Testing and Modeling of Compressive and Tensile Viscoelastic Effects in High Performance Concrete

by

Bo Meng

A dissertation submitted in partial fulfillment
of the requirements for the degree of
Doctor of Philosophy
(Civil Engineering)
in the University of Michigan
2019

Doctoral Committee:

Professor Will Hansen, Chair
Professor E.A.B. Koenders, Technische Universität Darmstadt
Professor Jason P. McCormick
Professor Jwo Pan

Bo Meng

mengbo@umich.edu

ORCID iD: 0000-0003-4053-5598

Acknowledgements

I wish to thank the many individuals who assisted me in the completion of this dissertation. First, special thanks to my advisor, Prof. Will Hansen, for providing support, encouragements, and suggestions during this research. His knowledge and dedication have made this work possible. I also wish to thank my committee members Prof. Jwo Pan, Prof. Jason P.McCormick, and Prof. E.A.B. Koenders for spending time reviewing my work and providing comments.

I would also like to express my appreciation to the faculty and staff of the Department of Civil and Environmental Engineering at the University of Michigan. The professors, technicians, and office staff have offered me endless support throughout my study here. Thank you to Jan Pantolin, Robert Spence and Steve Donajkowski for helping me to finish all the laboratory work as well as collaborate with me for teaching work for CEE 351 in many years. Thank you to Zhichao Liu and Yuguo Zhong for their friendship and support. Finally, thank you to my family who are always supportive and patient.

Table of Contents

List of Tables

List of Figures

List of Appendices

List of Abbreviations

ACI	American Concrete Institute
CEB	Comité Euro-International du Béton
CTE	Coefficient of Thermal Expansion
FIB	Fédération Internationale de la Précontrainte
GGBFS	Ground granulated blast-furnace slag
HPC	High performance concrete
LWA	Lightweight aggregate
NSC	Normal strength concrete
RILEM	The International Union of Testing and Research Laboratories for Materials and Structures
SCM	Supplementary cementitious materials
TD	Thermal Dilation
TSTM	Thermal Stress Testing Machine

List of Symbols

A_c	The cross section area of concrete
A_s	The cross section area of steel
C_{SCM}	The SCM content by mass
C_u	Ultimate creep coefficient
$E_{v,cr}$	Viscoelastic creep modulus
E_e	Young's elastic modulus of concrete
$E_{e,t}$	Young's elastic modulus of concrete, in tension
E_s	Modulus of steel reinforcement
E_{sh}	Viscoelastic shrinkage modulus
ε_{cr}	Sealed basic creep strain
$\varepsilon_{cr,0}$	The ultimate basic creep strain
ε_e	Elastic strain
ε_s	Deformation of steel reinforcement
ε_{sh}	Free autogenous shrinkage
$\varepsilon_{sh,r}$	Restraint autogenous shrinkage
$\varepsilon_{sh,0}$	Ultimate free autogenous shrinkage
$\varepsilon_{sh,P}$	Shrinkage contributed by pozzolanic reaction
$\varepsilon_{sh,S}$	Free autogenous shrinkage with slag
ε_{tot}	Total load dependent strain
$\varepsilon_{tot,0}$	Ultimate total load dependent strain

f_{cm}	The compressive strength
g	Volumetric Aggregate content
J_{cr}	The creep compliance
$J_{cr,0}$	The ultimate creep compliance
J_e	The elastic compliance
J_{tot}	The total compliance
$J_{tot,0}$	The ultimate total compliance
M	Maturity index
λ	The coefficient of viscosity
R	Relaxation in percent
Re	Degree of restraint
RH	The internal relative humidity
RH_u	Ultimate relative humidity
$\sigma_{cr,t}$	The axial stress due to tensile creep
σ_{fe}	Fictive elastic stress
σ_0	The external load applied on specimens for creep
σ_{sh}	Internal shrinkage stress
σ_{re}	Relaxation in stress
w/c	Water/cement ratio in weight
w_t/c	Total water/cement ratio
w_e/c	Effective water/cement ratio
w_{ic}/c	Internal curing water/cement ratio
ɳ	Percentage of IC water

Abstract

This thesis deals with experimental tests and numerical simulation of compressive and tensile viscoelastic behavior at later ages (since 7 days and curing at 20 °C) of high performance concrete (HPC), here defined as low water-cementitious ratio (0.35) concrete, which is cured under sealed moisture conditions. Previous studies have focused on early-age cracking, which is complicated by the rapid changing thermal effects. The viscoelastic effect starting from later ages (7 days), when the thermal effect is not major concern, still needs to be studied. The main objectives are to evaluate experimentally the compressive and tensile viscoelasticity effects on HPC, autogenous shrinkage stress development associated with full deformation restraint on the tensile cracking susceptibility, and to develop a modeling tool for incorporating effects of viscoelasticity in total stress analysis.

HPC is studied for its popularity in structure and building. The experimental program can be split into three parts for creep, autogenous shrinkage and restraint net tensile stress evaluation and modeling respectively. The viscoelastic behavior under sealed condition of HPC is studied in this thesis for its prevalence in structure and buildings. Normal strength concrete is also studied for comparison.

Basic creep under sealed condition is studied for HPC with w/c = 0.35. A rheological based model is used for simulating and predicting the basic creep of HPC under sealed condition due to its ability to capture underlying physical parameters. The relaxation under compressive mode is numerically simulated for investigating the contribution of relaxation in stress on the resistance to cracking. Viscoelastic creep modulus is defined in a similar way as elastic modulus for characterizing the resistance of concrete to be deformed viscoelastically in compressive mode due to external load. The effect of material parameters and aging on the viscoelastic modulus are also studied.

Autogenous shrinkage tests under sealed condition for HPC and normal strength concrete (NSC) are conducted in a long-term study on the effect of water/cement ratio, aggregate contents and addition of LWA for internal curing. A direct approach for estimating the shrinkage stress under full restraint condition is proposed based on twin tests of free shrinkage and partial restraint autogenous shrinkage with reinforcement. The mitigation effect of LWA on shrinkage is directly shown by its significant effect on maintaining the internal RH concluded from internal RH and wrapping tests conducted in this research.

For direct testing for net tensile stress development associated with full deformation restraint, a servo-hydraulic system known as a Temperature Stress Testing Machine, TSTM is implemented here for detailed long-term continuous measurement starting at the age of 7 up to 60 days. These results are augmented with free and restrained shrinkage tests. Shrinkage stress is shown to be significant and the major factor in viscoelastic stress contribution and is combined with elastic stresses for assessing crack susceptibility of HPC. Tensile viscoelastic effect on HPC is shown insignificant after early age (7 days) by TSTM test with LWA mitigation on shrinkage. Relaxation modulus as in plastics is not needed for the estimation of tensile stress of HPC with restraint. The addition of LWA is also proven to be effective for reduction in internal stress due to its mitigation effect in shrinkage.

Chapter 1 Introduction

1.1 Background

Concrete, the commonly used building materials, is the one whose parameters and properties are changing with time. Shrinkage and creep and its associated stress relaxation are the key viscoelastic behavior which functions importantly in evaluating the risk of cracking or performance in long-term use. With the higher demand in the performance of concrete used for industry, concrete with excellent properties are needed not only in terms of strength but also low shrinkage and creep. In the recent decades, high performance concrete (HPC) with much higher strength and better durability are introduced with wide use in building foundations, bridges and prestressed structures, etc. However, most of former work on viscoelastic behavior of HPC are focused on the very early age, only few did extend the study to long term, like 3 months to one year, and most importantly in compression. For further potential improvement in the viscoelastic performance of HPC, a comprehensive understanding of viscoelastic behavior of concrete in compression and tension is needed for accurate performance prediction such as transfer in compression in reinforced columns and of risk of tensile cracking if restrained in tension.

The high strength concrete with compressive strengths 50-100 MPa, here defined as high performance concrete (HPC) is important in structural applications such as reinforced columns in high rise buildings, as compressive creep and shrinkage result in significant time-dependent stress transfer between concrete and steel. Of particular interest in this thesis is the creep and shrinkage under sealed moisture condition, referred to as basic creep and autogenous shrinkage. Basic creep is prevalent in a thick cross section. This eliminates the need for drying shrinkage correction effects for drying creep analysis as basic creep develops without a moisture gradient.

In HPC of low water-cement (w/c) ratio (e.g. 0.35), sealed curing results in significant chemical shrinkage, which at the macro-level causes autogenous shrinkage. Although both creep and shrinkage originate from the hydration of cement and movement of water, the driving forces are different. While creep is originated from sustained external loading, shrinkage is believed to originate from the volume change due to moisture loss or movement towards equilibrium condition. Therefore, they are treated as independent properties for their distinct mechanisms under external and internal load (Harank, 2009).

In terms of compressive or tensile stress concrete is applied on, creep can be separated into compressive creep and tensile creep. Due to the difficulty in the measurement of tensile creep under uniform distributed tensile stress, tensile creep is assumed the same as compressive creep by many researchers in the past decades. As mentioned before, few studies were conducted on the tensile viscoelasticity of HPC at later ages and it is inaccurate to assess the tensile viscoelasticity by just using compressive creep value. Therefore more study on later age viscoelasticity effects on HPC is needed.

Pre-soaked lightweight aggregate is known as the material for reducing the self-desiccation because of internal curing effect. Many researchers (Cussion *et al*. 2008, Lura, 2003) associated the effect of internal curing by the internal curing water/cement ratio. In this study, the direct measurement of relative humidity development with various aggregate contents and the addition of lightweight aggregate are done for investigating the effect of internal curing on the relative humidity, the key factor for development of viscoelastic behaviour of concrete.

1.2 Objective and Scope of research

The primary objective of this research is to explore and better understand the mechanisms of viscoelastic behavior of HPC and its associated influence on stress development in compression and tension modes. While no consistency in lab and experimental conditions exists for the previous research on tensile and compressive viscoelastic behavior, this research is able to conduct comprehensive experiments and study on the viscoelastic behavior of concrete under sealed condition with consistency in materials and lab environments. This study can also help to extend the limited study on the long-term viscoelastic behavior of high performance concrete under sealed condition.

With wide use in structures and buildings, the accurate prediction and estimation of viscoelastic creep behavior are essential for evaluating the life cycle of concrete, especially high performance concrete with high self-desiccation. Experimental tests are therefore necessary for verifying mathematical models with fine-tuned parameters. While many models were developed based on data from other reference, the quality of data lacks confidence which may lead to larger error in the long term behavior prediction. The thesis instead implements a model with parameters of physical meaning for simulating the long-term creep behavior of HPC under sealed condition with effect of materials and aging parameters.

In this research, autogenous shrinkage tests are conducted with study in the effect of materials parameters for better understanding of shrinkage of HPC and normal concrete and its association with internal stress development. A new proposed method is introduced for easy assessment of shrinkage stress under restraint condition. A better understanding of autogenous shrinkage development in long term of HPC and the effect of materials parameters are expected to be achieved. Moreover, as one of the major influential factors, internal humidity is directly measured and modelled associated with its effect on shrinkage. The self-desiccation mechanisms of autogenous shrinkage is directly measured through internal relative humidity.

Cracking risk is the biggest concern for long–term use of concrete, especially in tensile mode because of the relative low split tensile strength of concrete. While the internal stress grows up to about 60%-70% of the strength, concrete has larger probability of propagation of micro and macro cracking. As a result, axial stress growth of concrete under tensile mode cannot be ignored and experimental measurement and mathematical simulation are studied for accurate evaluation of risk of failure with the effect of materials parameters in this thesis.

1.3 Organization of the thesis

This doctoral thesis is organized in eight chapters. A short review about the mechanical properties of concrete is discussed in Chapter 2 together with the basic correlation with material parameters.

A literature review of the state-of-art study on the viscoelastic behavior of creep and shrinkage behavior of concrete is presented in Chapter 3. Some of the important material parameters

controlling the viscoelastic properties are also discussed as well as some of the prevalent mathematical modeling of simulating the viscoelastic behavior.

After the introduction of experiential program as well as the materials used in this thesis are listed in Chapter 4, the basic creep behavior of HPC and NSC under sealed condition are studied with various aggregate contents, water/cement ratio, loading stress and addition of LWA as well as GGFS(SCM) in Chapter 5. A constitutive rheological viscoelastic model is involved in this research for modeling and predicting the basic creep behavior with the effect of materials parameters and loading condition.

Autogenous shrinkage plays an important role in controlling the growth of internal stress and risk of failure. A series of direct measurement of autogenous shrinkage with various aggregate contents, water/cement ratio, internal moisture are studied in Chapter 6. The internal curing effect with the presence of LWA is also studied for its importance in restraining the growth of shrinkage. An innovative method for evaluating the capacity of limit of cracking is proposed for evaluating the shrinkage stress under restraint condition.

In Chapter 7, TSTM test for analyzing the axial stress of concrete with fixed length was conducted. The tensile viscoelasticity under sealed condition is studied as well as the effect of aggregate content and LWA.

Finally in Chapter 8, the summary and conclusion are given along with the recommendations for future work.

Chapter 2 Mechanical Properties of High Performance Concrete

2.1 Introduction

Concrete is a composite material that continuously changes with transient material properties. From the mixing of each composite at the beginning, concretes starts as the material with liquid state and then transfer to a viscoelastic state within a few hours. Concrete finally becomes the hardened material with almost elastic properties after a long-term development.

A lot of focus has been put on the development of HPC in buildings, offshore structures, bridges and other prestressed structures in the last two or three decades. High strength, high durability and good workability at site are some of the main reasons for wide use of HPC. Among all the mechanical properties, high strength is one of the most important advantages over ordinary concrete for HPC and it can reach 140 MPa even in some parts of the world. But besides the high strength and modulus of elasticity, low permeability and resistance to some forms of attack are also required. In order to be classified as HPC, a list of specifications must be met such as impermeability, dimensional stability besides the common requirements of durability specified by ACI committee 201. Some study has been conducted on the reasons why HPC has better performance than NSC. Aıtcin (2003) claims that high performance concrete that have a water/ binder ratio between 0.30 and 0.40 are usually more durable than ordinary concrete not only because they are less porous, but also because their capillary and pore networks are disconnected due to the development of self-desiccation. Neville *et al.* (1998) attributed the reasons to the low water / cement ratio and the wide use of supplementary cementitious materials such fly ash, ground blast furnace slag. Also a smaller maximum size of aggregate is used for the sake of smaller differential stress as the aggregate-cement paste interface.

It is well known that many factors affecting the mechanical properties of HPC such as mix proportioning and temperature. Many studies have been conducted on the mechanical properties

because of the convenient of experimental setup. Contrast to mechanical properties, viscoelasticity property is more important in term of durability. However because of the close correlation between mechanical and viscoelasticity property, most of the modelling of viscoelasticity property are built using mechanical variables and therefore mechanical properties are quite important for characterizing viscoelastic behavior of concrete.

The main purpose of this chapter is to give a short review of some of the existing knowledge about the mechanical properties of HPC and the factors affecting mechanical properties. Some of the prevalent models for simulating the time effect on strength and elastic modulus and their dependence are also discussed.

2.2 Mechanical properties

2.2.1 Compressive and tensile strength

Compressive and tensile strength are the most important mechanical properties that have been widely studied for mature and young concrete. Compared to tensile strength, compressive strength is easy to determine and provides a good picture of the general quality of concrete. But for tensile strength, it is complicated to carry out and the interest has been concentrated on the compressive capacity of concrete.

It is easy to conduct the compressive strength test at different ages. Many mathematical models have been created to predict and characterize the development of strength with time. Maturity laws and degree of hydration are two of the most important concepts which are widely used as the parameters in the mathematical models. Other concepts used to describe the growth of compressive strength are porosity concept, the gel – space ratio and the chemistry – oriented strength laws which are described in Kanstad *et al.* (1999), Jonasson (1984) and Byfors (1980). CEB–FIP MC 1990 provides a widely use expressions for characterizing the development of compressive strength versus time given in Eq. 2-1.

$$f_c(t_0) = f_{c28} \cdot \left\{ exp\left[s \cdot \left(1 - \sqrt{\frac{28}{t - t_0}} \right) \right] \right\} \qquad \text{Eq. 2-1}$$

In where t_0 corresponds to the the time when the strength and stiffness are defined to be zero. The coefficient s depends on the type of cement and compressive strength. f_{c28} is the

compressive strength at 28 days. Tests on HPC with w/b ratio of around 0.4 and with different cement types and variable silica contents have shown that t_0 varies typically between 9 to 12 hours at 20 °C.

The tensile strength can be measured in a uniaxial tensile test or alternatively by tensile splitting. The tensile splitting test is widely used for determining the split tensile strength due to its simplicity method procedure. Ring test and flexural test are other testing methods used for testing of tensile strength. The main factors that affecting the growth of tensile strength are similar to those that affecting the growth of compressive strength. Some study (Kasai *et al.* 1974 and Khan *et al.*,1996) reported that the tensile strength grows faster than the compressive strength.

2.2.2 Modulus of elasticity

Modulus of elasticity is also an important property for characterizing the general quality of concrete. ASTM Standard C469 provided the method and procedure to measure the modulus of elasticity from compressive strength test. An exponential equation by CEB-FIP code 90 is widely used for predicting the development of modulus of elasticity at various ages.

$$E_{cmt} = E_{cm28} \cdot \left\{ exp\left[\frac{s}{2} \cdot \left(1 - \sqrt{\frac{28}{t/t_0}} \right) \right] \right\} \quad \text{Eq. 2-2}$$

As a part in modeling of creep behavior, modulus of elasticity can also be modeled in various methods. In ACI model, modulus of elasticity can be modeled as a function of unit weight of concrete and the mean compressive strength at the time of loading (ACI committee 209):

$$E_{mcto} = 0.043\gamma_c^{1.5}\sqrt{f_{cmto}} \quad \text{Eq. 2-3}$$

Where γ_c is the unit weight of concrete (kg/m^3) and f_{cmto} is the mean concrete compressive strength at the time of loading. In addition to Eq. 2-3, ACI also recommends the following expression for high strength concrete:

$$E_{mcto} = 3320\sqrt{f_{cmto}} + 6900 \quad \text{Eq. 2-4}$$

Onken *et al.* (1995) claimed that elastic tensile modulus after 28 days should be about 15% higher than that in compression at the same day due to the less non-linearities in tension. This is

consistent with the findings by Hagihara *et al*.(2002) the ratio of tensile and compressive modulus should be in range of 1.07-1.18.

2.3 Factor affecting mechanical properties

2.3.1 Aggregate content

Modulus of elasticity is greatly influenced by material properties and mineral admixtures. Neville (1970) stated two equations for elastic moduli of composites listed below:

$$\mathrm{E} = (1-g)E_m + gE_p \quad \left(composite\ hard\ material\ when\ E_m\ >\ E_p\right) \qquad \text{Eq. 2-5}$$

$$\mathrm{E} = \left(\frac{1-g}{E_m} + \frac{g}{E_p}\right)^{-1} \left(composite\ soft\ material\ when\ E_p\ >\ E_m\right) \qquad \text{Eq. 2-6}$$

Where E is the modulus of elasticity of concrete. E_m is the modulus of elasticity of the matrix, E_p is the modulus of the particle phase and g = fractional volume of the particles. Matrix for normal concrete without special fiber or reinforcement usually has elastic modulus E_m much smaller than aggregate E_p. Therefore Eq. 2-6 should be applied in this study.

The relations of stress and strain for aggregate, cement paste and concrete are shown in Fig. 2-1 by Neville (1997). It needs to be noted that both the aggregate and the hardened cement paste have a perfect linear stress-strain relation while concrete develops nonlinearly with strain. The rate of increase in induced strain at the interface of aggregate and cement paste was much higher than the rate of applied stress development beyond a certain range. As mentioned by Neville (1997), the particles of cement at the interface zone are unable to become closely packed against large particles of aggregate which leads to large void around the aggregate not filled by the cement. The difference of modulus of elasticity between aggregate and cement paste plays an important role in modulus of elasticity of concrete. In HPC the difference of modulus of elasticity between aggregate and cement paste was smaller than normal concrete, which resulted in better bond of aggregate and cement and higher modulus of elasticity of concrete. In HPC the linear part in a stress-strain curve was high as 85% of ultimate strength and even higher was observed.

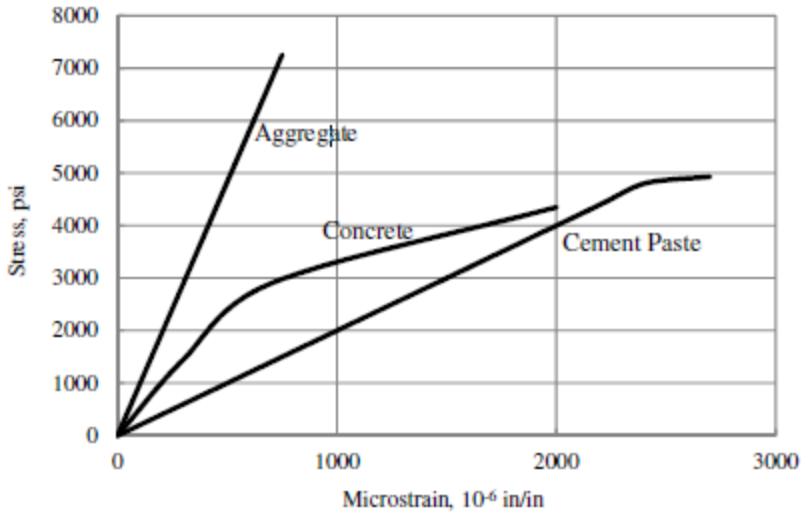

Fig. 2-1 The typical relation between stress and strain for aggregate, concrete and concrete paste (Neville A. M., 1997)

Lightweight aggregate is another type of aggregate with rough surface of texture and large volume of open surface pores. Similarly, the elastic modulus of lightweight aggregate is low and close to that of matrix which is beneficial to the bond between matrix and aggregate. Moreover, lightweight aggregate is always absorbing water and the water becomes available for the hitherto unhydrated remnants of cement particles. This happens in the interface zone so that the bond between aggregate and hardened aggregate can be improved. The good bond leads to the absence of early age microcracking, which can be seen by the linear stress-strain curves up to 90 % of the ultimate strength as shown in Fig. 2-2.

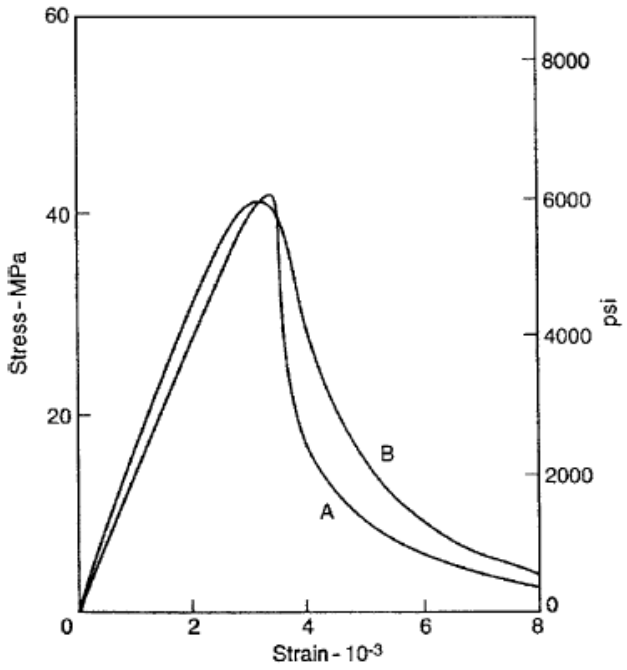

Fig. 2-2 Stress-strain curves for lightweight aggregate; A = all lightweight aggregate, B = normal weight fine aggregate (Neville, 1997)

2.3.2 Supplemental cementitious materials(SCM)

Mineral admixtures are typically added in HPC as partial replacement materials of Portland cement. The influence of slag on modulus of elasticity of concrete is small (ACI 233R, 2003). In the study by Brooks (1992), the effect of 0%, 30%, 50% and 70% slag replacement of Portland cement on the property of concrete was investigated. No significant influence of slag on elastic moduli was observed at later ages even though a reduction in the elastic modulus can be observed with increase in the level of slag at early age. It was indicated that dry-stored slag concrete had higher elastic moduli at early ages, but lower at later ages comparing with concrete without slag, and the opposite trend was found for water-stored concrete.

Fly ash has also slightly influence on modulus of elasticity of concrete, including Class F fly ash (Best, J.F, 1982) and Class C fly ash (Yildirim, 2011). From Fig. 2-3 (Yildirim, 2011), it can be seen that the modulus of elasticity is not affect substantially with the use of fly ash even though for water/cement ratio of 0.75, the modulus increases slightly with fly ash content.

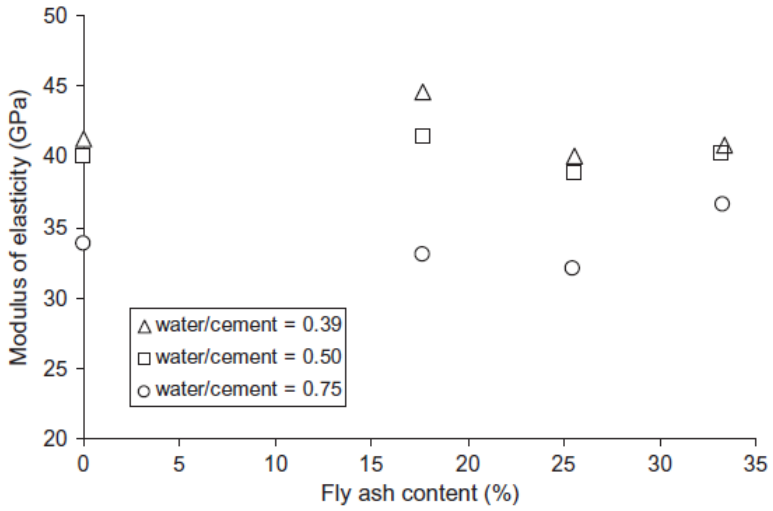

Fig. 2-3 Effect of fly ash content on the static modulus of elasticity of concrete (Yildirim, 2011)

According to the study by Alfes (1992), it was indicated that 10% silica fume as the replacement of Portland cement can help to increase elastic moduli of concrete by 12% at 28 days, but 20% silica fume increased it by 7% at 28 days comparing with concrete without silica fume as shown in Fig. 2-4.

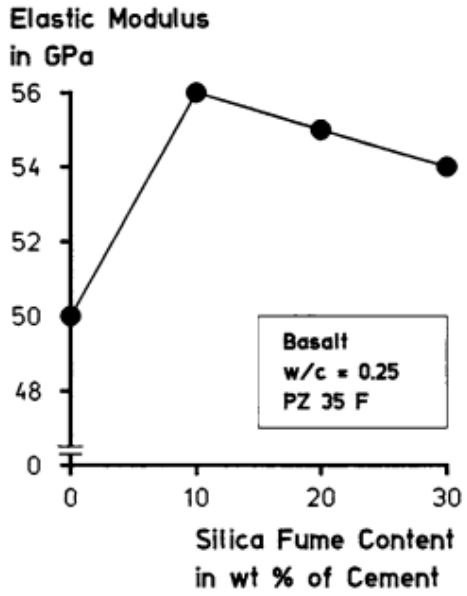

Fig. 2-4 Dynamic elastic modulus of high strength concrete as a function of the silica fume content (Alfes, 1992)

In the study by Mazloom *et al*. (2004), effect of four levels of replacement of Portland cement with silica fume including 0%, 6%, 10% and 15% on modulus of elasticity of concrete were investigated. It was found that secant elastic moduli increased within 10% at 7 days and 28 days with an increase of silica fume content as shown in Table 2-1. Moreover, Mazloom *et al*.(2004) also mentioned that the sealed and drying specimens had similar values of secant modulus. Even after comparing the secant modulus of measured elastic modulus recovery after long term creep test and estimated elastic modulus recovery, it is shown that the loading age and silica fume replacement level had no influence on the elastic modulus recovery.

Table 2-1 7 and 28 days compressive strength and secant modulus of elasticity (Mazloom et al. 2004)

Kind and age of concrete		Compressive strength (MPa)	Measured modulus (GPa)	Predicted modulus by Eq. (1) (GPa)
OPC	7 days	46	28.8	30.2
	28 days	58	34.4	34
SF6	7 days	50.5	31	31.7
	28 days	65	35.5	36
SF10	7 days	52	31.1	32.2
	28 days	67.5	37	36.6
SF15	7 days	53	31.5	32.5
	28 days	70	38.1	37.3

2.3.3 Temperature

Temperature also has a big effect on the modulus of elasticity. Temperature can be associated with maturity:

$$\mathrm{M(t)} = \int_0^t exp\left[\frac{E_a}{R}\left(\frac{1}{273+T_{ref}} - \frac{1}{273+T(t)}\right)\right]dt \qquad \text{Eq. 2-7}$$

M(t) refers to the equivalent age under target climate with give target temperature profile. Based on this equation, the strength in concrete increases more quickly under higher temperature. For concrete with sealed curing and drying curing, the effect of temperature is different. For concrete under drying curing, the modulus decreases due to the loss of load-bearing evaporable water.

For mass-cured (sealed) or water stored concrete, the modulus is also reduced as the temperature rises, the effect even being greater than when water can be expelled from the concrete. For concrete which is heated a short time and then being subjected to load, the rise in temperature leads to the mobility of moisture and as a result the stiffness of the solid structure is reduced.

But for the sealed concrete which is cured under elevated temperature throughout the whole life or a long time before the starting of the loading, the effect of temperature will lead to the acceleration of the hydration which leads to the a slight increase in the modulus but not significantly, reported by Nasser *et al.*(1965). Liu *et al*.(2017) also mentioned that instabilities of prediction of mechanical behavior of concrete structure may arise in the presence of transient heating which confirms the significant effect of temperature on mechanical property.

Chapter 3 Viscoelastic Behavior of HPC under Sealed Condition

3.1 Introduction

Creep is generated due to sustained loads of concrete. Besides the instantaneous deformation at the time of loading, a long-term deformation exists during the whole period of loading. At the same time, concrete may also undergo other deformation because of thermal and volumetric deformation due to the change in water and hydration process. Because of this fact that creep always goes with other deformation, it is hard to investigate the behavior of creep alone and decouple the creep deformation from others. The viscoelasticity of HPC under sealed condition is important as its prevalence in use as the foundations of structure, and many references has been already done with it (Brooks et al.1992, Koenders et al., 1997, Kovler 1994). However since lots of research are related to the very early age, additional research is still needed for comprehensive knowledge of the viscoelasticity for long term.

Creep and shrinkage are the two most important viscoelastic behavior of concrete. As mentioned in the description of the effect of shrinkage on long term use and cracking risk estimation of concrete, creep is critical. For concrete under tensile stress, the magnitude of relaxation, which is always associated with the creep, partially determines the increase rate of self-induced stress for accessing the growth of internal crack. Relaxation is supposed to occur under both compressive and tensile load and there is no all-agreed conclusion that whether tensile relaxation is the same as compressive relaxation. Several viscoelastic models have been created by the superposition rule to study creep without dependence on other behavior. Even though good fit can be achieved for most of the creep data by many models, there is no single model that explains perfectly the creep behavior in both short term and long term. The models which can simulate the very early beginning stage of creep always has problems fitting to the long term

data with good accuracy. Bosnjak *et al*. (2001) states that the theoretical creep modeling is not very reliable and the uncertainty in creep prediction is still considerable. Due to the lack of enough creep data, especially for high performance concrete, the bias cannot be prevented and lead to inevitable large deviations of the parameters for concrete used in different fields (Bazant, 2008). The long-term creep data such as 1-10 years is still well needed.

In this thesis, the mechanisms of viscoelasticity of HPC under sealed condition including the basic, drying creep and relaxation are investigated. The effect of materials parameter such as aggregate, cement, stress, water/cement ratio and temperature, etc on creep and shrinkage are discussed based on previous reference. The current prevalent numerical modeling of shrinkage and creep are discussed with the advantages and disadvantages.

3.2 Viscoelastic behavior of concrete

The mechanisms of the deformation of concrete is various. For study on shrinkage and creep, the following terms are needed listed in ACI 209.1R:

- Total Strain
- Shrinkage
- Autogenous shrinkage
- Drying Shrinkage
- Carbonation Shrinkage
- Swelling
- Load-induced strain
- Initial strain at loading or nominal elastic strain
- Creep strain
- Basic creep
- Drying creep
- Compliance
- Specific creep
- Creep coefficient

The deformation of concrete can be decomposed into three fundamental types: elastic, plastic and viscous as well as elasto-plastic or viscoelastic. In term of time correlation, the deformations can be categories: time-independent and time-dependent deformations as shown in Table 3-1 (Atrushi, 2003). The deformation can be classified into stress-dependent and stress- independent in terms of stress. Creep and elastic deformations are stress-dependent while shrinkage and thermal dilation are stress independent. The deformation of concrete can also be split into reversible and irreversible deformation. For both the instantaneous and creep strain, they are composed of both the reversible and irreversible deformation. The table below gives a clear illustration about the different classification method. The various terms of mechanical deformation behavior are shown in Fig. 3-1.

Table 3-1 Classification of strains (Atrushi, 2003)

Strain	Load-dependent		Load-independent
	Instantaneous	Time-dependent	
Reversible	Elastic (ε_{el})	Delayed elastic ($\varepsilon_{el,d}$)	Thermal dilation* & Shrinkage or swelling*
Irreversible	Inelastic (ε_{nel}) (*Plastic flow*)	Delayed inelastic ($\varepsilon_{nel,d}$) (*Viscous flow*)	

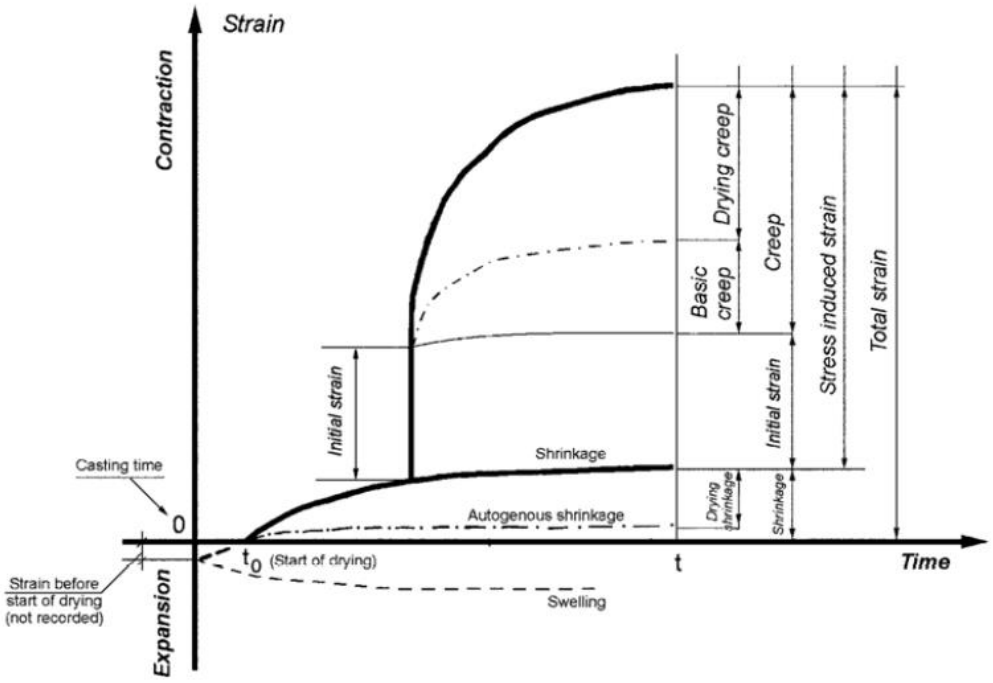

Fig. 3-1 Relationship between various measured and derived strain values (ACI 209.1R)

3.2.1 Basic creep and drying creep

Total load-dependent strain is composed of basic creep, elastic strain and drying creep if moisture loss condition. Basic creep refers to the time-dependent increase in strain under sustained external load in which moisture losses or gains are prevented (sealed specimen). When specimens are exposed to the environment and allowed to dry, additional creep called drying creep is applied on specimens. To obtain the drying creep, one can subtract the total load-dependent of sealed specimen and shrinkage of drying specimen from the total strain of drying specimen as shown in Eq. 3-1. The activation of drying and basic creep is different. For drying creep, the tensile stress induced in the outer part of concrete is one of the major factors while uniform drying occurring only in the inside of concrete without moisture exchange with outside.

$$\varepsilon_{total} = \varepsilon_{el} + \varepsilon_{cr} + \varepsilon_{dr} \quad \text{Eq. 3-1}$$

Many theories were proposed for the mechanisms of creep. Some argues that the creep is due to the delayed elasticity as the cement matrix acts as a restraint on the elastic deformation of the skeleton formed by the aggregates. Other prevalent theories believe that creep is due to

consolidation seepage in form of adsorbed water or the decomposition of interlayer hydrate water. The main reason that no a universal theory is reached is that no one theory can explain the whole creep process.

Right after the loading started, a small inelastic component exists along with the elastic part besides the recoverable elastic strain. It should be noticed that the loading of specimens under creep test takes some time and the first reading from the starting of the creep test is not only elastic strain immediately generated with the loading. Instantaneous deformation is defined as the total load dependent strain after a short amount of time. The basic creep is thus the difference between total strain and the instantaneous strain. However, there is no standard for determining the time of instantaneous strain and therefore different definitions of instantaneous deformation are used and even some authors just regard that as the elastic deformation.

Bazant *et al*. (1982) claimed that the instantaneous deformations, which is the total strain of elastic and inelastic component right after loading, can be that for 1 to 10 mins (typical the duration of strength tests) while others use 0.0001s for that. There are great differences among all the definitions of elastic modulus E(t') which will lead to the diversion in the magnitude of creep strain. Bazant suggested to use quasi-elastic analysis to give good results for short-time loading while for the loading more than one day, it makes little difference between using 1 or 2 hours for determining the E(t'), show in Fig. 3-2. And for practical structural analysis, an equation is also given, in Eq. 3-2.

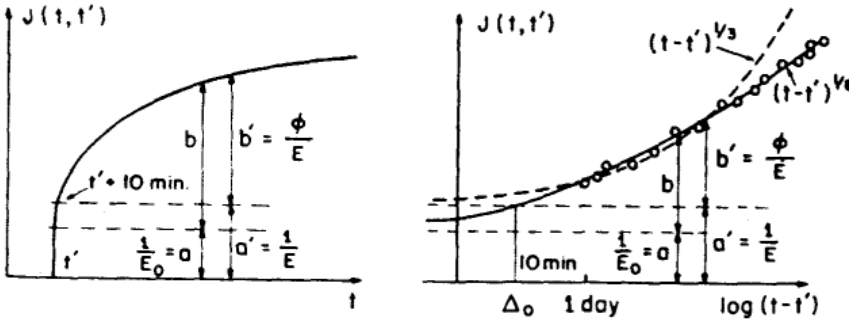

Fig. 3-2 Creep curves in actual and log time scales (a = true elastic deformation, b = true creep, a' =conventional elastic deformation, b'=conventional creep) (Bazant, 1982)

$$E(t') = \frac{1}{J(t'+\Delta,t')} \qquad \text{Eq. 3-2}$$

In Fig. 3-2 it can be seen that the elastic deformation and the subsequent creep are not easily separated from the other. The instantaneous deformation represents almost the vertical part of the response curve. In compression, the basic creep is expected to be linear with the applied load, however the linearity of tensile creep is very difficult to confirm because of the data scatter by various researches. The drying creep is expected to be in much larger magnitude compared to the basic creep as well as the creep rate.

3.2.2 Creep recovery

Creep recovery occurs after the unloading of sustained force. Since the elastic modulus at age of unloading is higher than that at the age of loading, the recovered deformation is smaller the elastic deformation at the loading age. Similar to the creep, creep recovery also undergoes a gradient decrease procedure. The initial recovery can correspond to the elastic deformation and creep recovery can correspond to the delay elastic deformation, shown by Arushi (2003):

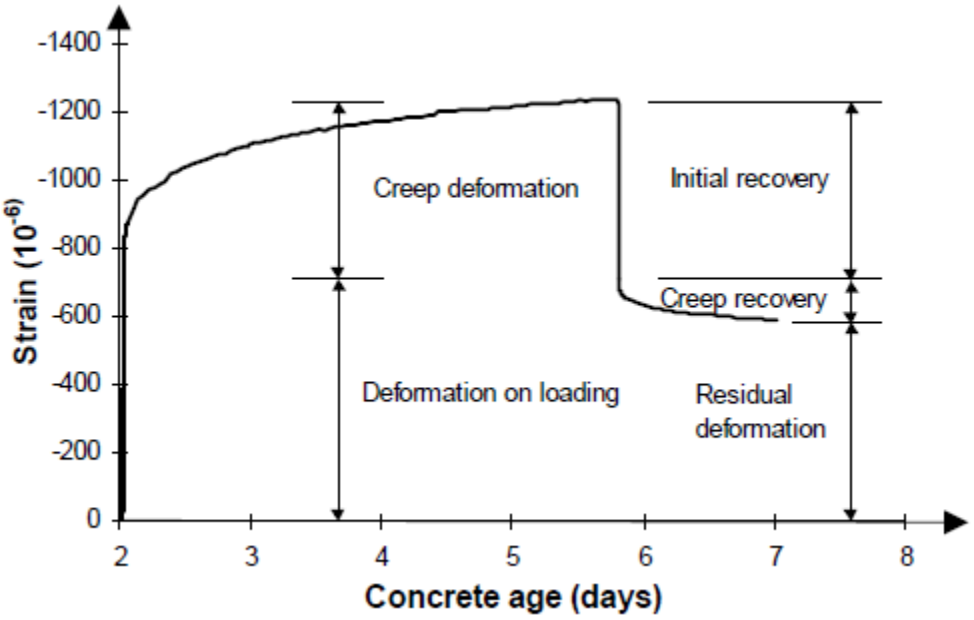

Fig. 3-3 Creep recovery and initial recovery after the unloading of specimens (Atrushi, 2003)

The knowledge of creep recovery is important for the study on the concrete specimens under stress variation with time. Some study (Yue *et al*, 2014) found out that similar to creep, creep recovery is also linear to the preloaded stress level. When the load is applied on specimens

before 28 days, creep recovery is affected and tends towards a final high value for earlier ages. For specimens with loading starting after 28 days, the final value for creep value is stable. The creep recovery of high performance concrete is higher than that of normal strength concrete. Creep/recovery ratio can be used as a key factor for study the mechanisms of creep recovery. But since few study has been done on creep recovery but just discuss creep recovery as a secondary finding, not many mathematical models are present. Yue *et al* (2014) also proposed a mathematical model for predicting the creep recovery behavior of concrete:

$$\varepsilon_r = \frac{\sigma}{E} \emptyset_{cr}(t_0, t_1) \beta_{cr}(t, t_0, t_1) \qquad \text{Eq. 3-3}$$

In which the final value of creep recovery is $\emptyset_{cr}(t_0, t_1) = 0.35/\sqrt{\propto}$

The development of creep recovery can be predicted by

$$\beta_{cr}(t, t_0, t_1) = \left[\frac{t - t_1}{t - t_1 + 300\propto}\right]^{0.24} \qquad \text{Eq. 3-4}$$

Smadi, M. M *et al* (1987) concluded that with the lower stress level, the percentage of creep strain recovered and initial strain covered on unloading are greater. The total recovery (initial + creep) is approximately proportional to the applied stress which is consistent with Yue's findings, shown in Fig. 3-4. Based on Bazant *et al.* (1979), the creep recovery is supposed to be able to be modeled with a pseudo external loading in the opposite direction with the same magnitude of the real external loading, as shown in Fig. 3-5.

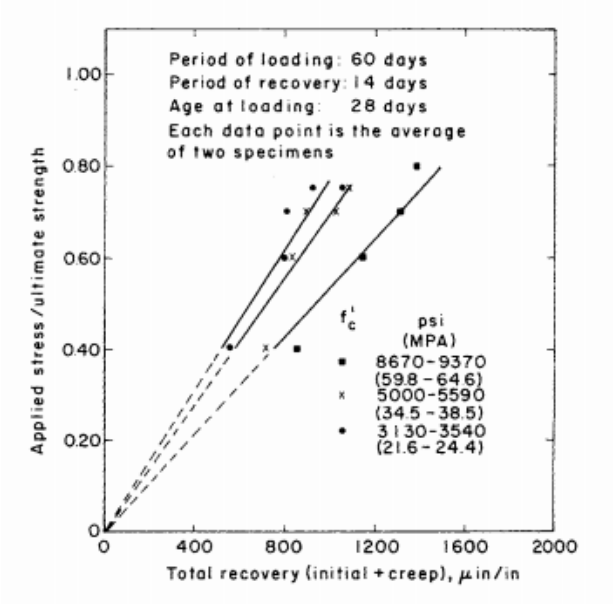

Fig. 3-4 Relation between stress-strength ratio and total recovery strain for high, medium and low stress concrete under sustained uniaxial compressive stresses (Smadi, M. M *et al*, 1987)

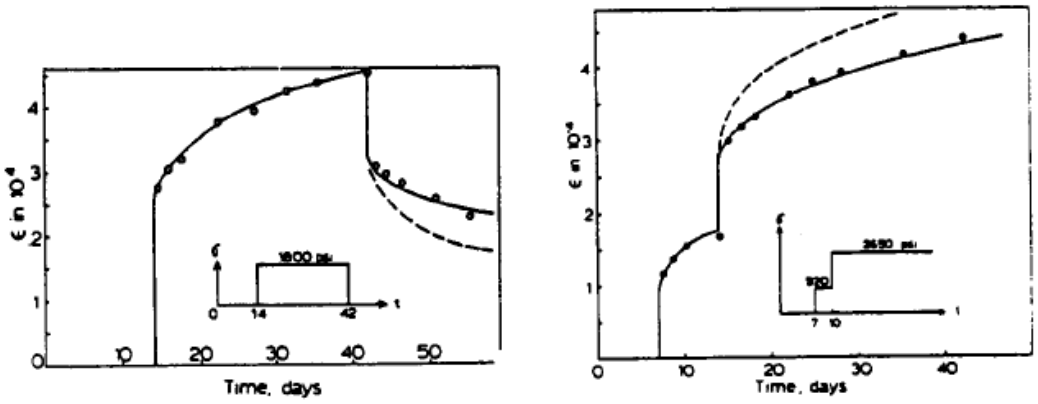

(a) (b)

Fig. 3-5 Deviation from the superposition principle when a loaded concrete is (a) unloaded (creep recovery) (b) further load [Bazant and Kim (1979)]

3.2.3 Creep relaxation

Compared to the creep behavior of deformation under constant loading, relaxation refers to the reduction in the stress for concrete with constant strain (compressive or tensile). A sustained strain produces an initial stress at time of application and a deferred negative stress increasing

with time at a decreasing time. Relaxation is important for evaluating the risk of cracking under tensile restraint condition since the internal stress due to autogenous shrinkage can be reduced by relaxation behavior. The relaxation modulus $R(t,t')$ is used for evaluating the stress development under relaxation effect. The volterra integral equation (Neville *et al.* 1983) can be used to transform the creep compliance $J(t,t')$ into relaxation modulus:

$$\int_0^t J(t,t')dR(t') = 1 \qquad \text{Eq. 3-5}$$

Creep compliance $J(t,t')$ is the compressive creep compliance. The volterra integral equation can be used for tensile creep with the assumption that tensile creep compliance is the same as compressive creep compliance.

The restrained tensile stress in concrete can be numerically evaluating by applying Eq. 3-6:

$$\sigma(t_{i+1}) = \sum_{j=1}^{i} \Delta\sigma_j(t_{i+1}) = \sum_{j=1}^{i} \frac{\alpha_t \Delta T_j + \Delta\varepsilon_j}{2}\left[R\left(t_{i+1}, t_{j-1}\right) + R\left(t_{i+1}, t_{j+1}\right)\right] \qquad \text{Eq. 3-6}$$

It is well established from other studies (Ross *et al*, 2013, Bazant et al, 1988. etc.) that compressive stress relaxation develops as a result of creep under constant strain. It should be emphasized that this relaxation modulus is fictitious modulus used for complex stress analysis.

A relative reduction in 30%-60% of modulus by relaxation in compression is observed by many previous study. For tensile relaxation, most of previous studies are focused on the early age (0-7 days) potential for normal concrete. Atrushi (2013) did comprehensive study on early age (0-7 days) tensile relaxation and found the effect of stress relaxation is relatively large and significant in the development of self-induced stress. Based on restrained ring test, Hossain et al (2004) evaluated the stress relaxation also by the comparison of residual and theoretical elastic stress and also detected pronounced relaxation and the relaxation is more pronounced with thicker steel wall. During the very early age, concrete is undergoing substantial change in mechanical properties and volume due to initial significant thermal effect. The conclusions derived from these studies support substantial relaxation effect on concrete stress development. However, some different conclusions are also drawn. Morimoto *et al* (2014) ran both compressive and tensile relaxation tests on concrete at early age. It is concluded in his research that tensile relaxation is smaller and terminates in shorter time (2-3 hours) to reach the ultimate value. If the

specimen is loaded at 3 days, the relaxation is only by about 15% while it can be 25% if loaded at 1 day.

Relative few studies have investigated the potential of the stress reduction at later ages for constant strain (some tests last for 1000 days). Bissonnette *et al.* (2007) and Forth (2015) concluded that significant amount of tensile creep and some even states that the magnitude of tensile creep is larger than compressive creep. Bissonnette *et al.* (2007) even concluded that creep in tension, as in compression, increases sharply under drying conditions, and tensile creep coefficients (under drying conditions) of up to 6.2 were determined. Tensile creep coefficient decreases with the age at loading, and that up to 50% of the ultimate short-term strength, tensile creep of concrete varies linearly with the applied load. Weiss *et al*. (1997) and Schachinger *et al.* (2002) stated that tensile creep significantly reduces tensile stress development and creep of concrete in tension increases sharply under drying conditions. By conducting comparison test of specimens with and without tensile creep, it was shown that shrinkage of specimens under tensile creep is larger than that of non-loaded ones (Reinhard *et al*., 2006).

3.2.3 Principles of superposition for linear viscoelastic creep

Many study and test already show that for creep test with sustained load smaller than 30-40% of compressive strength, the creep deformation follows linear behavior and it is common agreed that linearity principle can be used for studying the creep including drying and basic creep behavior as well as the other viscoelastic behaviors. With the assumption of linearity, superposition rule can be applied to creep of concrete under sustained external load. The principle of superposition proposed by Boltzmann (1876) makes it possible to do the stress analysis for the structure under various stress profile as the effect of creep and shrinkage. The sum of two stress can be regarded as the sum of the response to each of them taken separately.

Based on the rule of superposition rule, creep can be expressed as the integral of strain due to the each small stress increments in the form as below, in Eq. 3-7 and illustrated in Fig. 3-6.

$$\varepsilon(t) = \int_0^t J(t,t')d\sigma(t') + \varepsilon_0(t) \qquad \text{Eq. 3-7}$$

Where

t: The total time starting from the cast of concrete

t': concrete age at the time of loading

$d\sigma(t')$: stress increment at time t'

$\varepsilon(t)$: Total strain

$\varepsilon_0(t)$: Stress-independent strain (Shrinkage and thermal dilation)

$J(t,t')$: Compressive creep compliance (Creep strain over external stress)

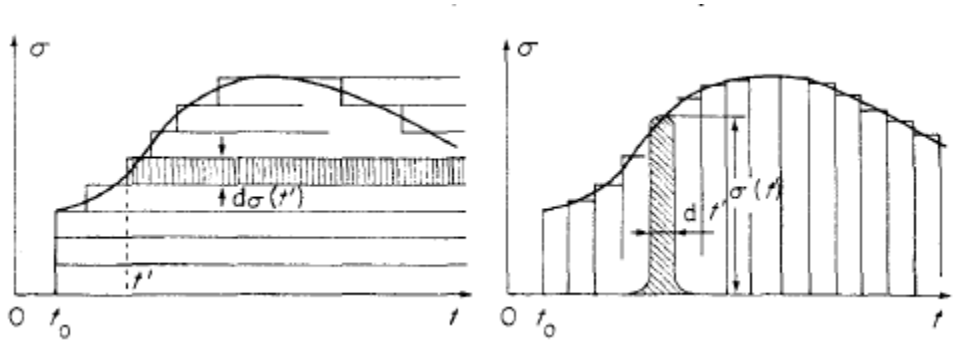

(a) (b)

Fig. 3-6 Decomposition of stress history into (a) stress steps and (b) stress impulses (Bazant *et al*.1982)

There are several conditions under which the rule of superposition will yield accurate prediction, as stated by Bazant *et al* (1982).

1. The stresses are within the service stress range, i.e. less than about 40% of the strength
2. Unloading, i.e. strain of decreasing magnitude, does not take place
3. There is no significant change in the moisture content distribution during creep
4. There is no large sudden stress increase long after the initial loading

What needs to be mentioned is that, the above restrictions can seldom be held for young concrete. For condition (1), the crack risk is high as the result of comparative high stress/strength ratio. Because of the dramatic heating and cooling phases at the early age of hydration, the significant change in moisture content cannot always be avoided. Moreover, the self-desiccation may also cause some internal drying because of the coupling effect of creep and autogenous shrinkage.

Also substituting $d\sigma(t') = [d\sigma(t')/dt']dt'$, one can transfer the equation to the following form, obtained by Maslov(1941). Then the strain history can be decomposed into the integral of vertical strips and can be transferred to a function of time t', shown in Fig. 3-6(b):

$$\varepsilon(t) = \frac{\sigma(t')}{E(t)} + \int_0^t L(t,t')\sigma(t')t' + \varepsilon_0(t) \qquad \text{Eq. 3-8}$$

The uniaxial stress by arbitrary strain history can also be derived by changing the form of the Eq. 3-8 to Eq. 3-9. When the strain history is given, one can calculate the stress history and relaxation function by solving this equation for the strain history specified as a step function.

$$\sigma(t') = \int_0^t R(t,t')[d\varepsilon(t') - d\varepsilon_0(t)] \qquad \text{Eq. 3-9}$$

3.2.4 Autogenous Shrinkage

Contrast to creep behavior which takes place as the result of external loading, shrinkage takes place from the internal stress as the result of the movement towards the moisture equilibrium with the environment where it is located. Shrinkage is load-independent behavior contrast to load-dependent creep. With regards to whether the concrete is sealed or dry, shrinkage can also be split to autogenous shrinkage and drying shrinkage. During the early age hydration two active mechanisms are involved in producing these movements, starting with thermal effects which dominate during the first 24-48 hours while self-desiccation is another consequence of cement hydration as this process consumes water into solid hydration products (Copeland, L. E *et al*. 1955). ACI209 mentioned that autogenous shrinkage occurring in the absence of moisture exchange due to the hydration reactions taking place inside the concrete matrix. With the increase use in the high performance concrete, autogenous shrinkage becomes a more and more important factor since it is comparatively larger than the autogenous shrinkage for normal strength concrete. Based on research from Tazawa(1995), for concrete with water-cement ratio less than 0.40, autogenous shrinkage may be a significant component of the total measured shrinkage. Drying shrinkage, on the other hand, refers to the shrinkage occurring in a specimen that is exposed to the environment and allowed to dry. For normal strength concrete, autogenous shrinkage can be neglected and drying shrinkage can be accounted for the whole shrinkage. And also because moisture movement and moisture loss occurs during the drying shrinkage, the magnitude and development of drying shrinkage depends on the size and shape of the specimen.

One popular theory of the mechanisms of autogenous shrinkage is the formation of capillary menisci as shown in. With the continuous cement hydration consumes water, drying takes place in pore structure with the formation of capillary menisci that cause tension in pore liquid. With the pore wall is in compression, the shrinkage happens. The capillary pressure can be evaluated by Eq. 3-10(a) and Eq. 3-10(b). In the study in volume changes in hardening cement-based materials, Koenders (1997) stated that surface tension in the adsorption layer at the pore walls can be considered as the (internal) driving force behind the mechanism to cause autogenous shrinkage. He also mentioned that the internal relative humidity in the empty pore space reaches between 100% and 75% due to self-desiccation effect. A thermodynamic-based numerical model is then made to simulate the effect of surface tension development and humidity change in porous structure (Koenders *et al*, 1997).

$$P_c - P_V = \Delta P = \frac{2\sigma cos\theta}{r} \qquad \text{Eq. 3-10(a)}$$

$$\frac{M}{\rho} \cdot \frac{2\sigma}{r} \cdot cos\theta = RT\, ln\frac{P_0}{P_r} \qquad \text{Eq. 3-10(b)}$$

Pre-wetted lightweight aggregate (LWA) is reported that can be used as internal source of water that can replace the water consumed by chemical shrinkage during hydration. As mentioned by Bentz and Weiss (2011), lots of benefit of internal curing can be observed such as reducing shrinkage, increasing cement hydration and improving curing when short cure time are permitted. Fig. 3-7 shows a schematic view of the effect of internal curing on the internal humidity. While external curing water is only able to penetrate several mm into low water to cement ratio concrete, whereas internal curing enables the water to be distributed more equally across the cross section (Bentz and Weiss, 2011). This finding was also confirmed by Lura (2003) in this PhD thesis by X-ray adsorption experiments that transport of water from saturated LWA to hydrating cement paste is observed, especially in the first days after casting. Properties of LWA that facilitate the internal curing process are essentially a high porosity, a fast water uptake when underwater, and an open pore structure that allows releasing water in the concrete at high internal RH (Lura, 2003).

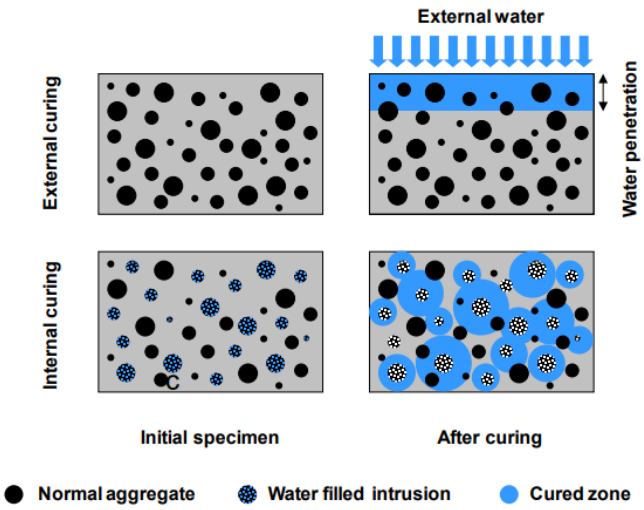

Fig. 3-7 Illustration of the difference between external and internal curing. The waterfilled inclusions should be distributed uniformly and spaced close enough to provide coverage for the entire paste system. (Bentz and Weiss, 2011)

The replacement level of pre-wetted LWA needed to ensure adequate water for complete curing of concrete is estimated by Bentz *et al*. (1999) using a simple equation in Eq. 3-11 where $\emptyset_{LWFA}$ is the porosity of LWA, S is the saturation degree and V_{wat} is the volume of water. Assuming the porosity of LWA is 15%, then 50% of the fine aggregate needs to be replaced by pre-wetted LWA.

$$V_{LWFA} = \frac{V_{wat}}{S \cdot \emptyset_{LWFA}} \qquad \text{Eq. 3-11}$$

3.3 Factors affecting creep

As reported by many investigated, there are many factors affecting creep and many of them are coupled with some of the other. Generally, all the factors can be divided into intrinsic and extensive factors. According to Bazant *et al.* (1982), the intrinsic factors are the materials characteristics which can vary since the casting such as elastic modulus of aggregate, strength, fraction of aggregate in the concrete mix and the maximum aggregate size. Increase in those factors will lead to the reduction in creep as well as shrinkage. Extensive factors include those which may vary since the casting such as temperature, pore water content and age at the loading. There are local and external types of factors for extensive factors. The local, which is also called state variables, are those which treated as a point property of a continuum such as degree of hydration, relative vapor pressure in the pores, water content. On the other hand, the size of

specimen and humidity are not admissible as state variables in a constitutive equation even though they have a great effect on creep.

3.3.1 Aggregate content

The role of aggregate is about the restraint of creep and shrinkage. The elastic modulus of aggregate is one of the most important factors that influence the creep behavior. For obtaining the elastic modulus of concrete, the volume fraction of aggregate and paste are the two most important variables. Kaplan (1959) and Hansen (1960) developed the basic equations to establish the correlation among those.

$$\frac{1}{E_c} = \frac{g}{E_p} + \frac{1-g}{E_m} \qquad \text{Eq. 3-12(a)}$$

$$E_c = gE_p + (1-g)E_m \qquad \text{Eq. 3-12(b)}$$

Where E_c, E_p and E_m are moduli of elasticity of the concrete, aggregate and matrix and g is volume concentration of the aggregate. As explained by Hansen (1960), Eq. 3.12(a) should be used when the aggregate is stiffer than the matrix while it is better to use Eq. 3.12(b) when the aggregate is softer than the matrix. Two more complex equation shown in Eq. 3.13(a) and Eq. 3.13(b) were developed by Counto (1965) but drawbacks still exist. The sketch of the four models are shown in Fig. 3-8.

$$\frac{1}{E_c} = \left(1 - \frac{2Z}{\pi}\right)\left(\frac{g}{E_p} + \frac{1-g}{E_m}\right) + \frac{2Z}{\pi}\left(gE_p + (1-g)E_m\right) \qquad \text{Eq. 3-13(a)}$$

$$\frac{1}{E_c} = \frac{1-\sqrt{g}}{E_m} + \frac{1}{\left(\frac{1-\sqrt{g}}{\sqrt{g}}\right)E_m + E_p} \qquad \text{Eq. 3-13(b)}$$

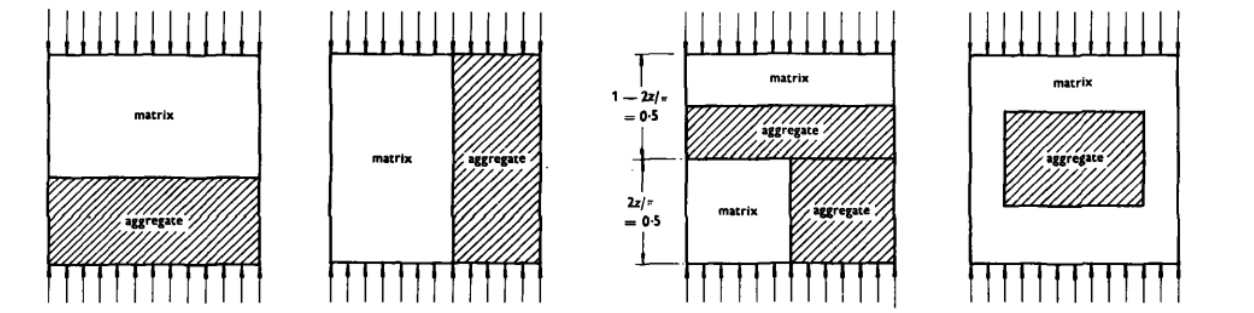

Fig. 3-8 Comparison among four models proposed by Kaplan (1959) and Hansen (1960) and Counto (1965)

There are common agreements that the modulus of concrete increase as the modulus of aggregate increases. For the aggregate whose modulus is smaller than that of matrix, with the increase volume fraction of aggregate, the elastic modulus of concrete decreases and the reverse is true while the modulus of aggregate is larger than that of matrix.

3.3.2 Cement and SCM

The type and strength of the cement influences the strength of concrete which will lead to the different magnitude of creep especially at early age. Water/cement ratio and volume of hardened cement paste are usually used to predict the effect of cement on creep and shrinkage. Pickett and Neville developed the equation shown in Eq. 3-14 and correlated the effect to the creep at a constant stress/strength ratio of cement paste d_p and the volume fraction of cement paste g_m with a parameter n which depends on elastic moduli and Poisson's ratios of aggregate and concrete.

$$d_C = d_p(g_m)^n \qquad \text{Eq. 3-14}$$

Based on Eq. 3-14, Brooks (1989) developed an equation:

$$R_c = R_p \left(\frac{g_m}{0.3}\right)^n = R_p R_g \qquad \text{Eq. 3-15}$$

Where R_p is the relative deformation of cement paste and R_g is the relative volume fraction of cement paste. For normal weight aggregate and light weight aggregate concrete, n=1.8 and n =1 are used.

The influence of supplementary cementitious materials (SCM) has been studied widely. It was stated by Brooks *et al*.(1992) that the influence of type of slag on strength, modulus of elasticity and long–term deformation is small and cannot be associated quantitatively with chemical composition. Although the increase in quantity of slag leads to the decrease in early strength and increase in initial basic and total creep, little improvement in effect of the raising replacement ratio from 30 to 70% on creep can be noticed and the major effect can be attributed to the effect on strength.

Not only slag, silica fume also has been studied that the silica fume replacement levels will have effect on basic and drying creep of concrete. Mazloom *et al*. (2004) stated that as the proportion of silica fume increased, the workability of concrete decreased but the short term mechanical properties such as 28-day compressive strength and secant modulus improved. With the increase in the silica fume replacement level, basic creep of concrete decreased and the reduction of silica fume on swelling effect was reported to be the main factor as shown in Fig. 3-9. Bissonnette *et al*. (1995) indicated that silica fume seems to enhance tensile creep as well as the drying shrinkage but the effect is relatively small.

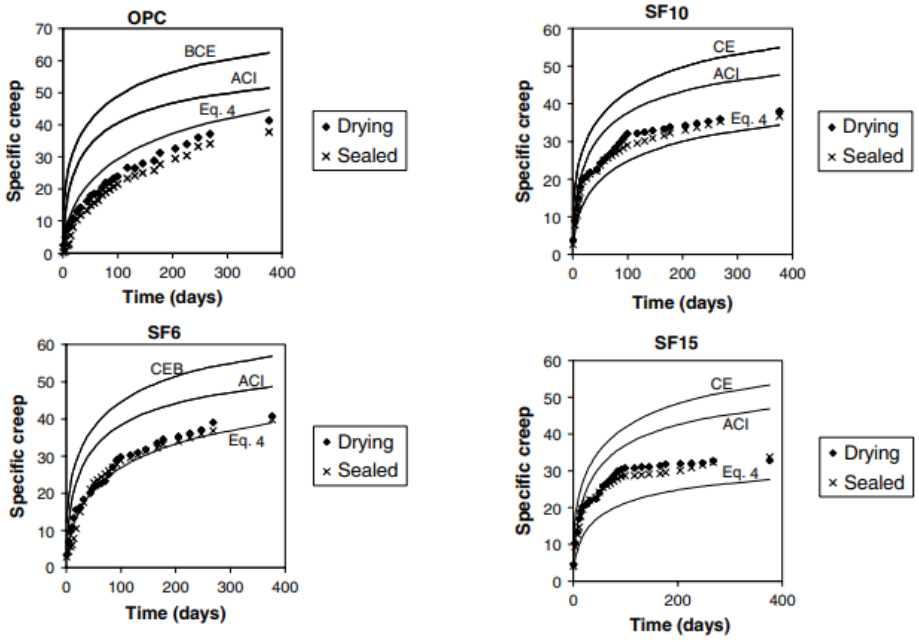

Fig. 3-9 The effect of various silica fume replacement level on specific creep: (a) OPC (b) SF10 (c) SF6 (d) SF15 (Mazloom *et al*.2004)

3.3.3 Stress level

It has been reported by many researchers that for a low stress level, which is lower than 30-40% of the corresponding strength, the creep develops as a linear behavior. By measuring the basic creep behavior of concrete with different stress/strength ratios for tensile, compressive and flexural load conditions, Ranaivomanana *et al*. (2013) indicated that the non-linearity was found for compressive creep while external load increases to somewhere between 30 and 50% of the compressive strength. As the variability in split tensile strength, it is difficult to conclude that for tesnile creep, the loading-induced damage appeared to have limited effects in the stress level range investigated (between 30% and 50% of the tensile strength). Rossi *et al*. (2013) found out by doing parallel tests of concrete under 30%, 50% and 70% stress/strength ratio at 28 days that the basic compressive creep is non-linear for loading level equal or greater than 70% of the compressive strength. Contrast to the basic creep, the specific creep rate is independent of applied compressive stress level for a creep duration greater than 100 days. The residual strain is a linear function of the creep strain independent of the hygral exchange conditions (sealed and unsealed specimens), the loading level and the loading age.

Similar finding was described by Atrushi (2003) that after the stress/strength ratio reaches 0.7, the magnitude of tensile creep seems to be linear whereas a non-linear behavior takes place at higher loading.

3.3.4 Water/cement ratio

Water/cement ratio influences the development of creep through strength and elastic modulus. For the same initial stress, the concrete with lower water/cement ratio is supposed to have higher strength and elastic modulus leading to the reduction of creep. In many models, w/c ratio is not a common parameter and it is usually incorporated into the compressive strength. Despite this effect, the degree of hydration, which is used to estimate the process of hydration, is important to control the development of creep. The details will be explained in the further chapter.

3.3.5 Elevated temperature

Temperature has a big impact on the development of hydration. With higher temperature, the chemical process of cement hydration is faster. However, the effect of temperature on creep is twofold, as concluded by Bazant *et al*. (2004), generated by two different mechanisms:

1. Increase in temperature accelerates the bond breakages and restorations causing creep, and thus increases the creep rate.

2. The higher the temperature, the faster is the chemical process of cement hydration and thus the aging of concrete, which reduces the creep rate.

Usually the former effect prevails and the overall effect of temperature rise is an increase of creep. While for young concretes where the hydration processes rapidly at elevated temperatures, heating can have the opposite effect. The pore humidity plays a similar role in aging and both the hydration and creep processes are slowed down by decrease in pore humidity. To describe the characteristics of the effect of temperature on concrete, Bazant *et al*. (2004) introduced two variables:

(1) The equivalent time for characterizing the degree of hydration.

(2) The reduced time for characterizing the change in the rate of bond breakages and restorations on the microstructural level.

What needs to be noted is that the elevated temperature during the period of curing preceding the application of load and during the application of load are different. The elevated temperature before the application of load accelerates the hydration process with a higher degree of maturity. The creep is reduced a lot compared to the creep at normal temperature. Regarding the elevated temperature during the application of load, it is reported by many researchers that basic creep can be enhanced by elevated temperature after a range and then decreases. Arthanari *et al*. (1940) states that the increase in temperature by several steps leads to a higher creep than a steady temperature after a certain period of loading.

3.3.6 Relative humidity

It was reported by many researchers that creep is higher with a lower relative humidity. The increase in the creep with lower relative humidity can be due to the large amount of shrinkage generated, especially at the very early age. The drying creep as the result of drying at the initial age is also supposed to be higher with reduced humidity.

However, reduction in relative humidity before the loading of specimen in a moisture equilibrium condition leads to reduced creep. The rate of hydration strongly depends on the relative humidity h in the pores of concrete. The effect of humidity is usually used as one of the variables for calibrating the so-called equivalent hydration period t_e which is the important variable for age-dependent materials parameters such as E_μ , η_μ.

$$t_e = \int \beta_h dt, \quad E_\mu = E_\mu(t_e), \quad \eta_\mu = \eta_\mu(t_e) \qquad \text{Eq. 3-16}$$

β_h is an empirical function of pore humidity h and can be fitted by $\beta_h = [1 + (a - ah)^4]^{-1}$.The relative humidity plays an important role in the assumption that the creep rate depends on the magnitude of the flux of microdiffusion of water between the macropores and the micropores in the cement gel, mentioned by Bazant (1985). The effect of microdiffusion can be attributed to effect of rate of pore humidity on the creep viscosity. So does the shrinkage coefficient which also defined as the ratio of increments of shrinkage stain and pore relative humidity.

Humidity gradient is significant for controlling the cracking in concrete. The drying shrinkage, which is the major driving force behind cracking, is induced by external drying through diffusion. The drying process begins while the balance between pore water pressure pushing the microstructure apart and attractive forces binding it together breaks. Once the pores are emptied to a radius about 50nm, concave capillary menisci develops. The Laplace equation relates the change in the pore fluid pressure to the meniscus curvature as:

$$p'' - p = \frac{2\gamma}{r} \qquad \text{Eq. 3-17}$$

Where p'' is the pressure in the gaseous phase, p is the pore fluid pressure, γ is the surface tension of water and r is the radius of the meniscus curvature. The Kelvin-place equation then relates the internal humidity (RH) to pore fluid pressure by:

$$p = \frac{\ln(RH)RT}{v} \qquad \text{Eq. 3-18}$$

By implementing this method for prediction of development of stress gradient model, one can estimate the internal stress and risk of cracking in concrete. Grasley *et al*. (2006) developed a single model to estimate the stress gradient associated with drying in both free and fully restrained concrete specimens and obtained with the conclusion that the stresses in the surface layer of restrained concrete exceed the tensile strength of the material prior to complete specimen failure.

Humidity variation is one of the most difficult aspects of creep to model, especially the drying creep effect, also called Pickett effect. A number of models have been proposed such as:

1. Pickett's model with creep nonlinearity.

2. Microdiffusion of hindered adsorbed or interlayer water and changes of disjoining pressure (manifested as stress-induced shrinkage).

3. Shrinkage reduction due to tensile cracking (Klug *et al*. 1974) or by tensile strain softening (Bažant, 1974).

4. Microprestress of highly localized creep sites in cement gel caused by humidity (and temperature) changes

3.4 Numerical modeling of creep

3.4.1 Rheological models

Rheology refers to the subject of time dependent relation between stress and strains. The idealized deformations such as elastic, viscous or plastic behavior are represented by basic mechanical devices such as spring for elasticity, dashpot and fiction for viscosity or plasticity.

The basic representation of viscoelasticity of concrete can be represented by the combination of spring and dashpot after being simplified. The model with a series connection of a spring and a dashpot is called the Kelvin-Voigt model as shown in Fig. 3-10(a). The model with a parallel connection of a spring and a dashpot is called Maxwell model, shown in Fig. 3-10(b). The correlation between the stress and strain for kelvin-Voigt model and Maxwell model are shown in Eq. 3-19(a) and Eq. 3-19(b):

$$\sigma + \frac{\eta}{E} d\sigma = \eta d\varepsilon \qquad \text{Eq. 3-19(a)}$$

$$\sigma = E\varepsilon + \eta d\varepsilon \qquad \text{Eq. 3-19(b)}$$

The difference between Kelvin-Voigt and Maxwell model is that the Maxwell model predicts the stress relations well but does not predict creep accurately. While Kelvin-Voigt is extremely good with modeling creep behavior but not so accurate for predicting the relaxation behavior.

Few models by various combination of Kelvin-Voigt and Maxwell model were also proposed. Thomson model, the series connection of a spring and Kelvin-Voigt unit, can be used for simulating the total loading-dependent deformation including elastic and creep. The mathematical form of Thomson model is shown in Eq. (3-19(c)).

$$\varepsilon = \frac{1}{E_1} + \frac{1}{E_2}\left[1 - exp\left(\frac{t}{\tau}\right)\right] \qquad \text{Eq. 3-19(c)}$$

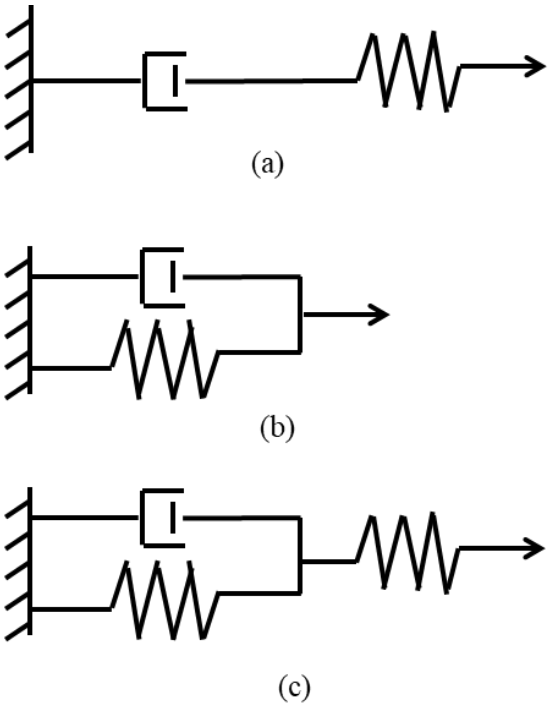

Fig. 3-10 (a) Maxwell model (b) Kelvin model (c) Thomson model

3.4.2 Solidification theory

Bazant et al (1988) proposed the solidification theory in a constitutive numerical form of equation. The primary base of the model is that the hydration products are non-aging viscoelastic

materials and that aging effects are present on the bulk scale as a result of the gradual solidification of new hydration products. Each layer of the hydration products must solidify in a stress-free state, implying that layers which form at an age t are only stressed by loads applied after ' . The constitutive equation for uniaxial loading and deformation is

$$\frac{\partial \varepsilon(t)}{\partial t} = \frac{J_0}{v(t)}\frac{\partial \sigma(t)}{\partial t} + \frac{1}{v(t)}\int_0^t \frac{\partial J_g(t-t')}{\partial t'}\frac{\partial \sigma(t')}{\partial t'}dt' + \frac{\partial \varepsilon^f(t)}{\partial t} \qquad \text{Eq. 3-20}$$

Where J_0 is the instantaneous elastic uniaxial compliance, $v(t)$ is the aging function for the materials. $J_g(t-t')$ is the non-aging viscoelastic uniaxial compliance of the cement gel and $\varepsilon^f(t)$ is the free strain. The final equation for predicting the compliance of concrete creep is shown in:

$$J(t,t_0) = q_1 + C_o(t,t_0) + C_d(t,t_o,t_c) \qquad \text{Eq. 3-21}$$

Where q_1 is the instantaneous strain due to unit stress. $C_o(t,t_0)$ is the compliance function for basic creep. $C_d(t,t_o,t_c)$ is the additional compliance function for drying creep. The basic creep compliance function can then be split into three terms which present the aging viscoelastic compliance, non-aging viscoelastic compliance and aging flow compliance respectively.

$$C_o(t,t_0) = q_2 Q(t,t_o) + q_3 \cdot [1 + (t-t_o)^n] + q_4 \cdot \ln\left(\frac{t}{t_o}\right) \qquad \text{Eq. 3-22}$$

One of the limit of the solidification theory is that the constitutive equation requires numerical integration for many load histories and aging functions. In contrast to the time–shift approach, the solidification theory is not physically represented by a simple change in the rate of viscoelastic response. For example, for a solidifying material represented by a Kelvin chain, the spring constants and dashpots are both age dependent (with the same aging function for all springs and dashpots), in contrast to the age-dependent viscosities implied in the time–shift approach.

3.4.3 Dissolution-precipitation approach

Suter, M *et al*. (2006) proposed a new dissolution-precipitation method for describing the long-term response of stress hardening concrete like creep, recovery and relaxation, etc. Creep is described as the vicoelastic behavior caused by the gradual transformation of stressed reactant solid phases into stress- free solute before reaction, based on the explanation of dissolution-precipitation mechanism. This approach assumes that creep of concrete is the result of

dissolution and subsequent precipitation. It is similar and different from solidification theory from the following summed by Grasley *et al*. (2007):

1. The solidification theory assumes that the dissolution of cement gains or any other species does not affect the stiffness of bulk materials while precipitation of hydration does.
2. The solidification theory treats the solidifying materials as viscoelastic while dissolution-precipitation treats the precipitating or solidifying material as strictly elastic as creep or stress relaxation is accounted for in the reduction of the bulk scale elastic modulus caused by dissolution process
3. The dissolution-precipitation is unable to account for long-term creep or aging that in absence of reaction while solidification theory is unable to account for the long term aging, but can account for long term creep since solidifying product is assumed to be viscoelastic.

3.4.4 Review of other numerical models

In ACI 209R-92 model, the compliance can be represented as a function of creep coefficient $\emptyset(t, t_0)$and the modulus of elasticity E_{cmto} at the time of loading in Eq. 3-23.

$$J(t, t_0) = \frac{1+ \emptyset(t,t_0)}{E_{cmto}} \qquad \text{Eq. 3-23}$$

Where the creep coefficient is defined as the ratio of creep strain to initial strain.

$$\emptyset(t, t_0) = \frac{(t-t_0)^{\varphi}}{d+(t-t_0)^{\varphi}} \emptyset_u \qquad \text{Eq. 3-24}$$

Where $\emptyset_u$ is the ultimate creep coefficient and d (days) and φ are the constant for a given member shape and size. Ultimate creep coefficient $\emptyset_u$ depends on the dimensions of specimens, temperature, moisture and loading age, etc. ACI 209R model is recommended for its easy fitting to the short-term test data by modifying the ultimate creep coefficient. The drawback, however, is its limitation in its accuracy and particularly the method of accommodating size when its simplest form is used. Moreover, ACI 209R is derived empirically and it doesn't help to explain the mechanisms of creep or shrinkage.

The form of CEB MC90-99 model is similar to that of ACI 209R

$$J(t, t_0) = \frac{1}{E_{cm28}} [\eta(t_0) + \emptyset_{28}(t, t_0)] = \frac{1}{E_{cmto}} + \frac{\emptyset_{28}(t,t_0)}{E_{cm28}} \qquad \text{Eq. 3-25}$$

Where $\eta(t_0) = \frac{E_{cm28}}{E_{cmto}}$, E_{cm28} is the mean modulus of elasticity of concrete at 28 days.

$$\emptyset_{28}(t, t_0) = \emptyset_0 \beta_C (t - t_0) \quad \text{Eq. 3-26}$$

Where $\emptyset_0$ is the notional creep coefficient, $\beta_C(t - t_0)$ is the coefficient that describes the development of creep with time after loading. The notional creep coefficient $\emptyset_0$ can be determined by a function of relative humidity, strength and temperature. The priority of CEB MC90-99 over ACI 209R is that it does not require any information about the duration of curing or curing condition. Since this model was developed by European researchers, it underestimated the shrinkage and creep of concrete containing particular aggregates in North American.

The Double-Power Law by Bažant *et al*. (1978) is another well know compliance function with its extension to Triple Power Law by Bažant *et al*. (1985). As mentioned by Bažant *et al*. (1978), Double-Power Law is suitable for predicting the short term creep at the very beginning of the creep when $t - t_0 \ll t_0$. m, n should be used as the same value as in solidification model developed by Bažant *et al*. (1988). The Triple-Power Law by Bažant *et al*. (1985) was thus derived for a better simulation of long-time creep, shown in Eq. 3-26(b). Emborg (1989) modified the Triple-Double Law by adding additional function $G(t, t_0)$ and $H(t, t_0)$ of exponential type as shown in Eq. 3-26(c):

$$J(t, t_0) = \frac{1}{E_0} + \frac{\emptyset}{E_0}(t_0^{-m} + \alpha)(t - t_0)^n \quad \text{Eq. 3-27(a)}$$

$$J(t, t_0) = \frac{1}{E_0} + \frac{\emptyset}{E_0}(t_0^{-m} + \alpha)[(t - t_0)^p - B(t, t_0; p] \quad \text{Eq. 3-27(b)}$$

$$J(t, t_0) = \frac{1}{E_0} + \frac{\emptyset}{E_0}(t_0^{-m} + \alpha)[(t - t_0)^p - B(t, t_0; p] + \frac{G(t,t_0)}{E_0} + \frac{H(t,t_0)}{E_0} \quad \text{Eq. 3-27(c)}$$

3.5 Factors affecting shrinkage

3.5.1 Quantity of aggregate, elastic property of aggregate and lightweight aggregate

Pickett model by Pickett (1956) states that the quantity of aggregate is the most important factor in affecting the development of shrinkage:

$$S = S_P(1 - g)^n \quad \text{Eq. 3-28}$$

Where S and S_P are the shrinkage of the concrete and paste and g is the volumetric content of aggregate and n is a constant variable. The restraining bodies such as aggregates, unhydrated cement grains and stable micro-crystalline products of hydration act from the beginning of drying to reduce shrinkage. Shown in Fig. 3-11, the data for w/c = 0.35 are represented fairly well by a straight line while data for $w/c = 0.5$ is not represented well by a straight line.

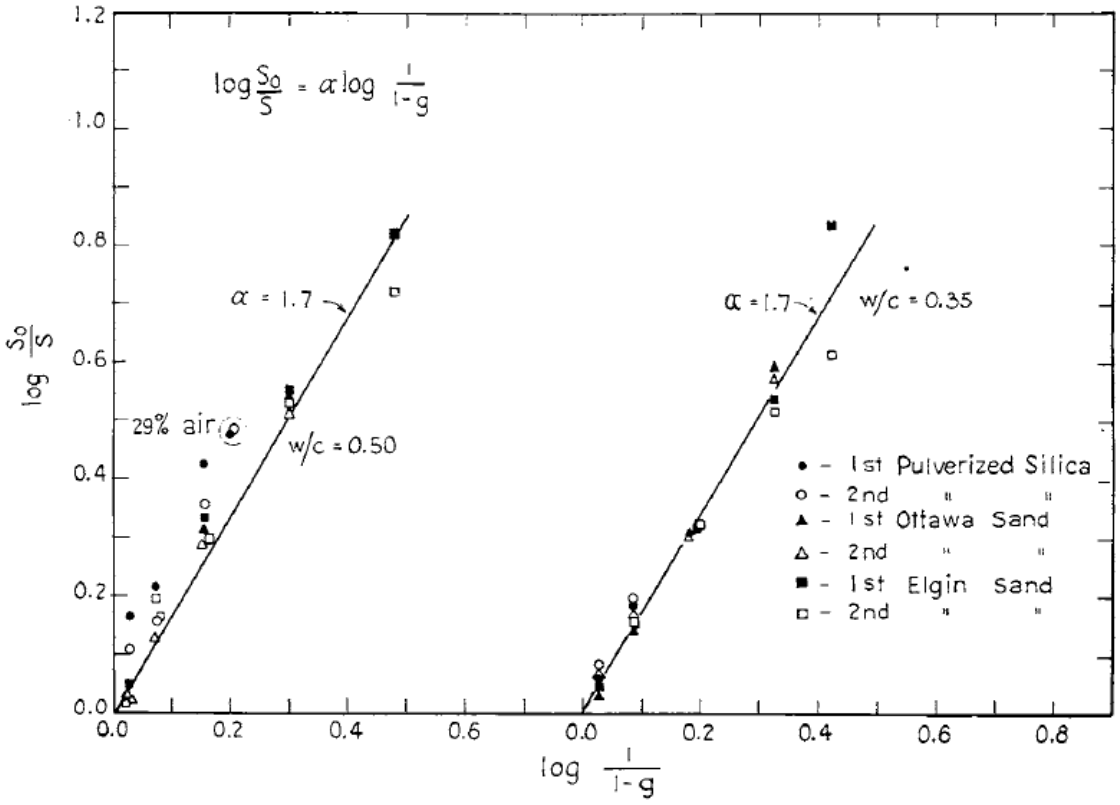

Fig. 3-11 Effect of aggregate on shrinkage (Picket, 1956)

Hansen *et al.* (1965) confirmed this findings by extending Picket model to include the effect of shrinkage of aggregate and elastic modulus of cement paste and aggregate. It was stated in the paper that the degree of restraint offered by aggregate particles is determined by the quantity of aggregate in the concrete as well as by the elastic properties and the shrinkage of cement paste and aggregate particles. A spherical particle of aggerate within a concrete sphere is used as to simulate the interface between aggregate and paste shown in Fig. 3-12. Two equations are derived for correlating the shrinkage with the elastic modulus of aggregate and paste as shown in Eq. 3-29(a) and Eq. 3-29(b). S, S_p and S_g are the shrinkage of concrete, paste and aggregate. E_g and E_p are the elastic modulus of aggregate and paste.

$$\frac{S}{S_p} = \left(1 - \frac{S_g}{S_p}\right) \frac{\left(\frac{E_g}{E_p} - 1\right) g^2 - 2\frac{E_g}{E_p} + \frac{E_g}{E_p} + 1}{\frac{E_g}{E_p} + 1} + \frac{S_g}{S_p} \; while \; E_g \geq E_p \qquad \text{Eq. 3-29(a)}$$

$$\frac{S}{S_p} = \left(1 - \frac{S_g}{S_p}\right) \frac{\left(\frac{E_g}{E_p} + 1\right) g - \frac{E_g}{E_p} - 1}{\left(\frac{E_g}{E_p} - 1\right) g - \frac{E_g}{E_p} - 1} + \frac{S_g}{S_p} \; while \; E_g < E_p \qquad \text{Eq. 3-29(b)}$$

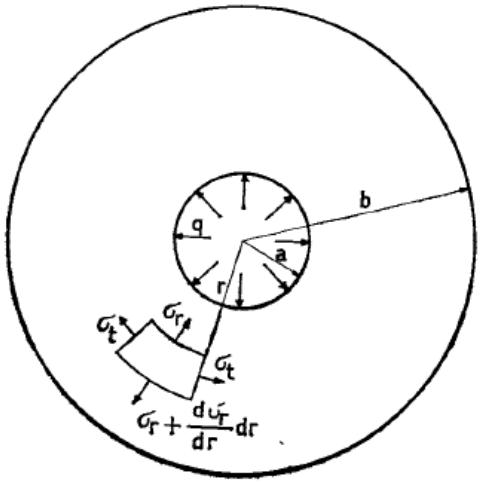

Fig. 3-12 Small spherical particle of aggregate with a concrete sphere (Hansen *et al. 1965)*

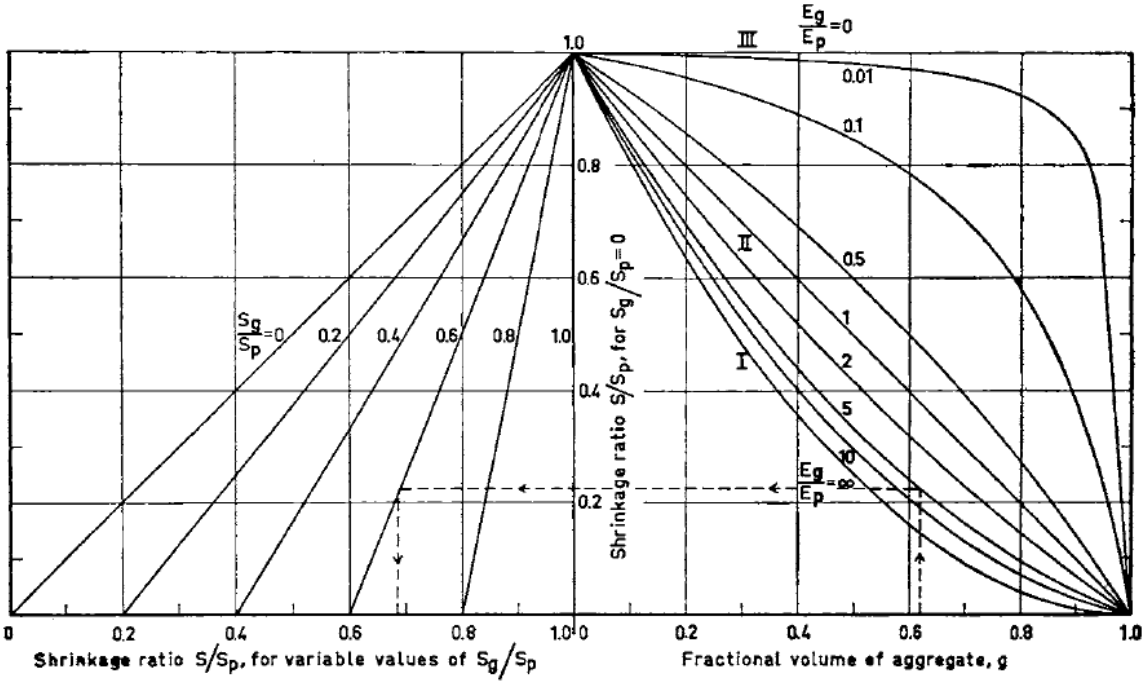

Fig. 3-13 Shrinkage ratio $\frac{S}{S_p}$ in terms of $\frac{S_g}{S_p}$ and $\frac{E_g}{E_p}$ (Hansen *et al. 1965)*

When aggregate functions as a restraint for the shrinkage of paste, the concrete containing aggregate with higher modulus of elasticity tends to have a lower shrinkage than the concrete containing aggregate with lower modulus of elasticity. It can be seen from Fig. 3-13 that minor aggregate shrinkage can seriously affect the concrete shrinkage. For most of the common use normal aggregate, no shrinkage of aggregate could be assumed with minimal loss of accuracy of fitting, according to Hansen *et al.* (1965).

3.5.2 Water content, cement content and slump

With more water content, cement content tends to increase shrinkage since the aggregate content is reduced. Slump can be increased by adding more water and result in the same situation that the aggregate content is reduced. Many studies (Zhang *et al*. 2003, Tazawa *et al*.1995, Lee *et al*.2006, Bissonnette *et al*.1999) have been conducted to prove that the shrinkage, for both drying and autogenous shrinkage, is decreased with the increase in the water/cement ratio.

3.5.3 Air content

It was reported (Davis *et al*. 1954) that normal range of air content does not have any significant effect on the shrinkage development. When the air content is in the amount of 3 to 5 percent air, there is no effect on the magnitude of dry shrinkage.

3.5.4 Relative humidity, temperature

The environment where the concrete is cured, placed and mixed has big impact on the drying of concrete. With low humidity, high temperature and wind, the concrete tends to be dry in a faster rate. Environment effect can usually be characterized by relative humidity and temperature. There are various mathematical equations being used for simulating the effect of humidity on shrinkage. Generally most of prevalent equations follow the correlation shown in Eq. 3-30. However, this equation cannot be applied to h lower than 50% because little data exists for this condition.

$$shrinkage \propto 1 - \left(\frac{h}{100}\right)^b \qquad \text{Eq. 3-30}$$

In the test for study on the key parameters controlling the drying shrinkage, Bissonnette *et al*. (1999) figured out that compared to the linearity between humidity and relative shrinkage for paste, the slope between 48 and 75% relative shrinkage is lower while it increases in the 75% and 100% range for mortar.

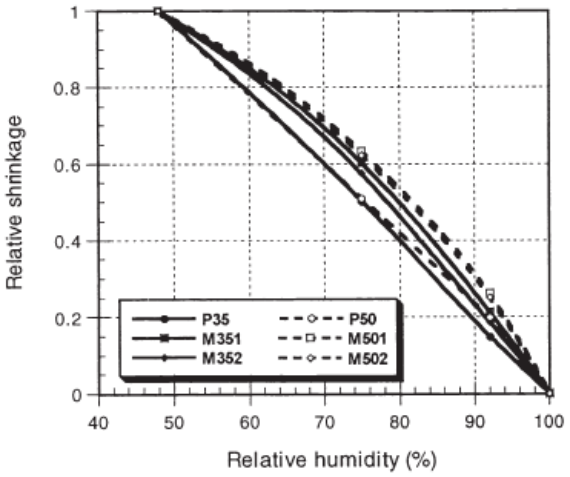

Fig. 3-14 Relation between relative ultimate shrinkage and relative humidity (Bissonnette *et al*. 1999)

For early age concrete and shrinkage, Zhang *et al.* (2010) observed a multiple stage development of internal relative humidity. Followed by a vapor-saturated stage with 100% relative humidity, a gradually reducing stage occurs and the ending of the first stages just corresponds to the point of concrete setting, at which point fresh concrete transformed from a liquid-like plastic state to a solid state. A linear correlation between shrinkage and internal relative shrinkage exists, as shown in Fig. 3-15.

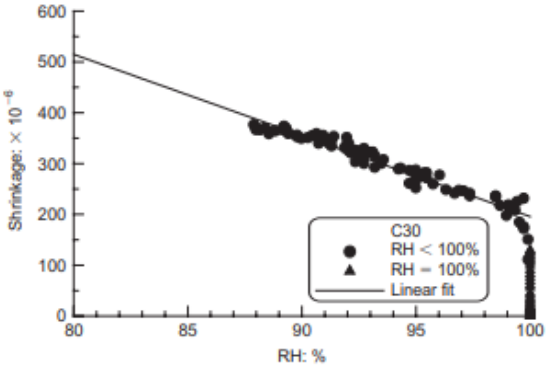

Fig. 3-15 Relationship between free shrinkage strain and interior RH of C30 concrete by Zhang *et al.* (2010)

The effect of temperature on shrinkage is not as large as relative humidity. Some study (Lura *et al.* 2001 Bjøntegaard *et al.* 1999) has been done and conclusions have been drawn that the higher temperature do not necessarily lead to higher deformation. What is more important is that, higher temperature generally leads to faster growth of shrinkage as well as self-induced stress and finally a higher risk of cracking happens.

3.5.5 Period of curing

Work by Perenchio (1997) already showed that with period of curing greater than 4 to 8 days and less than 35 to 50 days may increase the drying shrinkage. For various w/c, the effect of period of curing also varies. From the study by Perenchio (1997) shown in Fig. 3-16, for various w/c concrete, the drying shrinkage after 1 year is highest for the concrete with initial moist curing about 100 hours.

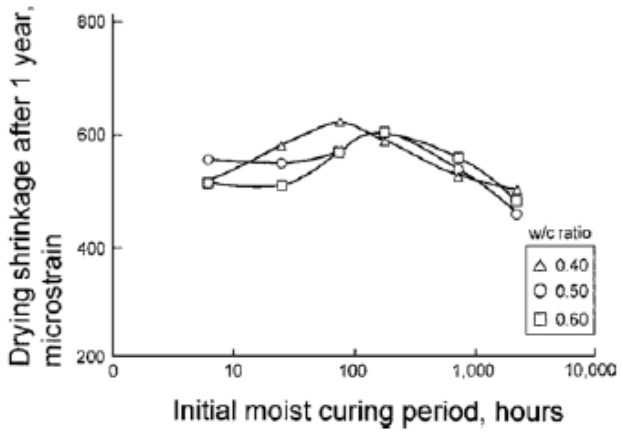

Fig. 3-16 Effect of curing period on drying shrinkage after 1 year for specimens with different w/c (Perenchio, 1997)

3.5.6 Size and shape of the specimens

Larger members of concrete leads to slower rate of drying, and therefor thick concrete shrinks slower than the thin concrete specimens. A general equation can explain the relationship between shrinkage and ratio of volume to surface area:

$$Shrinkage \propto \frac{1}{(V/S)^2} \qquad \text{Eq. 3-31}$$

Where V = volume and S = surface area. Shrinkage test from Hansen *et al.* (1966) also suggested the similar tendency. After comparing the shrinkage of cylindrical and I-shaped specimens after 100 and 1200 days since loading, it can be seen that for specimen with same volume to area ratio, the shrinkage of I-shaped specimen is smaller than that of cylinders. So a conclusion can be drawn that volume to area ratio does not account perfectly for variation in size and shape and more complex function needs to be developed to explain the internal mechanisms.

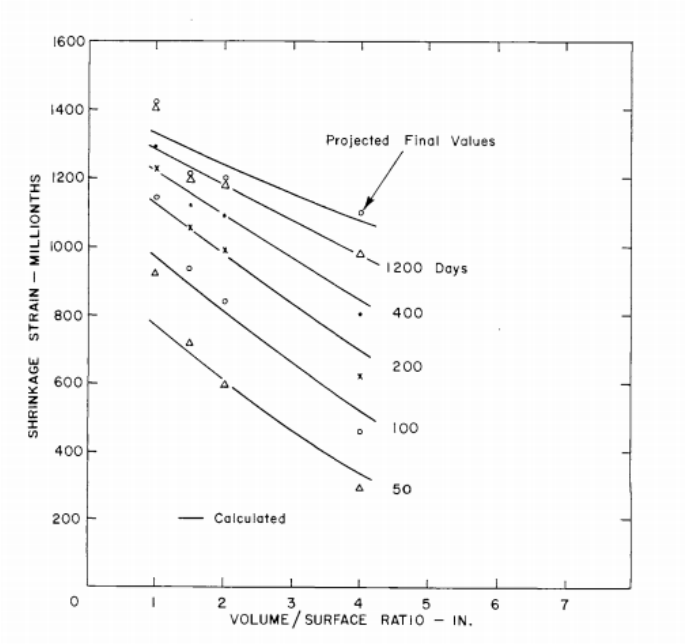

Fig. 3-17 Variation of shrinkage with volume/surface ratio at different ages (Hansen *et al.*, 1966).

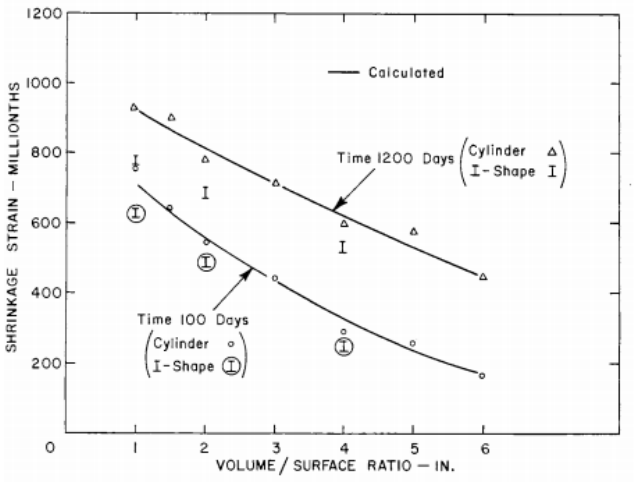

Fig. 3-18 Comparison of shrinkage of cylinders and I-shaped specimens (Hansen *et al.*, 1966).

Because that moisture gradient is a key parameter for controlling the drying of specimen, McDonald *et al.* (1993) stated that the influence of size and dimension on shrinkage is mainly by affecting the moisture gradient which affects the shrinkage and stress concentration.

3.6 Modeling of development of shrinkage

There are also many models for predicting the development of shrinkage for coupling the modeling of creep behavior:

ACI model:

$$\varepsilon_{sh}(t, t_c) = \frac{(t-t_c)^{\alpha}}{f+(t-t_c)^{\alpha}} \cdot \varepsilon_{shu} \quad \text{Eq. 3-32}$$

Where f and α are constant parameters for the shape and size effect. ε_{shu} is the ultimate shrinkage strain and $(t - t_c)$ is the time from the end of initial curing.

B3 mode:

$$\varepsilon_{sh}(t, t_c) = -\varepsilon_{sh\infty} k_h S(t - t_c) \quad \text{Eq. 3-33}$$

Where $\varepsilon_{sh\infty}$ is the ultimate shrinkage strain and k_h is the humidity dependence factor and $S(t - t_c)$ is the time curve

$$\varepsilon_{sh\infty} = -\varepsilon_{s\infty} \frac{E_{cm607}}{E_{cm}(t_c+\tau_{sh})} \quad \text{Eq. 3-34}$$

Where $\varepsilon_{s\infty}$ is a constant and E_{cm607} and $E_{cm}(t_c + \tau_{sh})$ is a factor to account for the time dependence of ultimate shrinkage.

CEB MC90:

$$\varepsilon_{sh}(t, t_c) = -\varepsilon_{cso} \beta_s(t - t_c) \quad \text{Eq. 3-35}$$

Where ε_{cso} is the notional shrinkage coefficient and $\beta_s(t - t_c)$ is the coefficient describing the development of shrinkage with time of curing. t is the age of concrete (day) at the moment considered and t_c is the age of concrete at the beginning of drying (day).

3.7 Evaluation of cracking risk by self-induced stress

To investigate the self-induced stress directly from the experimental test, various experimental apparatus have been developed. With Temperature Stress Testing Machine (TSTM) developed by Springenschmid (1994), stress measurement under any degree of stress restraint and stress profile can be measured directly with the recording of the temperature file. The stress relaxation which is critical for affecting the development of self-induced stress can also be measured by the

machine and some study has been conducted on that (Atrushi, 2003) shown in Fig. 3-19. The assessment of cracking risk can be made by comparing the calculated stress to the concrete tensile strength at a time.

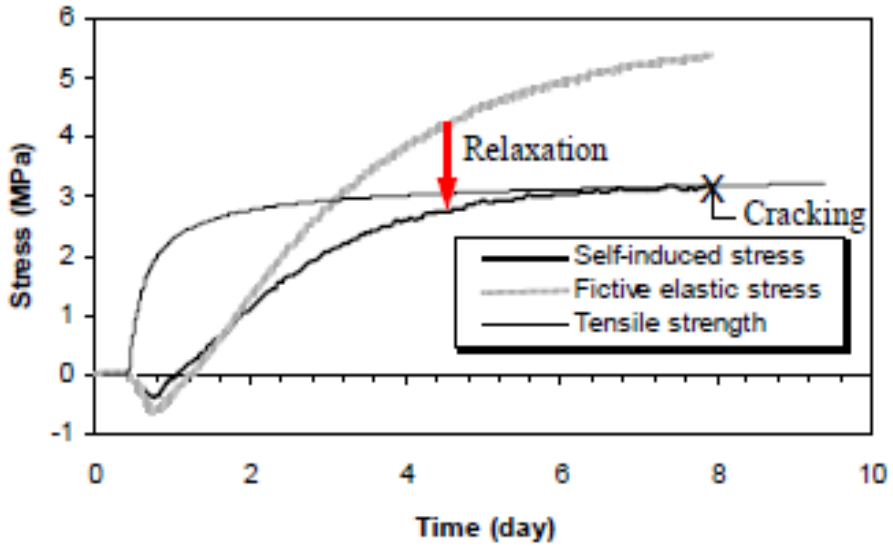

Fig. 3-19 Schematic pattern of crack development when self-induced stress due to restrained strain are relieved by relaxation (Atrushi, 2003)

Besides the shrinkage deformation, the thermal dilation is another major factor which controls the development of self-induced stress, especially at early age. For more accurate investigation of individual influence of shrinkage and thermal dilation on self-induced stress, Bjøntegaard (1999) tested early age TSTM axial stress and development of autogenous shrinkage simultaneously at the every early age, as shown in Fig. 3-20. After initial t_0 hour when initial thermal effect is large, the development of autogenous shrinkage and TSTM axial stress develops at similar rates. The two curves of stress and autogenous shrinkage development are parallel with a constant net internal viscoelastic modulus of about 11 000 MPa, considerably smaller than the Young's modulus. The result suggests that tensile stress relaxation is either instant or not a major factor.

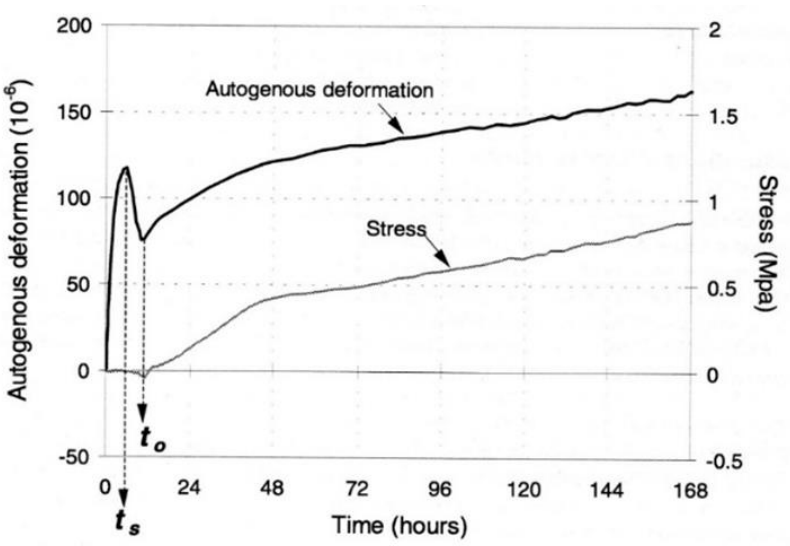

Fig. 3-20 TSTM and free shrinkage measurements on 0.40 water-cementitious ratio concrete where thermal effects are ceased within 48 hours (Bjøntegaard, 1999)

For evaluating the capacity of resistance of cracking under tensile mode, Hansen *et al*. (2014) proposed a straightforward method to calculate the viscoelastic modulus by comparing the different strain between free and restrained shrinkage with rebar, shown in Fig. 3-21. A series of equations can be used to calculate the viscoelastic modulus:

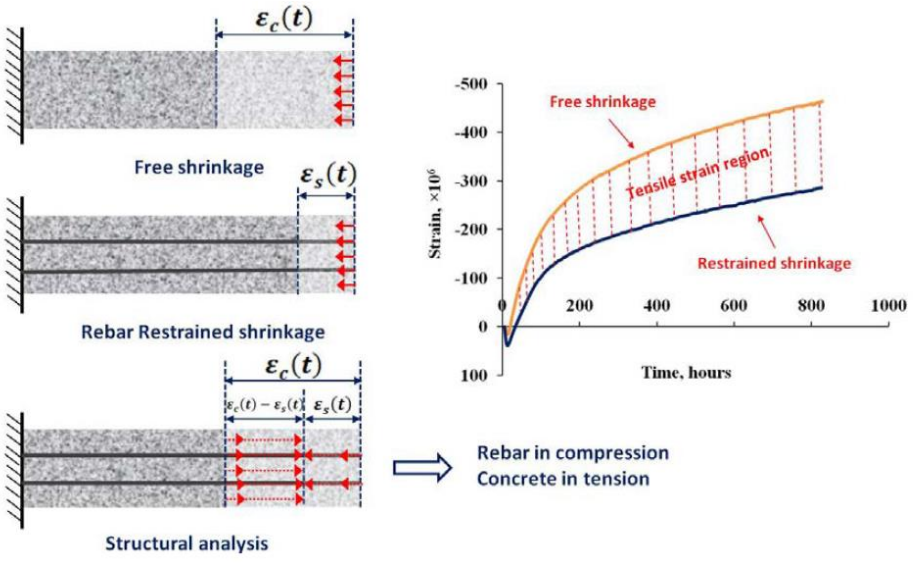

Fig. 3-21 Illustration of free shrinkage and restrained shrinkage by concentrically placed rebars (Hansen *et al*. 2014)

$$\varepsilon_s(t)E_sA_s = [\varepsilon_{sh}(t) - \varepsilon_s(t)]E_vA_c \qquad \text{Eq. 3-36}$$

Where $E_v = E_s\rho/\left(\frac{\varepsilon_{sh}(t)}{\varepsilon_s(t)} - 1\right)$, $\varepsilon_{sh}(t)$ = free shrinkage, $\varepsilon_s(t) =$ deformation of steel in reinforced mix. A_c , A_s are the area of plain mix and steel. A constant E_v can be derived without much effect on the aggregate content, shown in Fig. 3-22.

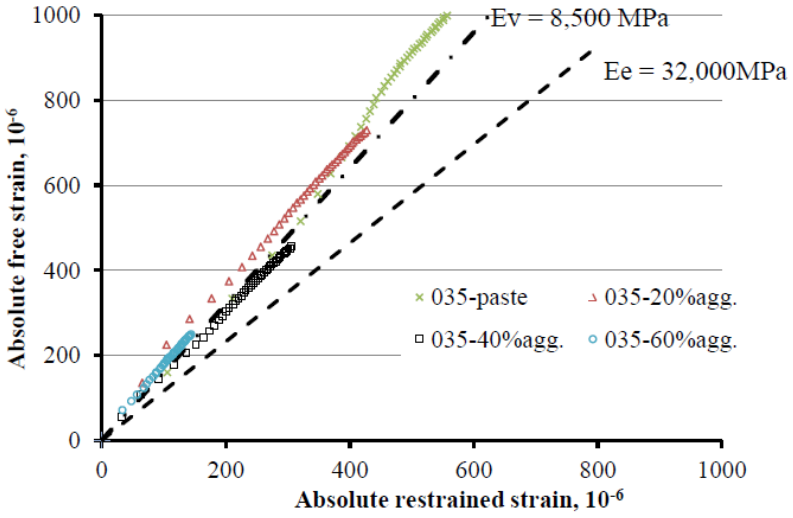

Fig. 3-22 Effect of steel reinforcement on viscoelastic hydration modulus (Hansen *et al*. 2014)

An experimental based method for evaluating the tensile creep without conducting direct tensile creep was done by Kovler (1994) by simultaneous twin specimens that one under restrained shrinkage and one under free shrinkage. The individual elastic $\epsilon_e(t)$, creep $\epsilon_c(t)$ and shrinkage $\epsilon_{sh}(t)$ have the relation as shown in Eq. 3-36 under fully restrained condition with the methodology shown in Fig. 3-23. A variety of mechanical characteristics of the concrete such as shrinkage stresses, moduli of elasticity, creep coefficient can be determined in one test.

$$\epsilon_e(t) + \epsilon_c(t) + \epsilon_{sh}(t) = \epsilon(t) = 0 \qquad \text{Eq. 3-37}$$

The creep/shrinkage ratio can be used as the index for evaluating the reduction of the development of tensile strain in the restraint concrete, and consequently, the degree of stress relaxation as mentioned by Altoubat *et al*. (2001). Moreover, the relative humidity, stress history, tensile strength, internal curing and alternate drying/ wetting all have a big effect on the development of cracking.

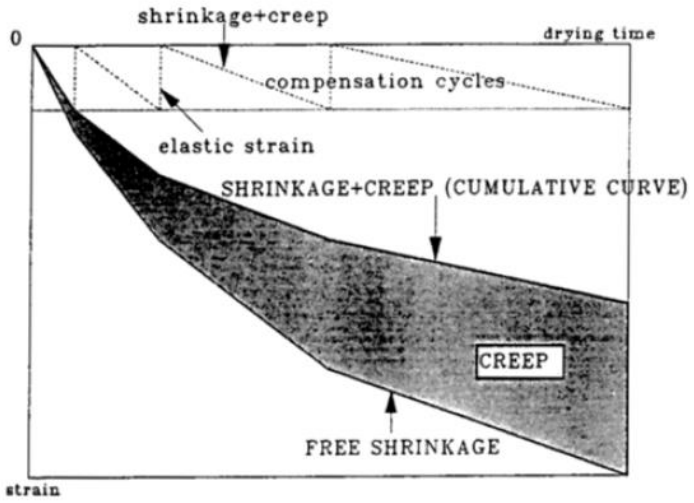

Fig. 3-23 Creep strain calculated from the data of restrained and free shrinkage tests (Kovler, 1994)

The internal curing effect by pre-soaked fine lightweight aggregate is also an effective approach for prevention of cracking, especially for HPC with low water/cement ratio. Based on Rilem TC-196, the pre-soaked lightweight aggregate (LWA) can supply an internal source of water and replace the water consumed by chemical shrinkage during cement hydration. The internal curing water is naturally drawn during cement hydration from the relatively large pores of the lightweight aggregate into the smaller pores of the cement paste, as discussed by Cusson *et al*. (2008). After comparing with the self-induced stress by different LWAs replacement level, it is found by Cusson *et al*. (2008) that only with sufficient internal curing water provided by pre-soaked LWA, the autogenous shrinkage can be eliminated almost completely.

3.8 Summary

In this chapter, the literature about definition, affecting factors and numerical modeling of viscoelastic behavior of concrete was reviewed .What needs to be noted from the current available study of viscoelastic behavior is that: (1)For creep behavior, no single one numerical model can explain the mechanisms of creep from very early to later age. As the lack of study in viscoelasticity field of HPC, more comprehensive experimental test and numerical modeling is need for the better understanding of viscoelastic effect on HPC. (2) The current available study on autogenous shrinkage and tensile viscoelasticity focus on very early age (less than 7 days). As

the minimal thermal effect after 7 days, it should be noted that large difference in tensile viscoelasticity could be observed. Even though tensile creep/relaxation is important for the development of axial stress at early age, more study needs to be made to determine whether same behavior can be observed for the axial stress with loading starting from later age (7 days) .

Chapter 4 Experimental Equipment and Test Program

4.1 Introduction

In this chapter, the concrete mixes used in the thesis are introduced. It also includes the details in the preparation and testing procedure of all the tests involved in this study. The basic mechanical property of concrete with effect of materials parameters is discussed briefly.

4.2 Materials and Specimens

Concrete mixes of 0.35 w/c ratio for HPC and 0.40 and 0.45 w/c ratio for NSC and 0%, 20%,40%, 60%, 70% and 75% aggregate content by volume are prepared in the laboratory according to ASTM C192 for the common use as the mix in industry. The mix design listed in Table 4-1 consists of type I portland cement, natural sand and lime stone coarse aggregate (25 mm nominal maximum size) with gradation curves shown in Fig. 4-1. Two sets of cylindrical specimens (150 mm diameter by 300 mm height for creep, 60 mm height by 100 mm width by 1000 mm length for shrinkage and 100 mm diameter by 200 mm height for strength and elastic modulus) are cast and cured for one day before demoulding. All specimens are wrapped by plastic and cured sealed before testing. For investigating the effect of SCM and LWA on the viscoelastic behaviour, some mix with one of the SCM, Ground granulated blast-furnace slag (GGBFS) is used and S in the denotation means that slag with 50% replacement level is used. L in the denotation means that LWA with 50% replacement level is used. SL in the denotation means that GGBFS with 50% replacement level is used together with 50% replacement ratio of LWA. The microscopic cross-sectional photo of hardened concrete with various aggregate contents 70%, 40%, 20% are shown in Fig. 4-2.

Table 4-1 Mix design (kg/m^3)

Type	cement	gravel	sand	water	LWA	GGBFS
0.35-0%	1497	0	0	524	0	0
0.35-20%	1198	0	530	420	0	0
0.35-40%	900	0	1060	315	0	0
0.35-60%	600	940	648	210	0	0
0.35-70%	450	1093	753	157	0	0
0.35-75%	375	1175	810	131	0	0
0.35(SL)-70%	225	1097	378	157	252	224
0.35(S)-70%	225	1097	756	157	0	224
0.35(S)-60%	300	940	648	210	0	300
0.35(S)-40%	450	627	432	315	0	450
0.35(S)-20%	600	313	216	420	0	600
0.35(L)-40%	898	0	530	315	353	0
0.35(L)-70%	450	1097	567	157	126	0
0.45-20%	1041	0	530	468	0	0
0.45-40%	781	0	1060	351	0	0
0.45-70%	390	1097	756	175	0	0
0.40-40%	835	0	1060	334	0	0

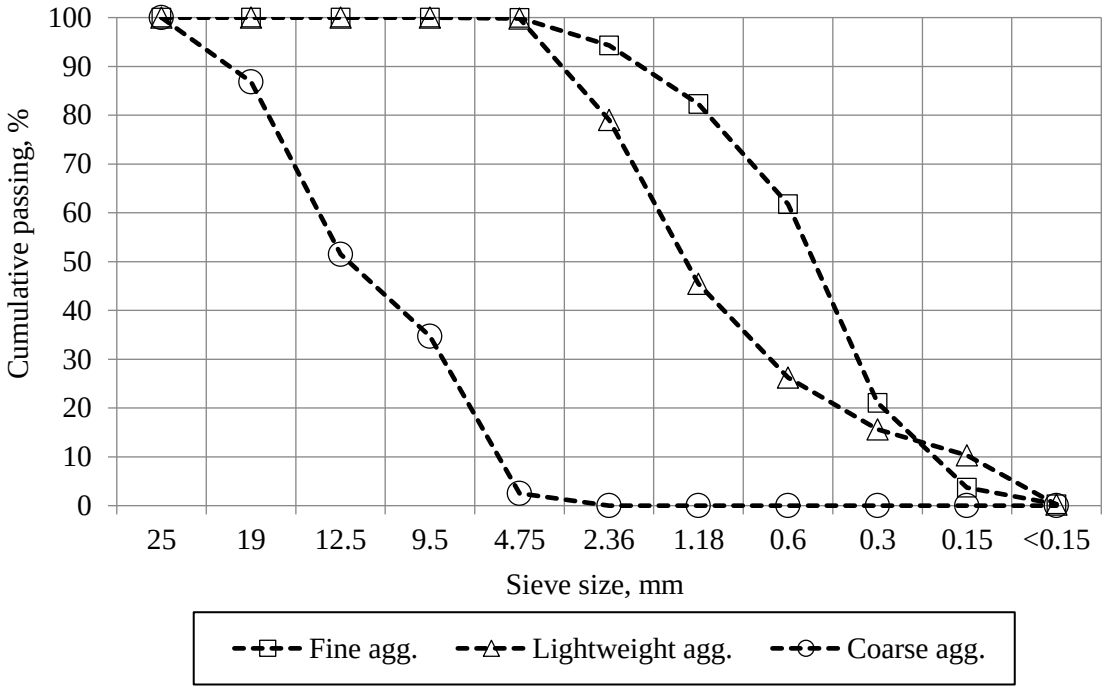

Fig. 4-1 Gradation curves for different aggregates.

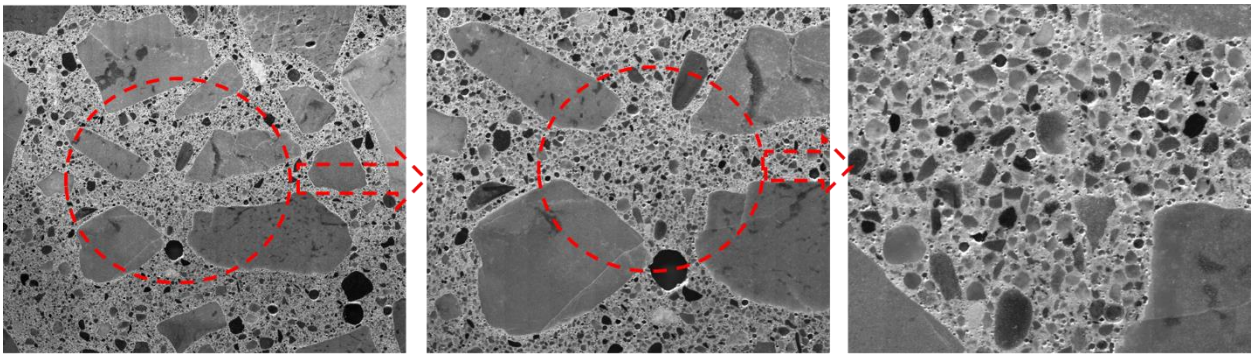

0.35 w/c ratio concrete (25% paste-70%aggregate-5% air)

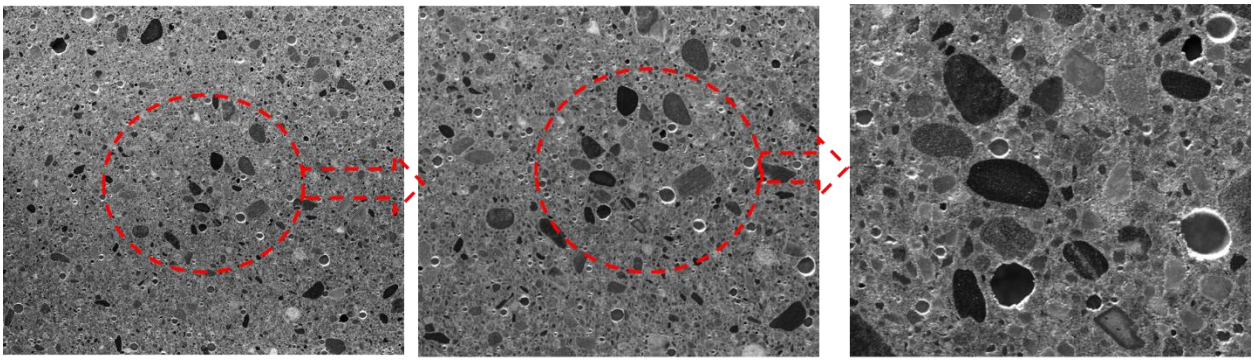

0.35 w/c ratio mortar (56% paste-40%aggregate-4% air)

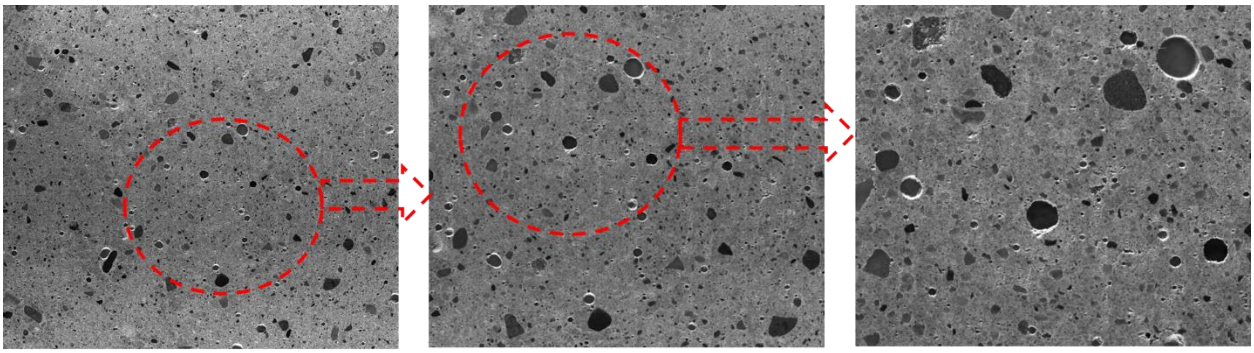

0.35 w/c ratio mortar (74% paste-20%aggregate-6% air)

Fig. 4-2 The microscopic picture of 0.35 w/c concrete with 20%, 40% and 70% aggregate contents

4.3 Strength and compressive elastic modulus test

Compressive elastic modulus is obtained from the stress-strain curve of two 300 mm × 600 mm cylinders based on the simultaneous measurement of uniaxial compressive load by a static

hydraulic system shown in Fig. 4-3(a), and linear deformation by a motion capture system (Fig. 4-3(b)) at 1, 3, 7 and 28 days. The stress strain curve of two cylinders at various ages are plotted in Fig. 4-4.

Compressive strength is tested at 1, 3, 7, 28 and 91 days on the 100 mm × 200 mm cylinders according to ASTM C39, respectively. The test results of three specimens on various ages are plotted in Fig. 4-5 together with the ACI simulation and elastic modulus.

(a) (b)

Fig. 4-3 (a) The static hydraulic system (b) Motion capture system

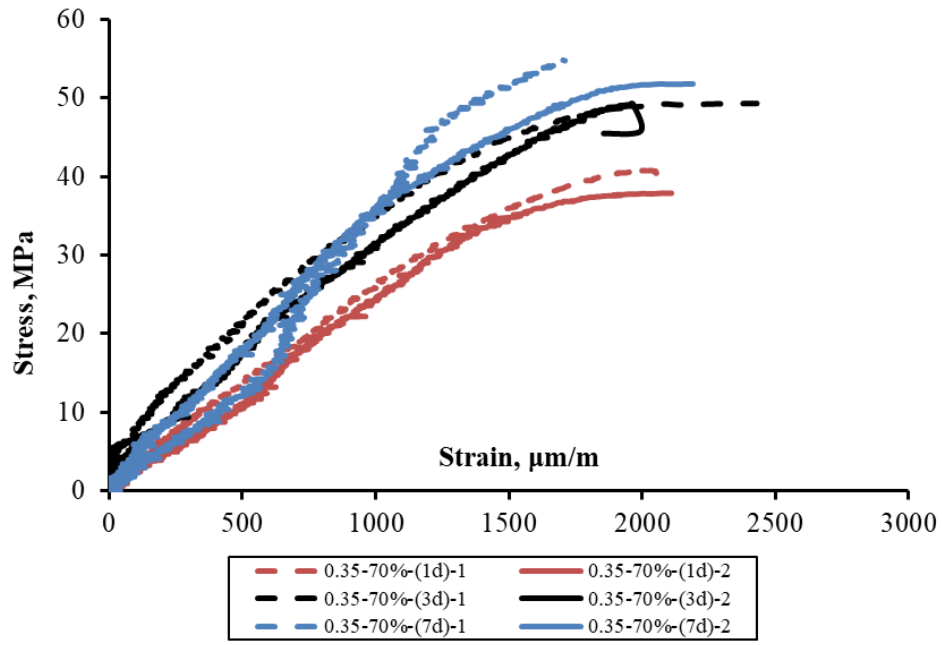

Fig. 4-4 The compressive stress strain curve for duplicate specimens of 0.35-70% at various ages (1 day, 3 days and 7 days)

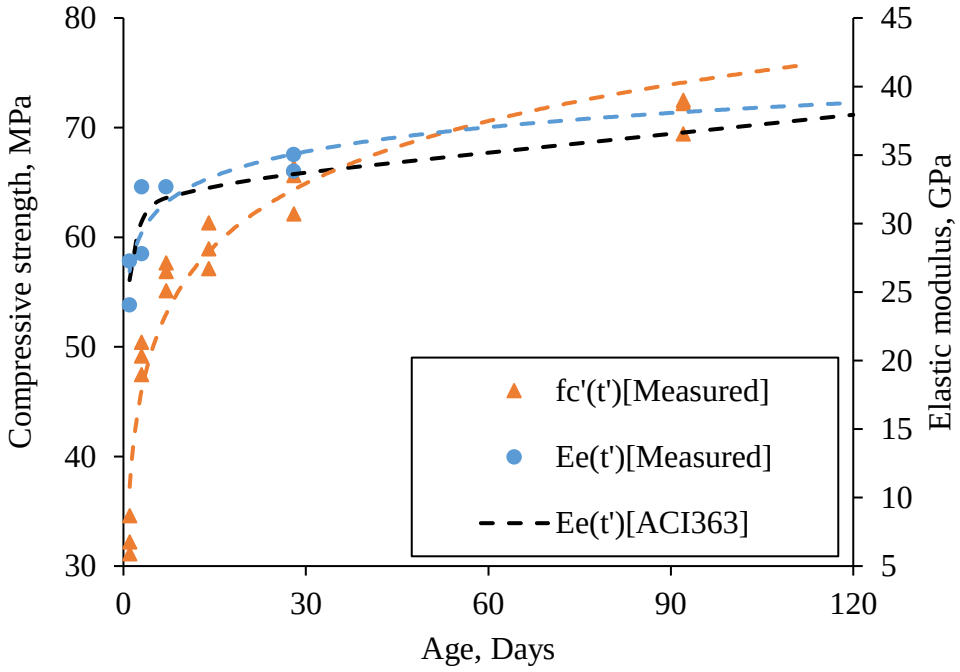

Fig. 4-5 Compressive strength and elastic compressive modulus versus age with ACI363 model fitting

4.3.1 The effect of water/cement ratio

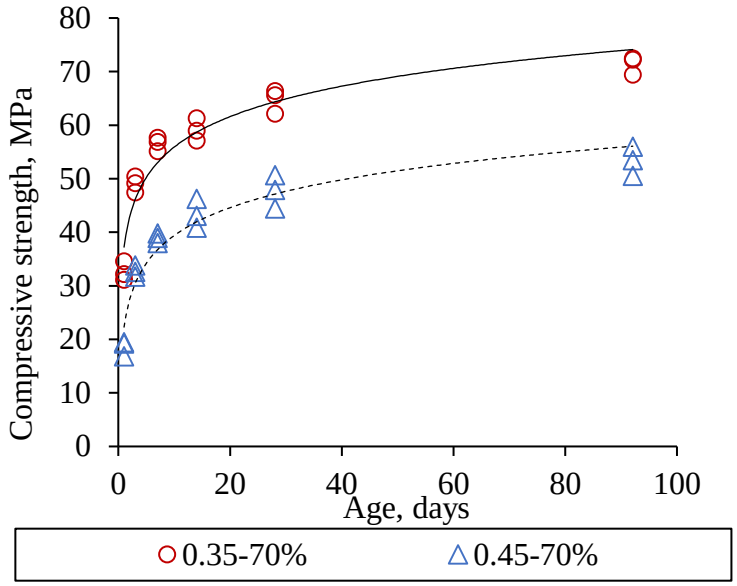

(a)

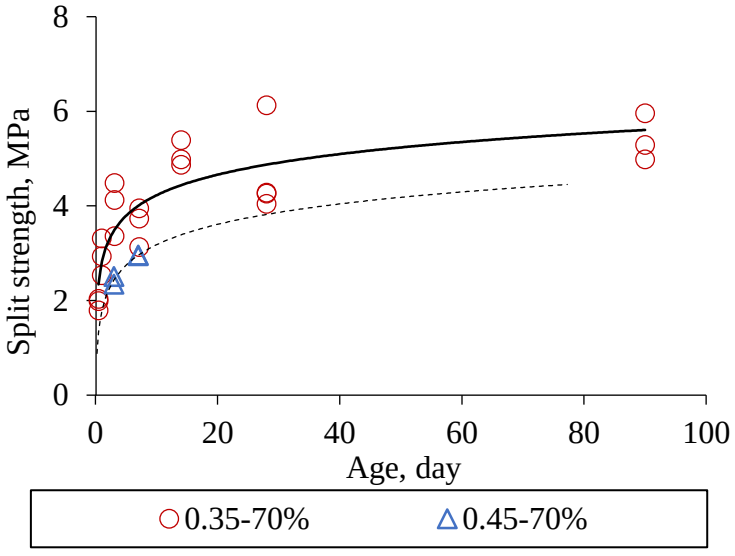

(b)

Fig. 4-6 (a) Compressive and (b) split strength of 0.35-70% and 0.45-70% versus age

The compressive and split strength of 0.35-70% and 0.45-70% are plotted in Fig. 4-6(a) and (b) for comparing the effect of water/cement ratio on development of strength. It can be seen that the compressive and split strength of HPC with 0.35 w/c are both much higher than that of NSC with 0.45 w/c for both compressive and split strength. Compressive and split strength are two of the most important factors affecting the elastic and viscoelastic behavior of concrete, thus the strength test versus aging is always needed for any form of viscoelastic research.

4.3.2 The effect of aggregate content

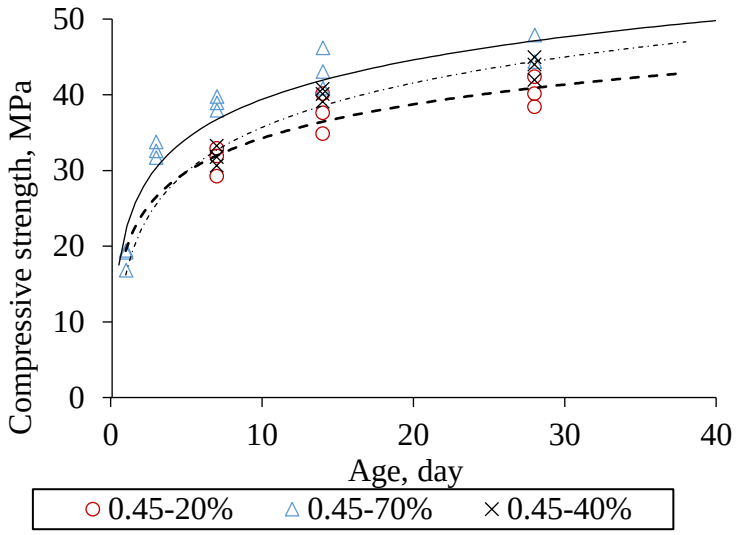

Fig. 4-7 The compressive strength of 0.45 with various aggregate content (20%, 40% and 70%) versus age

The compressive strength of 0.45 with various aggregate contents (20%, 40% and 70%) are plotted in Fig. 4-7 versus time. It can be seen that with higher aggregate content, the compressive strength is higher. It can be attributed to the much larger elastic modulus of aggregate compared with paste modulus. With more aggregate content, the composite elastic modulus is larger.

4.3.3 The effect of SCM

The compressive and split strength versus ages for 0.35-70% and 0.35-70% with 50% GGBFS replacement are plotted in Fig. 4-8(a) and (b). It can be seen that the compressive strength of

0.35(S)-70% with GGBFS is lower than the one without slag before 7 days and then exceeds the strength of 0.35-70% after 7 days. The split strength is affected similarly by the addition of slag. It can be concluded from these test results that the addition of slag can increase the strength of concrete, especially in later age.

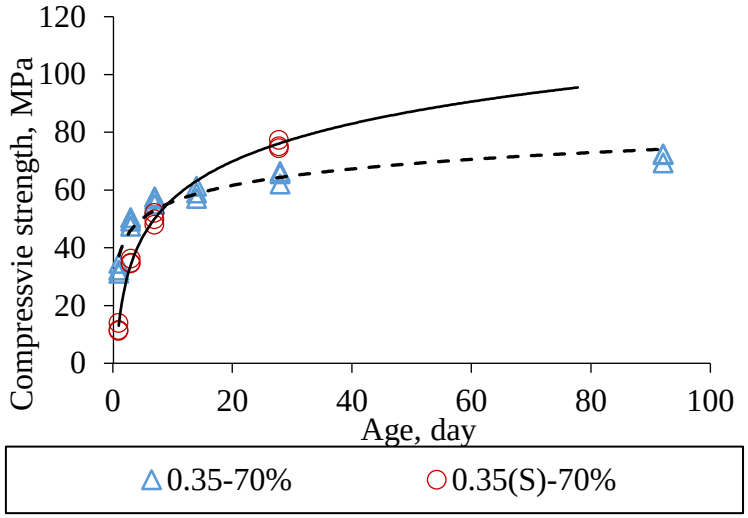

(a)

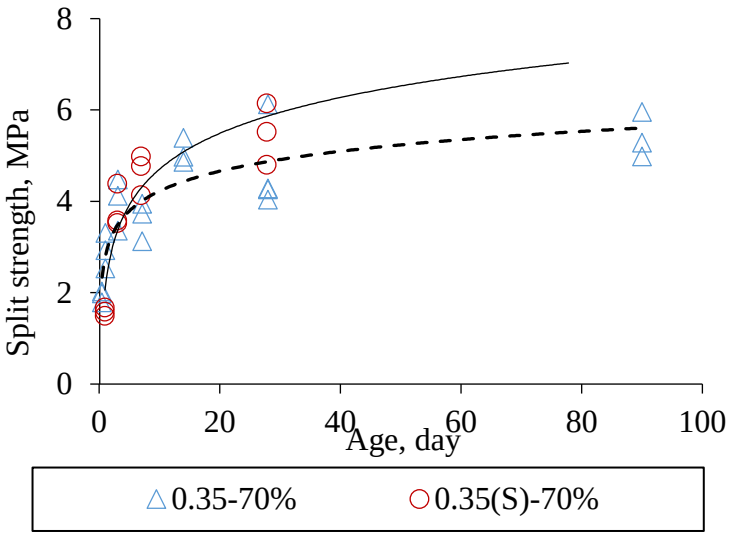

(b)

Fig. 4-8 (a)The compressive and (b) split strength versus ages for 0.35-70% and 0.35(S)-70% with 50% slag replacement

4.3.4 The effect of Lightweight aggregate (LWA)

To investigate the effect of the LWA on the strength of concrete, the compressive and split strength of HPC with and without LWA replacement are plotted in Fig. 4-9(a) and (b). It can be seen that 0.35-70% without LWA bear much higher compressive and split strength compared to the 0.35(L)-70% with 50% LWA replacement. It can be attributed to the much lower elastic modulus of LWA compared to normal fine aggregate.

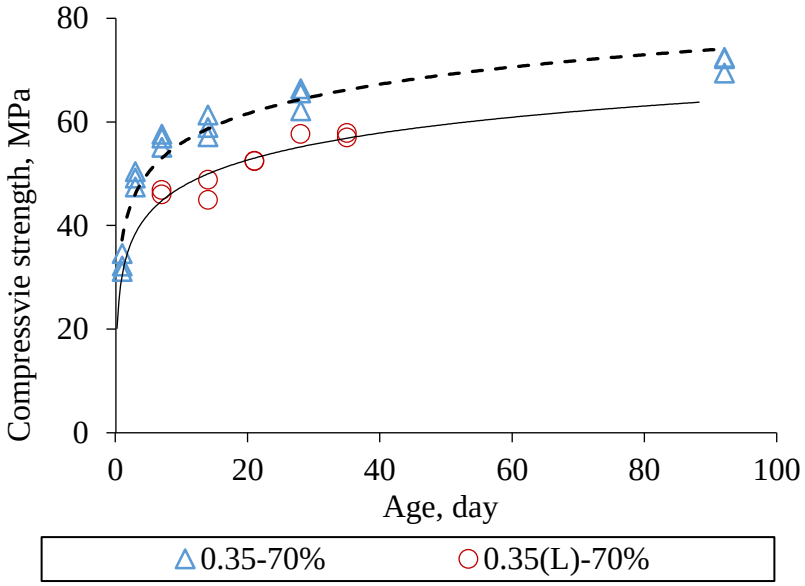

(a)

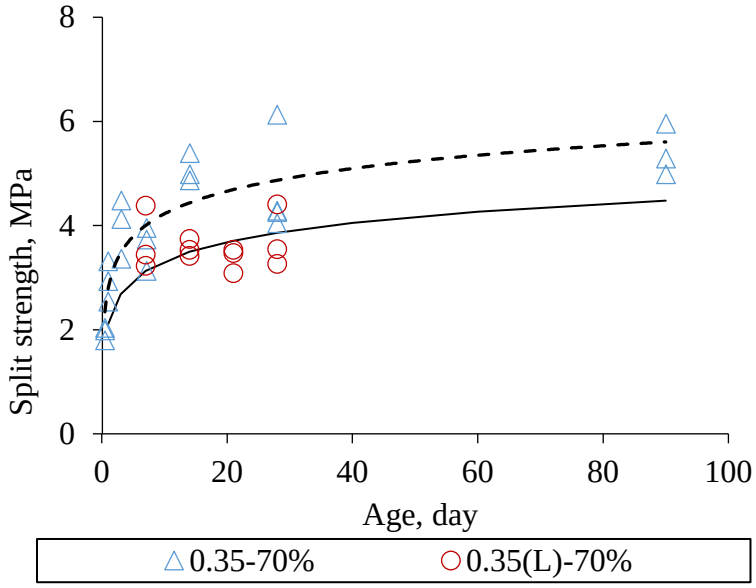

(b)

Fig. 4-9 (a) Compressive strength and (b) split strength of 0.35-70% and 0.35(L)-70%

4.4 Creep test

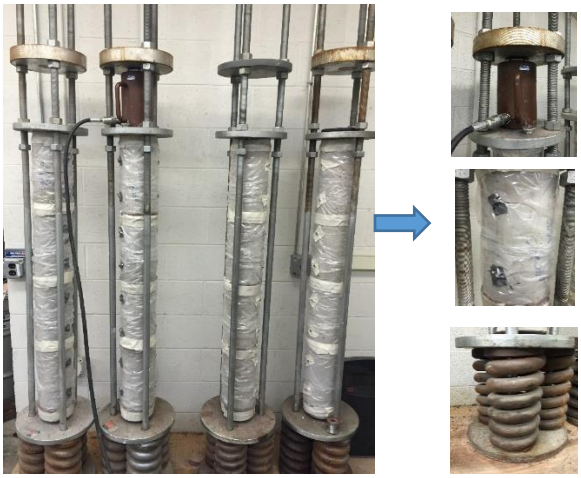

Fig. 4-10 Sealed compressive creep test

Basic creep is investigated for three different ages (7 days; 28 days and 120 days), while drying creep is done for two ages (7 days and 28 days) for certain mixes for reference. A spring-loaded system containing three heavy duty coil springs at the bottom was used as shown in Fig. 4-10. The concrete cylinders, which are capped at both ends, are stacked between two plates. Loading is applied to the top-plate of the frame by manually increasing the hydraulic pressure with a pump. When the desired load is reached, nuts are tightened down on the plate above the load cell and the hydraulic jack is removed. The creep pressure on the specimens is maintained by the springs below the bottom plate of the frame. Periodic load adjustments are applied to maintain the initial load. For each specimen, four brass inserts with conical shaped steel pins are placed. A mechanical strain measurement gauge is used. Creep loading started at 7, 28 and 120 days after casting for two stress levels (5 and 10 MPa). During the entire test period, a sealed moisture condition is achieved by wrapping each cylinder in plastic and no moisture loss is assumed.

4.5 TSTM and tensile elastic modulus test

The frame used here is composed of a load cell and an actuator with servohydraulic control (Fig. 4-11). While one end is fixed, the other end, which is on the side of actuator, can be moved freely. Since the volume of concrete changes due to shrinkage, the actuator is programmed to move cyclically relative to its original place. The amplitude of the actuator controlled to move

cyclically is smaller than 3 μm relative to its original position and at a time interval of 2s. The specimen can be considered as full restrained because the cyclic moves for the length adjustment are small compared to the amplitude of size of specimen. The specimen is directly cast into the foam-insulated mold which is already positioned in the test rig. Two ends of the specimen are enlarged to ensure a uniform stress distribution at the central part. A thin vinyl sheet is placed between the specimen and the mold to avoid frictional resistance. Immediately after casting, the upper surface of the specimen is covered with a plastic sheet to prevent any water evaporation. The mold is equipped with copper pipes that could circulate constant temperature (23°C or 33°C) water from a heating-cooling control bath. Two gauges whose distance is about 200 mm are inserted into the matrix vertically in the middle span of the specimen for measuring the deformation of the concrete during test. During the entire testing period, the specimen is sealed cured. The temperature field in the specimen is measured at three locations along the specimen depth. It is found that the specimens have a quite uniform temperature distribution along the depth at all times. The stress measurements start immediately after casting.

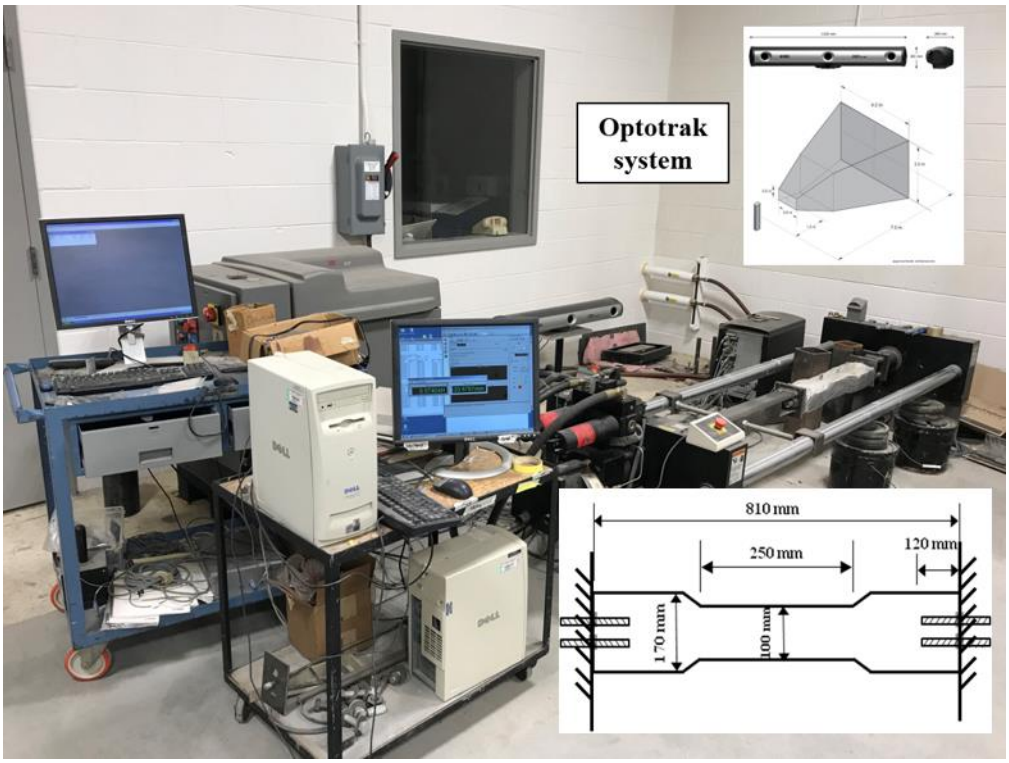

Fig. 4-11 TSTM apparatus and Optotrak camera system

The development of deformation of specimens is captured by the Optotrak system with NDI First Principles software for collecting, managing and presenting 3D and 6 DOF measurement data in real time. It can capture 3D measurements to an accuracy of 0.1mm and resolution of 0.01mm, independent of sampling rate, with minimal latency and noise. Pre-calibration is done to allow the immediate data collection and will maintain calibration even if the optical tracker is moved. During the test, one set of data containing the time profile, the coordinates of markers are collected each second and synchronized to the load information of TSTM. The tensile elastic modulus is measured by the use of TSTM and Optotrak system with loading recorded by TSTM and deformation recorded by Optotrak. The specimen is loaded to a certain stress level and unloaded by multiple times to get a more accurate value of elastic tensile modulus. The specimen is finally loaded to failure to calibrate the load by comparing with the result from split strength test. The stress strain curve of loading and reloading and loading to failure of a specimen is shown in Fig. 4-12 as an example. One can see the good linearity between the stress and strain correlation with small variation. The slopes of three consecutive loadings are identical which proves the stability and consistency of the test.

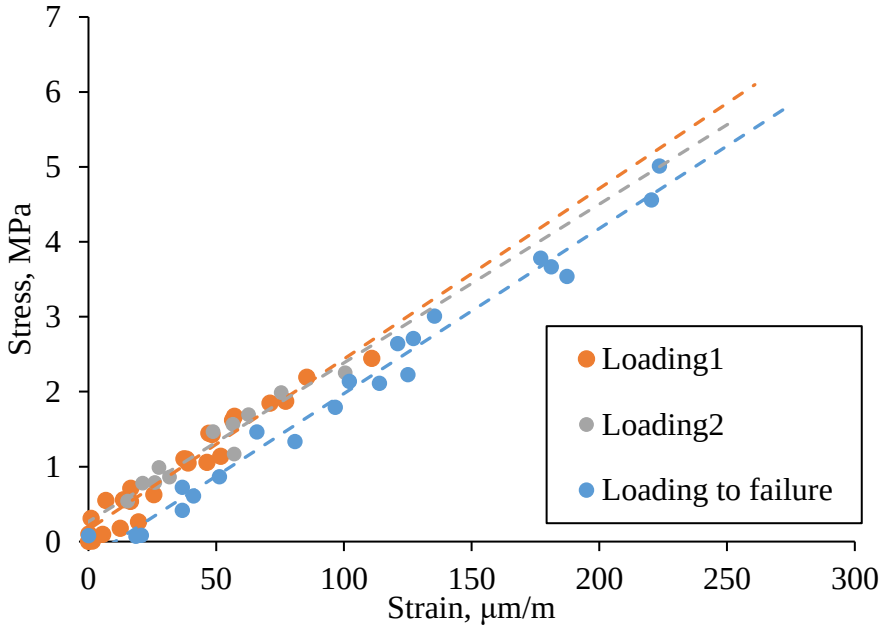

Fig. 4-12 Measured tensile stress strain point from multiple loading test by TSTM and Optotrak camera

4.6 Shrinkage test

Autogenous shrinkage and temperature are measured simultaneously on duplicate specimens of dimensions 60 mm (height) by 100 mm (width) by 1000 mm (length) embedded in a double layer polystyrene for sealed moisture testing. The test system is shown in Fig. 4-13. While one end of the specimen is fixed by a metal hook, the other end can be moved freely and connected with LVDT sensor shown in Fig. 4-13(b). LVDT sensor does not touch the specimen before the concrete reaches initial setting. The length after initial setting is used as the reference for calculating the shrinkage strain. For some of the free shrinkage test, a twin reinforced autogenous shrinkage test is also done with the use of four bars as shown in Fig. 4-13(a). The location of the four steel bars is represented in Fig. 4-13(a) and the twin free and reinforced autogenous shrinkage tests are from the same mix with cured and measured under the same condition.

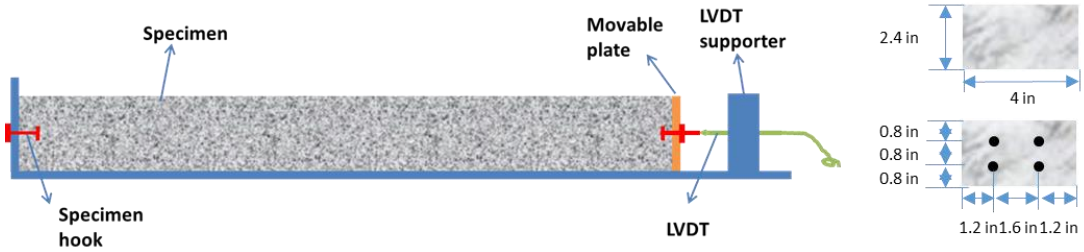

(a)

(b)

Fig. 4-13 Autogenous shrinkage test system

4.7 Internal RH measurement

Internal RH and temperature is measured concurrently on mortar specimens with 40% aggregate volume by the Vaisala® HMP110 probes positioned in a prefabricated hole of the specimen (Fig. 4-14). Humidity accuracy is 1.7 % for RH < 90 % and 2.5 % for RH ⩾ 90 %. Cylindrical specimens of 150×300 mm are cast for internal RH measurement. A sealed plastic sleeve with a diameter of 12.5 mm is inserted from the top into the fresh mixes during casting (Fig. 4-15(a)). This makes the space to accommodate the humidity probe for the RH measurement. The typical measuring depth is 150 mm from the top and two more depths are also used (50 mm and 275 mm) to evaluate the RH variation over depth. One day after casting, the moisture-rich zone surrounding the bottom of the sleeve is removed along with the plastic sealing by a chisel, while the top of the sleeve remains sealed. Specimens are sealed cured at 20±1 °C for all the time unless the effect of temperature is tested and various temperature is applied.

RH is measured regularly up to 90 days. A technique is utilized to improve the test accuracy by chiseling off a fraction of fresh mortar particles at the test surface prior to the insertion of the probe (Fig. 4-15 (b) and (c)). This procedure releases the moisture and increases the contact area with the RH probe. During testing, the probe is inserted into the hole in contact with the fresh mortar particles while the RH values are continuously monitored on a computer. A reading is taken when RH and temperature had reached equilibrium.

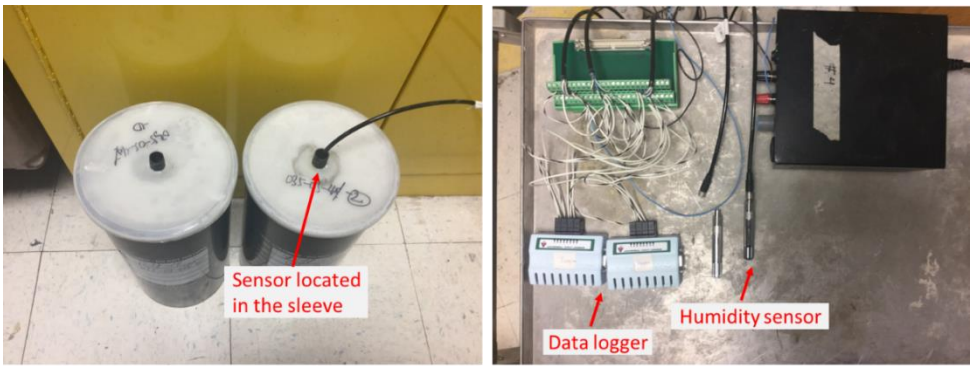

Fig. 4-14 Internal RH measurement system

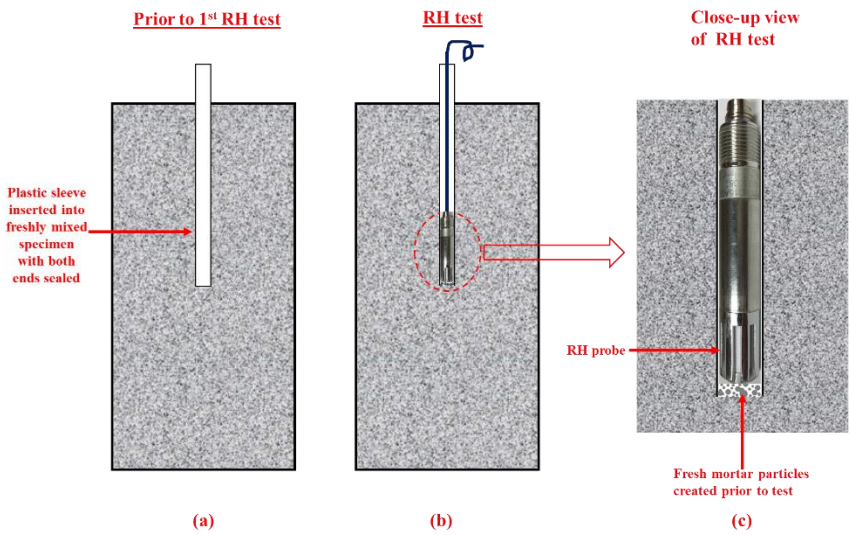

Fig. 4-15 Detailed test configuration for internal RH measurement

4.8 Moisture warping measurement

Warping associated with moisture gradient is measured on a concrete beam of 0.15×0.2×2.3 m (Fig. 4-16) for two mixes (0.35-70% and 0.35(L)-70%). The beam is cast on a steel frame with five evenly-spaced spacers in between. After 28-day sealed curing, the bottom of the beam is exposed to a water reservoir while the other sides remain sealed by plastic sheets. One end of the beam is fixed to the frame by two bolts while the other end is free to move. Two dial gauges are positioned at the two ends to monitor the change in vertical displacement with time.

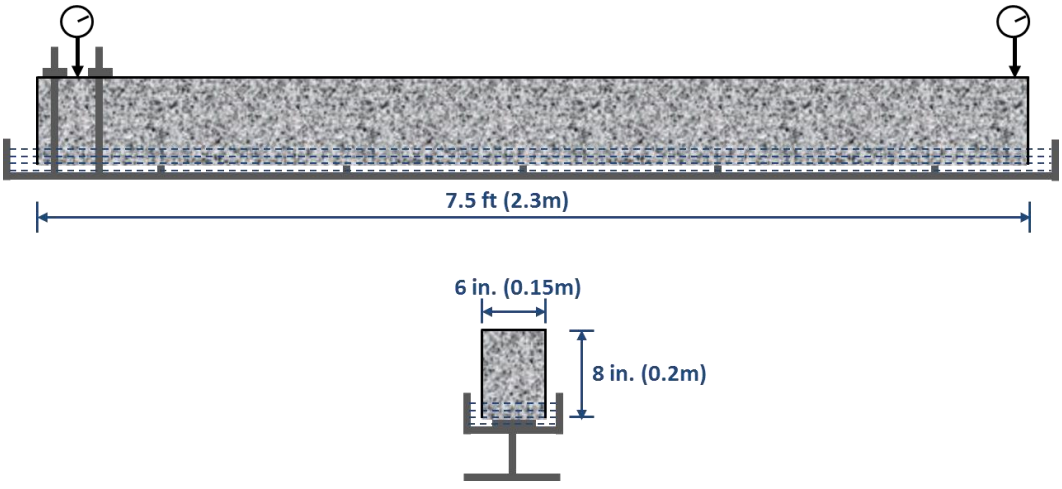

Fig. 4-16 Illustration of moisture warping test

4.9 Summary

The concrete proportioning used in this study is introduced in this chapter. The detailed preparation and procedure of experimental tests including basic creep, autogenous shrinkage and TSTM full restraint tests, etc. are discussed. The basic mechanical property of concrete with effect of materials parameters is also tested.

Chapter 5 Testing and Modeling of Compressive Creep of HPC

5.1 Introduction

Creep can be divided into basic creep and drying creep if concrete is exposed to air. For the concrete sealed without moisture loss, the basic creep deformation is just equal to the total creep. Since the moisture loss of the large concrete member for long term period is minimal, basic creep is the focus for this research. Creep behavior is regarded as linear with load under stress/strength ratio lower than 0.3. Although many literatures develop various linear or nonlinear continuous models for simulating the mechanics of basic creep (Bazant *et al*. 1988), there is no agreement on one universal model which can be used to explain the mechanics of creep perfectly from short-term to long term. While many models claim that the parameters should be universal regardless of type of cement and mix specification, the coefficients of all the models still need to be fine-tuned by experiment data. In the chapter, a practical rheological model with physical parameters fine-tuned by experimental data is used to characterize the compressive viscoelastic creep behavior of HPC under sealed condition. With the basic creep of normal concrete being tested at the same time, the difference between creep behavior of normal and high performance concrete are also studied.

A comprehensive investigation of basic creep of HPC is done in this chapter. With the use of Thomson rheological model, viscoelastic creep modulus is defined to characterize the resistance of concrete to creep deformation under external load. The study on effect of aging, water/cement ratio, aggregate content, SCM content and presence of lightweight aggregate on the rate and magnitude of basic creep are involved and a modified Thomson type rheological model with w/c ratio, aggregate content, SCM and LWA content, etc. as the variables is developed based on respective experimental data. A constant ratio of creep modulus and.

compressive strength is found for approximate estimation of magnitude of basic creep. Finally, drying creep is also measured for investigating the effect of curing condition on creep behavior The creep recovery from unloading and further development of creep with reloading to same loading stress and elevated stress are also tested.

5.2 Long–term basic creep measurement under sealed condition

Various mixes of concrete are done for sealed creep test. For each mix, at least two loading ages 7 and 28 days) are included with two different loading stress (5MPa and 10 MPa).The magnitude of stress is chosen to keep a low stress/strength ratio for creep test. Two specimens are tested for each test specification and the final deformation is the derived by averaging the two readings from each of the side of the two specimens. Total deformation results are measured every 2-4 hours during the first 24 hours, followed by testing every 3-6 days. Measurement of each test lasts at least 100 days since the staring of the loading. Since the specimen is kept sealed all the time, autogenous shrinkage is insignificant with the 100 days testing compared to magnitude of creep and therefore neglected during the strain calculation. Generally, the basic creep strain is obtained by Eq. 5-1.

$$\varepsilon_{cr} \approx \varepsilon_{tot} - \varepsilon_{e} \qquad \text{Eq. 5-1}$$

The sealed creep test for 0.35-70%, 0.35(S)-70%, 0.35(SL)-70%, 0.35-40%, 0.35-20%, 0.45-70%, 0.45-20% under two stress levels (5MPa and 10MPa) starting from three loading ages (7. 28, and 120 days) are shown from Fig. 5-1 to Fig. 5-7**.** The curve in each figure represents the average measured strain from two sets of gauges from one specimen. Since two specimens are used for each mix and testing condition, duplicate total strain measurement can be obtained for verification of stability and consistency of creep test. It can be seen that the total strain is larger with larger external load and earlier loading ages when test results are compared within each of the concrete mix. The rate of creep is minimal after about 30-40 days since the start of loading regardless of mix and test specimens. The creep strain after the creep reaching the minimal creep rate is called ultimate creep with respect to the period of testing. Creep is expected to keep increasing for a much longer time after 100 days because of viscous flow. For evaluating the creep performance within 100 days after loading, ultimate creep is used here for approximation and simplification.

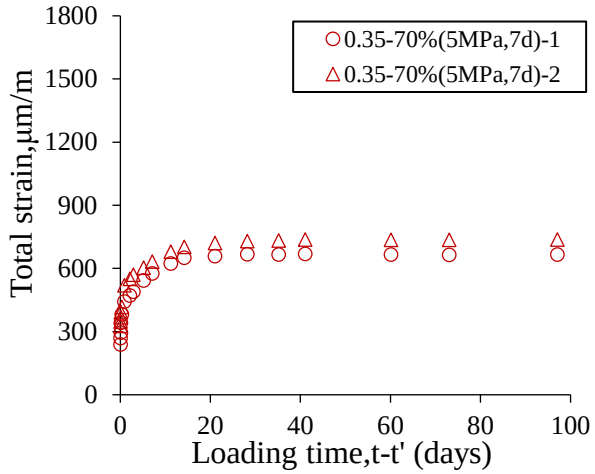
0.35-70%(5MPa,7d)-1
0.35-70%(5MPa,7d)-2
Total strain,μm/m
Loading time,t-t' (days)

(a)

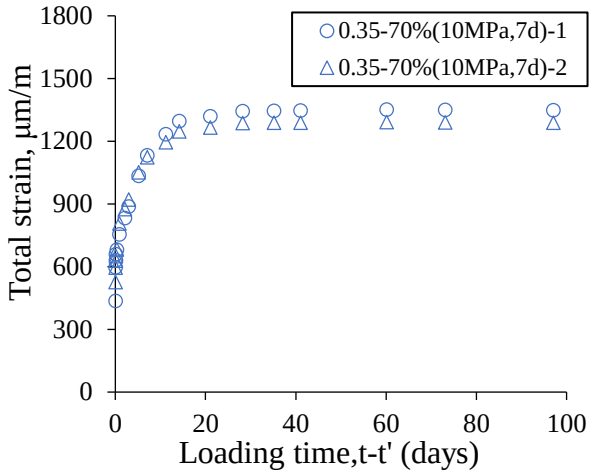
0.35-70%(10MPa,7d)-1
0.35-70%(10MPa,7d)-2
Total strain, μm/m
Loading time,t-t' (days)

(b)

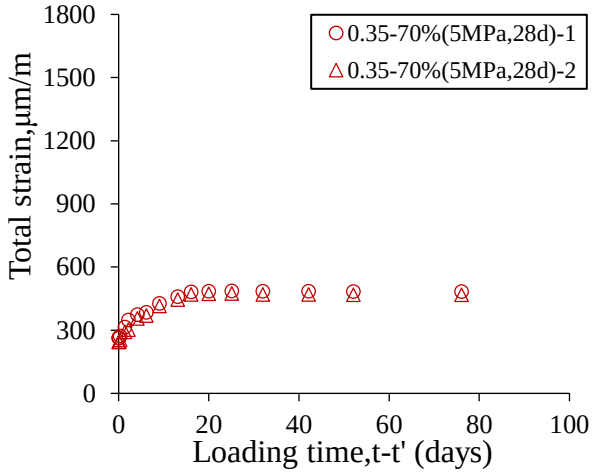
0.35-70%(5MPa,28d)-1
0.35-70%(5MPa,28d)-2
Total strain,μm/m
Loading time,t-t' (days)

(c)

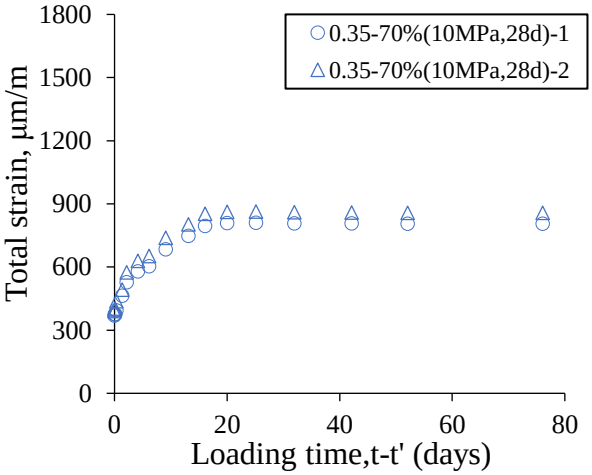
0.35-70%(10MPa,28d)-1
0.35-70%(10MPa,28d)-2
Total strain, μm/m
Loading time,t-t' (days)

(d)

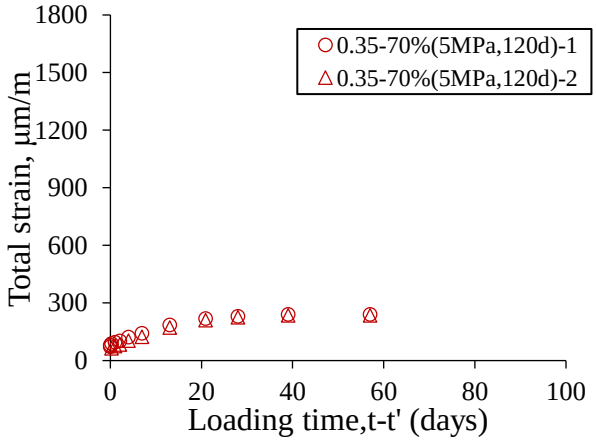
0.35-70%(5MPa,120d)-1
0.35-70%(5MPa,120d)-2
Total strain, μm/m
Loading time,t-t' (days)

(e)

Fig. 5-1 The total strain of concrete under sealed condition for 0.35-70% starting at 7 days with (a) 5MPa and (b) 10MPa, and starting at 28 days with (c) 5MPa and (d) 10MPa and starting from 120 days with (e) 5MPa

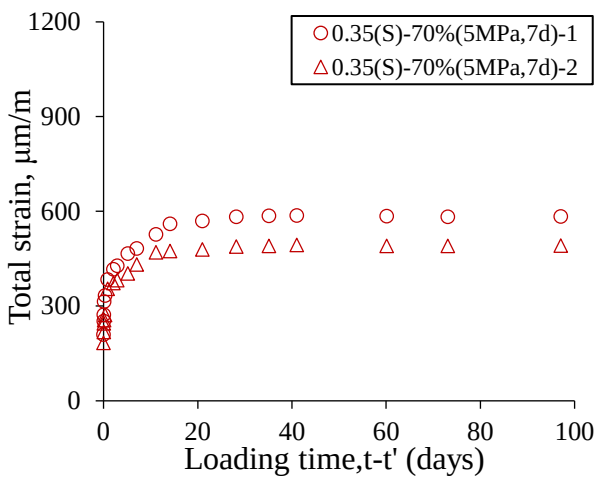

(a)

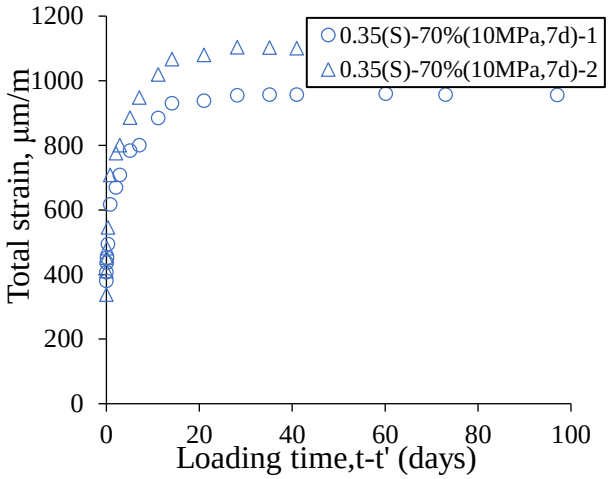

(b)

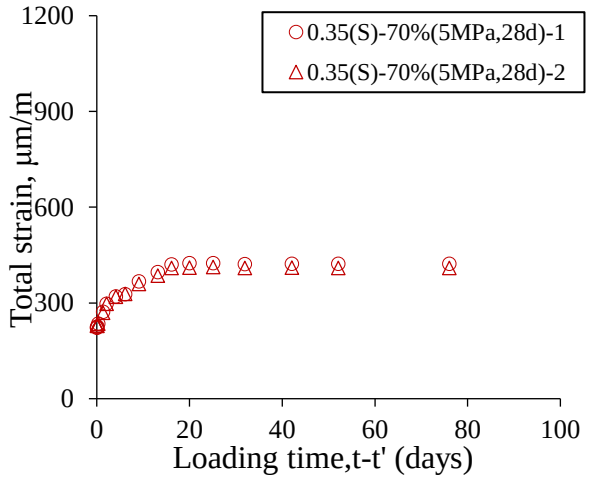

(c)

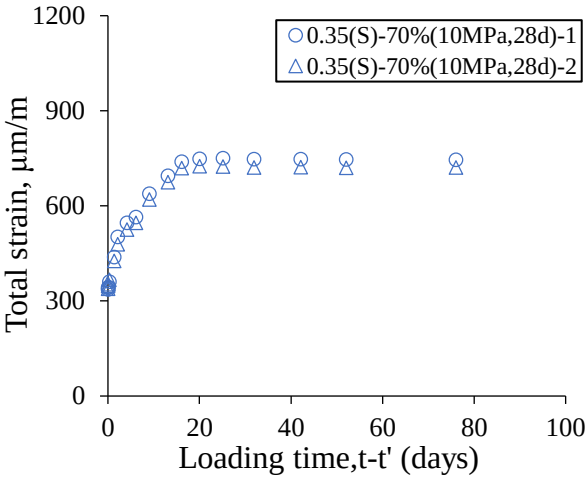

(d)

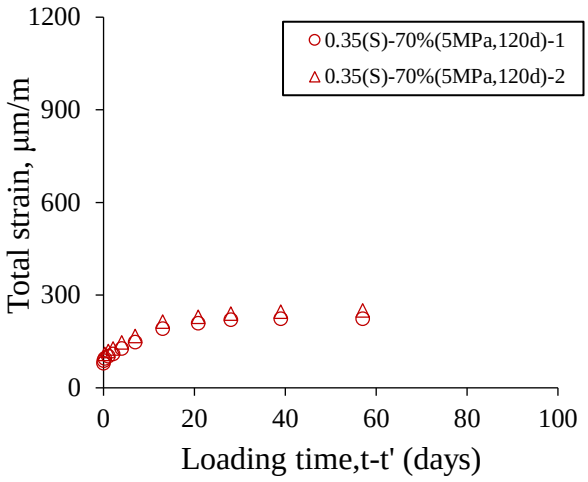

(e)

Fig. 5-2 The total strain of concrete under sealed condition for 0.35(S)-70% with 50% slag replacement starting at 7 days with (a) 5MPa and (b) 10MPa, and starting at 28 days with (c) 5MPa and (d) 10MPa and starting from 120 days with (e) 5MPa

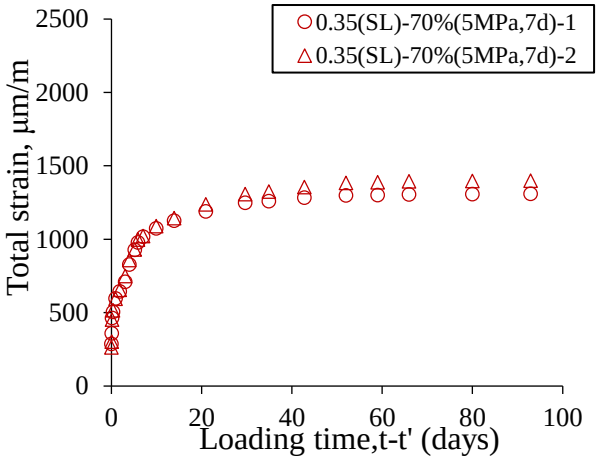

(a)

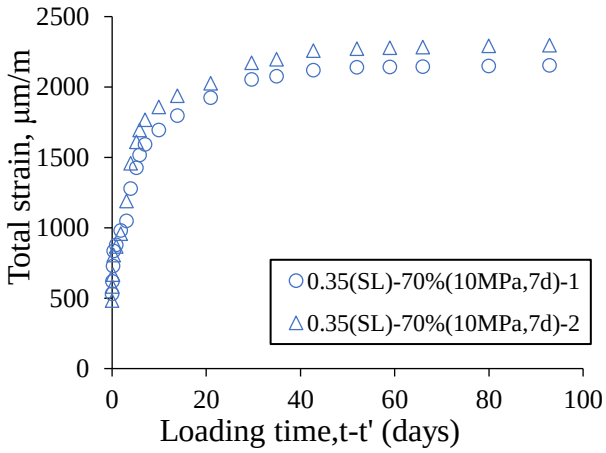

(b)

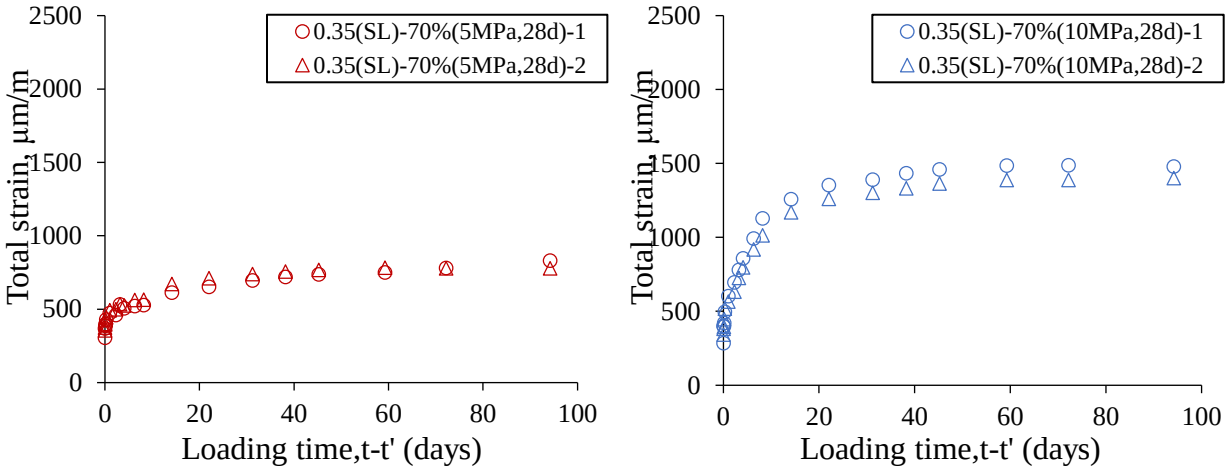

(c)

(d)

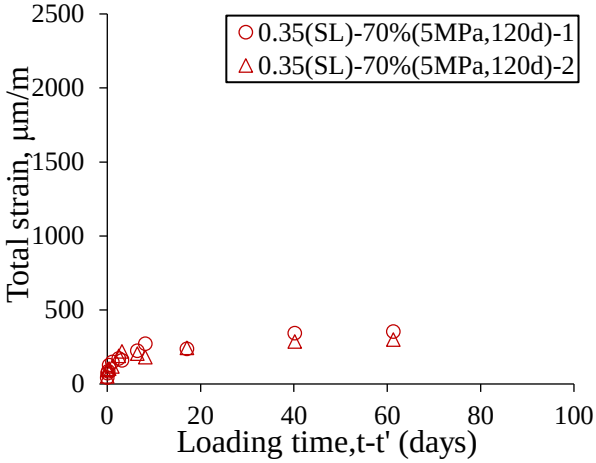

(e)

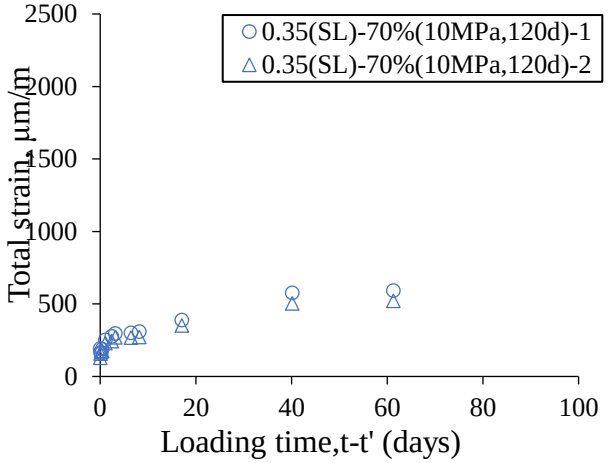

(f)

Fig. 5-3 The total strain of concrete under sealed condition for 0.35(SL)-70% with 50% slag replacement and 50% LWA replacement starting at 7 days with (a) 5MPa and (b) 10MPa, and starting at 28 days with (c) 5MPa and (d) 10MPa and starting from 120 days with (e) 5MPa and (f) 10MPa

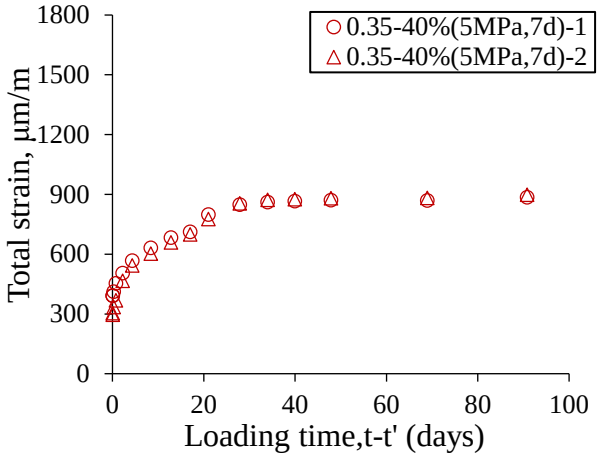
0.35-40%(5MPa,7d)-1
0.35-40%(5MPa,7d)-2
Total strain, μm/m
Loading time,t-t' (days)

(a)

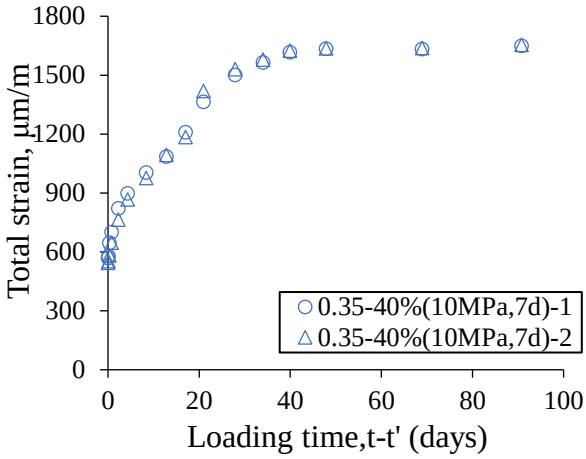
0.35-40%(10MPa,7d)-1
0.35-40%(10MPa,7d)-2
Total strain, μm/m
Loading time,t-t' (days)

(b)

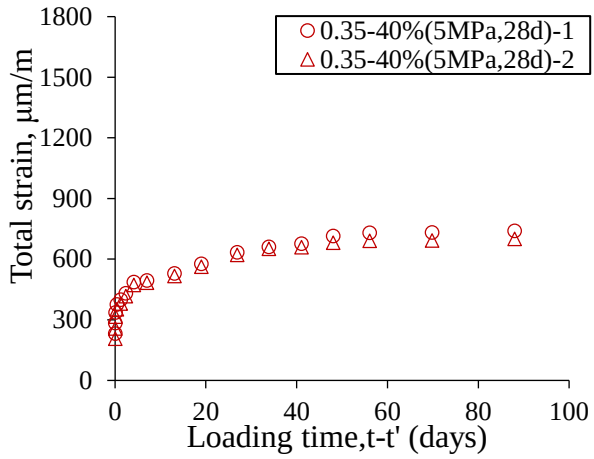
0.35-40%(5MPa,28d)-1
0.35-40%(5MPa,28d)-2
Total strain, μm/m
Loading time,t-t' (days)

(c)

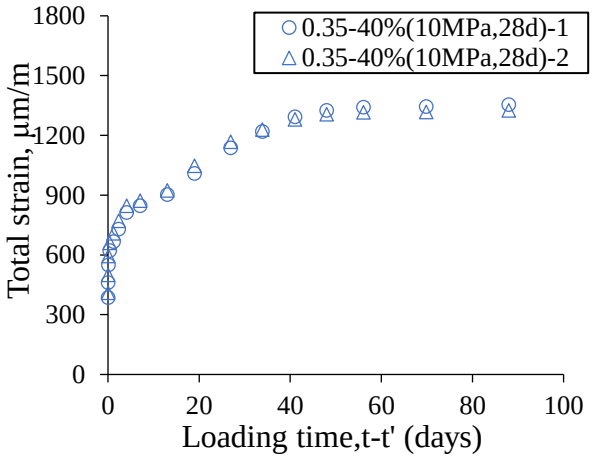
0.35-40%(10MPa,28d)-1
0.35-40%(10MPa,28d)-2
Total strain, μm/m
Loading time,t-t' (days)

(d)

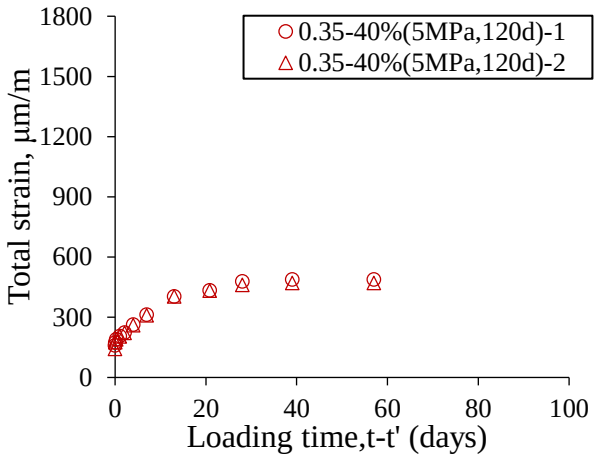
0.35-40%(5MPa,120d)-1
0.35-40%(5MPa,120d)-2
Total strain, μm/m
Loading time,t-t' (days)

(e)

Fig. 5-4 The total strain of concrete under sealed condition for 0.35-40% starting at 7 days with (a) 5MPa and (b) 10MPa, and starting at 28 days with (c) 5MPa and (d) 10MPa and starting from 120 days with (e) 5MPa

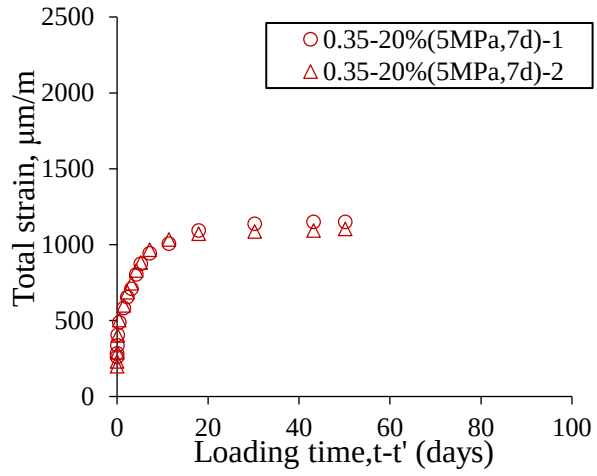

(a)

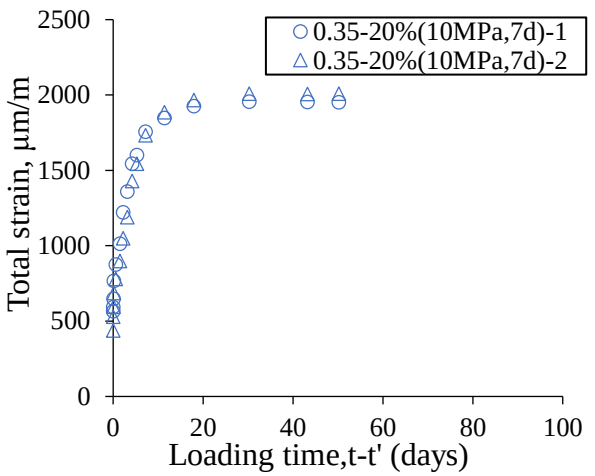

(b)

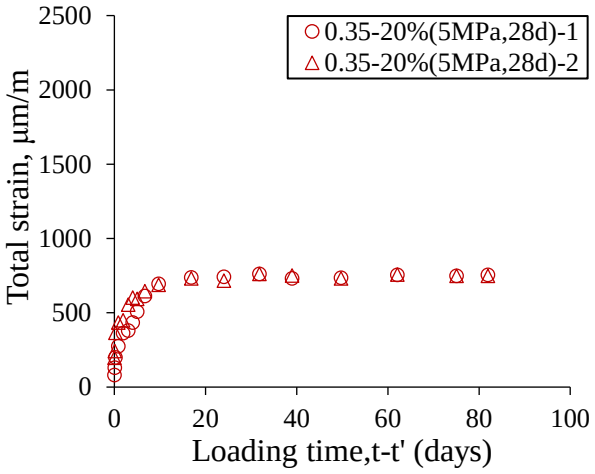

(c)

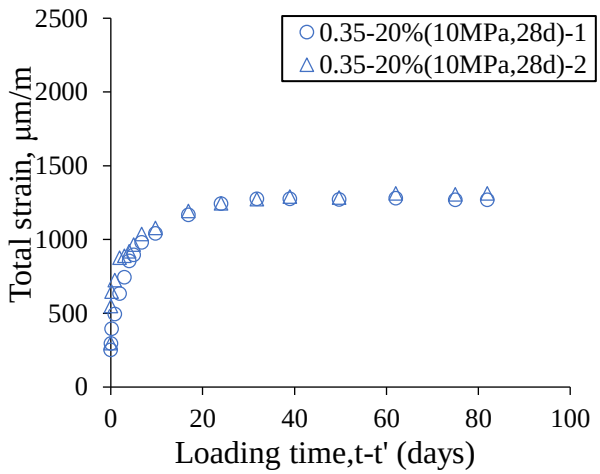

(d)

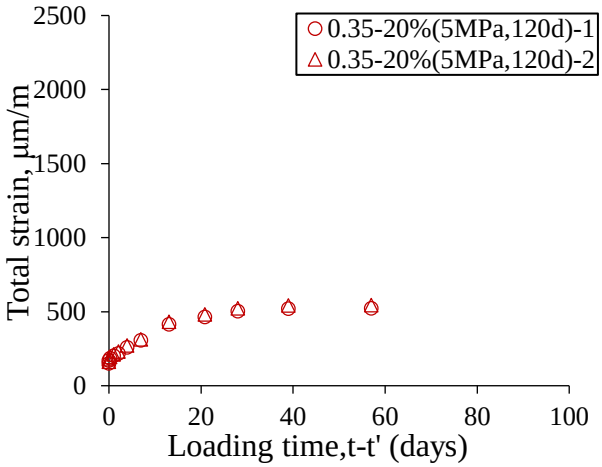

(e)

Fig. 5-5 The total strain of concrete under sealed condition for 0.35-20% starting at 7 days with (a) 5MPa and (b) 10MPa, and starting at 28 days with (c) 5MPa and (d) 10MPa and starting from 120 days with (e) 5MPa

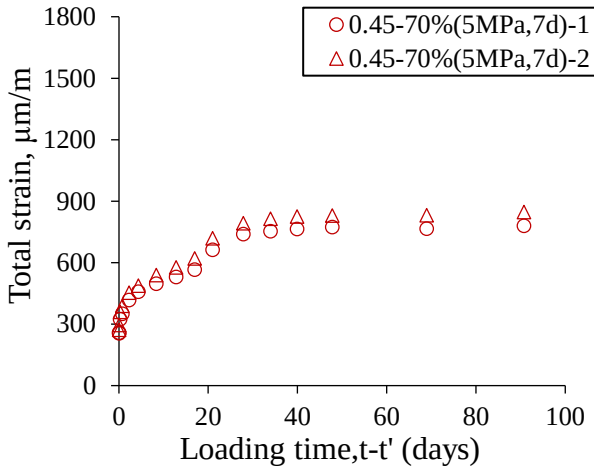

(a)

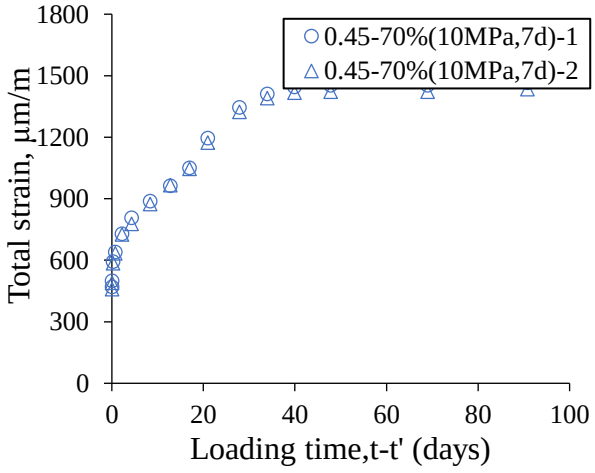

(b)

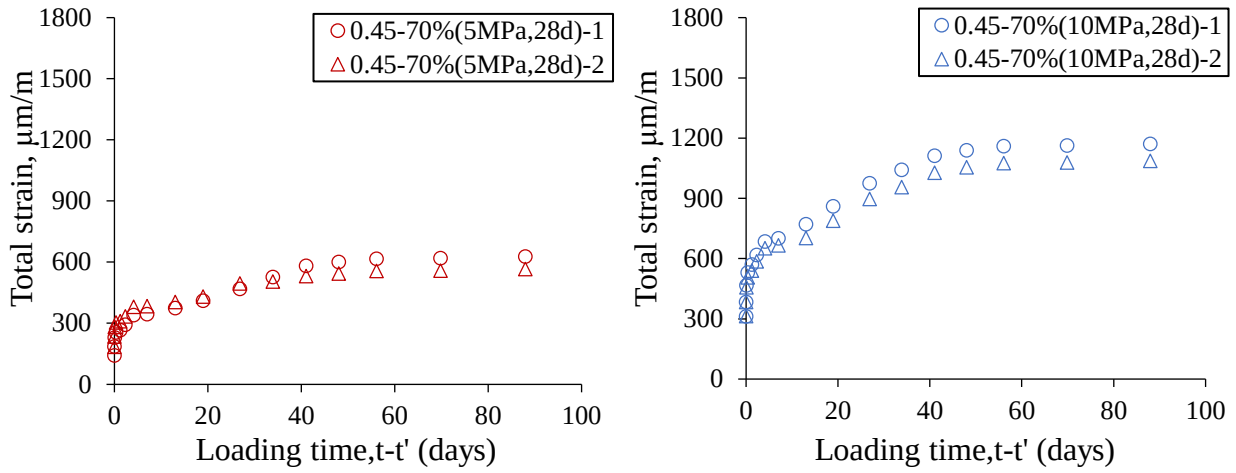

(c) (d)

Fig. 5-6 The total strain of concrete under sealed condition for 0.45-70% starting at 7 days with (a) 5MPa and (b) 10MPa, and starting at 28 days with (c) 5MPa and (d) 10MPa and starting from 120 days

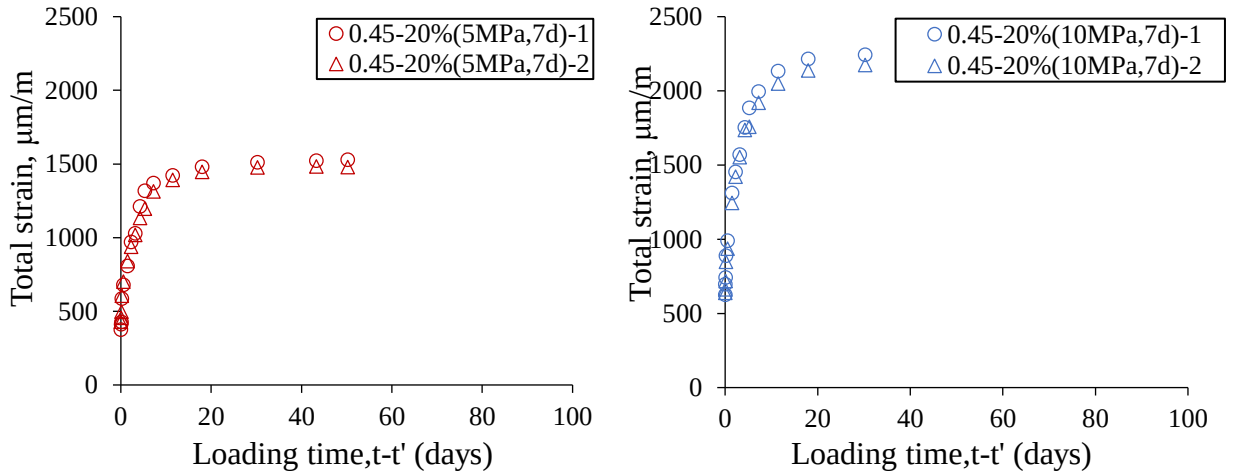

(a) (b)

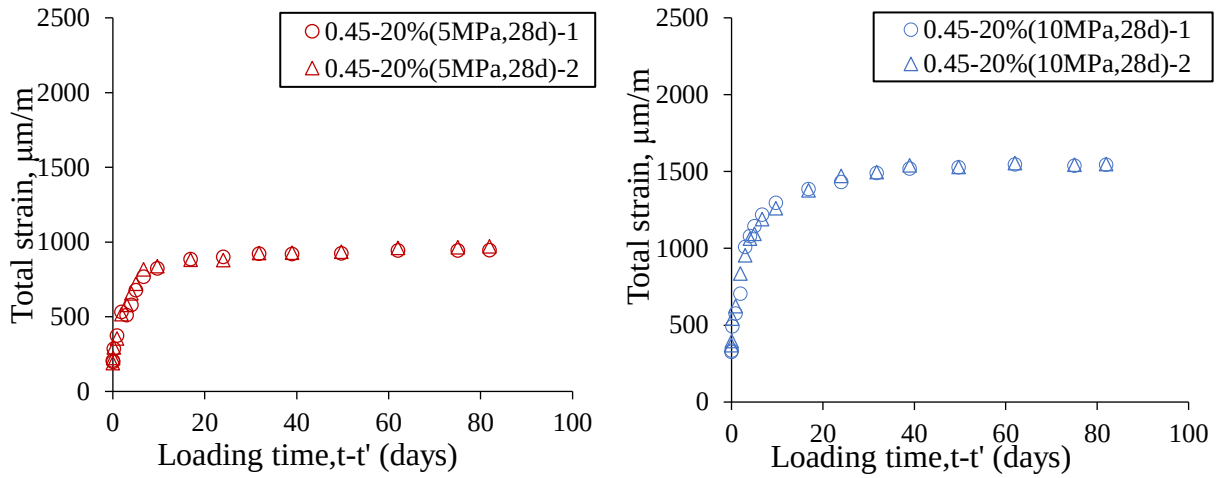

(c) (d)

Fig. 5-7 The total strain of concrete under sealed condition for 0.45-20% starting at 7 days with (a) 5MPa and (b) 10MPa, and starting at 28 days with (c) 5MPa and (d) 10MPa and starting from 120 days

The method for deciding elastic strain is not unique. Since the loading and specimen deformation may not be stable at the beginning of loading, the total strain at 1 hour after loading is assumed as the elastic strain. Logarithmic regression is used for back extrapolating to 1 hour since loading to obtain the initial elastic strain. Fig. 5-8 shows as an example how to estimate the initial elastic strain by extrapolating back to 1 hour.

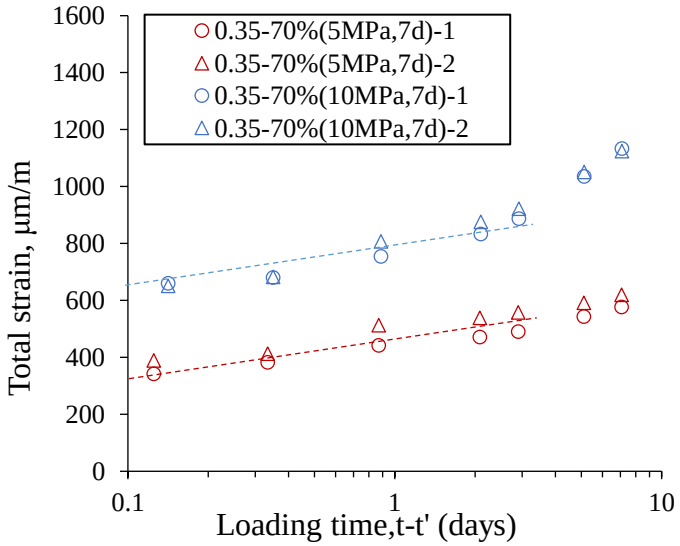

Fig. 5-8 Estimation of the elastic strain by extrapolating back to 1 hour since loading

After elastic strain is subtracted from total strain, the basic creep can be obtained directly. The basic creep of 0.35-70% with two different stress (5MPa and 10MPa) starting from 7 days are shown in Fig. 5-9(a).

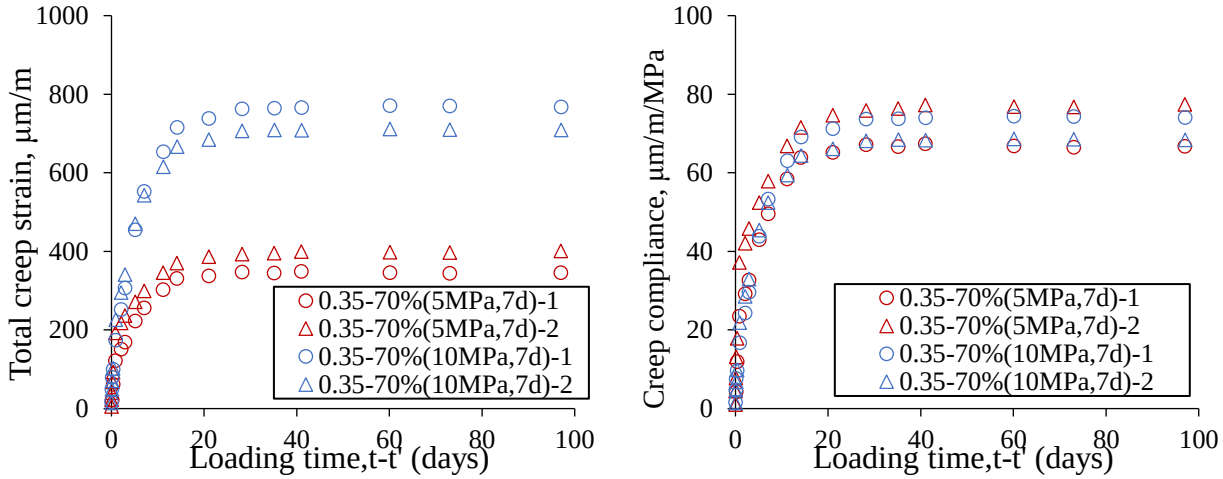

(a) (b)

Fig. 5-9 (a) The basic creep strain and (b) creep compliance for 0.35-70% on 7 days with (5MPa and 10MPa) external loading

Creep compliance (also called specific creep) is defined as the basic creep deformation under unit external loading. The equation for creep compliance is shown in Eq. 5-2.

$$J_{cr}(t,t') = \frac{\varepsilon_{cr}(t,t')}{\sigma_0} \qquad \text{Eq. 5-2}$$

Fig. 5-9(b) shows the normalized creep strain under different stress for 0.35-70% loading from 7 days. While normalized by the external stress, the creep compliance, is the same regardless of the amplitude of external stress. The result from Fig. 5-9(b) is consistent with the definition of creep compliance. The total creep strain and creep compliance for other mix systems are shown in APPENDIX A.

5.3 Modeling of basic creep

Currently there are many wildly used viscoelastic models for modelling the development of basic creep of concrete as well as the effect of variables quantitatively. As mentioned from the chapter 3, rheology theory is one of the basis mechanisms to explain the basic creep behavior by the combinations of spring and dampers. The aging viscoelastic term from the solidification theory

is also the series connection of multiple kelvin model units. Since this thesis is not focusing on development of new models for explaining the mechanisms of creep or comparison between the performances of various models, Thomson model is used here for its simplicity and parameters with physical meaning for characterizing the creep behavior. The Thomson model, which can be represented as the series connection of spring and kelvin unit, is shown in Fig. 5-10.

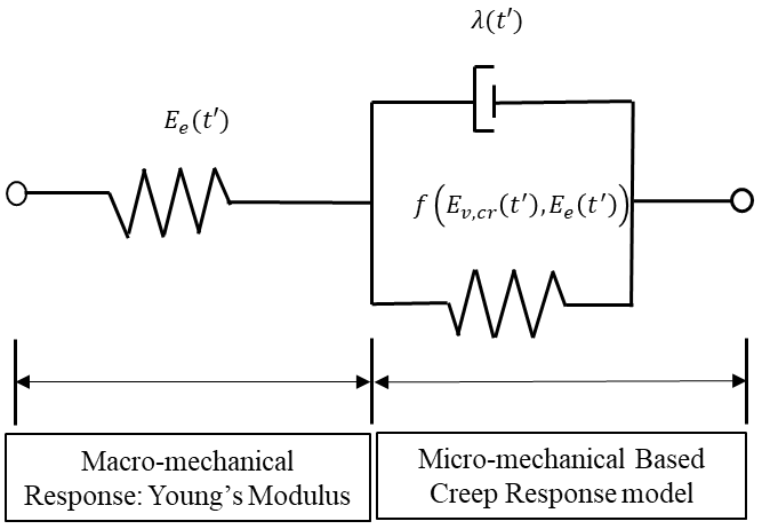

Fig. 5-10 Sketch of Thomson model, which is composed by the series connection of spring and a parallel connection of spring and damper

The total compliance can be represented as the sum of elastic term $J_e(t,t')$ and creep compliance $J_{cr}(t,t')$ shown in Eq. 5-3.

$$J_{tot}(t,t') = J_e(t,t') + J_{cr}(t,t') \quad \text{Eq. 5-3}$$

In which $J_e(t,t') = \frac{1}{E_e(t')}$. $E_e(t')$ is the elastic modulus on the loading age t'. The parallel connection of damper and spring can be simulated using Kelvin model shown in Eq. 5-4.

$$J_{cr}(t,t') = J_{cr,0}(t,t') * \left(1 - exp\left(-\frac{(t-t')}{\lambda(t')}\right)\right) \quad \text{Eq. 5-4}$$

t is the total age since the curing of the concrete. $\lambda(t')$ is the coefficient of viscosity which controls the creep development rate and supposed to be dependent on the loading age, t'. $J_{cr,0}(t,t')$ is the ultimate creep compliance. The 0.35-70% with two loading stress (5MPa, 10MPa) and three loading ages (7, 28 and 120 days) are plotted in Fig. 5-11 with regression

curves by Thomson model. The compliance data with regression by Thomson model for other mixes are added in APPENDIX B.

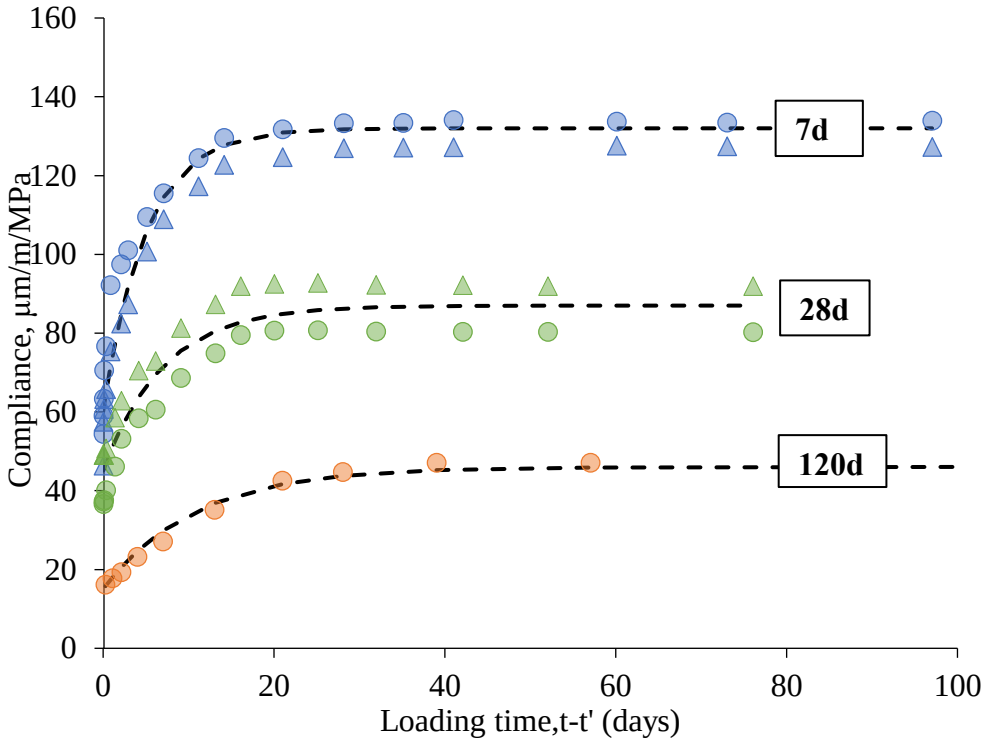

Fig. 5-11 Compliance with regression from Thomson model for 0.35-70% with two loading stress (5MPa and 10MPa) and three loading ages (7, 28 and 120 days)

After fine-tuning the parameter in Thomson model, it can be seen from Fig. 5-11 that Thomson model fits the development of compliance with various loading stress and ages well. Viscoelastic creep modulus, $E_{v,co}(t')$ is defined as the inverse of $J_{tot,0}(t,t')$ as shown in Eq. 5-5. Similar to elastic modulus which is used for evaluating the elastic behavior, viscoelastic modulus can be used for evaluating the viscoelasticity of concrete and the resistance of concrete to be deformed viscoelastically.

$$E_{v,cr}(t') = \frac{1}{J_{tot,0}(t,t')} \qquad \text{Eq. 5-5}$$

The ultimate creep compliance $J_{cr,0}(t,t')$ can be expressed as function of $E_{v,cr}(t')$ and $E_e(t')$ by plugging Eq. 5-5 and Eq. 5-4 into Eq. 5-6. As the dependent variable is only the loading age, t', one can conclude that with the same loading age t', the ultimate compliance should be the same

regardless of the loading stress. The Thomson model also can be changed to the form of Eq. 5-6(a) with $J_{cr,0}(t,t')$ as function of $E_{v,cr}(t')$ and $E_e(t')$ in Eq. 5-6(b).

$$J_{cr}(t,t') = J_{cr,0}(t,t') \quad * \left(1 - exp\left(-\frac{(t-t')}{\lambda(t')}\right)\right) \qquad \text{Eq. 5-6(a)}$$

$$J_{cr,0}(t,t') \quad = \frac{1}{E_{v,cr}(t')} - \frac{1}{E_e(t')} \qquad \text{Eq. 5-6(b)}$$

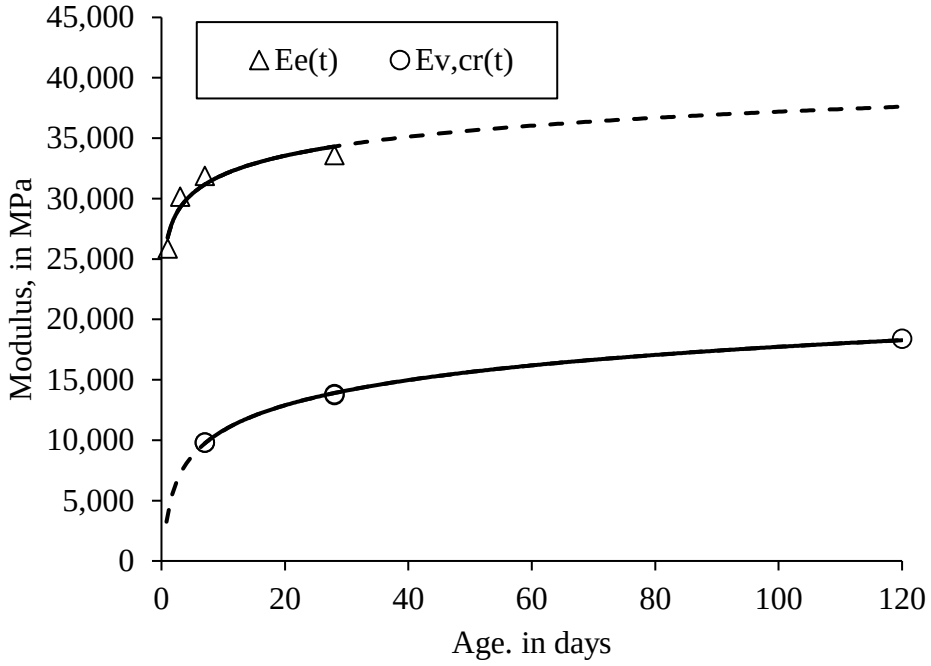

Fig. 5-12 Creep modulus and elastic modulus versus age

The estimated viscoelastic creep modulus versus loading ages are plotted in Fig. 5-12 with the elastic modulus. It can be seen that both elastic and viscoelastic modulus can be fitted using logarithmic function. A constant difference between $E_{v,cr}(t')$ and $E_e(t')$ can be seen which infers that $E_e(t')$ is always larger than $E_{v,co}(t')$. Fig. 5-13 is a schematic diagram illustrating the corresponding stress-strain development under multiple external stress levels. It can be pointed out from Fig. 5-13 that $E_{v,cr}(t')$ is never larger than $E_e\ (t')$ and it guarantees $J_{cr,0}(t')$ is non-negative, which is consistent with Eq. 5-6(b). It is also suggested that a unique relationship exists for a given concrete between viscoelastic modulus and elastic modulus at time of loading since the modulus of elasticity and creep are both related to cement hydration process.

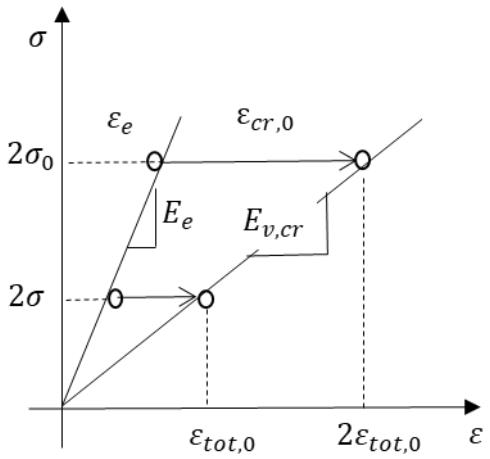

Fig. 5-13 Sketch of elastic and viscoelastic stress-strain relation in compression creep test

The total compliance, which is the sum of elastic and basic creep strain under unit stress, can be expressed as Eq. 5-7 after transformation:

$$J(t,t') = \frac{f}{E_{v,cr}(t')} + \frac{1-f}{E_e(t')} \qquad \text{Eq. 5-7}$$

Where $f = 1 - exp\left(-\frac{(t-t')}{\lambda(t')}\right)$

This equation infers that with the f increases to 1, $J(t,t') = \frac{1}{E_{v,cr}(t')}$ finally. The development creep behavior can be regarded as the process of concrete transferring from elastic to viscoelastic materials. While $f = 1$, the concrete becomes complete viscoelastic material.

5.4 Creep relaxation and modeling

For the creep strain, it can be expressed as the function of external loading $\sigma_c(t_0)$ and $J(t,t_0)$ in Eq. 5-8.

$$\varepsilon_{cr}(t) = \sigma_c(t_0)J(t,t_0) + \int_{t_0}^{t} J(t,t')d\sigma(t') \qquad \text{Eq. 5-8}$$

Where $J(t,t')$ = creep compliance function, representing the total stress dependent strain per unit stress. The relaxation modulus $\Delta R(t_k)$ at given time t_k can be numerically calculated by

$$\Delta R(t_k) = \frac{\sum_{i=1}^{k}\{[J(t_{k-1},t_i)+J(t_{k-1},t_{i-1})]-[J(t_k,t_i)+J(t_k,t_{i-1})]\}}{[J(t_k,t_k)+J(t_k,t_{k-1})]}\Delta R(t_i) \qquad \text{Eq. 5-9}$$

The calculation step to obtain $\Delta R(t_k)$ is attached in APPENDIX C. The simulated relaxation modulus for 0.35-70% starting from 7, 28 and 120 days are plotted together with elastic modulus and viscoelastic modulus in Fig. 5-14**.** One interesting finding about the simulated relaxation modulus is that it always starts from elastic modulus and ends at the value almost same as the corresponding viscoelastic modulus for given mix and loading ages. This simulation result validates the simulation of relaxation modulus since the viscoelastic modulus derived from creep test and relaxation modulus reach the identical result. The relaxation in percent is plotted against loading time with normalized basic creep for 0.35-70% (7d) in Fig. 5-15. It can be seen that the relaxation modulus reaches asymptotic value a bit faster than basic creep which is consistent with finding by Atrushi (2003). Calculations of relaxation is done by programming in MATLAB and the Matlab code is attached in APPENDIX D.

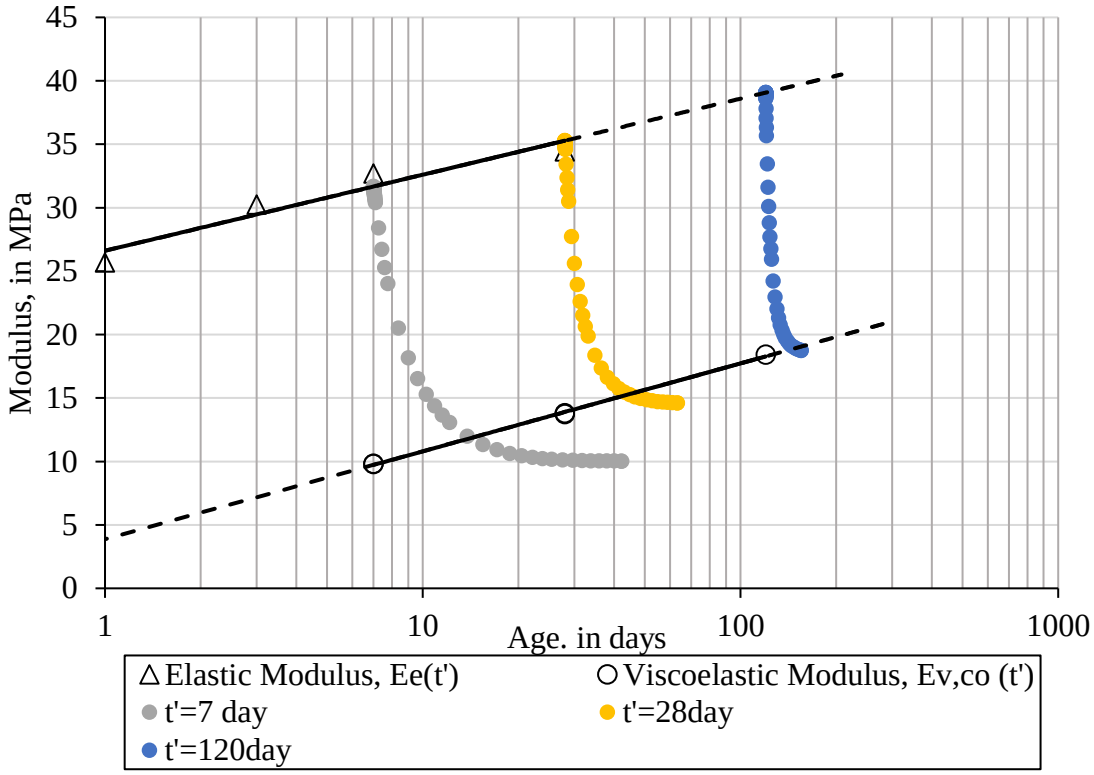

Fig. 5-14 The relaxation modulus for 0.35-70% at various ages together with elastic modulus and viscoelastic modulus

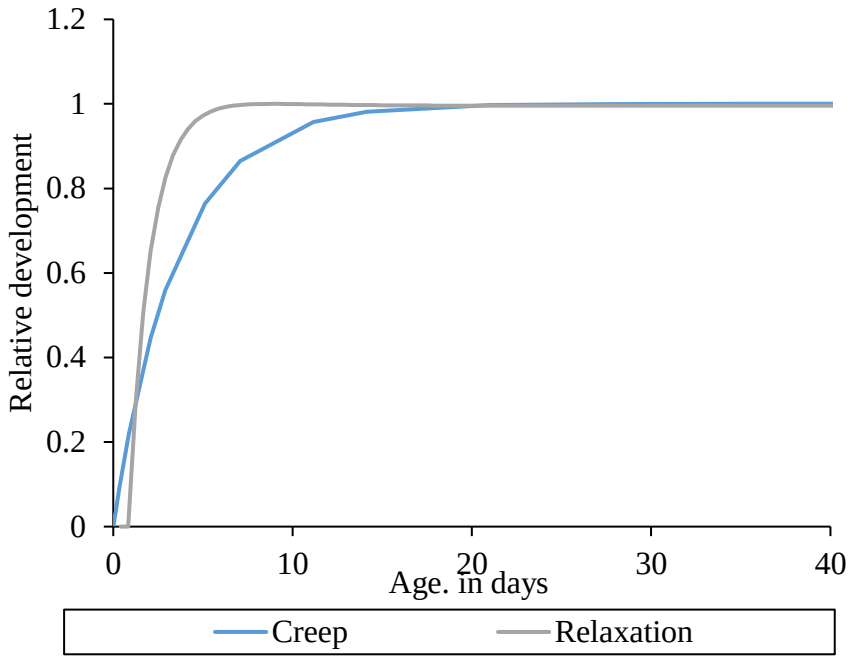

Fig. 5-15 Relative development of creep and relaxation of 0.35-70% with loading starts from 7d

5.5 Factors affecting basic creep

5.5.1 Aging effect

For investigating the effect of aging on the development of basic creep, the ultimate creep strain and ultimate creep compliance of various mixes are plotted against loading ages in Fig. 5-16**.** It can be seen the ultimate total strain decreases with loading age. The ultimate total strain $\varepsilon_{tot,0}$ and ultimate compliance $J_{tot,0}$versus age for other mixes are available in APPENDIX E**.** The tendency is consistent with the increasing viscoelastic modulus versus time.

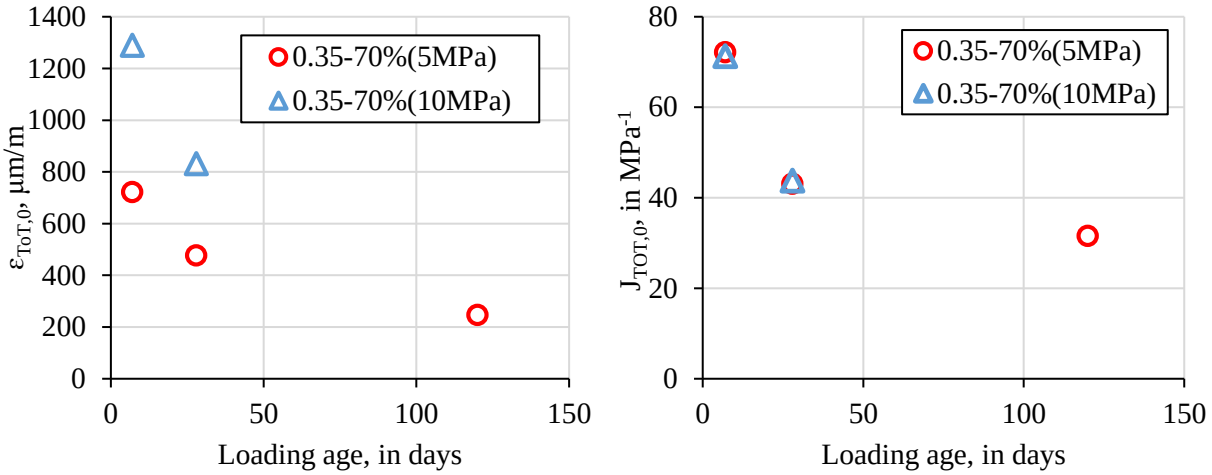

(a) (b)

Fig. 5-16 The ultimate total strain and compliance for 0.35-70% at 7, 28 and 120 days

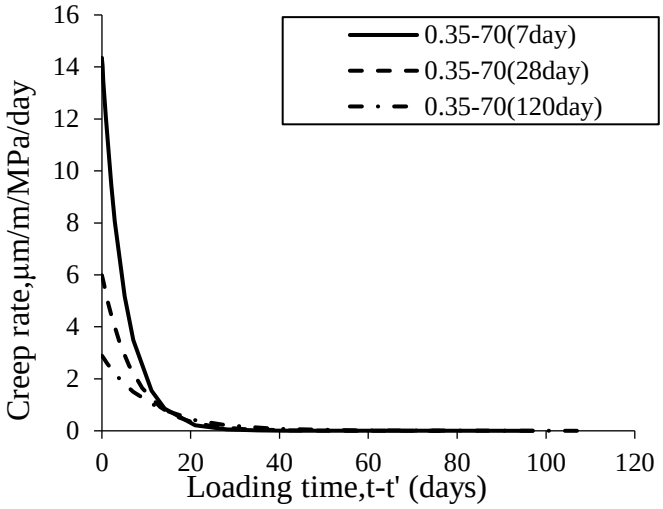

Fig. 5-17 The creep rate development versus loading time for 0.35-70%

With the creep rate plotted versus loading time for 0.35-70% with loading age of 7, 28 and 120 days in Fig. 5-17, a lower creep rate is observed with the increase in loading age. The coefficient of viscosity for various loading ages are plotted in Fig. 5-18. It can be seen that with increase in loading ages, the viscosity increases which means that rate of creep is lower for concrete loading from later ages. For better understanding the meaning of higher coefficient of viscosity, the f function in Eq. 5-7 for 0.35-70% (7, 20 and 120 days) is plotted against loading ages in Fig. 5-19. One can see that rate of transformation from elastic to viscoelastic materials for loading starting from later age is slower. Inverse to the aging effect on creep modulus, the percentage of

reduction in relaxation modulus R(t) is smaller at later age. Since generally the relaxation is the inverse of creep behavior, the ultimate relaxation should be higher at later age when ultimate creep is lower. Therefore a lower reduction in relaxation modulus is expected.

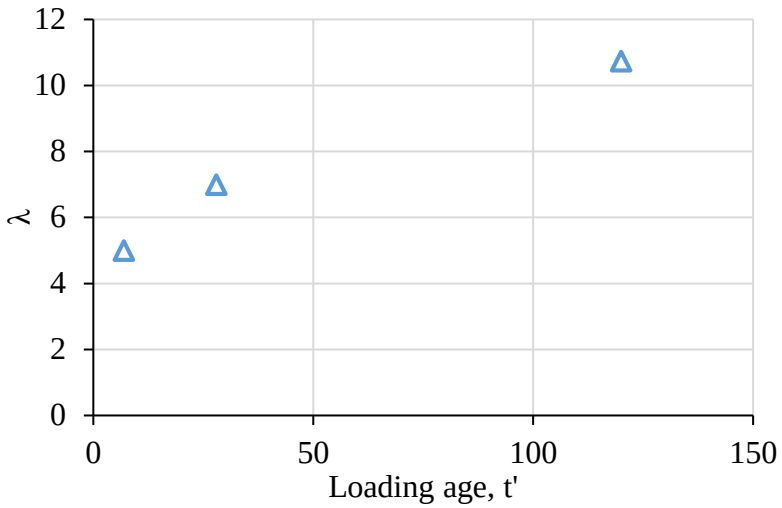

Fig. 5-18 The development of coefficient of viscosity at various loading ages for 0.35-70%

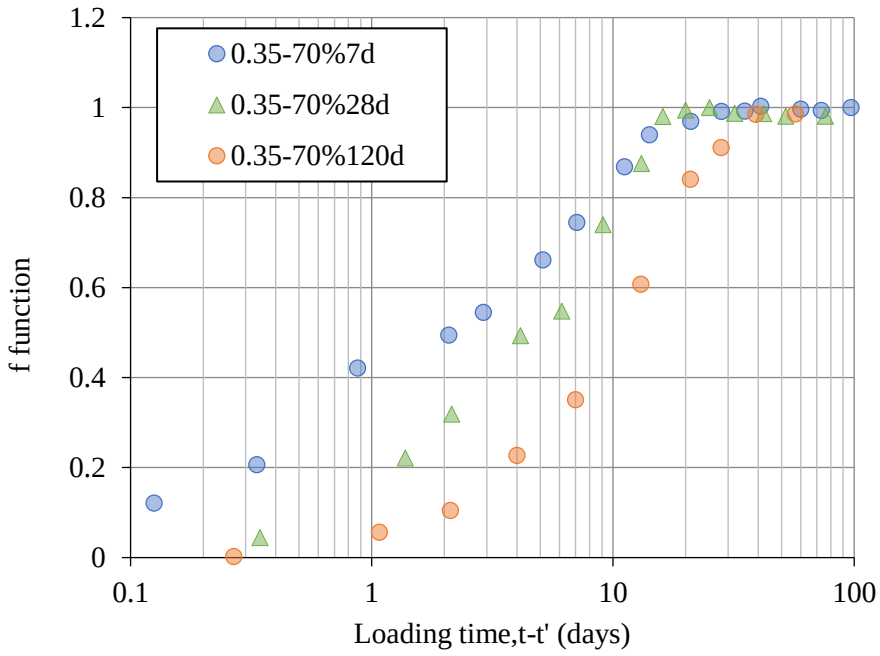

Fig. 5-19 The development of f function versus loading time for 0.35-70% (7, 28 and 120 days)

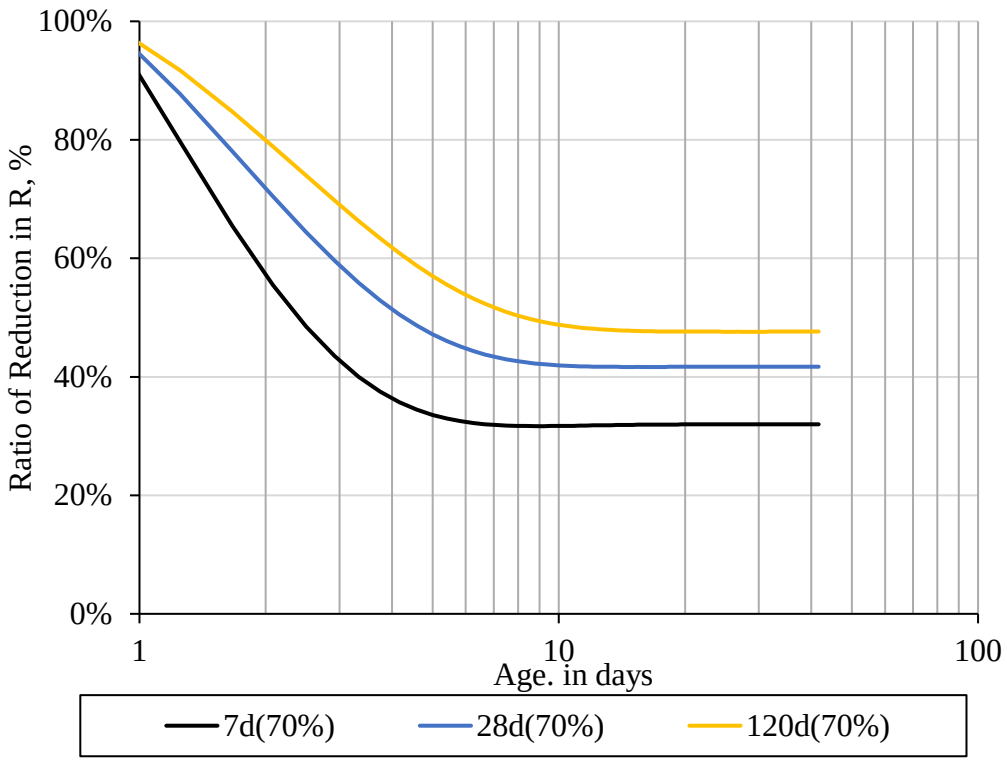

Fig. 5-20 The ration of reduction in R for 0.35-70% (7, 28 and 120 days)

Analogy to the definition of creep coefficient on ACI 209, the ultimate creep coefficient, $C_u(t')$ refers to the ratio of ultimate creep and elastic strain. $C_u(t')$ can be expressed as a function of $E_e(t')$ and $E_{v,cr}(t')$. In this work, only ultimate viscoelastic condition is expected to reflect real material properties. Eq. 5-10 can only be applied when creep strain reaches the ultimate value.

$$C_u(t') = \frac{\varepsilon_{cr,0}}{\varepsilon_e} = \frac{E_e(t')}{E_{v,cr}(t')} - 1 \qquad \text{Eq. 5-10}$$

Ultimate creep coefficient at loading ages of 7, 28 and 120 days are calculated by implementing Eq. 5-10 and shown in Fig. 5-21 together with literature data. For the aging factor, ACI model implements a loading factor with the form of exponential equation with the power of -0.118 to predict it:

$$\gamma_{c,to} = 2.35 t_0^{-0.118} \qquad \text{Eq. 5-11}$$

It can be seen from Fig. 5-21 below that good fitting is obtained by directly applying this equation to predict the time effect on ultimate creep coefficient for both the data proposed in this

paper and reference. The reference data comes from the concrete database for creep and shrinkage in http://iti.northwestern.edu/ as described by Bazant *et al*, (2008). It can be seen that $C_u(t')$ is larger than 1 which infers $E_e(t') > 2 * E_{v,cr}(t')$. It infers a conclusion that viscoelastic deformation is linearly related to mechanical property of concrete and the contribution of mechanical properties on viscoelastic deformation is similar regardless of mix specification. In other word, the effect of mix specification on creep and elastic deformation is similar which leads to the almost identical creep coefficient across various mixes.

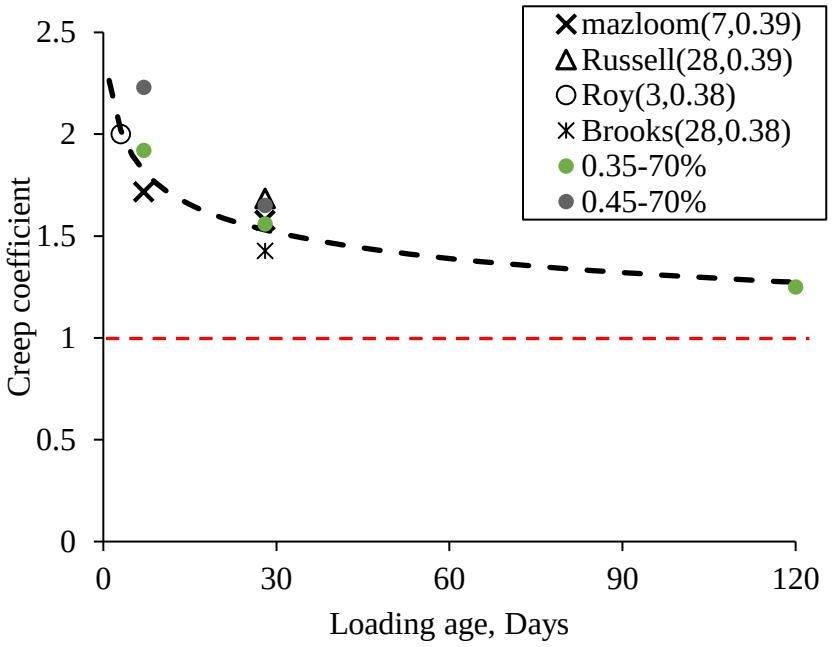

Fig. 5-21 Ultimate creep coefficient predictions based on this study and reference

5.5.2 Aggregation content

The most important effect of aggregate on concrete is the increase in the strength and modulus of concrete. As mention in Chapter 2, the modulus of elasticity can be represented as the equation of matrix modulus E_m , and aggregate modulus E_p:

$$\frac{1}{E} = \frac{(1-g)}{E_m} + \frac{g}{E_p} \qquad \text{Eq. 5-12}$$

In which g, E_m and E_p are the aggregate content, matrix modulus and aggregate modulus. While the g increases, the concrete elastic modulus also increases. As shown in Fig. 5-22, the total strain decreases with the increase in aggregate content. The development of strain over the whole loading period for 0.35 with different aggregate contents loading at 7 days under 5MPa is plotted in Fig. 5-23 as an example.

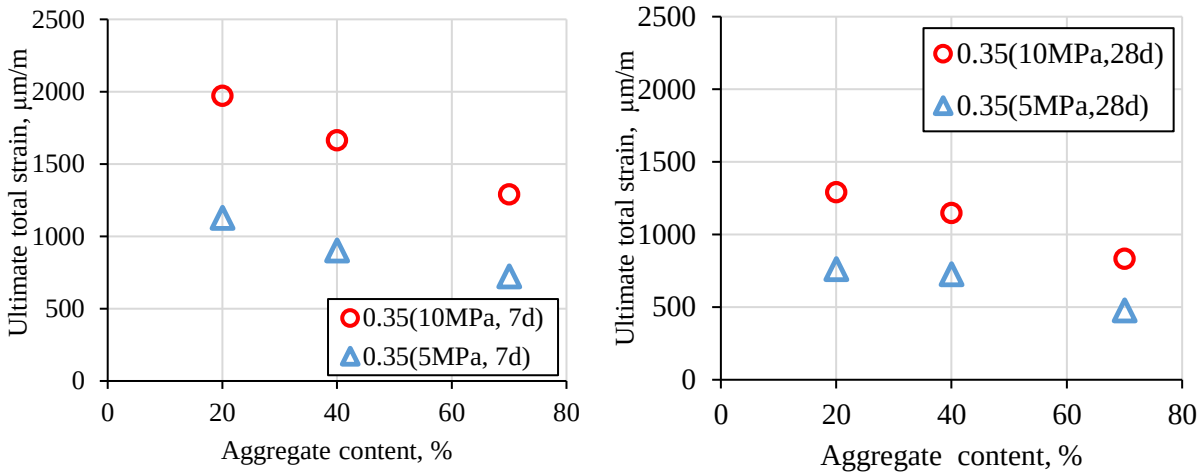

Fig. 5-22 The ultimate total strain of 0.35-70% starting from (a)7 days and (b) 28 days with two loading stresses (5MPa and 10MPa)

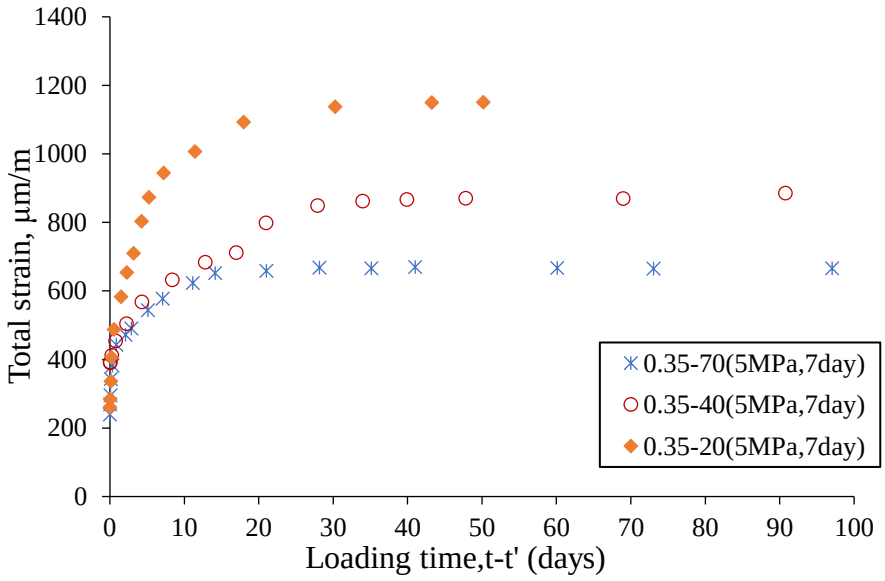

Fig. 5-23 The development of strain of 0.35 w/c with various aggregate contents loading at 7 days under 5MPa external stress

The ultimate creep compliance is normalized to that of the mix of paste for creep results of 0.35 and 0.45 with various loading ages. The compliance of paste is estimated by linear back extrapolation of the data shown in Fig. 5-22 to paste. It can be seen from Fig. 5-24 that $J_{tot,0}(g)/J_{tot,0}(0\%)$ is almost the same for various loading ages and two water/cement ratios. It can be concluded that an exponential correlation between compliance and aggregate content can be built and this correlation is independent on loading ages and water/cement ratio.

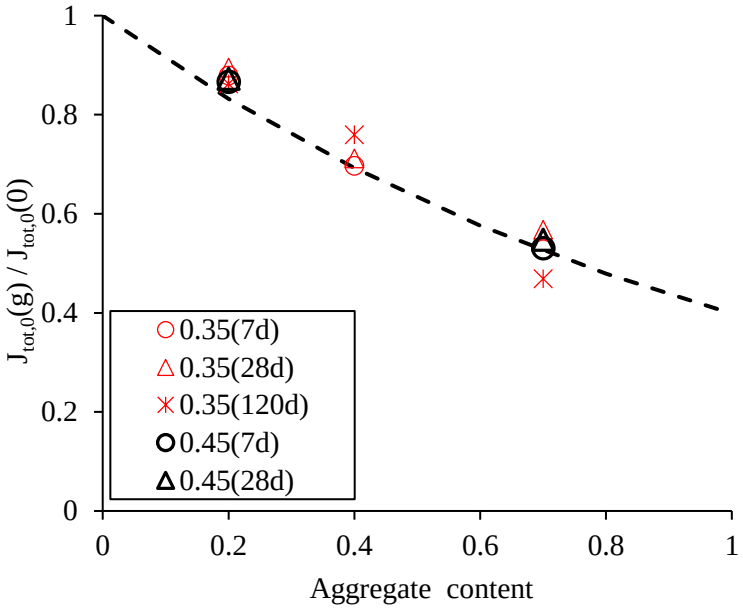

Fig. 5-24 Relative compliance versus aggregate content for HPC with 0.35-70% and NSC with 0.45-70%

To investigate the effect of aggregate on the creep rate, the total strain development for 0.35 mixes at 7 days and 28 days under 5 MPa are normalized by ultimate total strain and plotted in Fig. 5-25(a) and (b). It can be seen that there is no clear tendency of the effect of aggregate content on creep rate comparing the normalized compliance of same w/c mix for both 7 days and 28 days as the loading ages. The Thomson model with aggregate content as the variable can be modified to Eq. 5-13. The development of basic creep at any given aggregate content with same water/cement ratio can be estimated by linear interpolation with the known of reference mix result.

$$J(t,t',g) = \frac{f}{E_{v,cr}(t',g_0)\times(0.3*e^{0.01g})} + \frac{1-f}{E_e(t',g)} \qquad \text{Eq. 5-13}$$

The g_0 is 70% for the reference concrete. The simulated viscoelastic creep modulus for 0.35-70% with various aggregate contents for loading starting from 7, 28 and 120 days are plotted in Fig. 5-26. An exponential correlation can be found between viscoelastic modulus and aggregate content regardless of loading ages. The viscoelastic modulus at other given age and aggregate content can be predicted based on the exponential correlation with aggregate contents. After normalizing the creep modulus at other aggregate contents to the one at 70% aggregate for the creep starting from 7, 28 and 120 days, it can be seen in Fig. 5-27 that the one common regression line can be used to fit to all the data with various loading ages. It can be known that the aggregate effect on viscoelastic modulus is independent on loading age. The relative relaxation of 0.35 with 20%, 40% and 70% aggregate contents starting from 7 days are plotted in Fig. 5-28. The relaxation reduction rate is also shown unrelated to the aggregate content and consistent with the result shown in Fig. 5-25. As the same effect of aggregate content on viscoelastic modulus, the asymptotic relaxation in percent increases with the increase in aggregate content.

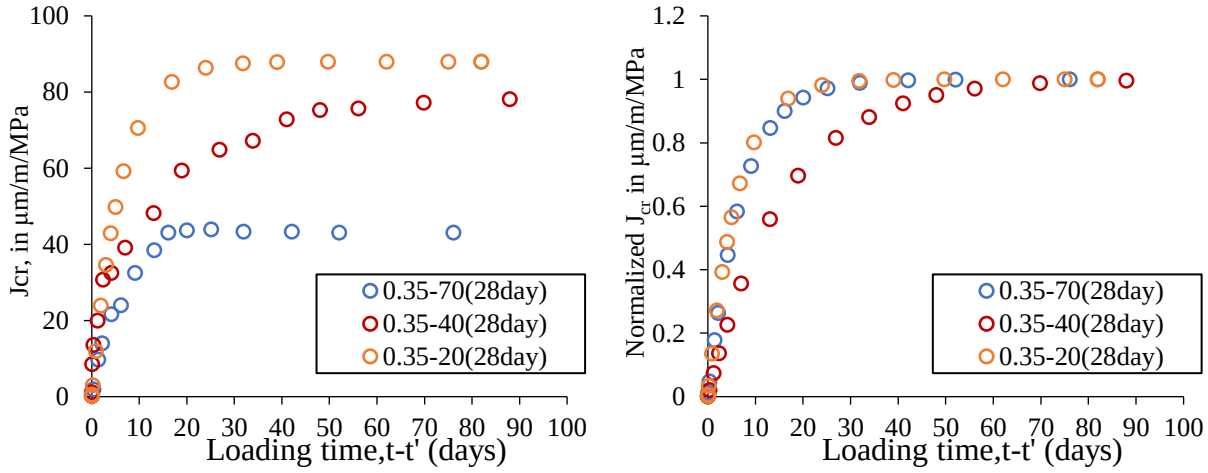

(a) (b)

Fig. 5-25 Normalized compliance for 0.35 with various loading ages

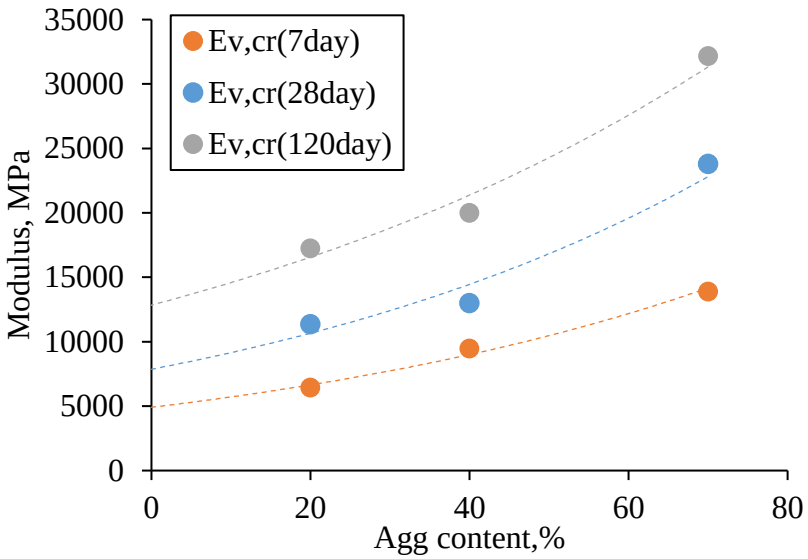

Fig. 5-26 Viscoelastic modulus versus aggregate content for loading starting from 7, 28 and 120 days

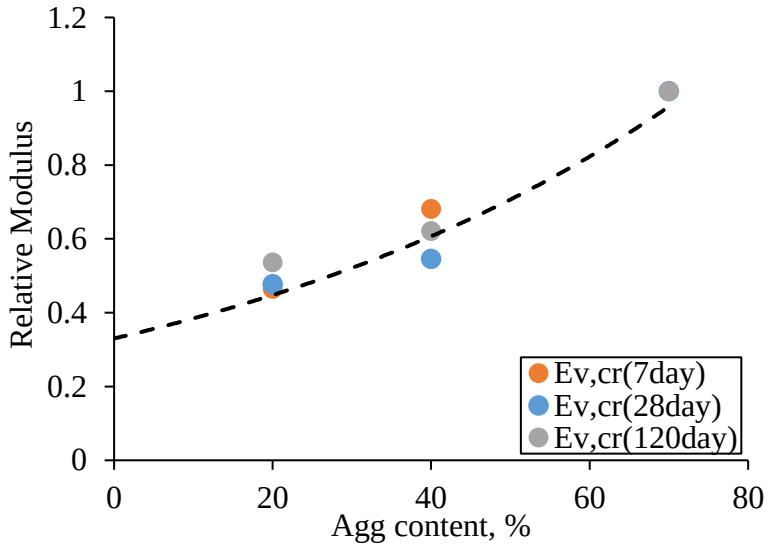

Fig. 5-27 Normalized viscoelastic modulus versus aggregate content for loading starting from 7, 28 and 120 days

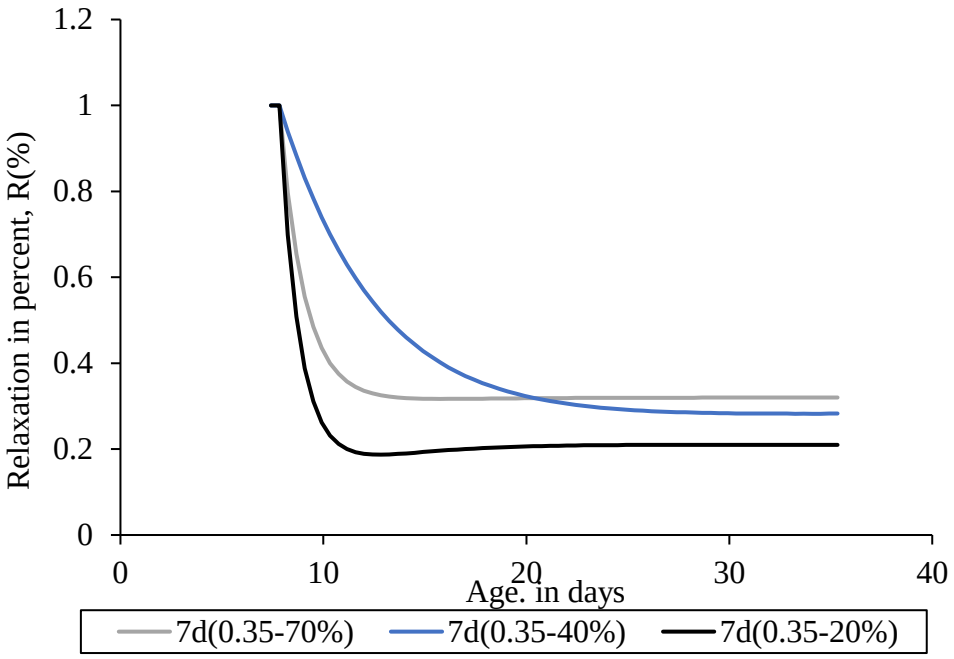

Fig. 5-28 The relaxation in percent R(t) for 0.35 with (20%, 40% and 70%) starting from 7 days

5.5.3 Water/Cement ratio

The creep compliance of 0.35-70% and 0.45-70% are plotted against loading time under two loading ages and two loading stresses (5MPa and 10MPa) in Fig. 5-29. It can be seen that the creep rate of 0.35-70 is larger than that of 0.45-70 while the magnitude is smaller than 0.45. The coefficient of viscosity λ is plotted in Fig. 5-30 versus the loading ages for 0.35 and 0.45 water/cement ratio concrete.

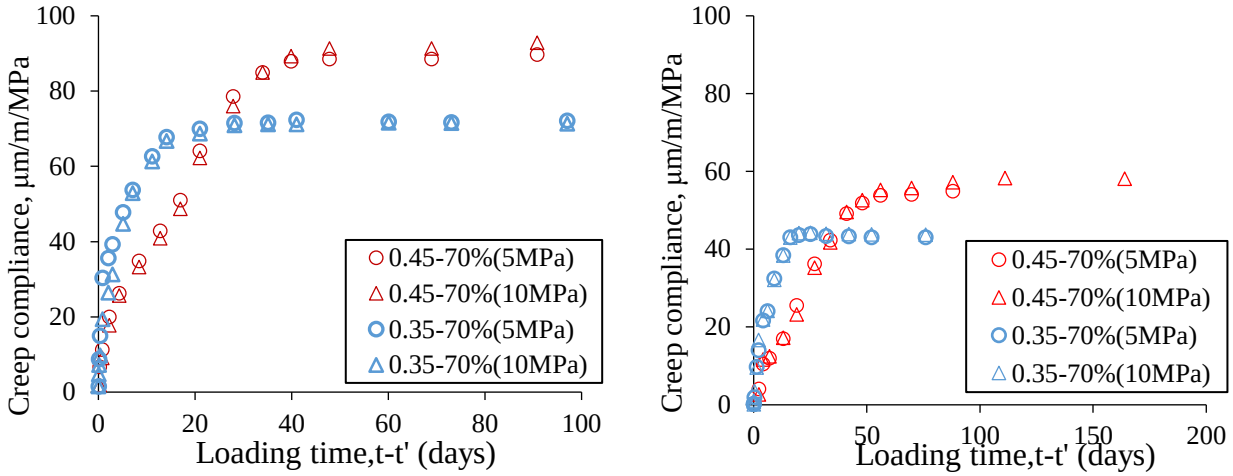

Fig. 5-29 The creep compliance for 0.35-70% and 0.45-70% with starting age at (a) 7 days and (b) 28 days

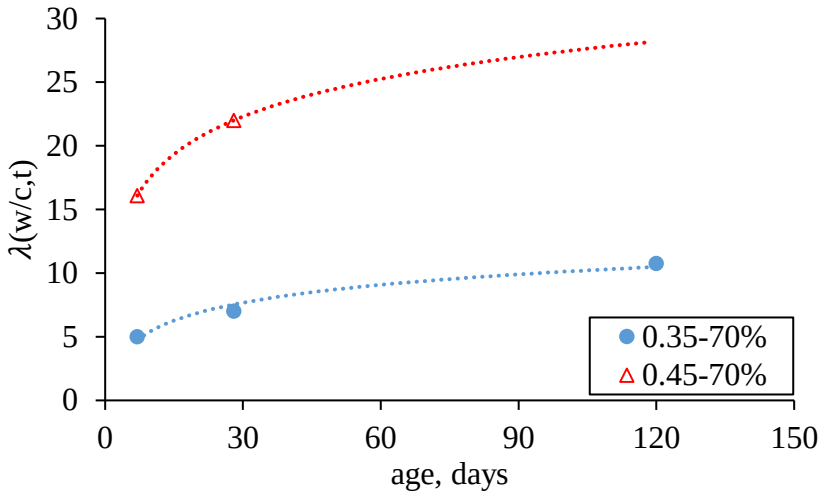

Fig. 5-30 Coefficient of viscosity for 0.35-70% and 0.45-70%

A log function with variable w/c and t' then can be used to fit the development of coefficient of viscosity $\lambda(t')$ versus loading ages for various water/cement ratio shown in Eq. 5-14.

$$\lambda(t', w/c) = f\left(\frac{w}{c}, t'\right) = \left[a * \left(\frac{w}{c}\right) + b\right] \cdot (\ln t' + c) \qquad \text{Eq. 5-14}$$

Analogical to elastic modulus which is proportional to compressive strength, the larger ultimate creep compliance of 0.45 system should be also due to the smaller strength of 0.45 concrete. After normalizing the creep compliance of 0.45-70% to HPC 0.35-70% by multiplying the ratio of 7 days compressive strength between 0.45 and 0.35 w/c concrete, one can see that the ultimate

creep compliance for 0.35 and 0.45 are the same, shown in Fig. 5-31. The ultimate creep compliance is thus approximately inversely proportional to the compressive strength. Thomson model can then be modified to a function of loading time t, loading age t', water/cement ratio w/c and aggregate content g. With knowing of the compressive strength with other w/c ratio and the same age and other materials specification, the development of creep compliance can be predicted by applying Eq. 5-15.

$$J(t,t',w/c,g) = \frac{f}{E_{v,cr}(t',0.35,70\%)\times(0.3*e^{0.01g})\times(-6*(w/c)+3)} + \frac{1-f}{E_e(t',w/c,g)} \qquad \text{Eq. 5-15}$$

Where $f = \left(1 - exp\left(-\frac{(t-t')}{\lambda(t',w/c)}\right)\right)$

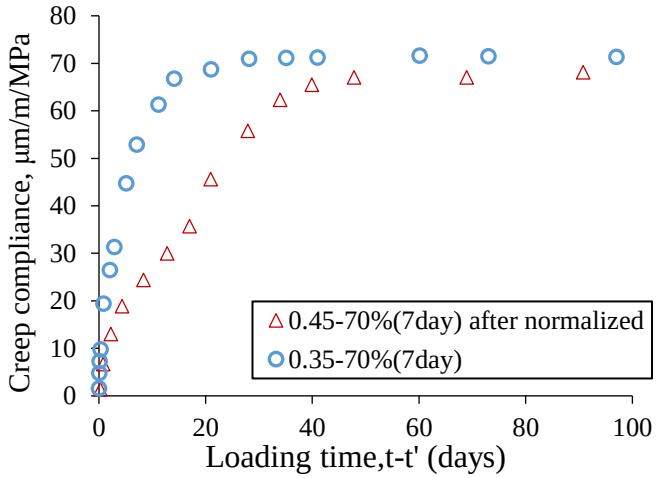

Fig. 5-31 Creep compliance for 0.35-70% and 0.45-70% after normalization

The w/c_0 and g_0 are 0.35 and 70% as the reference materials specification. For validating the test result in this research, several creep data of HPC with various w/c ratio from other research measured from the same starting loading age was added into Fig. 5-32 together with the measured 0.35-70% and 0.45-70% with all starting from 28 days. All the creep data are sealed curing and normalized to the creep data at 100 days after the starting of loading. It can be seen from Fig. 5-32(a) that the normalized creep data across various research are quite similar. The data of the reference is still coming from the concrete database for creep and shrinkage in http://iti.northwestern.edu/ as described by Bazant *et al*, (2008). While larger variation exits in the mixing environments, curing condition and mineral contents in the materials used in all the researches, larger variation also exists in the magnitude of creep. The external stress is

normalized by the 28 days compressive strength to modify all the loading levels to the same stress/strength ratio for investigating the basic creep intrinsic discipline. While it is already confirmed by 5.5.2 that aggregate contents have no effect on the creep rate, the creep rate is supposed to be only related to water/cement ratio. It can be seen that the creep curves from other reference are all between curves of 0.35 and 0.45 mix and the creep rate decrease with increase in w/c, which confirms the assumption on the water/cement effect on creep rate. The coefficient of viscosity λ for all the systems from reference are obtained by curve-fitting using modified Thomson model and plotted against w/c including the 0.35 and 0.45 system measured in this study in Fig. 5-32(b). It can be seen that roughly the coefficient of viscosity increases with water/cement ratio.

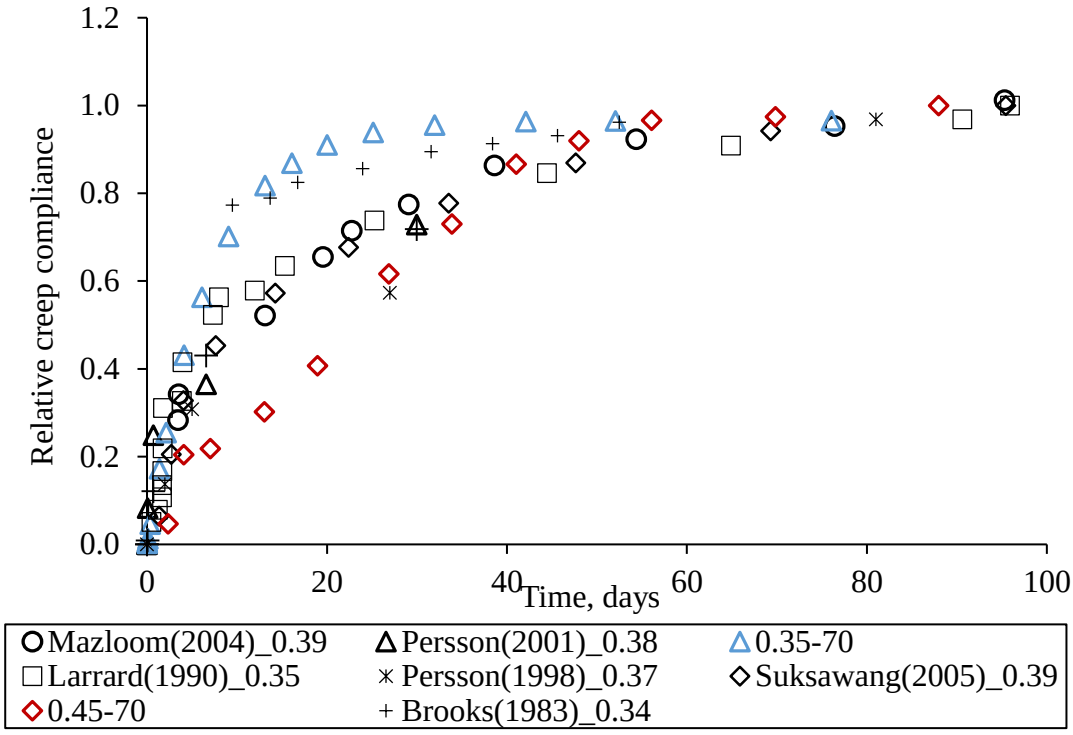

(a)

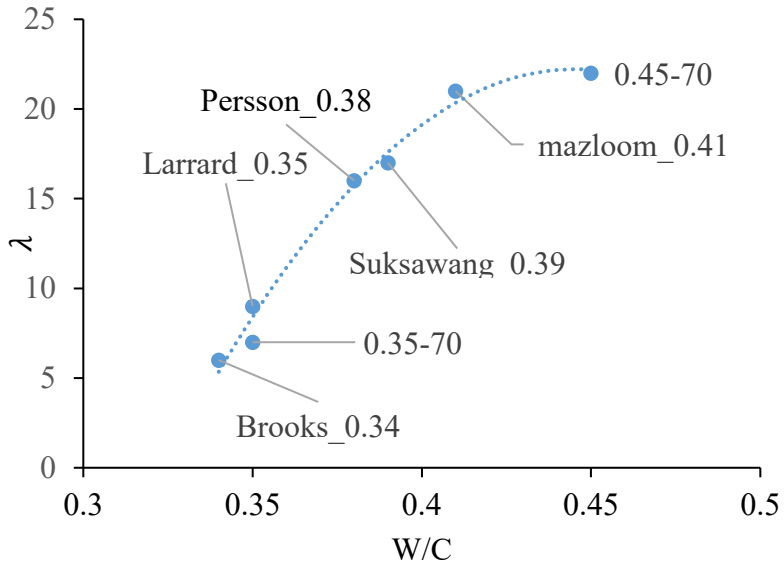

(b)

Fig. 5-32 (a) Normalized creep strain for various sealed creep test starting from 28 days (b) coefficient of viscosity versus w/c

5.5.4 SCM replacement ratio

Supplemental cementitious materials is usually used for improving the durability of concrete by reducing the permeability, improving the long term strength and consolidation. GGBFS is used here for comparing the effect of SCM on the development of basic creep of HPC.

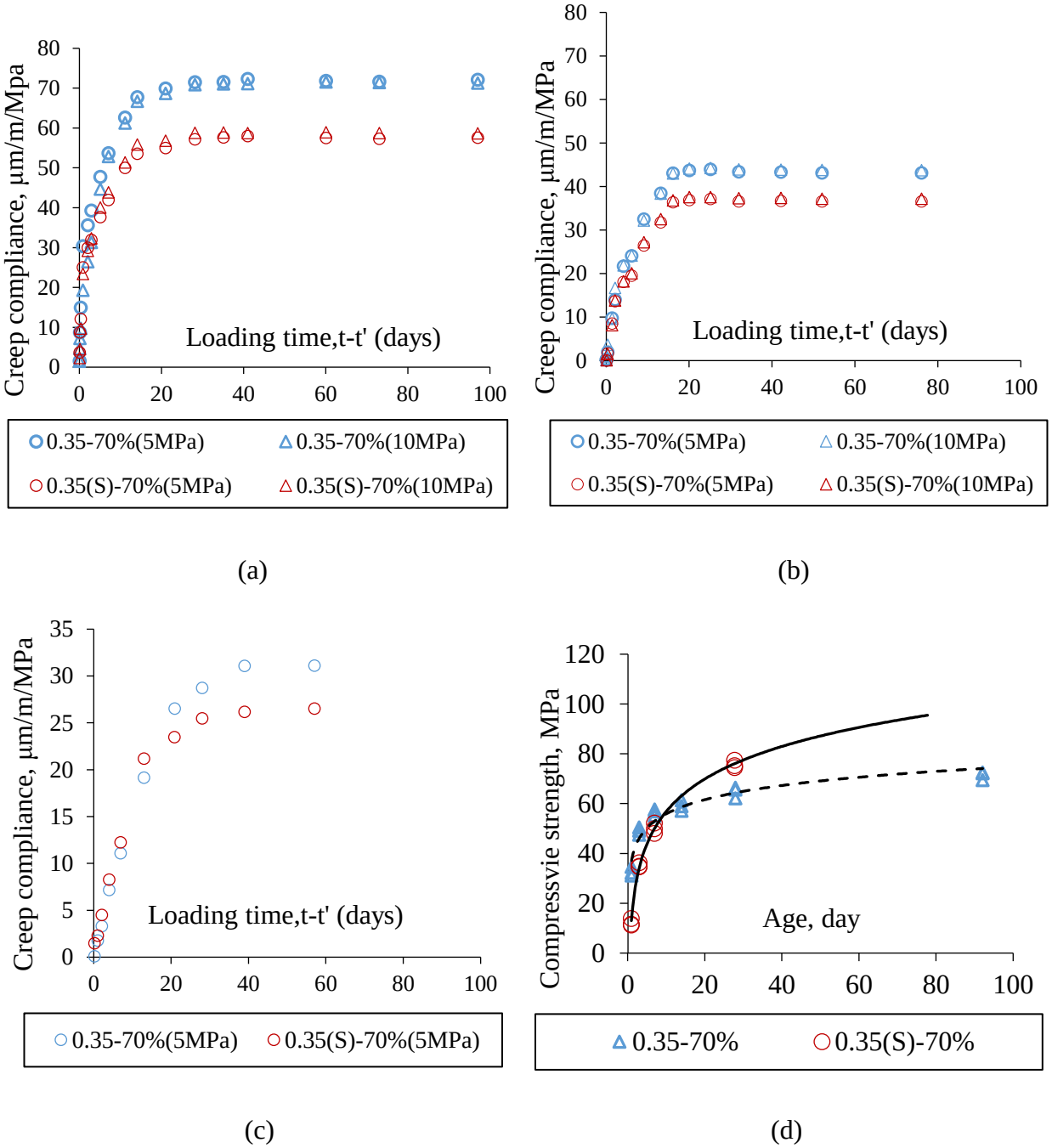

Fig. 5-33 The creep compliance of HPC with and without slag with the same w/c and aggregate content for (a) 7 days (b) 28 days and (c) 120 days and (d) compressive strength

It can be seen from Fig. 5-33(a), (b) and (c) that the creep compliance of 0.35-70 with 50% replacement by GGBFS is lower than that of 0.35-70 without GGBFS with small difference. The test result can be confirmed by the similar compressive strength test of 0.35-70% and 0.35(S)-70%. Since there is no large difference between the creep rate of the basic creep of HPC between the one with and without GGBFS, SCM affects basic creep by affecting the elastic modulus.

5.5.5 LWA effect

To investigate the effect of lightweight aggregate on the development of basic creep, the HPC with 0.35 w/c, 70% aggregate, 50% GGBFS and 50% LWA was conducted with creep test under two ages (7 days and 28 days) under two different loading stress (5MPa, 10MPa) and the creep compliance is shown below in Fig. 5-34.

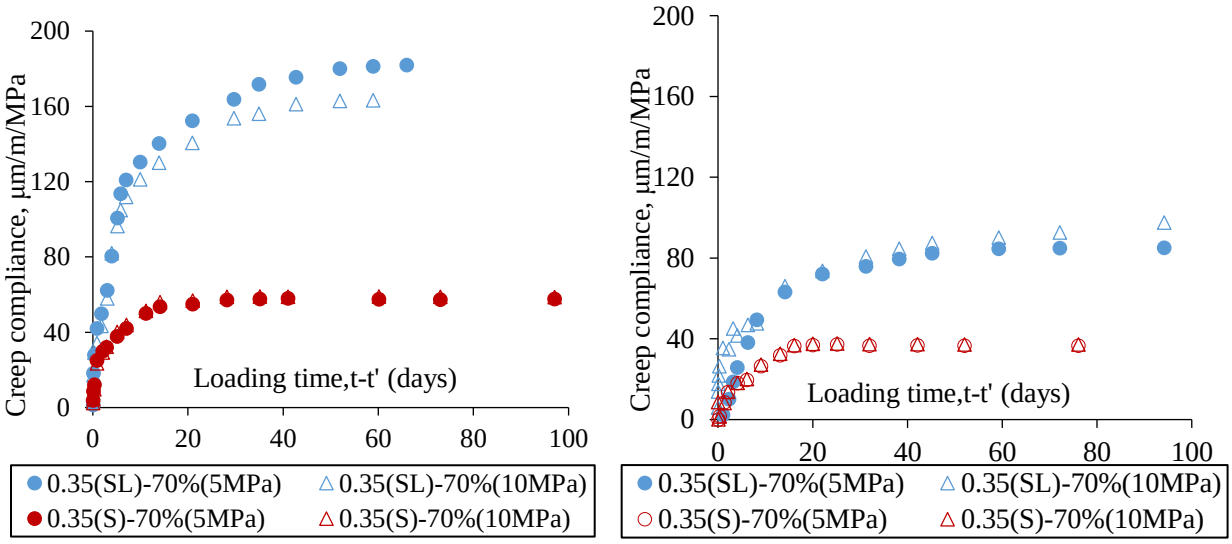

Fig. 5-34 The creep compliance of 0.35(SL)-70% and 0.35(S)-70% under two loading stress (5MPa and 10 MPa) and two loading ages (7 days and 28 days)

It can be seen that the creep compliance of HPC with LWA is much larger than that of HPC without LWA. This can be due to the lower compressive strength with the effect of LWA, shown in Fig. 5-35. After normalizing the 0.35(L)-70% creep compliance by the ratio of 7 days

compressive strength of 0.35(L)-70% and 0.35(SL)-70%, it can be seen from Fig. 5-36 that the ultimate creep compliance are very similar. The result confirms that the the effect of LWA on creep is only through affecting the magnitude by reducing the strength of concrete.

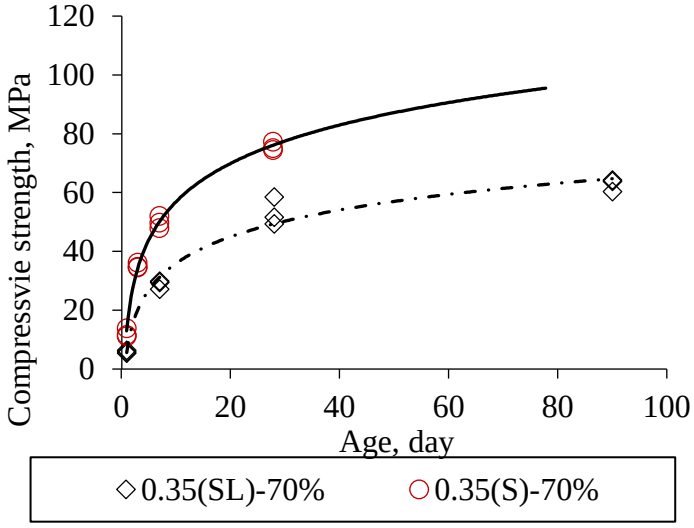

Fig. 5-35 The compressive strength comparison between 0.35-70%, 0.35(S)-70% and 0.35(SL)-70%

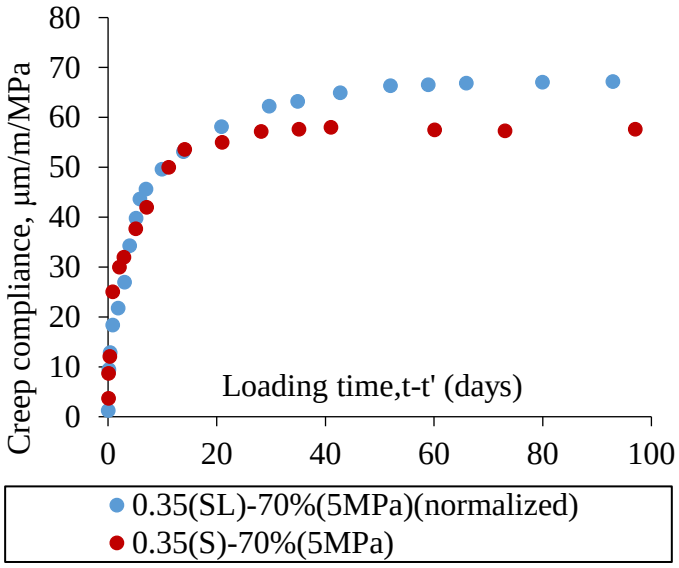

Fig. 5-36 The creep compliance versus loading time for 0.35(S)-70% and 0.35(SL)-70%

5.6 Approximate estimate of viscoelastic modulus

While plotting the normalized external stress versus the ultimate total strain about 90-100 days after the loading for both the data used in this research and other reference, a common linear correlation between normalized stress and ultimate total creep can be found, as shown in Fig. 5-37 and Eq. 5-16. The data of the reference is cited from the concrete database for creep and shrinkage in http://iti.northwestern.edu/ as described by Bazant *et al*, (2008).

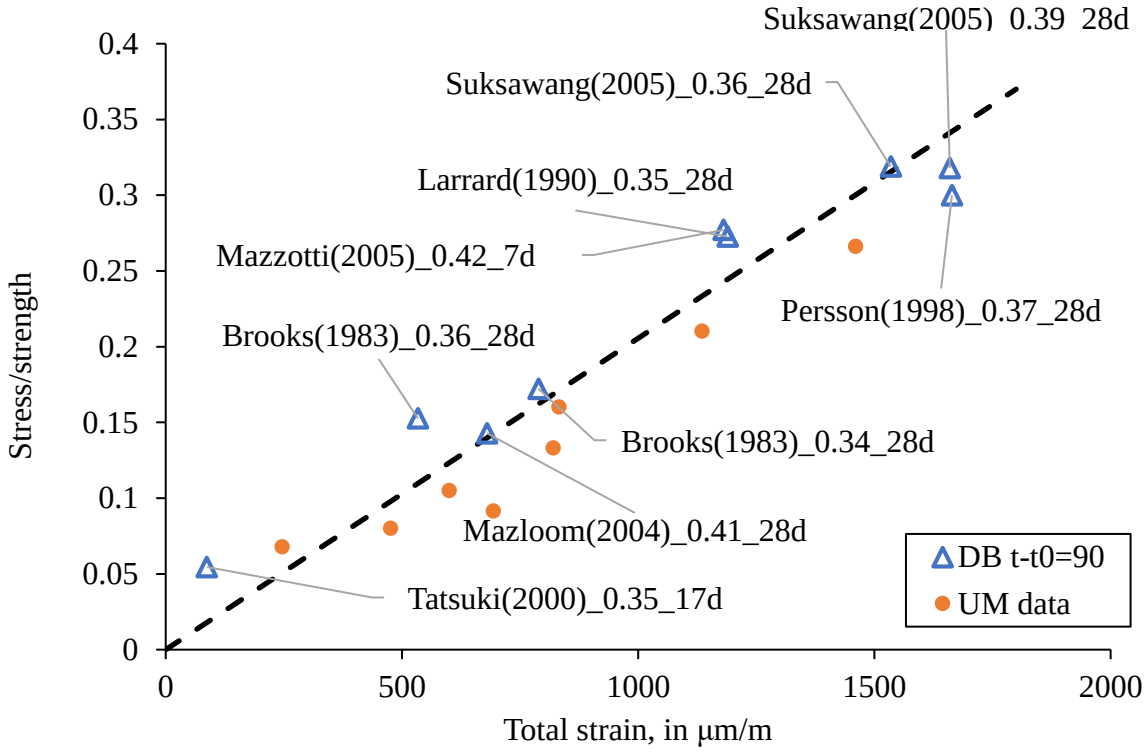

Fig. 5-37 The ratio of stress and ultimate creep versus ultimate basic creep for both literature and data in this research

$$\frac{\sigma_0/\varepsilon_{tot,0}}{f_{cm}(t')} = \frac{E_{v,co}(t')}{f_{cm}(t')} \approx const \qquad \text{Eq. 5-16}$$

Eq. 5-16 can be transferred to the form of the ratio of viscoelastic modulus and compressive strength. The same ratio across various mixes and loading ages infers that materials specification and loading ages play the important role on the magnitude of creep. With the removal of the effect of mix proportioning and loading ages by being normalized by compressive strength, the viscoelastic modulus is identical. Based on Eq. 5-16, the viscoelastic deformation

for short-term duration without knowing of any materials specification can be estimated as long as the compressive strength at the creep loading age is known.

To validate this conclusion, the development of normalized basic creep starting from various ages are plotted versus time in Fig. 5-38. After the aging effect and materials specification are removed by the normalizing the creep by stress/strength ratio, the creep development are almost identical for both HPC with 0.35 w/c and NSC with 0.45 w/c.

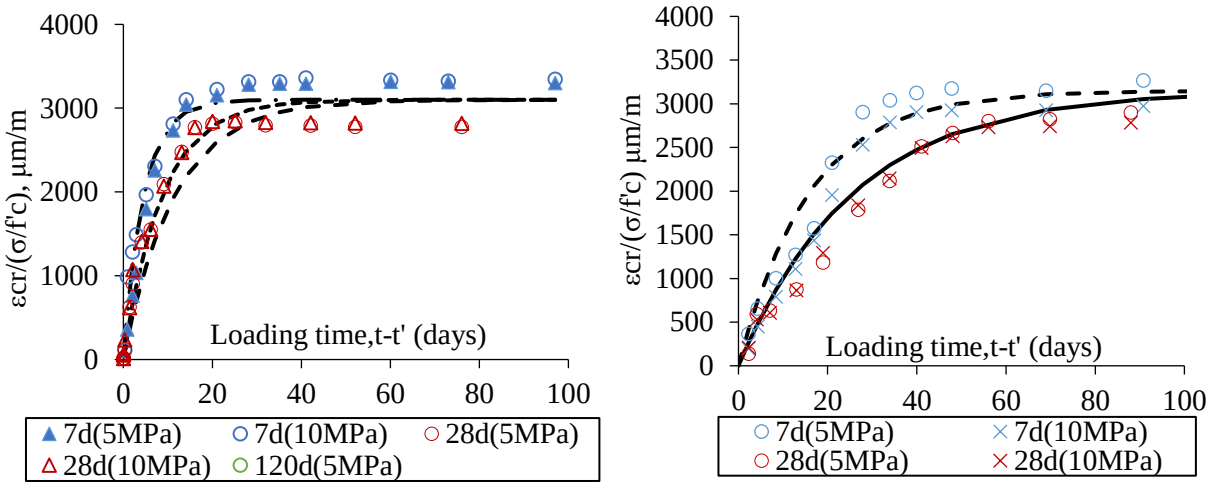

(a) (b)

Fig. 5-38 The normalized basic creep by stress/strength ratio for various loading ages for (a) 0.35-70% and (b) 0.45-70%

5.7 The comparison between drying creep and basic creep

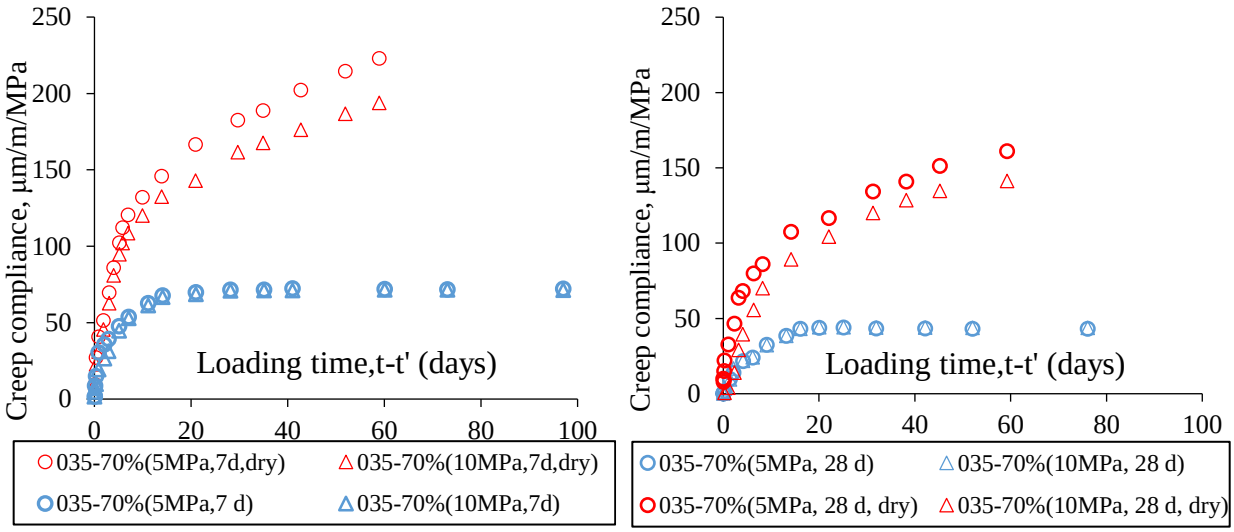

(a) (b)

Fig. 5-39 Creep compliance of 0.35-70% (a) under sealed condition and (b) under drying condition for 7 and 28 day

To verify the measured data, drying creep of 0.35-70% with 7 days and 28 days as the loading age under two stress levels were measured together with unloaded specimens for drying shrinkage measurement shown in Fig. 5-39 and Fig. 5-40. The drying creep strain can be fitted to the logarithmic equation in ASTM C512 in Eq. 5-17. Basic creep and drying creep are both obtained after subtracting the shrinkage from the total strain. While basic creep reaches the ultimate creep strain within 40-60 days since loading, drying creep is assumed to increase linearly with loading time in log scale for years which is consistent with findings in other references.

$$\varepsilon = (1/E) + F(k)\ln(t+1) \qquad \text{Eq. 5-17}$$

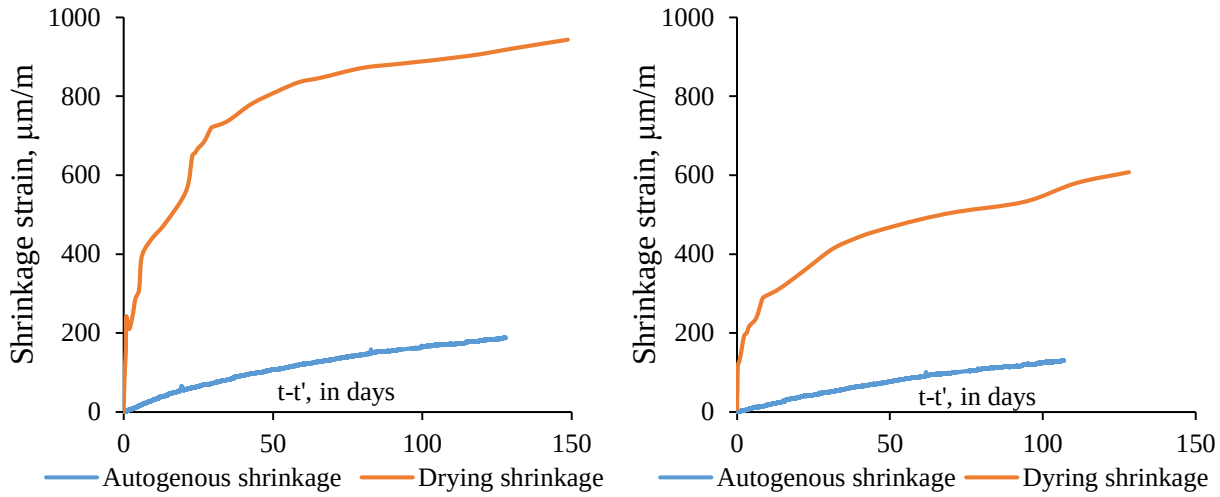

(a) (b)

Fig. 5-40 Free autogenous shrinkage and drying shrinkage for 0.35-70% with starting from (a) 7 days and (b) 28 days

5.8 The unloading and reloading of basic creep

To investigate the behavior of basic creep with unloading and reloading, 0.35-70% starting from 7 days and 28 days were unloaded after constant loading for about 100 days. Reloading was started after unloading for another 20 days to original loading level. 0.35-70% with 5MPa as the starting stress level was then loaded to 10MPa after reloading for 70 days. The corresponding strain development of 0.35-70% with various loading starting ages are shown in Fig. 5-41(a) and (b) with the loading profile shown in Fig. 5-41(c).

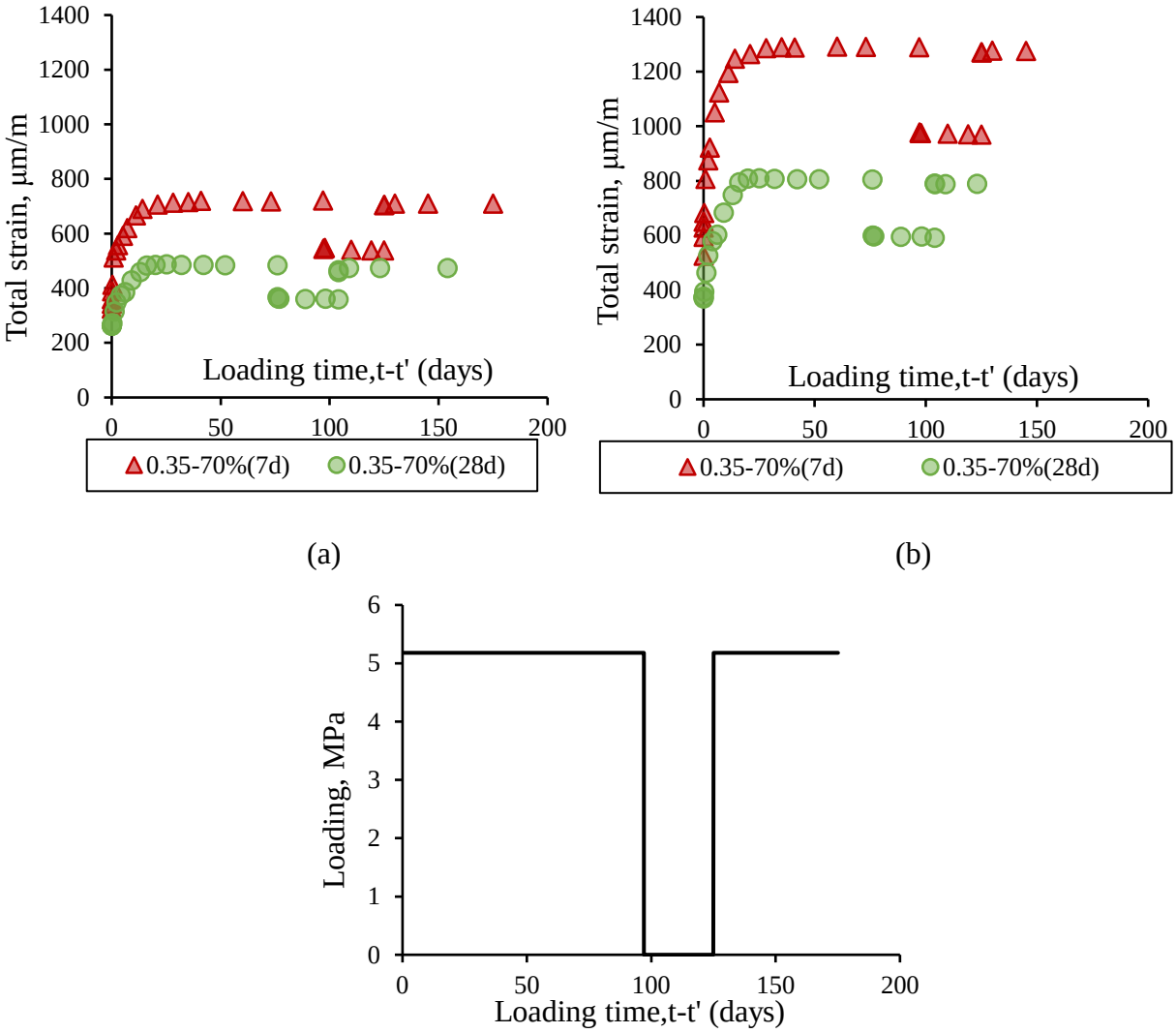

Fig. 5-41 Total strain of with loading and unloading for 0.35-70% under (a) 5MPa and (b) 10MPa with (c) Loading profile

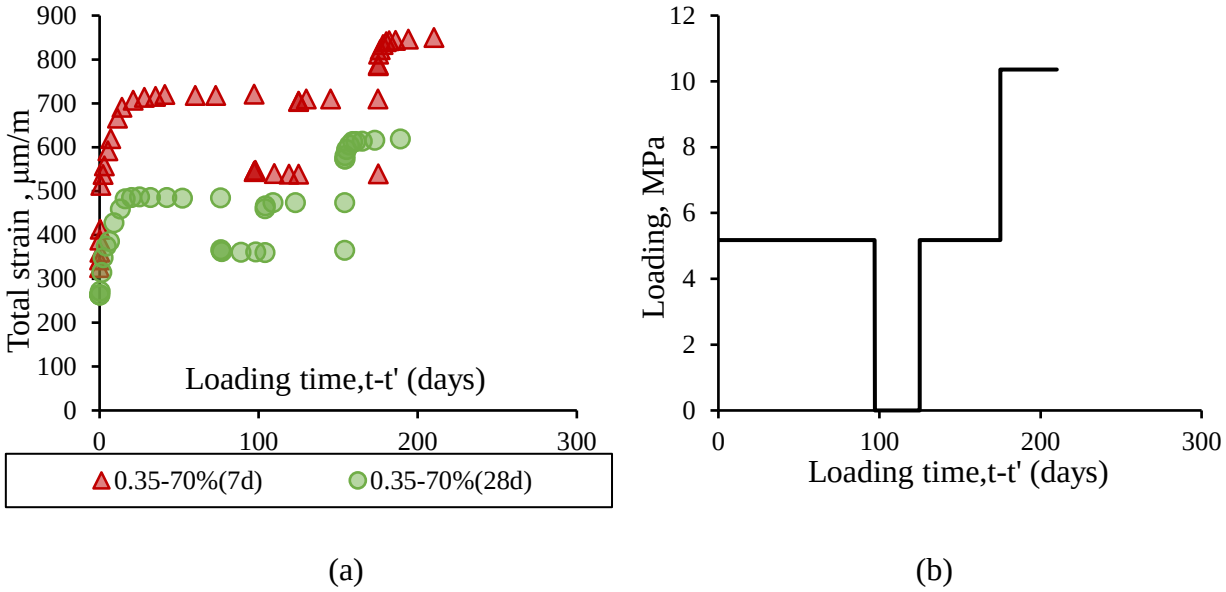

(a) (b)

Fig. 5-42 (a)Total strain of loading, unloading and reloading to 10MPa for HPC with 0.35-70% under and (b)corresponding loading profile

It can be seen that after the unloading, the elastic strain is immediately released with little creep recovery occurring. Except for the minor creep recovery seen from the curve in Fig. 5-41, most of the basic creep is permanent without recovery. After the specimen is reloaded to the same stress level, no significant additional creep strain is observed. It can be concluded from this result that no viscoelasticity exits if we reload the specimen to the same level after it reaches the equilibrium under the same stress level. HPC is assumed similar to elastic materials under this situation. While the specimen is loaded from 5 MPa to 10 MPa shown in Fig. 5-42, the additional creep is observed again and it takes about 30 days to reach the equilibrium strain. This phenomenon is consistent with the seepage theory that creep is arisen as the result of seepage of water. No further creep happens without further seepage of water after the balance is reached and then the balance is broken with the increase in the external loading.

5.9 Summary

In this chapter, the experimental testing and modeling of basic creep behavior under sealed condition of HPC and NSC are discussed. Concluded from long-term basic creep test (100 days) under constant temperature without moisture loss, basic creep reaches ultimate strain after 30-40

days since loading. A modified Thomson Rheological model with underlying physical parameters is applied for the simulation. With the definition of viscoelastic modulus, the magnitude of basic creep can be directly estimated and basic creep can be described as the procedure of concrete transferring from elastic to viscoelastic material. The viscoelastic modulus is also found to have an approximate constant ratio over compressive strength regardless of concrete specification. Finally, the simulation of basic creep behavior can be used to predict the stress distribution of reinforced HPC columns for estimation of risk of cracking.

Chapter 6 Internal Humidity and Autogenous Shrinkage Measurement

6.1 Introduction

Autogenous shrinkage is the shrinkage of concrete under sealed condition without moisture loss due to self-desiccation. Since it can be assumed that internal moisture of large concrete member is constant, autogenous shrinkage thus is one of major factors controlling the deformation of concrete under no moisture loss. The internal stress due to shrinkage with restraint is always important for evaluating the risk of rapid growth of cracking. Concrete will fail with high probability if shrinkage stress is close to the tensile strength of concrete. The accurate measurement of shrinkage is thus needed for assessment of growth of shrinkage stress. A new method for estimating the axial stress due to shrinkage is proposed in this chapter based on the twin test result of free and restraint autogenous shrinkage test.

The internal stress arisen from thermal expansion during the very early curing stage plays an important role for development of shrinkage. In this chapter, the internal temperature and relative humidity development are discussed for HPC with 0.35 water/cement ratio and various aggregate contents. A practical model for predicting the early age relative humidity as a function of curing time and water/cement ratio is developed. The effect of water / cement ratio, aggregate content, internal humidity and supplemental cementitious materials (SCM) on autogenous shrinkage are investigated with respective shrinkage measurement. A log function is shown to be capable of fitting the correlation between relative humidity and shrinkage at early age. Based on the.

proposed method for evaluating the shrinkage stress under various aggregate contents, a linear relationship between shrinkage stress and aggregate content is built. The effect of pre-wetted lightweight aggregate (LWA) is also studied by the measurement of internal RH and shrinkage with the addition of LWA. The potential for reducing the self-desiccation and autogenous shrinkage of LWA is discussed and verified by tests.

6.2 Internal temperature and shrinkage development at the very early age

At the very early age of autogenous shrinkage, the shrinkage strain as well as the internal temperature are plotted in Fig. 6-1. It can be seen that the internal temperature at beginning is about 20 °C followed by a large increase to about 38 °C and dropping back to about 20 °C after about 24 hours since the curing of the specimen. While within this period, expansion can be observed from the positive shrinkage strain in the same plot. The time for temperature going back to 20 °C is just equal to the time for the specimen going back to the initial length. Similar findings about the temperature and deformation of autogenous shrinkage was also found by other researchers. After 24 hours, no significant change in internal temperature can be observed. It can be inferred the thermal effect is only significant within the very early age of autogenous shrinkage and will greatly affect the internal stress development under restraint condition. However, the thermal deformation can be ignored after the very early age since curing. Daniel (2008) also observed the similar vibration of the temperature at the beginning hours after casting together with the development of internal relative humidity.

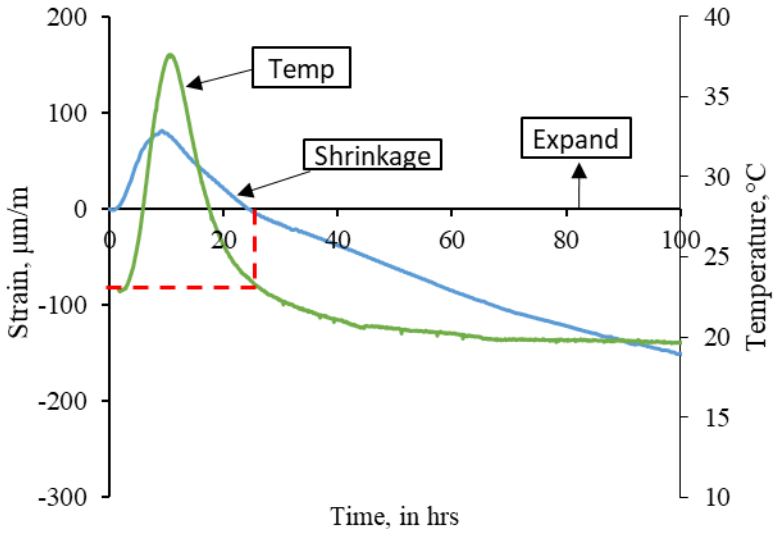

Fig. 6-1 Temperature and autogenous shrinkage for 0.35-40% at early age

6.3 Internal humidity for HPC

6.3.1 Self-desiccation effect in cementitious systems

90 days internal relative humidity for three mixes were measured and the results are shown in Fig. 6-2. Since coarse aggregate may prevent the probe from being inserted into the concrete vertically, the concrete with 40% aggregate content were selected. During the whole test procedure, the specimens were sealed cured under constant room temperature and constant humidity. It can be seen from Fig. 6-2 that the initial internal RH for the three mixes are quite close while 0.35-40% is smaller than the other two by 3-4%. The reduction of internal RH almost finishes at about 20-30 days for all the three mixes. By comparing the ultimate internal relative humidity, with the increase in water/cement ratio, the reduction in internal relative humidity is smaller. This result is consistent with the assumption of effect of self-desiccation on the internal moisture. For HPC with lower w/c, the self-desiccation is more severe which could lead to large reduction in the internal RH.

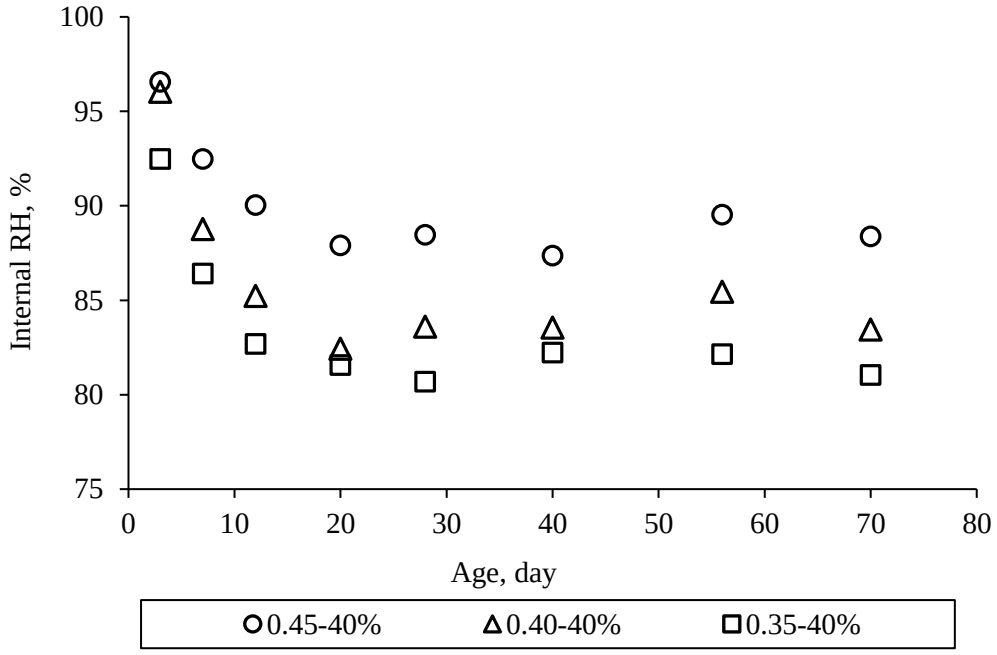

Fig. 6-2 Internal RH for 0.45-40%, 0.40-40% and 0.35-40%

It is also worth noticing that after 20-30 days since curing, a little increase in the internal RH for all the three test mixes can be observed. It can be due to the completion of cement hydration as well as the consumption of water during hydration. Generally the reduction in internal RH ends after 20-30 days and it can be concluded that the cement hydration process plays an important role in controlling the internal moisture.

6.3.2 Effect of aggregate content on internal RH

The effect of aggregate content on internal RH is also investigated here with the use of 0.35-40%, 0.35-70% with wet aggregate, 0.35-70% with dry aggregate and 0.35-0%. The test result is shown in Fig. 6-3. While checking the data for 0.35-0%, 0.35-40%and 0.35-70%, one can see no clear tendency for the effect of aggregate content on internal RH. While comparing the 0.35-70% with wet aggregate compared to 0.35-70% with dry aggregate, the reduction in internal RH of the one with wet aggregate is much smaller than the one with dry aggregate.

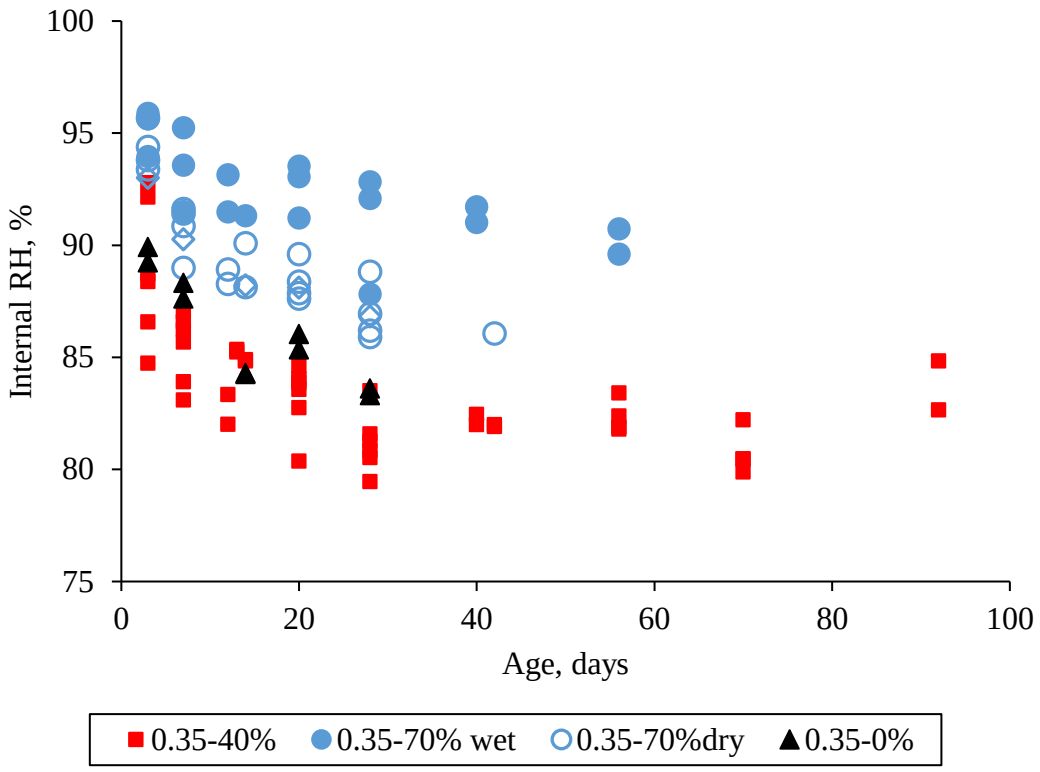

Fig. 6-3 The effect of moisture of aggregate on internal RH

6.3.3 Effect of depth of test position on internal RH

For investigating effect of the position of testing probe on the measurement of internal RH, the probe is inserted into 2 in, 6 in and 11 in from the top of the specimens. Fig. 6-4 shows the development of internal RH versus age for mixes with w/c of 0.35, 0.40 and 0.45 with 40% aggregate content with three different testing positions. It can be seen that the measured internal RH for testing at 2in and 11in position are almost identical. The result could be due to the fact that the two positions are symmetric and same distance from the bottom surface. While comparing the data from the two positions with the relative humidity at 6 in, which is in the middle span of specimen, one can see the reduction in relative RH for middle point is smaller than other places by 2-3 %. This result supports the conclusion that the internal moisture is not uniform across the length of the specimen. The internal RH is higher at the position in the middle span and far from the surface and decreases while closer to the surface. Therefore, the dimension of the specimens does influence the internal relative humidity measurement. For the accuracy of measurement of internal RH, it is important to choose the right position before

testing. All the internal RH measured in the study is at 6 in, the middle position from the side surface of specimens.

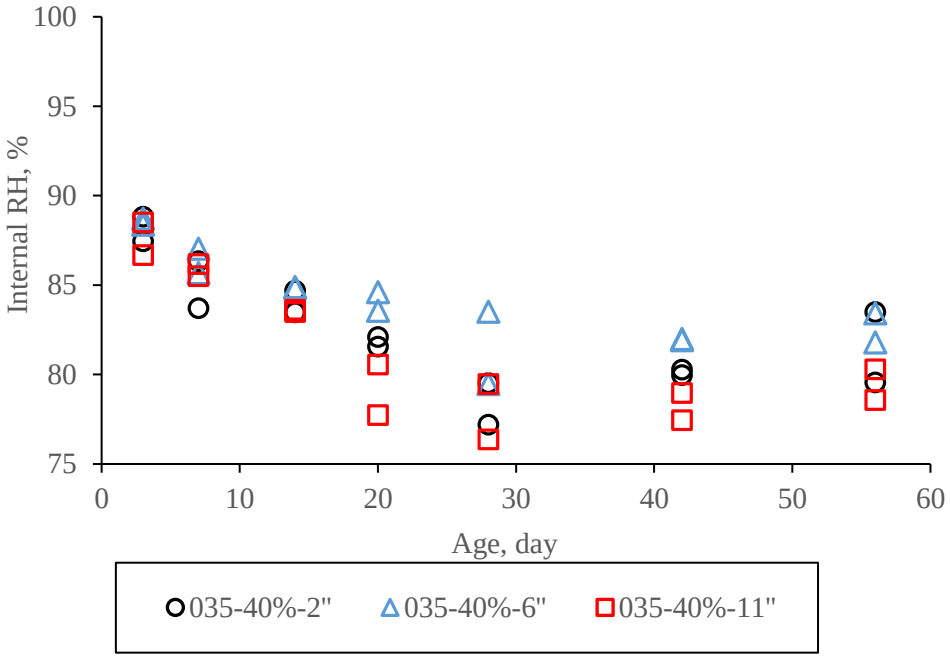

(a)

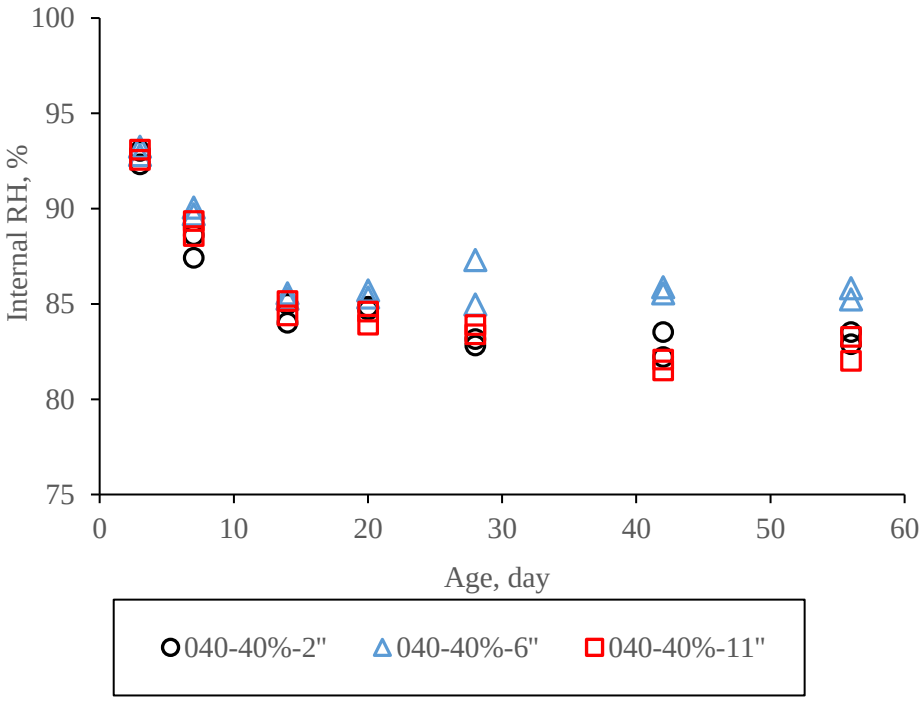

(b)

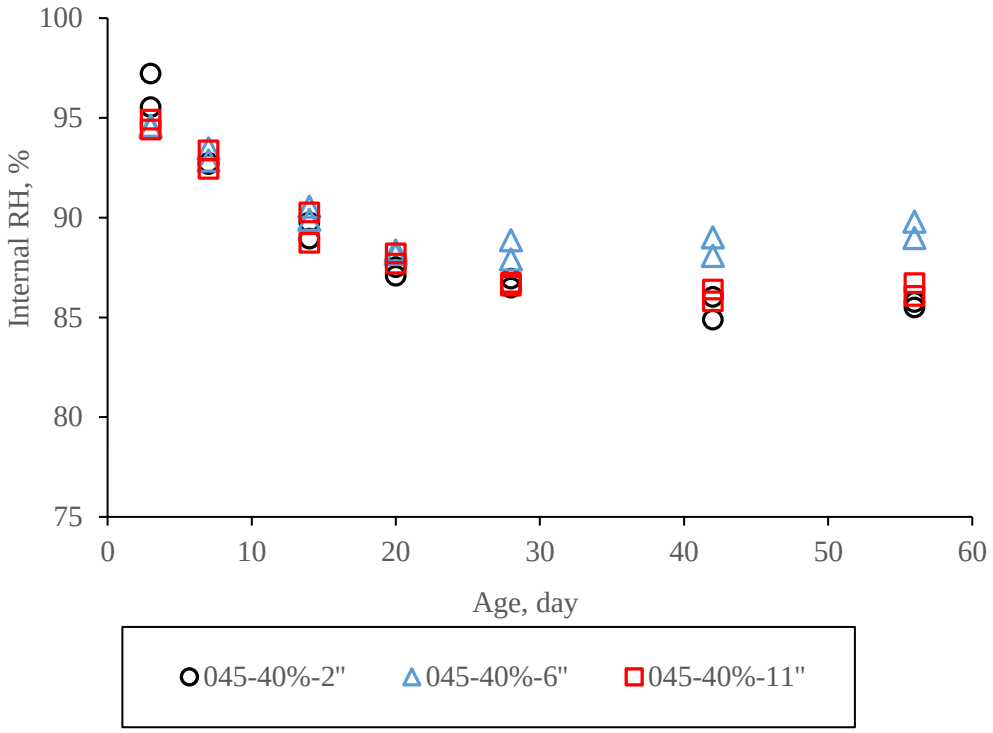

(c)

Fig. 6-4 The depth effect on RH at various depth for (a) 0.35-40%, (b) 0.40-40% and (c) 0.45-40%

6.3.4 Effect of maturity

It is known that with elevated temperature, the hydration process will be accelerated. The maturity can be calculated as the function of temperature by (Hansen, 1977):

$$M(t) = \int_0^t exp\left[\frac{E_a}{R}\left(\frac{1}{273+T_{ref}} - \frac{1}{273+T(t)}\right)\right]dt \qquad \text{Eq. 6-1}$$

For investigating the effect of maturity on the reduction in internal RH development, two specimens curing under 20 and 30 °C are tested. The results for RH result with mix of 0.45, 0.4 and 0.35 water/cement ratio are shown in Fig. 6-5. A general tendency of reduction regardless of w/c ratio can be observed. The internal RH at 20 °C is equal or smaller than that at 30 °C before 10 days. Then the internal RH between 10 and 20 days at 30 °C is higher than that at 20 °C. The

difference between development of RH at 20 and 30 °C after 20 days is that contrast to the constant internal RH at 30 °C since about 20 days, the internal RH at 20 °C is further reduced by 2-3% after 20 days since casting.

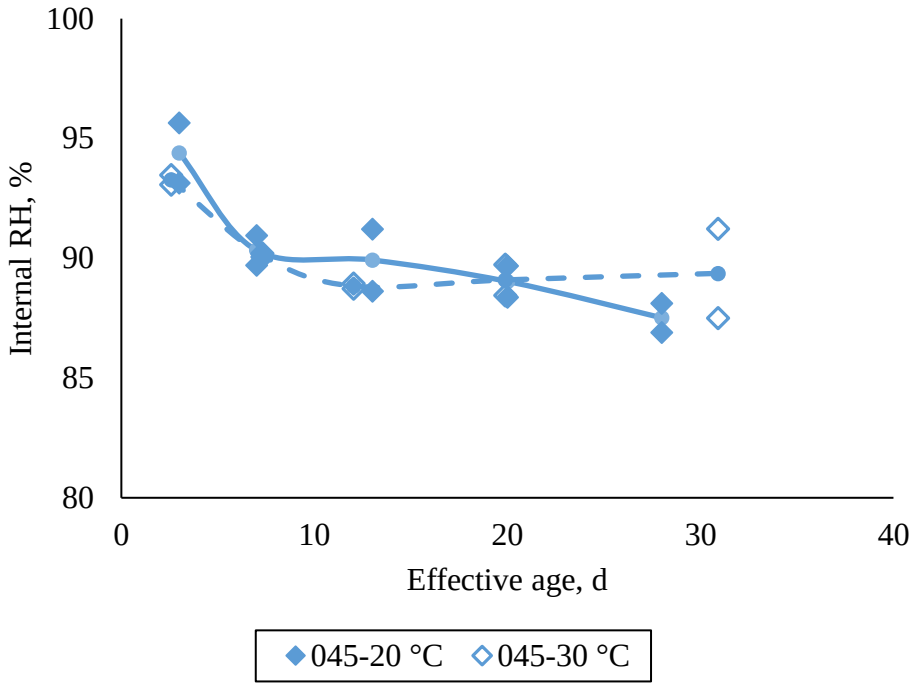

(a)

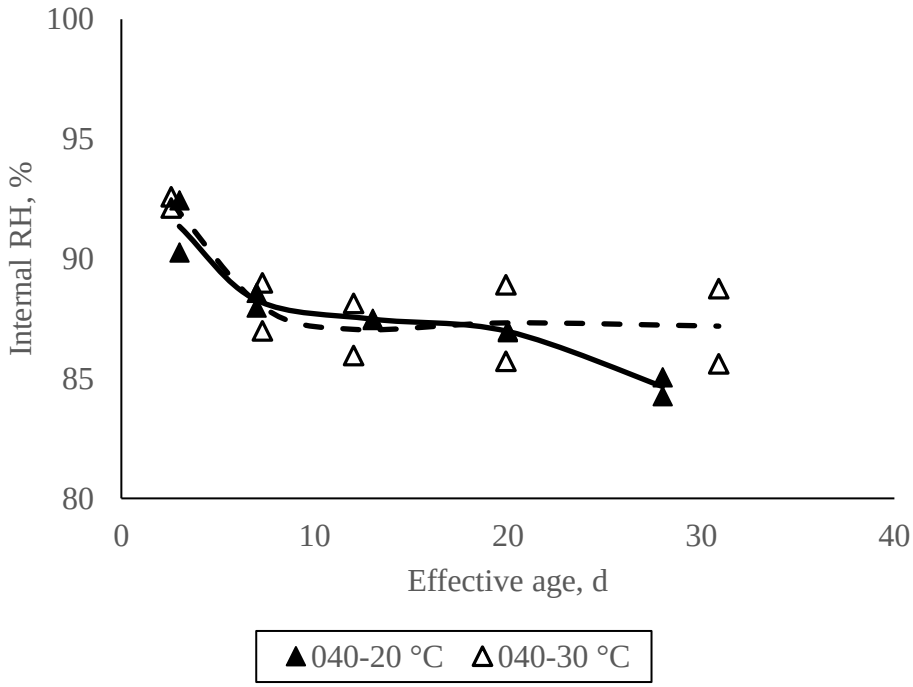

(b)

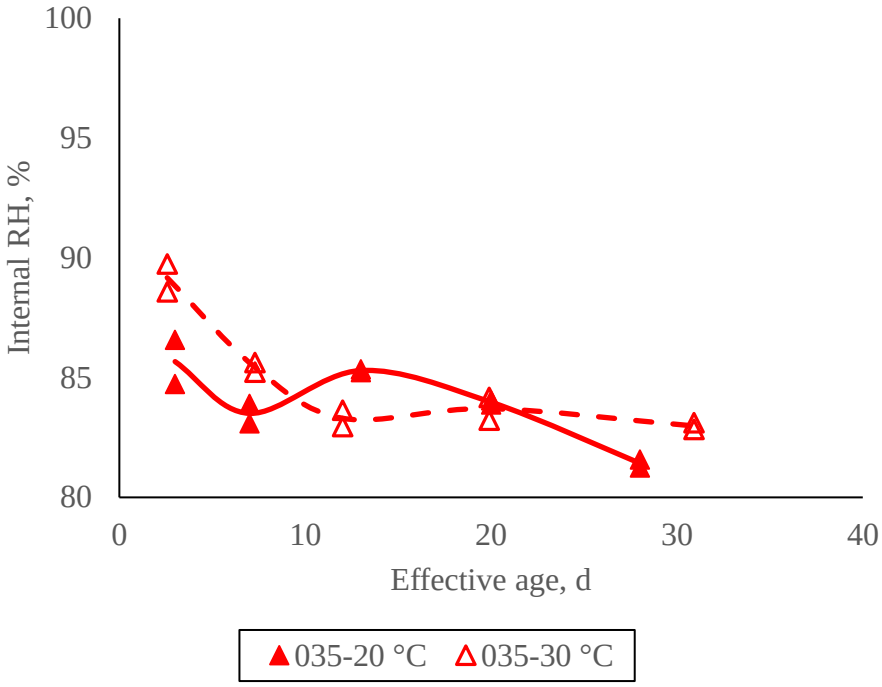

(c)

Fig. 6-5 The internal RH at 20 and 30 °C for (a) 0.45-40% (b) 0.40-40% and (c) 0.35-40%

6.3.5 Modeling of internal RH development

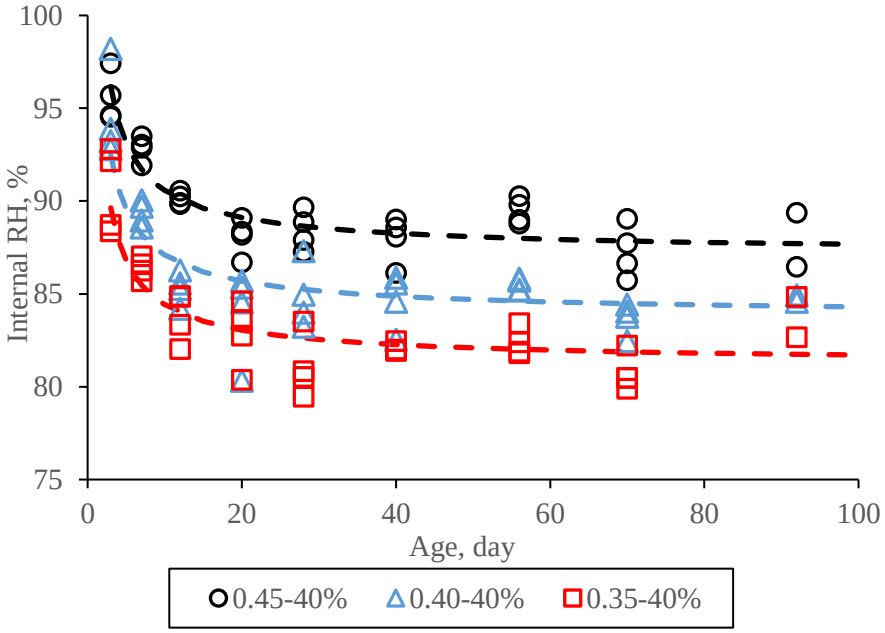

Fig. 6-6 Measured internal RH in mortar specimens of different w/c ratios.

Furthermore, close inspection of Fig. 6-6 reveals that internal RH can be modelled by the following equation as a function of time by Eq. 6-2.

$$RH = RH_u \times (1 + A \times \exp(-B \times t^c)) \quad \text{Eq. 6-2}$$

The three parameters can be obtained by the least-square regression analysis. It is found out that the optimized parameters A, B and C are 0.15, 0.2 and 0.8. RH_u, the ultimate relative humidity, is the relative humidity at 100 days since casting.

While plotting the RH_u versus water/cement ratio in Fig. 6-7, a simple linear regression equation can be used to fitted to the data points. Consequently, the relative humidity equation, as a function of time, can be modified to a function with both time and water/cement ratio. It can be seen that the ultimate relative humidity is linearly proportional to the water/cement ratio, which is logically right. With the modified relative humidity function, the relative humidity with given water/cement ratio and time duration with 40% aggregate content can be estimated.

$$RH = [61.3 \times (w/c) + 60.5] \times (1 + 0.15 \times \exp(-0.2 \times t^{0.8})) \quad \text{Eq. 6-3}$$

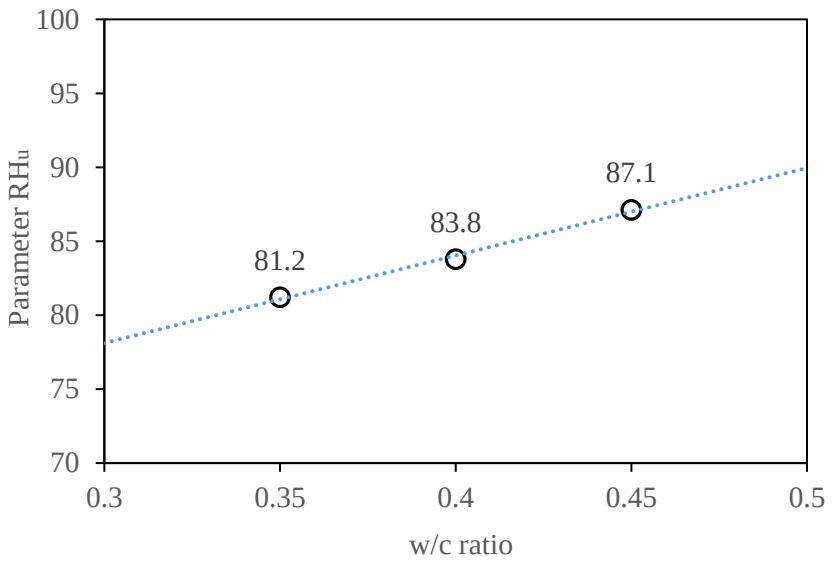

Fig. 6-7 The ultimate relative humidity versus water/cement ratio

Fig. 6-7 shows the correlation between the measured autogenous shrinkage versus modelled internal relative humidity for 0.35, 0.40, 0.45 water/cement ratio.

6.4 Factors for controlling the autogenous shrinkage

6.4.1 Aggregate content

Autogenous shrinkage with concrete and various aggregate contents are tested for long term. To investigate the full restraint shrinkage, the autogenous shrinkage fully restrained by reinforcement with 0%, 20%, 40%, 60% and 70% aggregate content were done at the same time. During the whole test, the specimens are sealed with the constant atmosphere temperature. The free autogenous shrinkage results for various aggregate contents of 0.35 and 0.45 w/c are plotted in Fig. 6-8(a) and (b). The shrinkage is plotted versus aggregate content for 3, 7, 21 and 28 days data for 0.35 w/c HPC and 0.45 w/c NSC and shown in Fig. 6-9(a) and (b). Due to various magnitude of shrinkage on various aging, the shrinkage is then normalized by the free shrinkage of paste at the same day to further investigate the aging effect alone.

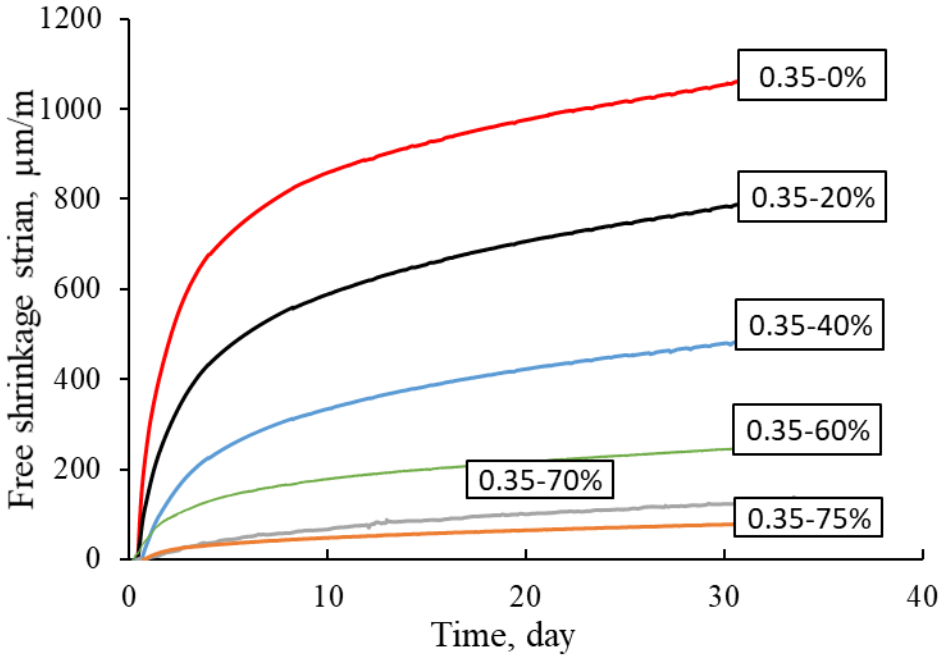

(a)

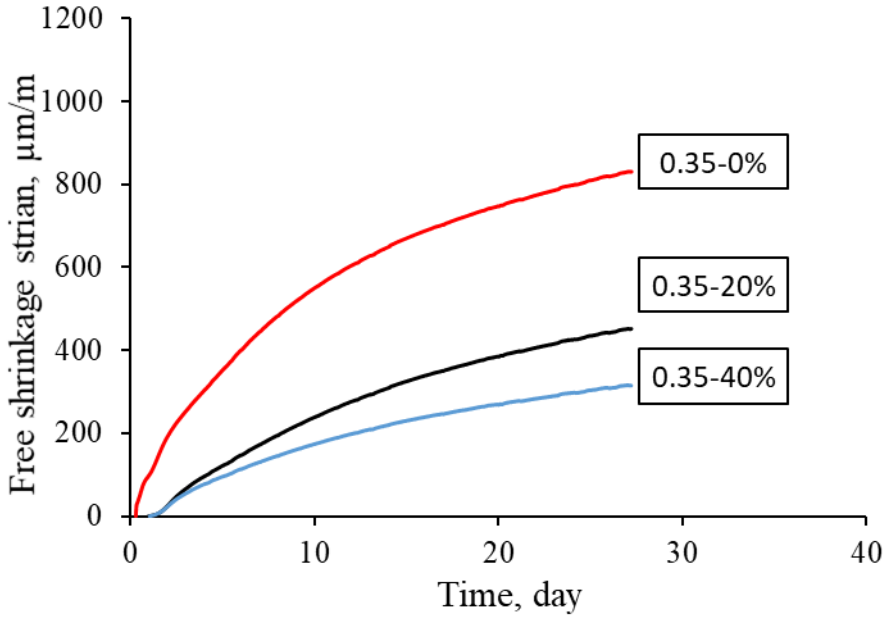

(b)

Fig. 6-8 Free shrinkage strain with various aggregate content for (a) 0.35 w/c and (b) 0.45 w/c

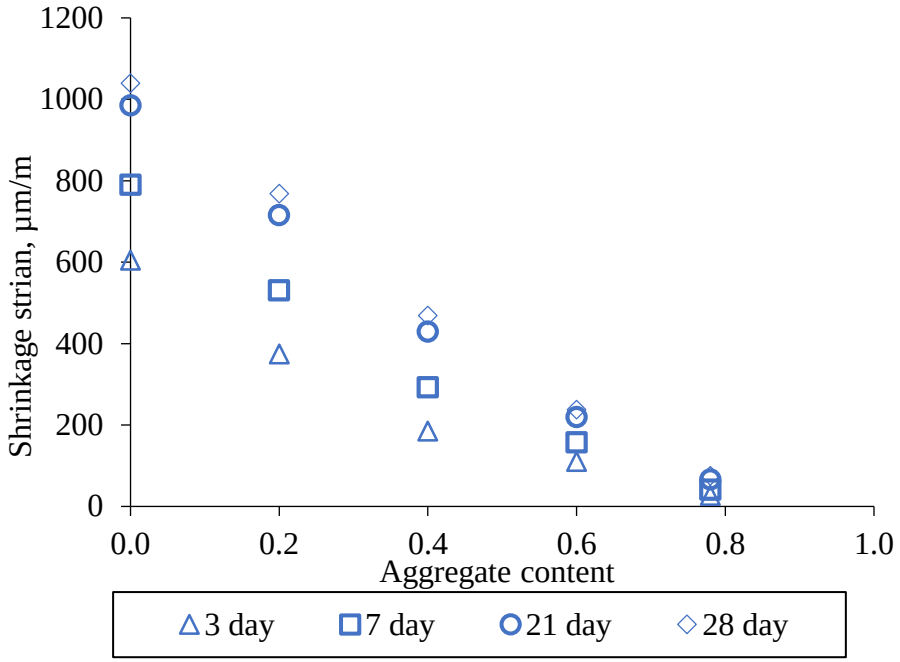

(a)

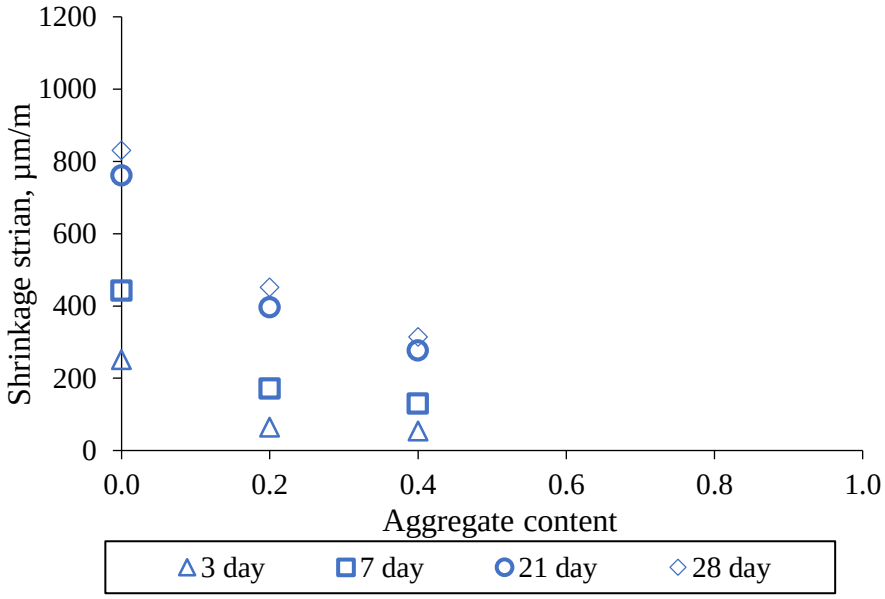

(b)

Fig. 6-9 The free shrinkage versus aggregate content for (3,7,28 and 90 days) for (a) HPC with 0.35 w/c and (b) NSC with 0.45 w/c

Based on Pickett model, the correlation between shrinkage and aggregate content can be represented by correlation:

$$\log\frac{\varepsilon_{sh,0}}{\varepsilon_{sh}} = \alpha \log\frac{1}{1-g} \quad \text{Eq. 6-4}$$

In which $\varepsilon_{sh,0}$ is the shrinkage that would occur if no aggregate were present and g is the aggregate content. After fine tuning the coefficient α, $\varepsilon_{sh}/\varepsilon_{sh,0}$ is plotted versus g for various aggregate contents in Fig. 6-10(a) . The autogenous shrinkage at 3, 7, 28 and 90 days are picked out together with the simulated relative shrinkage by Pickett model. Good fitting is achieved using Pickett model. One can predict the autogenous shrinkage at any aggregate content with the knowing of Pickett model equation. Compared to the relative creep compliance versus aggregate content for various loading ages as shown in Fig. 5-24, it can be seen that aging influence on the aggregate content effect on shrinkage is larger compared to that of creep. The relative deformation is almost linear versus aggregate content for basic creep while is in log-linear for shrinkage.

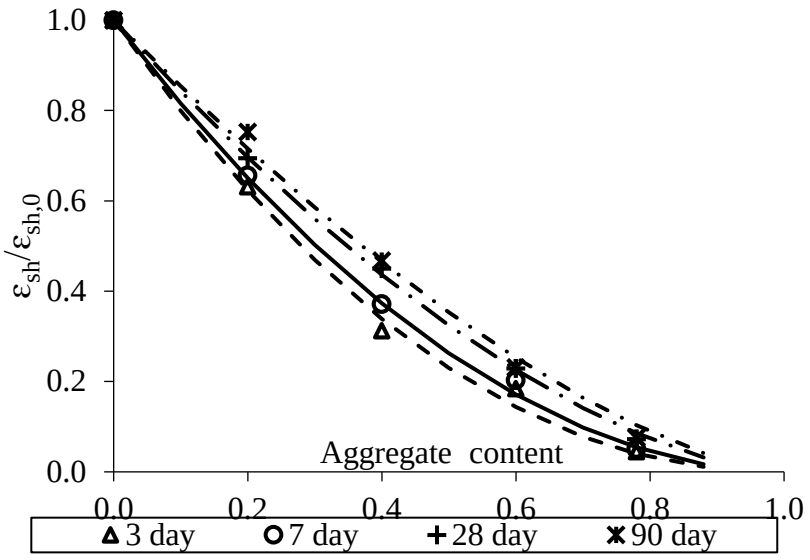

(a)

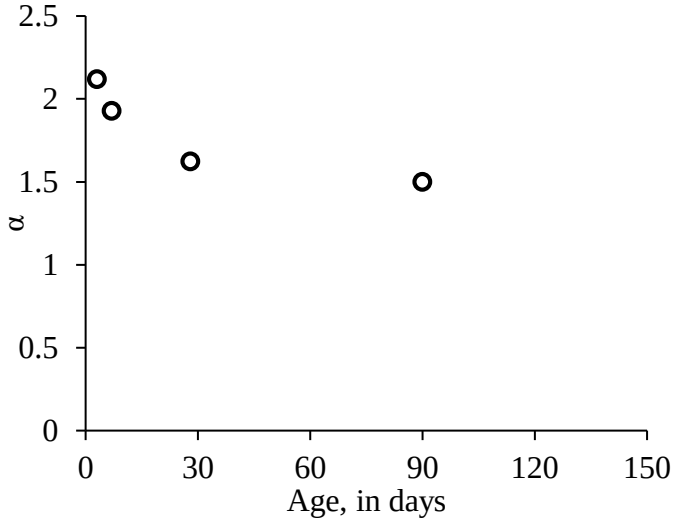

(b)

Fig. 6-10 (a) Relative shrinkage versus aggregate content for 0.35 w/c concrete on 3,7, 28 and 90 days (b) Value of α in Pickett model versus the age

6.4.2 Water/Cement ratio

As one of the important variables for controlling the performance of concrete, water/cement ratio is supposed to affect the development of autogenous shrinkage. Since the rate of autogenous

shrinkage is correlated to the rate of self-desiccation, high water/cement ratio is supposed to reduce the rate of self-desiccation. The free autogenous shrinkage strain with 0.35, 0.40 and 0.45 water/cement ratio are plotted in the same figure in Fig. 6-11. It can be seen that with higher water/cement ratio, the autogenous shrinkage is smaller.

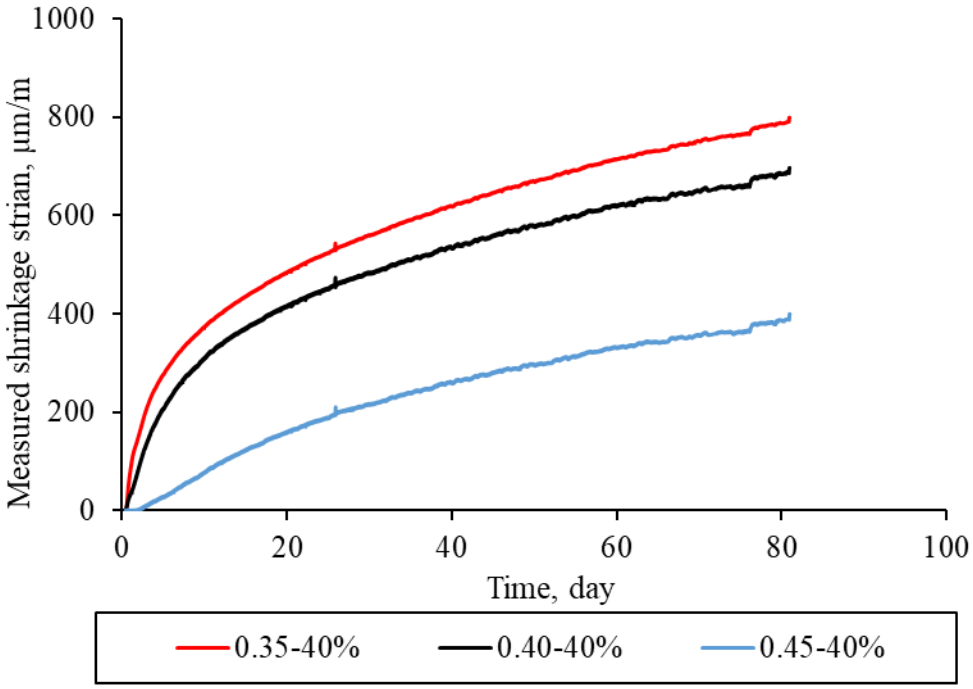

Fig. 6-11 Free shrinkage strain with different water/cement ratio (0.35, 0.40 and 0.45)

The measured shrinkage at 3 days, 7 days, 14 days, 28 days, 56 days and 90 days are picked out and plotted against water/cement ratio for mixes with 0.35-40%, 0.40-40% and 0.45-40% in Fig. 6-12. It can be seen that a linear regression curve can be used to fit the correlation between shrinkage and w/c.

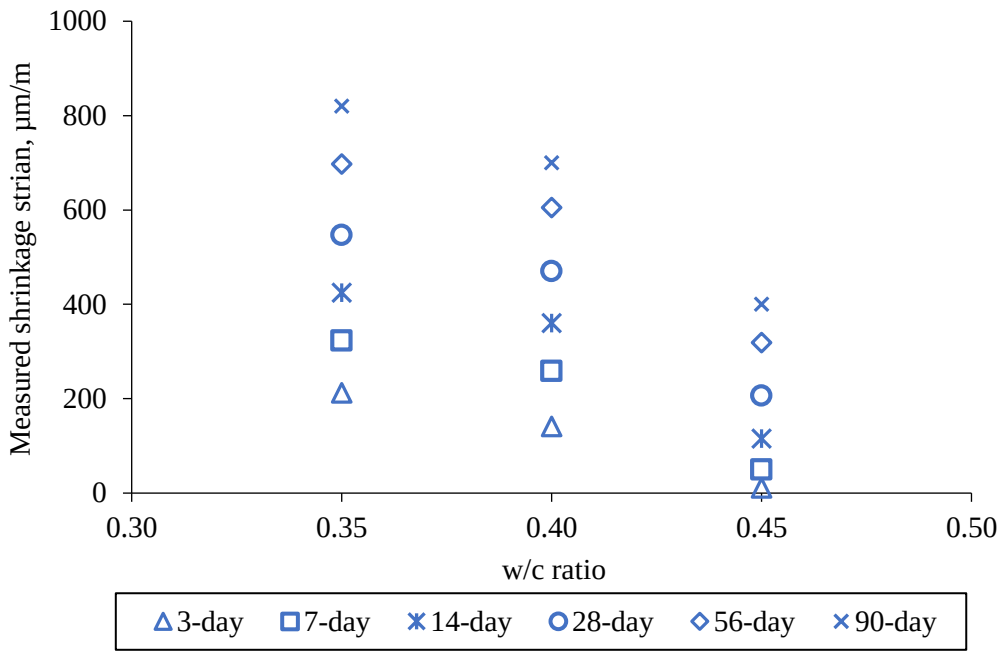

Fig. 6-12 The measured autogenous shrinkage versus water/cement ratio at 3 days, 7 days, 14 days, 28 days, 56 days and 90 days

6.4.3 Internal humidity

While plotting the autogenous shrinkage versus internal relative humidity, a log function can be used to fit the data, shown in Fig. 6-13. The rate of shrinkage versus internal RH can be regarded as one criterion for evaluating the self-desiccation speed. Therefore, with the increase in water/cement ratio, self-desiccation is reduced which is consistent with the lowest autogenous shrinkage at 0.45 water/cement ratio. It can be proposed that with more reduction in internal RH, the large autogenous shrinkage is supposed be developed. A log function can be used to fit the correlation between measured shrinkage strain and measured RH in Eq. 6-5. After combining with Eq. 6-4, Eq. 6-5 can be modified to the form of Eq. 6-6 with w/c and t as the variables.

$$\varepsilon_{40\%} = -3157 \times LN(RH) + 14476 \qquad \text{Eq. 6-5}$$

$$\varepsilon_{40\%} = -3157 \times LN\left([61.3 \times (w/c) + 60.5] \times (1 + 0.15 \times \exp(-0.2 \times t^{0.8}))\right) + 14476 \qquad \text{Eq. 6-6}$$

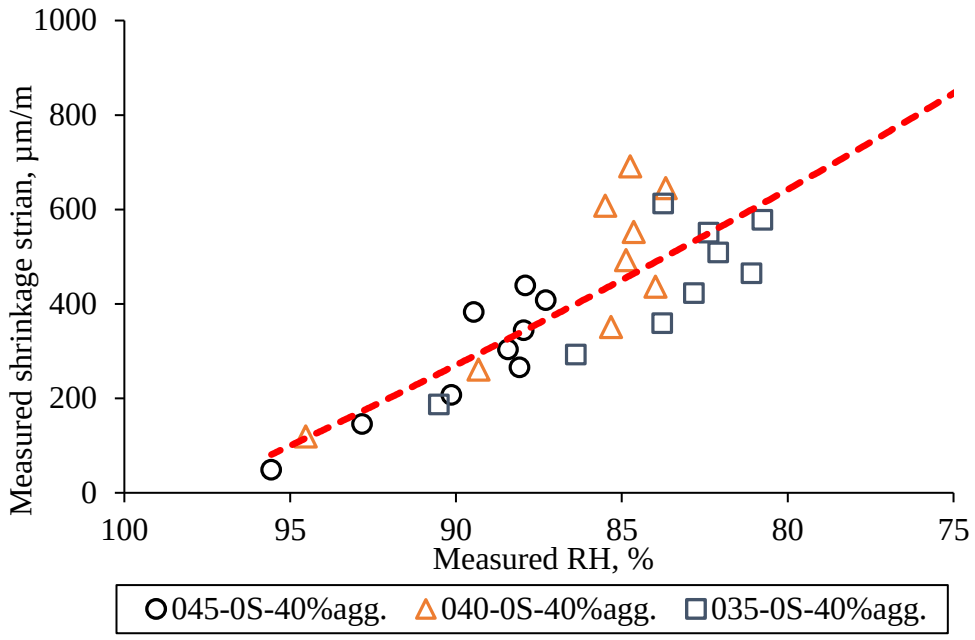

Fig. 6-13 The shrinkage versus modelled internal relative humidity for concrete with water/cement ratio

6.4.4 Supplemental cementitious materials

The autogenous shrinkage with GGBFS with varied aggregate contents were measured and plotted in Fig. 6-14.

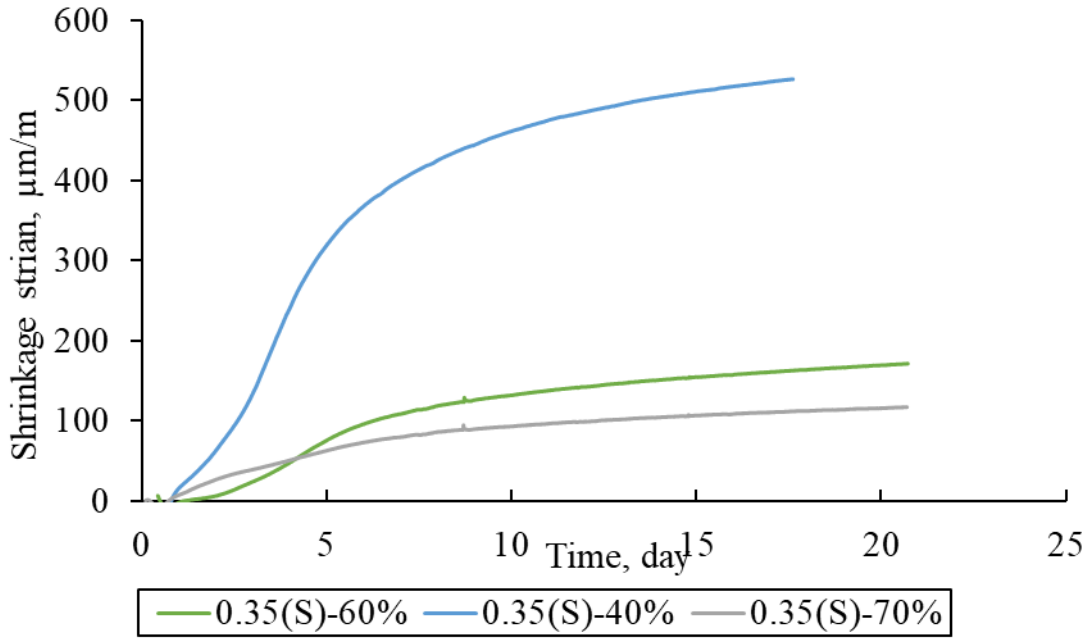

Fig. 6-14 The measured autogenous shrinkage strain versus time for varied GGBFS contents.

An equation mentioned in Wei et al (2008) can be used for describing the effect of pozzolanic reaction on autogenous shrinkage.

$$\varepsilon_{au,P} = \varepsilon_{sh} - (100 - C_{SCM}\%) \cdot \varepsilon_{au,C} \qquad \text{Eq. 6-7}$$

Where:

$\varepsilon_{sh,P}$=contribution from pozzolanic reaction

$\varepsilon_{sh,S}$= measured autogenous shrinkage of a blend system

C_{SCM}=the SCM content by mass in a blended system, in this case the SCM is GGBFS

ε_{sh} =measured autogenous shrinkage of OPC

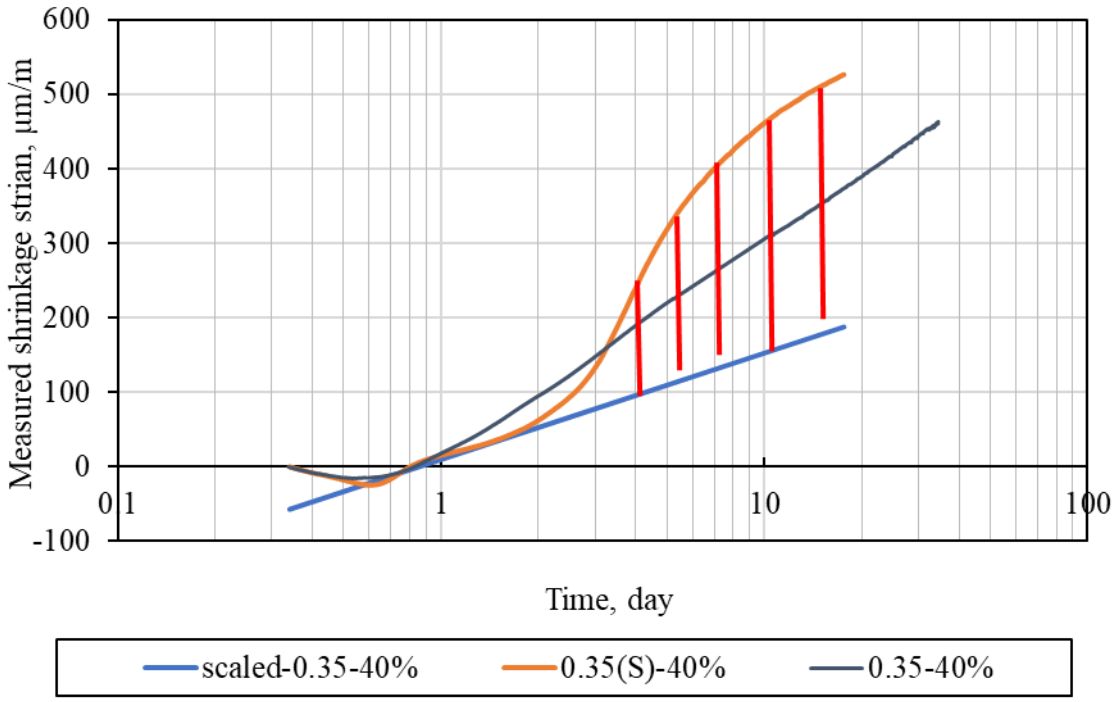
600
500
400
300
200
100
0
-100
Measured shrinkage strian, μm/m
0
1
1
10
100
Time, day
scaled-0.35-40%
0.35(S)-40%
0.35-40%

(a)

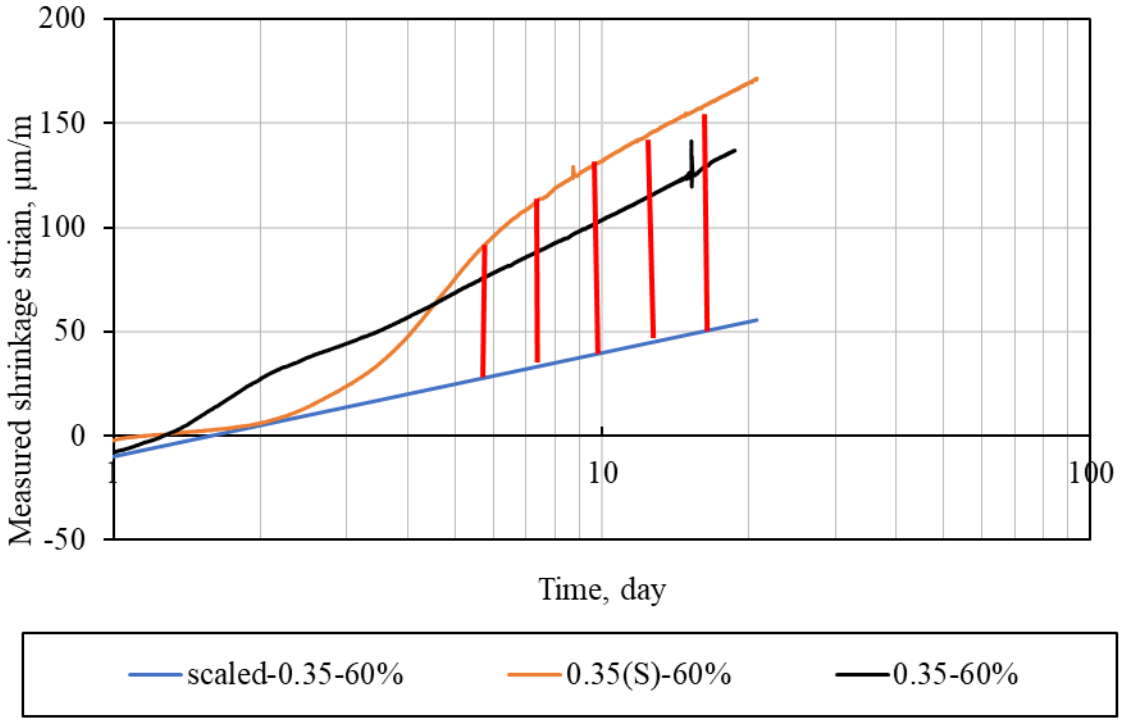
200
150
100
50
0
-50
Measured shrinkage strian, μm/m
1
10
100
Time, day
scaled-0.35-60%
0.35(S)-60%
0.35-60%

(b)

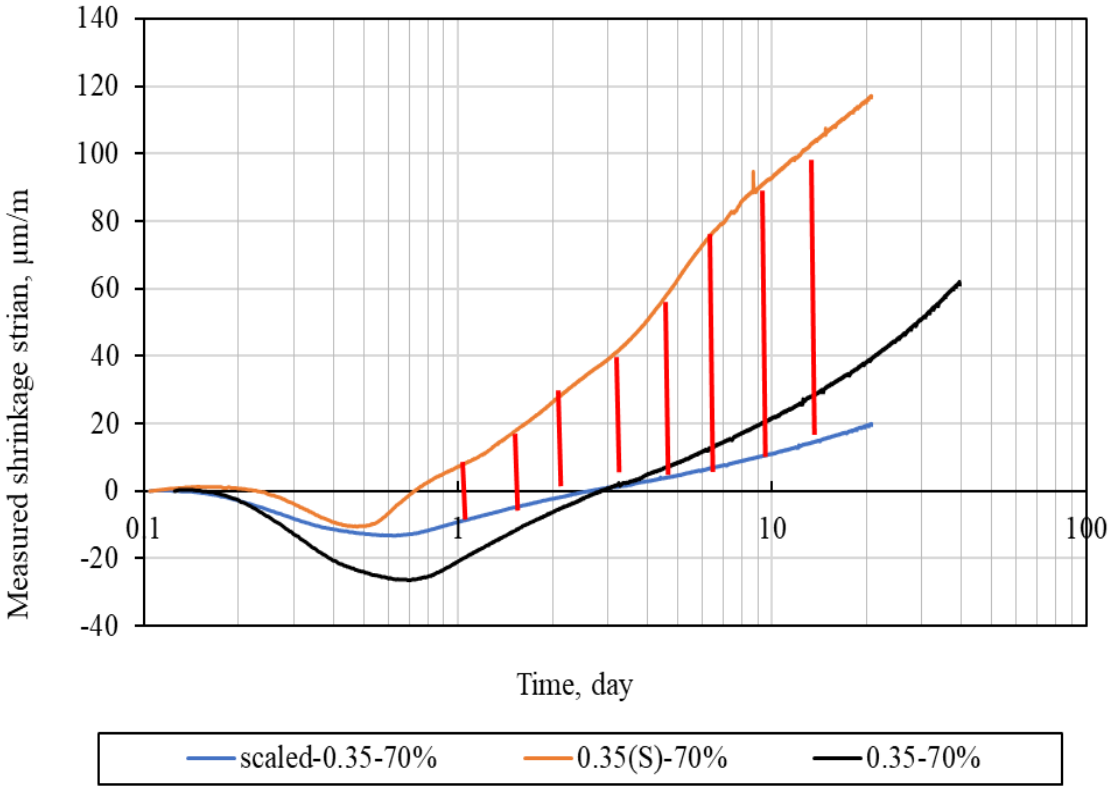

(c)

Fig. 6-15 The contribution of pozzolanic reaction to autogenous shrinkage for 0.35 w/c mix with (a) 40% aggregate (b) 60% aggregate and (c) 70% aggregate

Fig. 6-15 shows the contribution of GGBFS(SCM) for 0.35 w/c HPC with 40%, 60% and 70% aggregate content from autogenous shrinkage. It can also be seen that the autogenous shrinkage with the presence of GGBFS is larger than that of HPC without GGBFS after a few days since casting. One of the explanation from [Tazawa and Miyazawa 1995, Hanehara et al. 1999, Lura 2003, Lee et al. 2006] suggests that the pozzolanic reaction which consumes calcium hydroxide (CH) crystals, induces shrinkage as a result of removal of shrinkage restraints in the paste, e.g. the crystalline CH. This assumption is confirmed by the present study.

6.4.5 Modeling of autogenous shrinkage

F-H model, which originates used for fitting the cementitious hydration process, is used here for fitting the development of free autogenous shrinkage. F-H model is shown in Eq. 6-8:

$$\varepsilon_{sh} = \varepsilon_{sh,0} exp\left[-\left(\frac{\tau}{t}\right)^{\alpha}\right] \quad \text{Eq. 6-8}$$

Where $\varepsilon_{sh,0}$ is the proposed ultimate autogenous shrinkage

t is the time in days since the curing of concrete

τ is the time characteristics, in days

α is the curvature parameter

The shrinkage data for 0.35 w/c ratio concrete with 0%, 20%, 60% and 75% aggregate contents are included here for fitting the shrinkage data with F-H model with fine-tuned parameters. The fitting model is plotted with measured data in Fig. 6-16. It can be seen that F-H model can fit the development of autogenous shrinkage well.

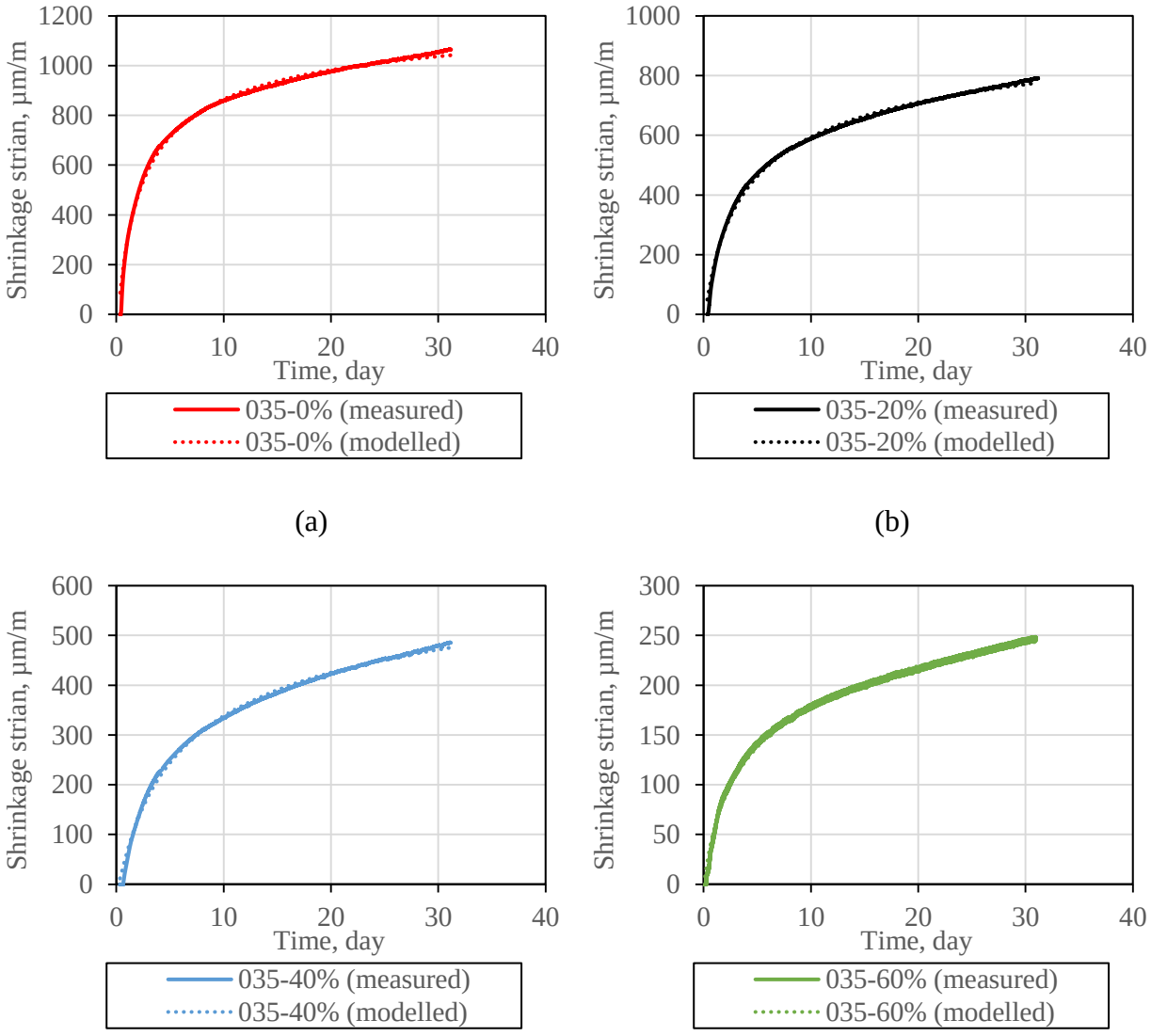

(c) (d)

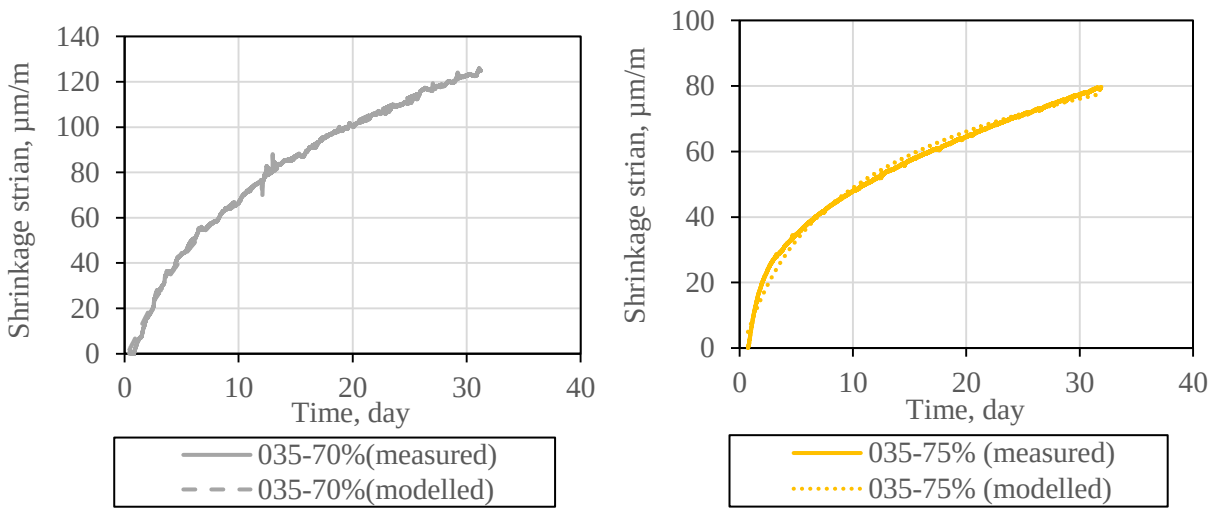

(e) (f)

Fig. 6-16 The measured and simulated free autogenous shrinkage for (a) 0.35-0% (b) 0.35-20% (c)0.35-40% (d) 0.35-60%, (e) 0.35-70% and (d) 0.35-75%

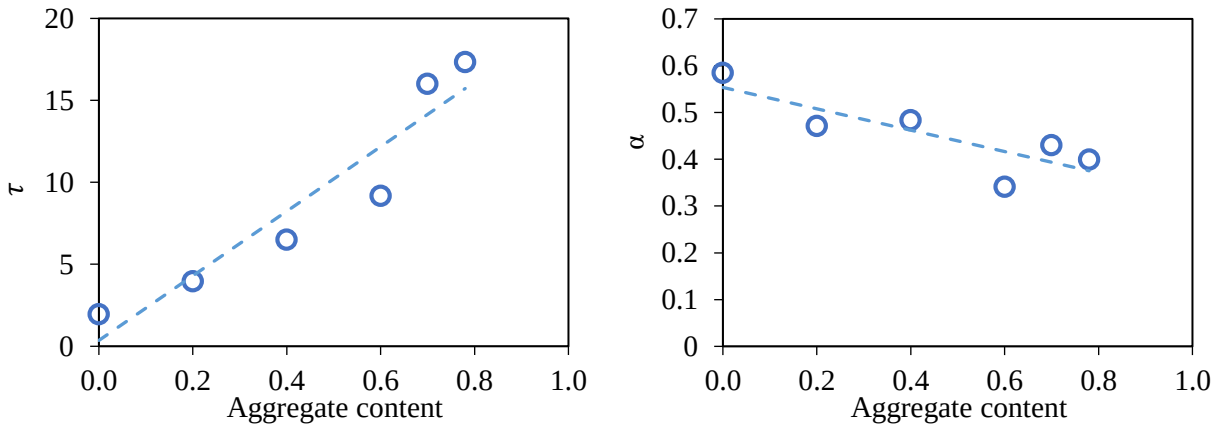

(a) (b)

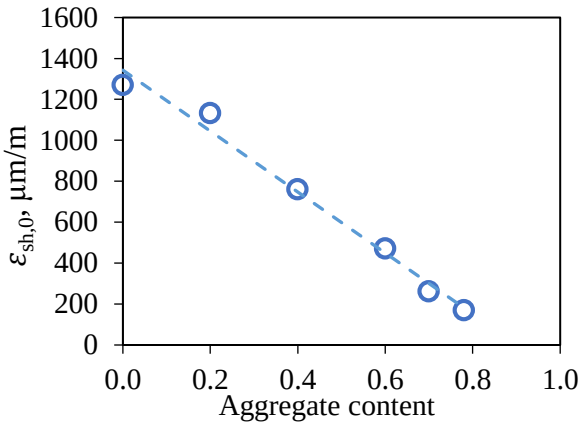

(c)

Fig. 6-17 The parameters of F-H model versus aggregate content

It can be seen in Fig. 6-17 that linear regression can be employed to fit the correlation between aggregate content and parameters τ, α and $\varepsilon_{sh,0.}$ The F-H model in Eq. 6-7 can be modified with the parameters as function of aggregate:

$$\tau = 19.699 * g + 0.3573 \quad \text{Eq. 6-9(a)}$$

$$\alpha = -0.2284 * g + 0.5535 \quad \text{Eq. 6-8(b)}$$

$$\varepsilon_{sh,0} = 1488.8 * g + 1342.8 \quad \text{Eq. 6-8(c)}$$

Predicted $\varepsilon_{sh,0}$ is then plotted versus aggregate content and plotted in the same figure with the relative shrinkage at 3,7, 28 and 90 days as shown in Fig. 6-18(a). It can be seen from Fig. 6-18(b) that a clear tendency of decreasing α versus age. The predicted α for ultimate shrinkage is 1, as shown by the red dash line.

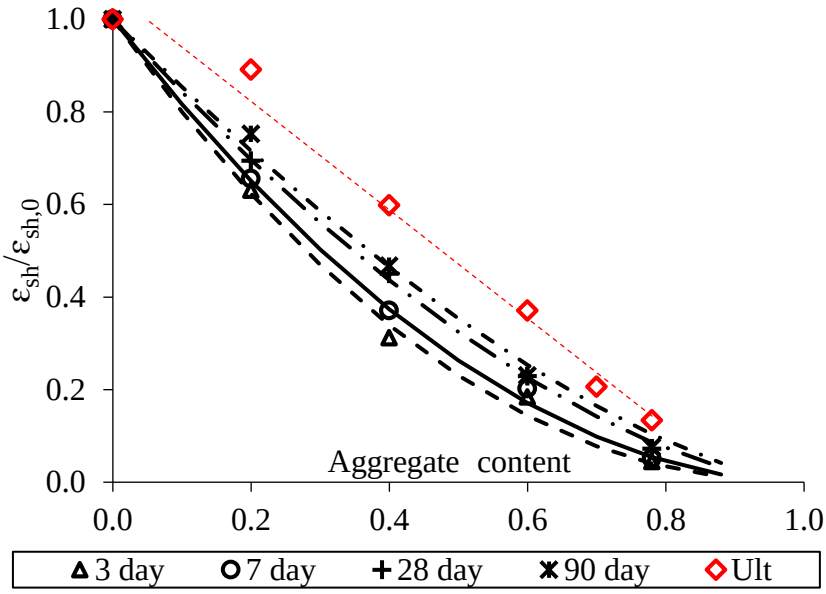

(a)

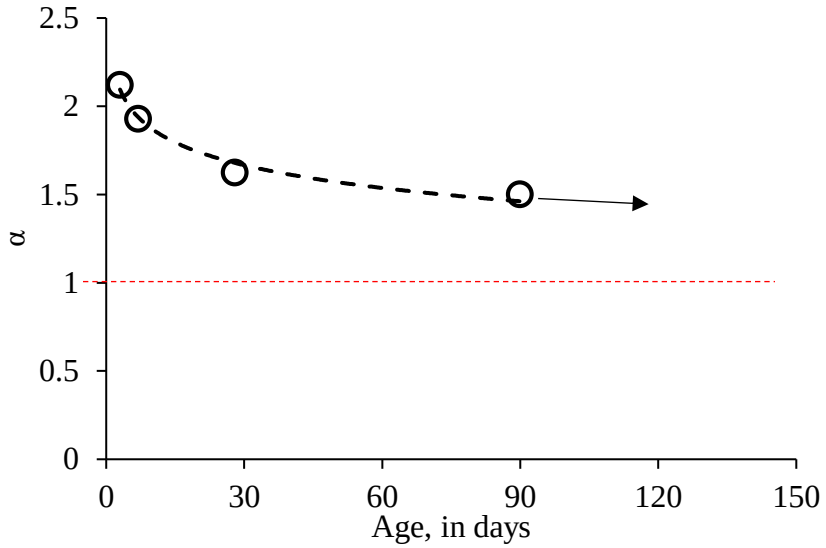

(b)

Fig. 6-18 (a)Relative shrinkage versus aggregate content for four ages (3, 7, 28 and 90 days) for 0.35 w/c concrete (b) Development of α versus the age

The correlation between α and time infers that comparing with the early age, the restraint effect of aggregate is smaller at the effect at later age. A log function can be used to fit the development of α versus age. With the knowledge of the α function at given age, the α function

at any other given age can be estimated. While using the log function for fitting to the α function, it can be seen that if $\alpha = 1$, then $x = 1079\ day \approx 3\ years$. It can be proposed that it takes about 3 years for the autogenous shrinkage to reach the ultimate value.

6.5 Estimation of autogenous shrinkage stress under full restraint

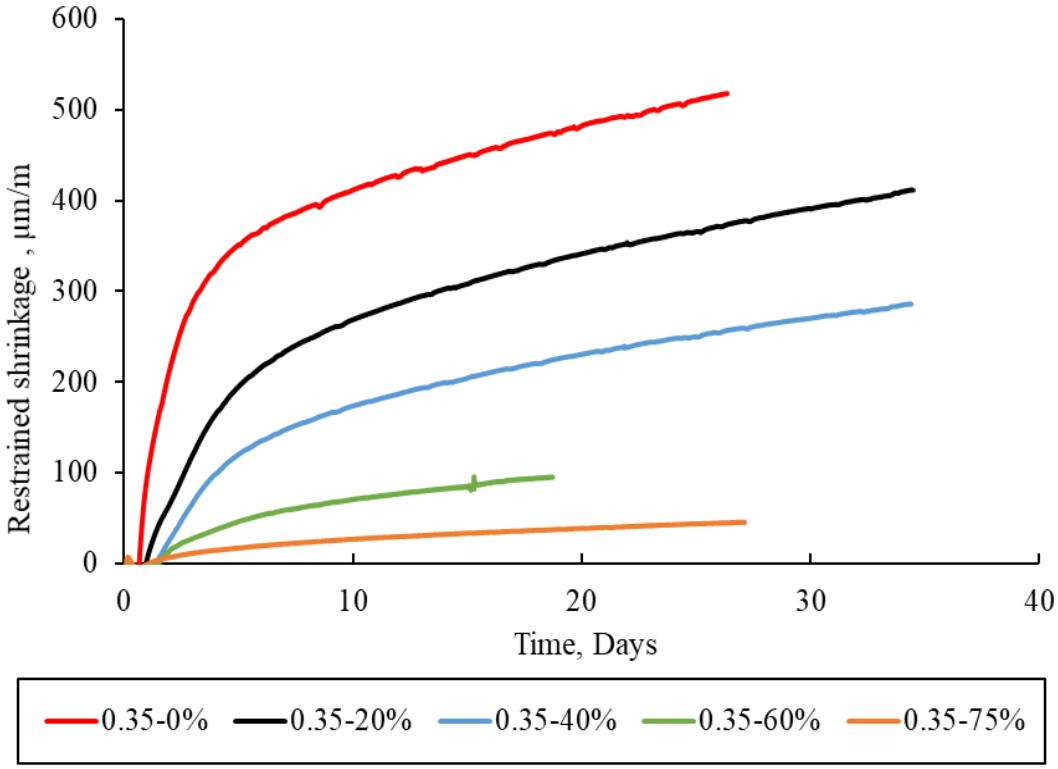

Fig. 6-19 Restrained shrinkage strain with various aggregate content

Sealed restrained autogenous shrinkage for concrete with 0.35 water/cement ratio and various aggregate content are plotted in Fig. 6-19. After comparing with free shrinkage shown in Fig. 6-8(a), it can be seen that the restraint autogenous shrinkage is much smaller than that of free autogenous shrinkage. In restrained shrinkage test, four rebars are used in each of the shrinkage frame and LVDT is connected with the free end for measurement of the deformation of shrinkage specimens.

The degree of restraint $Re(\%)$ with reinforcement for 0.35 w/c concrete with various aggregate content versus time can be obtained by applying the equation with the use of free and restrained

autogenous shrinkage data shown in Eq. 6-10. It can be seen in Fig. 6-20 that after about 10 days since the curing, the degree of restraint for various aggregate contents achieve constant value with the ultimate degree of restraint decreases with the increase in aggregate content. For the 0.35 w/c HPC with 0% aggregate, the ultimate degree of restraint is about 50% while that for 75% aggregate concrete reaches only 30%. The elimination of relaxation due to tensile creep could be attributed to the low degree of restraint from reinforcement.

$$Re(\%) = 1 - \frac{\varepsilon_{sh,r}}{\varepsilon_{sh}} \qquad \text{Eq. 6-10}$$

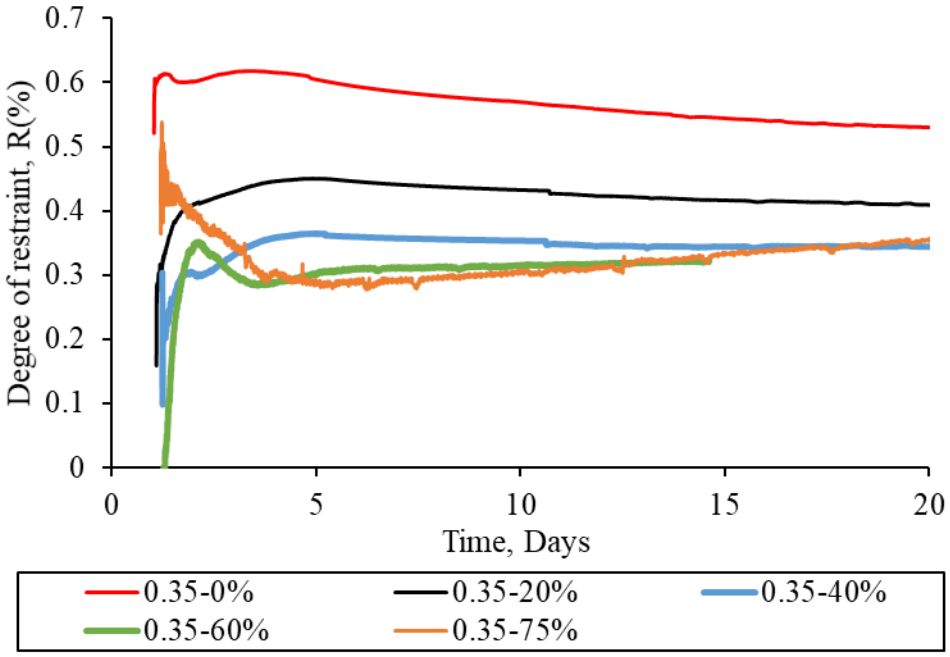

Fig. 6-20 The degree of restraint for various aggregate contents.

The internal shrinkage stress under full restraint can be calculated by the equation. Under fully restrained condition, the shrinkage stress is assumed to be equal to the external force that puls the specimens back to the same length. The shrinkage stress under full restraint when the degree of restraint equals to 100% can be obtained by:

$$\sigma_{sh} = \frac{\varepsilon_{sh,r} \times E_s \times A_s/A_c}{Re} \qquad 6.11$$

Where E_s is the modulus of steel reinforcement.

A_s is the cross section area of reinforcement.

A_c is the cross section area of concrete.

The estimated shrinkage stress at various aggregate contents under full restraint condition are plotted in Fig. 6-21. It can be seen that with less aggregate content, the estimated internal shrinkage stress is larger. The estimation is consistent with the large free autogenous shrinkage for concrete with lower aggregate content due to the lack of constraint from aggregate. One can use the method to predict the development of shrinkage stress for estimation of cracking risk with given mix and aggregate content.

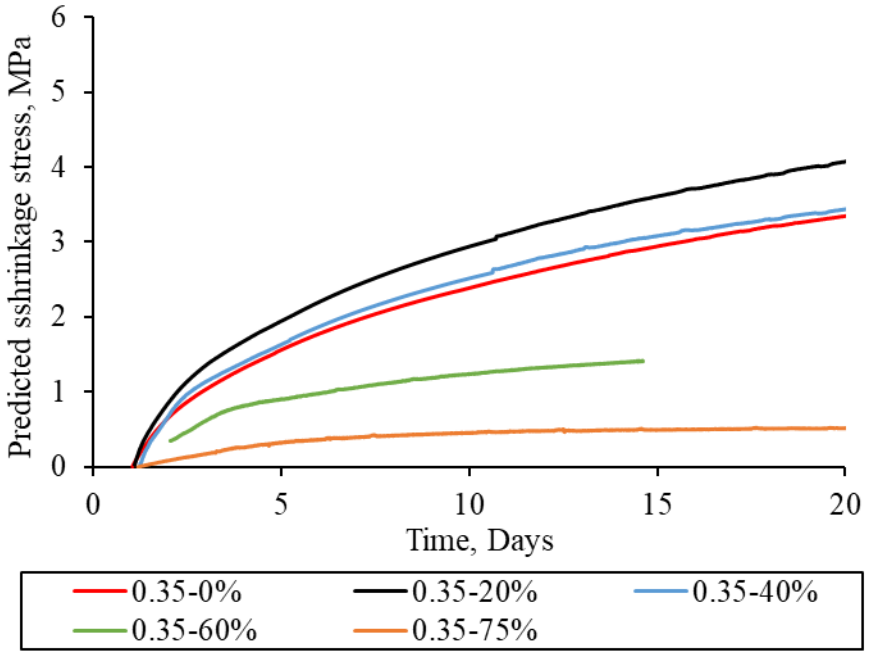

Fig. 6-21 The full restraint shrinkage stress with various aggregate contents.

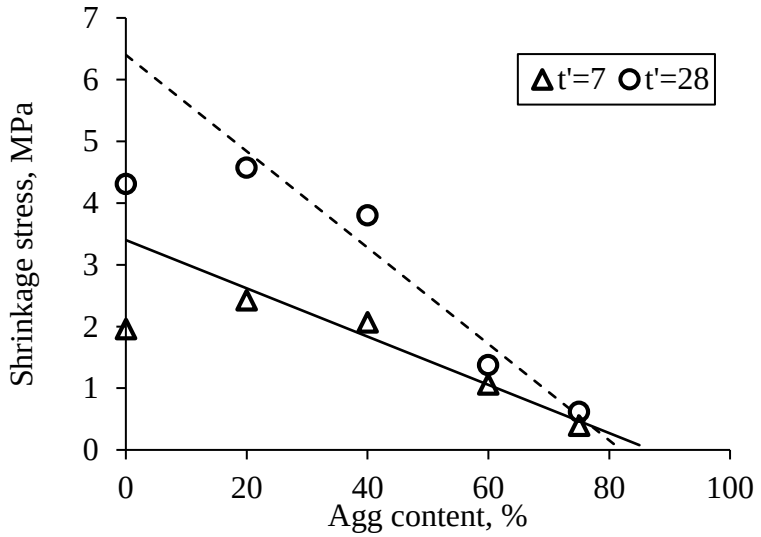

Fig. 6-22 Shrinkage stress versus aggregate contents for 7 and 28 days

The predicted full restraint shrinkage stress is plotted against free shrinkage strain for HPC with various aggregate contents in Fig. 6-22. Except for the shrinkage stress of paste, a linear correlation can be found between the shrinkage stress and aggregate content. The large deviation of paste specimen test can be due to the high hydration heat and inconsistence during casting. With knowing of the correlation between shrinkages stress and aggregate content, the shrinkage stress at given aggregate content can be estimated by this linear correlation.

6.6 Restraint of autogenous shrinkage by internal curing effect of LWA

6.6.1 Relative humidity prediction for internal curing

Addition of pre-saturated LWA in concrete can artificially entrain extra water to sustain cement hydration while maintaining a high RH level in the capillary pore system (Bentur et al., 2001; Lura, 2003; Wei, 2008). With sufficient internal curing, larger degree of saturation of pores can be obtained compared to sealed curing condition, as shown in Fig. 6-23 by D,Bentz (2006). This internal curing is a well-accepted remedy to reduce or even neutralize concrete deformation associated with internal moisture condition (such as autogenous shrinkage and moisture warping) (Bentur, 2001). The conclusion can also be validated by the conducted RH test seen in Fig. 6-24 where the RH in LWA mortar stays above 90% during the 4-month test period. As a result, the

autogenous shrinkage and moisture warping are substantially reduced in the 0.35-40% mortar (Fig. 6-25(a)). The effect of internal curing on autogenous shrinkage is strengthened with larger LWA replacement ratio, as shown also for 0.35-70% in Fig. 6-25(b) for autogenous shrinkage development with various LWA replacement ratios.

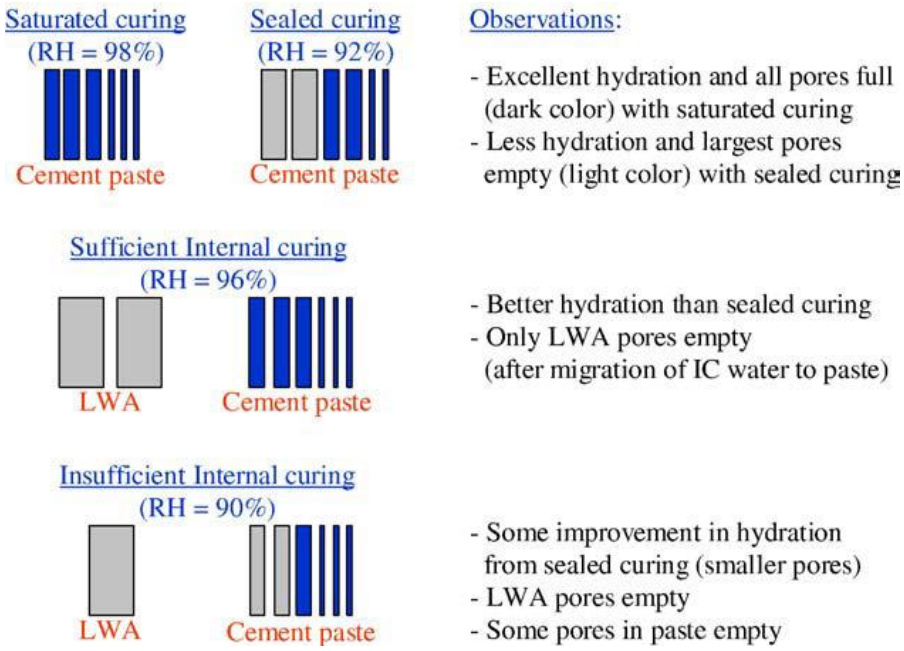

Fig. 6-23 Conceptual representation of cement paste pore systems under different curing conditions (D,Bentz (2006))

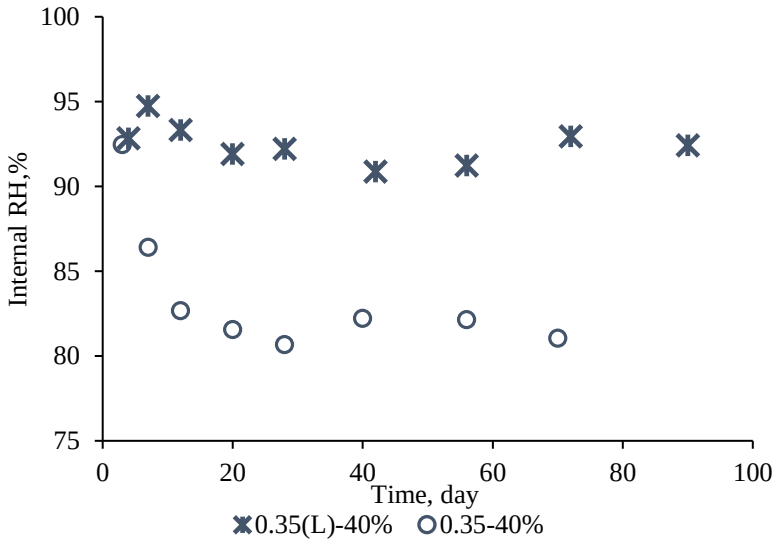

Fig. 6-24 Effect of LWA on internal RH of mortar specimens under sealed curing

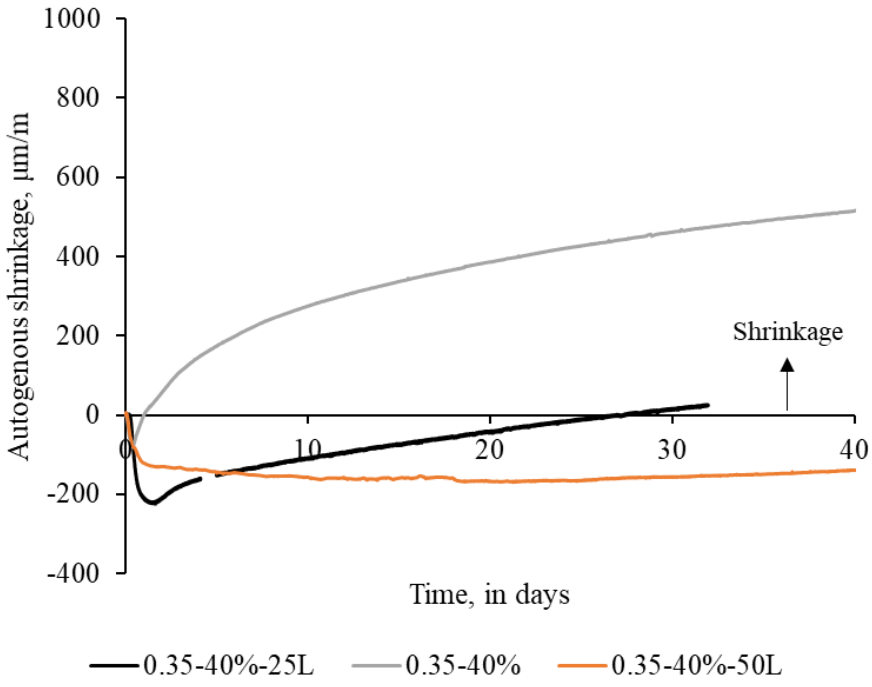

(a)

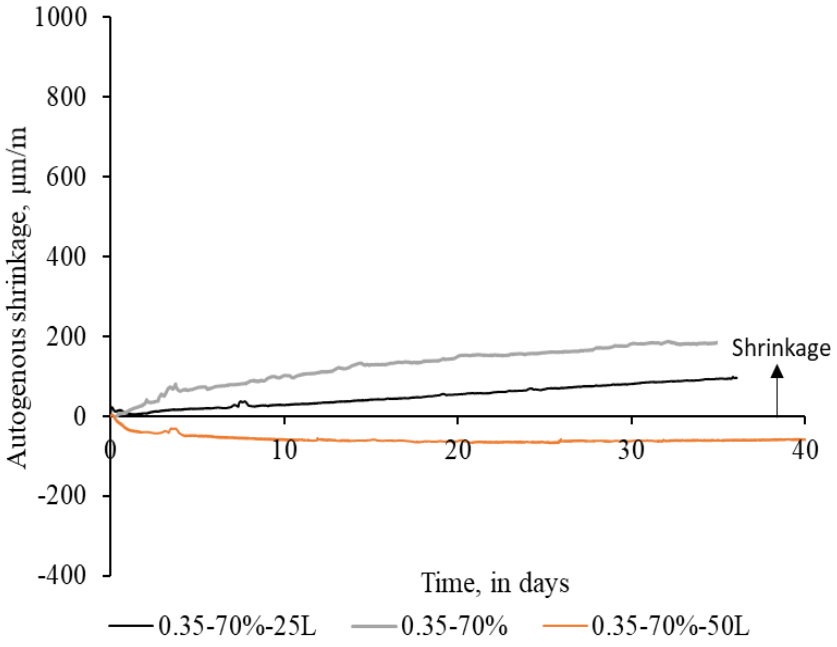

(b)

Fig. 6-25 Effect of LWA on autogenous shrinkage of 0.35 w/c for (a) mortar (40%) specimens and (b) concrete (70%) specimens

It is harder to predict the relative humidity with the presence of pre-wetted LWAs. Besides the mixing water, the water in LWA is also a big concern for affecting the relative humidity in HPC. It was reported by many researchers that not all extra water in LWA is immediately used for internal curing and some water in LWA only removed at low relative humidity. A commonly used method reported by Dejian (2017) and Daniel (2008) to study the case with pre-wetted LWA is using the total water/cement ratio defined as the sum of effective water/cement ratio where water is mixing water and the IC water where water is in pre-wetted LWA.

$$w_t/c = w_e/c + w_{ic}/c \qquad \text{Eq. 6-11}$$

The percentage of IC water actually provided in Mixtures can be calculated as:

$$\eta = \frac{m_{wat} \times W_{ic}/c}{C_f} \qquad \text{Eq. 6-12}$$

m_{wat} is the quantity of IC water needed to ensure adequate water for maximum degree of saturation. For fitting the equation to the prediction of relative humidity with presence of LWAs, the water/cement ratio needs to be refined as the working w/c ratio which only takes into account the water that is used for hydration and affects the self-desiccation process. By Dejian (2017), the water/cement ratio can be expressed as:

$$W_w/C = W_e/C + (\varphi \times t + \lambda) \times W_{ic}/C^{0.534} \qquad \text{Eq. 6-13}$$

With φ, λ is -0.0115 and 1.156 by fitting to test data show in Fig. 6-26. The fitting of internal RH versus age for internal curing condition with LWAs is plotted in Fig. 6-26(a) with the temperature development in Fig. 6-26(b). It can be seen that the model by Dejian (2017) does not fit to internal RH so well for system with LWA at the initial stage. While checking the temperature development versus shrinkage, it can be seen that when the temperature drops back to 22 °C, autogenous shrinkage stops increasing at the same time. It is thus convinced that the initial development of autogenous shrinkage with internal curing effect could be due to the effect of thermal expansion. After the thermal effect on autogenous shrinkage is done, no further development of autogenous shrinkage exists.

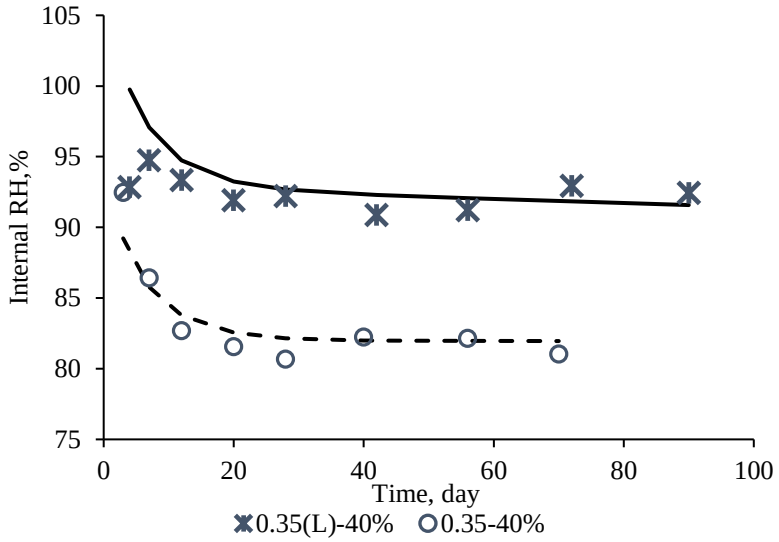

(a)

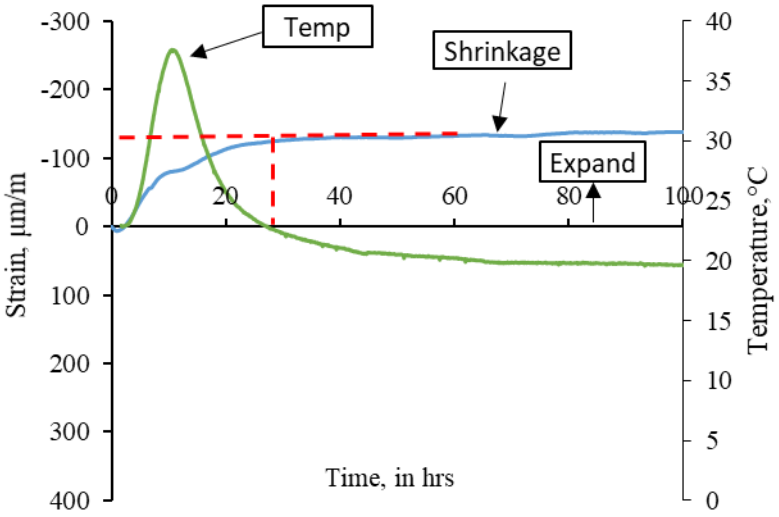

(b)

Fig. 6-26 (a) Internal RH for 0.35(L)-40% with fitting curve (b) Temperature development in the first 100 hours for 0.35(L)-40%

6.6.2 Aggregate effect with internal curing condition

From 6.3.1 it can be seen that when comparing the aggregate content effect on autogenous shrinkage, the autogenous shrinkage with less aggregate content is larger which can be explained by Pickett effect. The autogenous shrinkage with and without 50% LWA for 0.35 water/cement

ratio with 40% and 70% aggregate content are plotted in Fig. 6-27(a) and (b). It can be seen that autogenous shrinkage of 0.35(L)-40% and 0.35(L)-70% both keep constant after the initial expansion at the first 5 days while 0.35-40% and 0.35-70% without LWA increases with time. If shrinkage starts to be taken into account after early age (7 days), no autogenous shrinkage can be assumed occurring for 0.35(L)-70% and 0.35(L)-40%. The aggregate effect on internal curing is only shown by the initial larger expansion of 0.35 w/c HPC with lower aggregate content (40%).

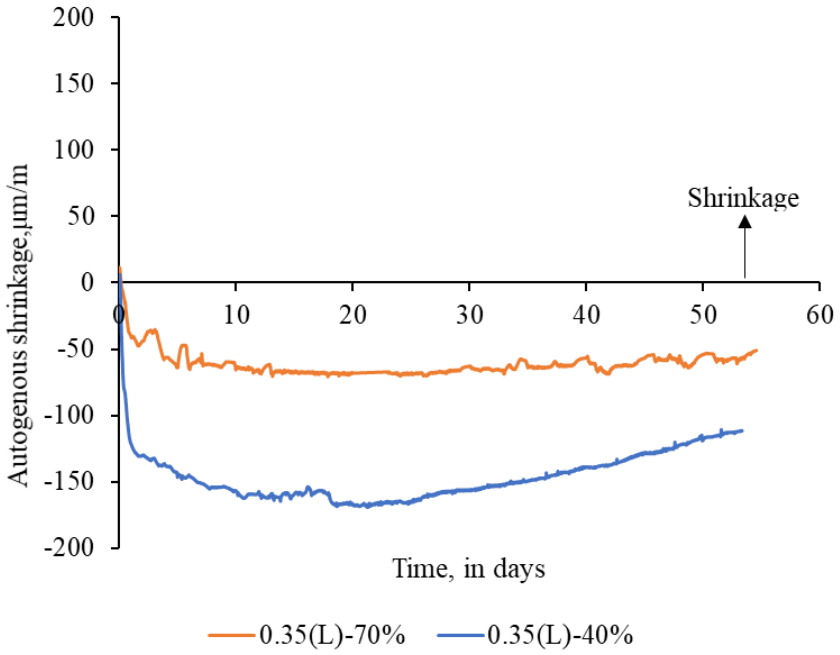

(a)

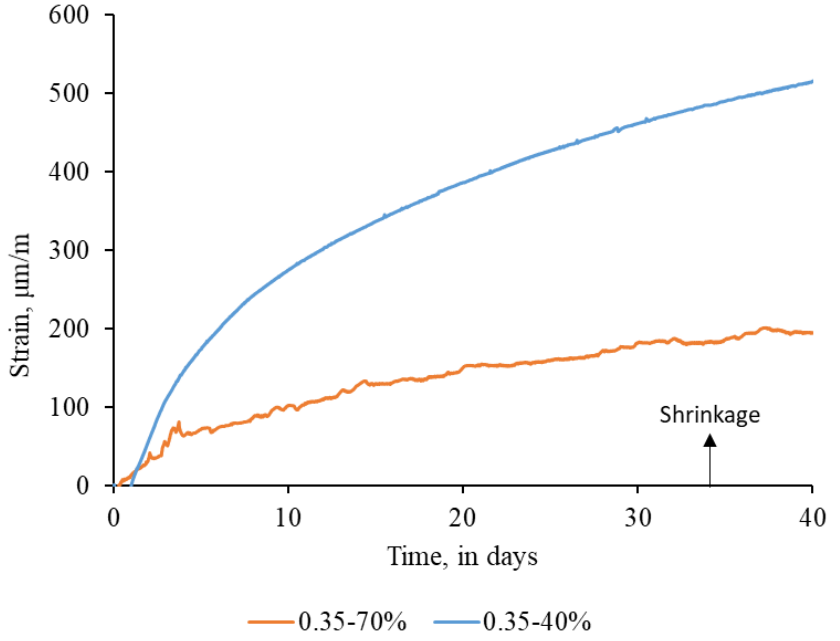

(b)

Fig. 6-27 (a) The autogenous shrinkage comparison between 0.35(L)-40% and 0.35(L)-70% and (b) The autogenous shrinkage comparison between 0.35-40% and 0.35-70%

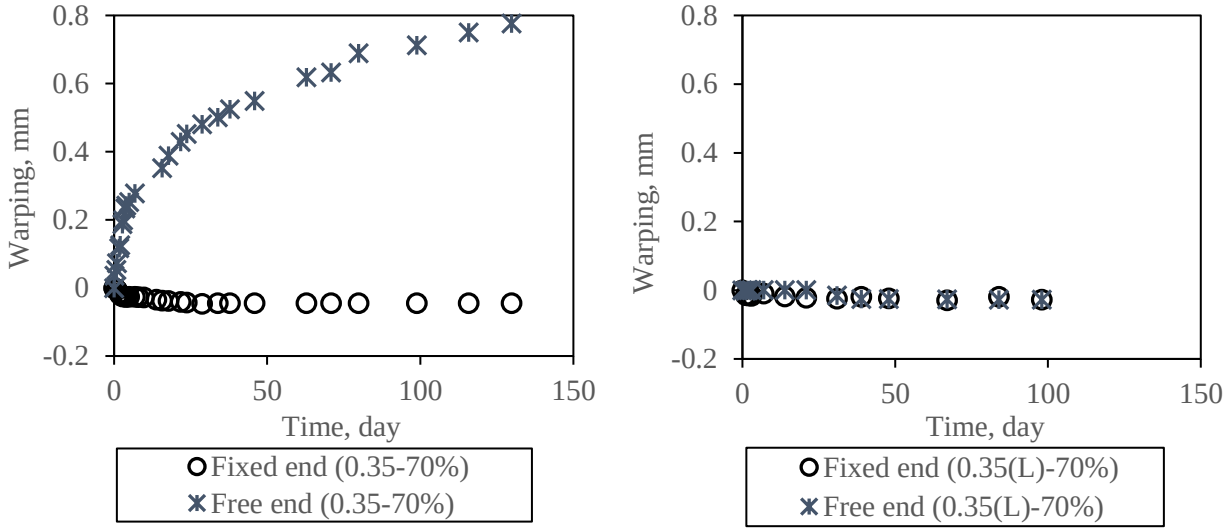

Fig. 6-28 Effect of LWA on the moisture warping of concrete beams for (a) 0.35-70% and (b) 0.35(L)-70% with 50% LWA replacement ratio

After comparing the warping measurement of 0.35-70% with and without LWA replacement in Fig. 6-28. One can see that there is almost no warping at the free end for the one with LWA replacement while there is 0.8 mm warping for the one without LWAs. The warping test confirms the internal curing of LWA can help to reduce the risk of cracking or severe deformation as the result of inhomogeneous moisture distribution.

6.7 Summary

The experimental testing and modeling of autogenous shrinkage of HPC and NSC are discussed in this chapter. The internal RH development versus time is directly measured out with the effect of maturity, aggregate content and depth of test position investigated. Pre-wetted LWA is found to mitigate the development of autogenous shrinkage by maintaining the internal RH over long time duration. A direct method by using the free and autogenous shrinkage test to estimate the shrinkage stress under full restraint is proposed for evaluation of risk of cracking. The shrinkage stress is found to be linearly proportional to aggregate content.

Chapter 7 Testing and Modeling of Tensile Viscoelasticity of HPC by TSTM

7.1 Introduction

TSTM test is the major topic in this chapter for measuring the tensile stress development of HPC under full restraint. While it is difficult for preventing the volume change in concrete as the result of hydration, the TSTM machine applied incremental loading method to pull the specimen back to the same length after each small deformation. While concrete under sustained tensile load externally, tensile creep is expected to develop in the similar way as the compressive creep. The TSTM machine provides the restraint load on the concrete and give us the access to measuring potential tensile viscoelasticity. Estimation of tensile creep is critical for evaluating the creep effect on restraining the growth of tensile stress. Conventionally, the tensile relaxation can be estimated by the difference between the fictive tensile stress and full restraint measured stress. Few studies on tensile restraint tests was done for evaluating the tensile viscoelastic behavior of HPC and only focusing on very early age, there is still need for more study on the tensile viscoelastic effects on HPC for a long term.

In this chapter, the axial stress under full restraint for 0.35 w/c HPC with 70% aggregate content are investigated with the effect of LWA. During the test, TSTM machine records the external loading with Optotrak camera system for recording any possible deformation. The measured full restraint tensile stress by TSTM is compared to the proposed self-induced stress proposed in Chapter 6. The great correlation between these two methods not only proves that the restraint stress is proportional to the degree of restraint, but also validates the method of estimation of tensile viscoelastic behavior of HPC without need to measure tensile relaxation. The effect of aggregate content on tensile creep is also studied.

7.2 Correlation between internal temperature and axial stress at very early age

With specimens under full restraint condition, the axial stress measured by TSTM machine was recorded together with the inner temperature for the first 100 hours since starting of curing. The axial stress and temperature of 0.35-70% and 0.35(L)-70% are plotted in Fig. 7-1. It can be seen from Fig. 7-1 that there is large change in axial stress within the first few hours after the casting of concrete. For both HPC with and without LWA, the internal curing temperature was raised by about 15 °C since about 10 hours after start of curing. This huge change in temperature lead to the expansion of specimens which can be detected from the reduction in axial stress. After about 1-2 days since the starting of curing, the internal temperature is stable and thermal strain is not an important factor anymore. All the TSTM restrained shrinkage tests in this study were started from 5-8 days since curing, and effect of the thermal expansion on axial stress can be ignored.

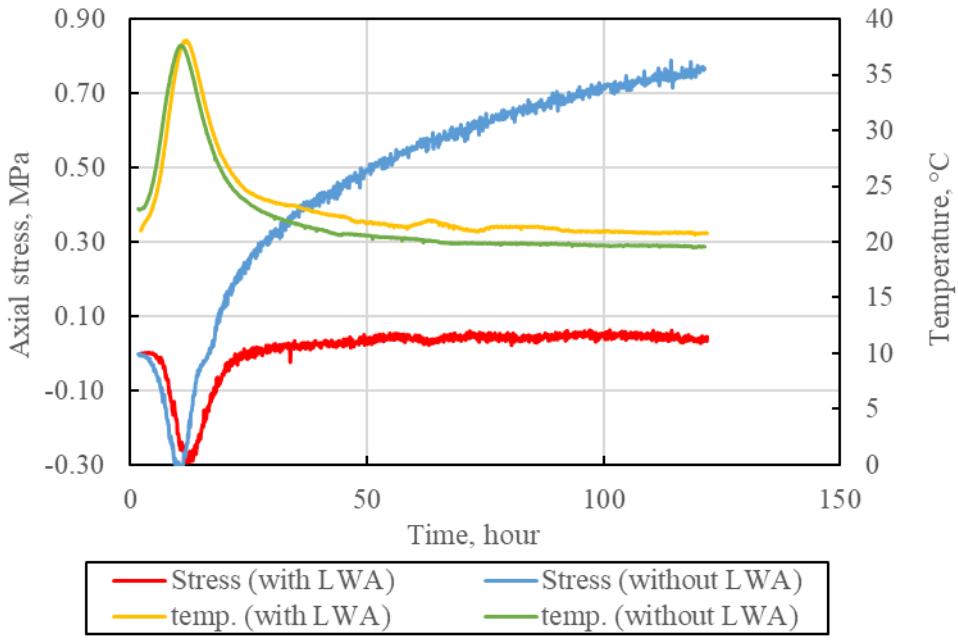

Fig. 7-1 The axial stress and internal temperature at the very early age after casting

7.3 Elastic tensile modulus measurement

With the aid of TSTM machine, the tensile elastic modulus can be directly measured by incremental loading. Optotrak camera is used for measuring the deformation of the specimen during the test. For the sake of accuracy of measurement, the specimen is first loaded and unloaded repeatedly to avoid any possible sliding between matrix and rebar before recording the data. Then the specimen is loaded and unloaded multiple times with the stress and strain recorded by TSTM. The tensile elastic modulus can thus be estimated by the averaged result from multiple tests. The stress/strain curves for 0.35-70 and 0.35(L)-70% at 7days, middle point during the test and the final loading to failure are plotted in Fig.7-2 and Fig. 7-3. A significant linear correlation between stress and strain can be observed from Fig.7-2 and Fig. 7-3 and the slope of the regression curve fitted by the data is the tensile elastic modulus.

In Fig. 7-4 (a) and (b), the measured tensile elastic modulus of 0.35-70% and 0.35(L)-70% were plotted versus ages with compressive elastic modulus. It can be seen that the tensile elastic modulus of both 0.35-70% and 0.35(L)-70% are both almost constant versus time. Different from the increase in compressive modulus versus time, no aging effect is shown to be related to the growth of tensile modulus.

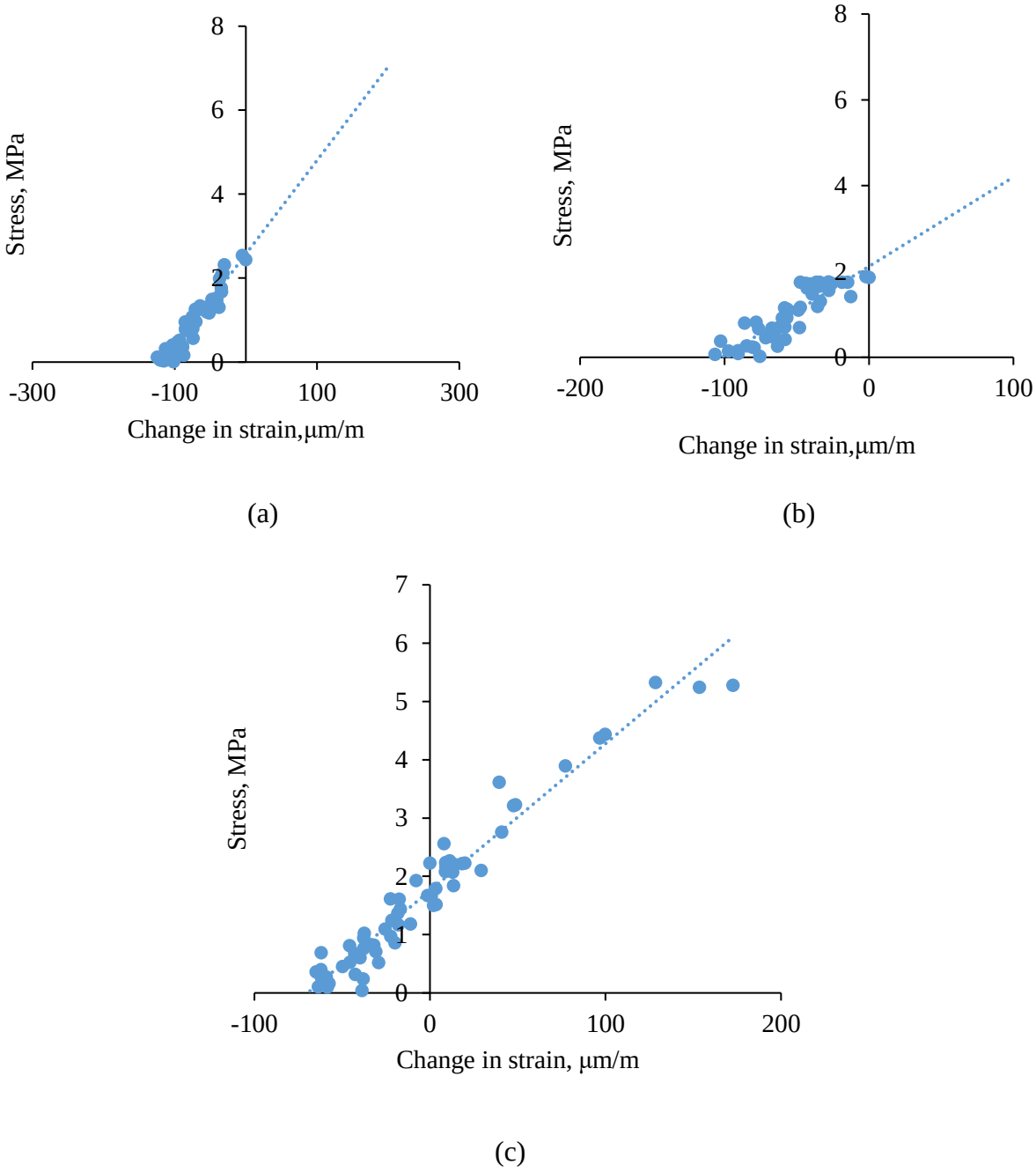

Fig. 7-2 The stress strain curve for tensile loading test by TSTM machine for 0.35-70% (a) at 7 days (b) at 28 days and (c) 35 days

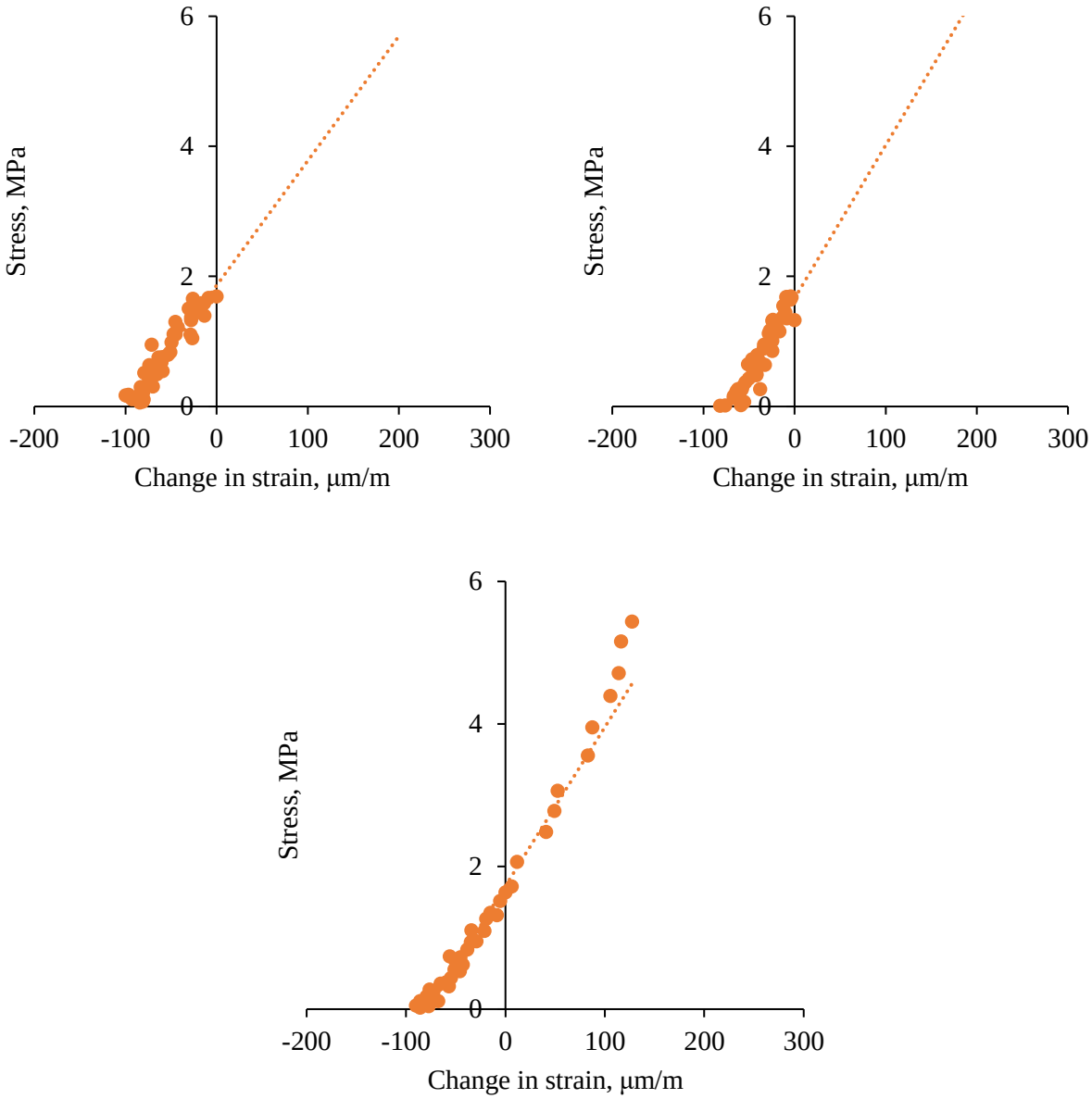

(c)

Fig. 7-3 The stress strain curve for tensile loading test by TSTM machine for 0.35(L)-70% (a) at 7 days (b) at 28 days and (c) 60 days

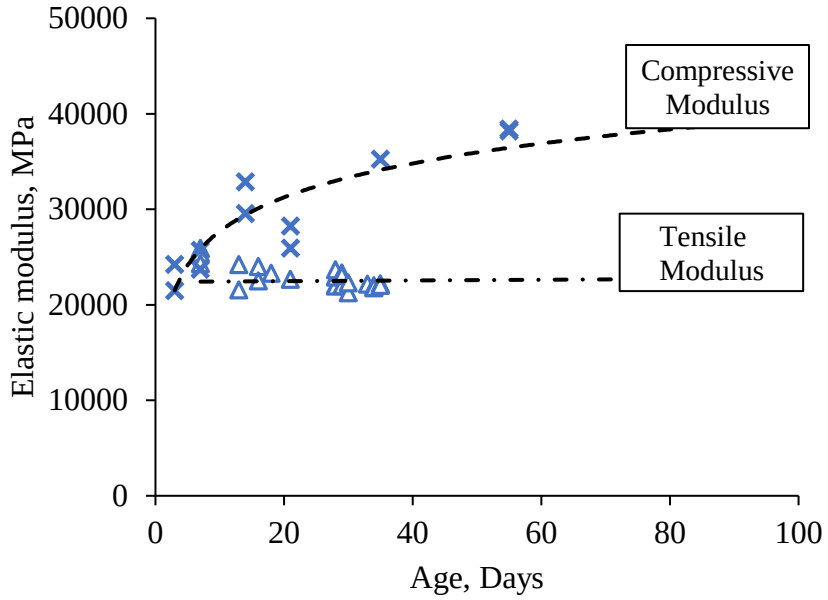

(a)

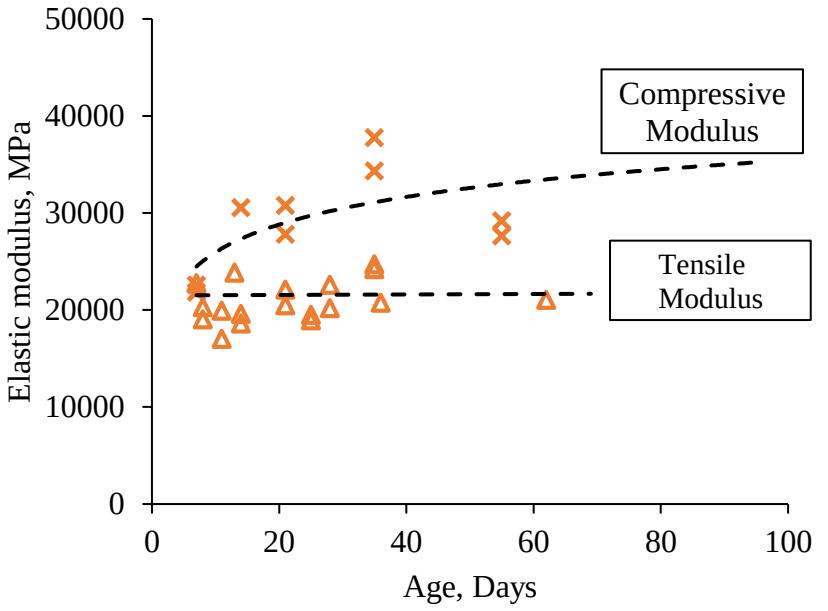

(b)

Fig. 7-4 The tensile and compressive modulus for (a) 0.35-70% and (b) 0.35(L)-70%

7.4 TSTM long term axial stress measurement under full restraint

The computer-controlled TSTM machine is used for holding the specimen with the same length. While shrinkage drives the concrete to deform, the loading cell of TSTM is programmed to adjust the load so that the specimen is always kept with the same length. Fig. 7-5shows the axial stress and axial displacement versus time during the loading for 0.35-70%. Based on the constant axial displacement, it can be guaranteed that the specimen is in constant length. The approximate zero relative development in strain measured by Optotrak camera shown in Fig. 7-6 also proves that no deformation developed in TSTM test. It can be seen that the axial stress for 0.35-70% increases from about 1.5MPa to 1.9 MPa linearly versus time.

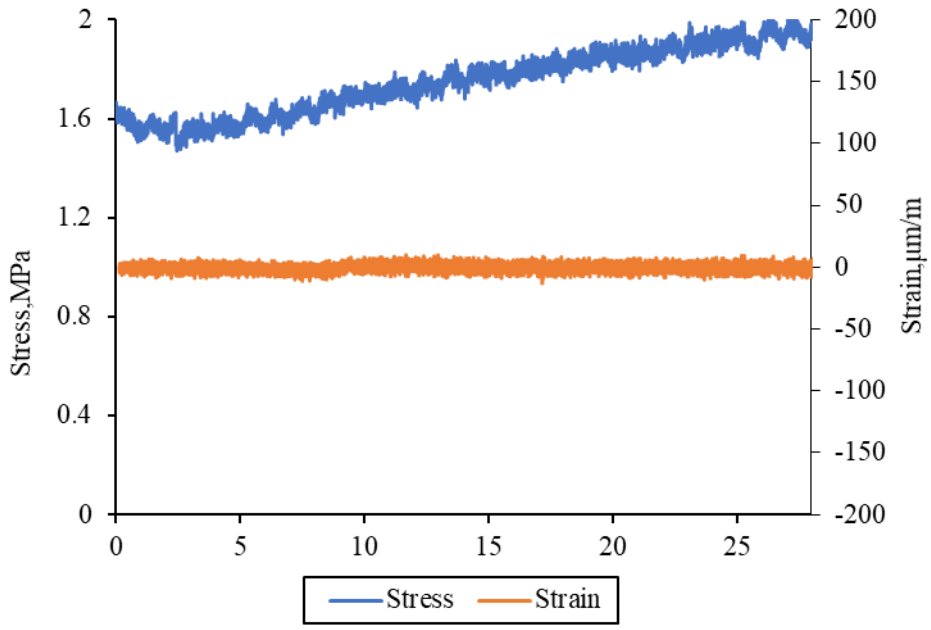

Fig. 7-5 The axial stress and relative strain for 0.35-70%

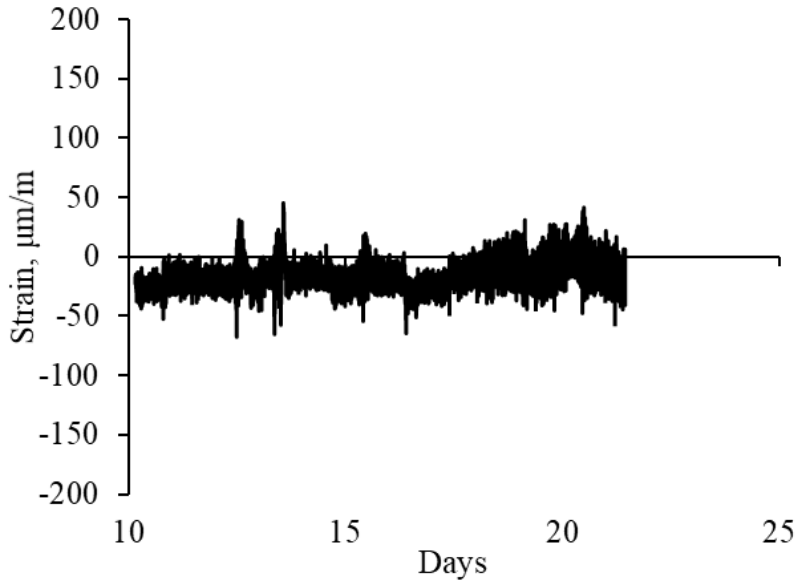

Fig. 7-6 The strain measured by Optotrak for 0.35-70% from 10 to 21 days

7.5 Tensile viscoelasticity estimation by restrained and free shrinkage measurement

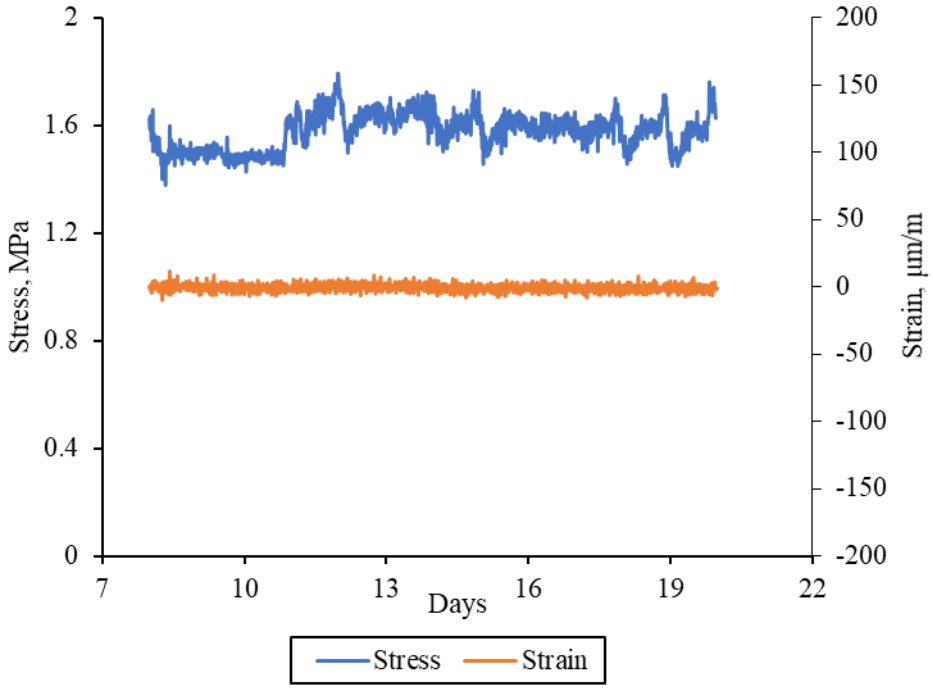

Fig. 7-7 The axial stress and relative strain for 0.35(L)-70%

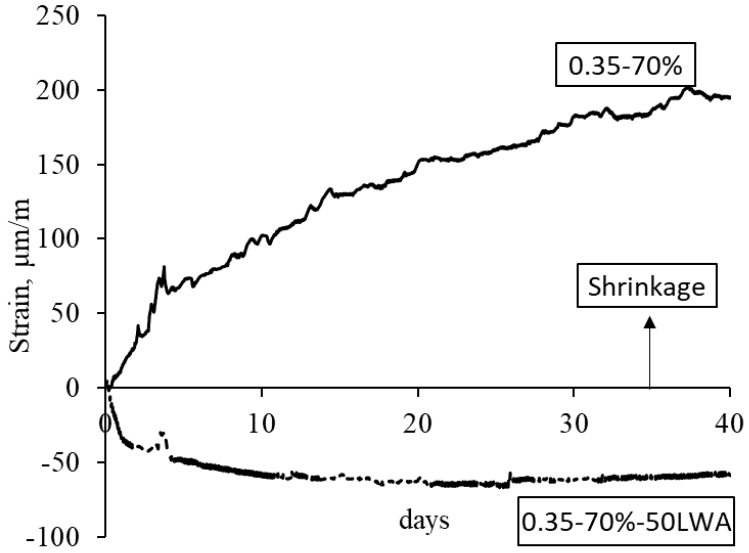

Fig. 7-8 Autogenous shrinkage for 0.35-70% and 0.35(L)-70%

The long term axial stress measurement by TSTM under full restraint for 0.35(L)-70% with 50% LWA replacement is also tested and plotted in Fig. 7-7. It has been investigated in Chapter 6 that with the presence of LWA, no shrinkage is developed since 7 days for HPC as shown in Fig. 7-8. Since the growth of shrinkage stress is proportional to the growth in autogenous shrinkage, no contribution of shrinkage to the growth of TSTM stress can be assumed for 0.35(L)-70% with 50% LWA replacement.

$$\Delta\sigma_{sh} \approx 0 \qquad \text{Eq. 7-1}$$

For the TSTM full restraint test, there are two possible factors that could potential reduce the total imposed tensile stress: (1) external tensile loading initially. It can be called creep loading because that it provides potential tensile creep with the external load. (2) Internal shrinkage stress, which increases with the shrinkage. Seen from section 7.3, it is known that the axial TSTM stress of 0.35(L)-70% HPC is constant versus time with shrinkage effect eliminated by LWA. By implementing internal curing and shrinkage mitigation, the effect of externally imposed tensile creep loading on the potential for tensile creep stress relaxation is directly tested.

No reduction in the TSTM tests shows that no tensile creep or relaxation from 7 days is observed. Moreover, in our tests for sustained constant strain between 7 and 30 days, and between 70 and 90 days no reduction in machine stress is found. Intermittent, short-term unloading/re-loading tests lasting less than 30 minutes in duration, show a continued linear elastic stress-strain behavior.

$$\Delta\sigma_{cr,t} = \Delta\sigma_{TSTM} - \Delta\sigma_{sh} \approx 0 \qquad \text{Eq. 7-2}$$

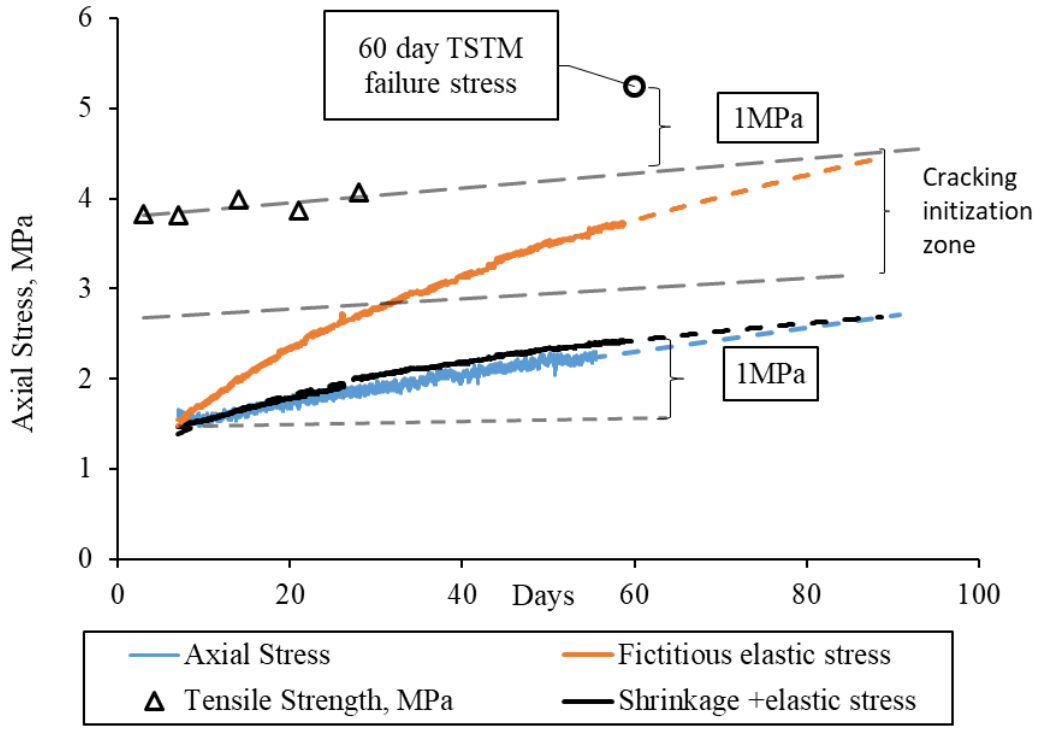

(a)

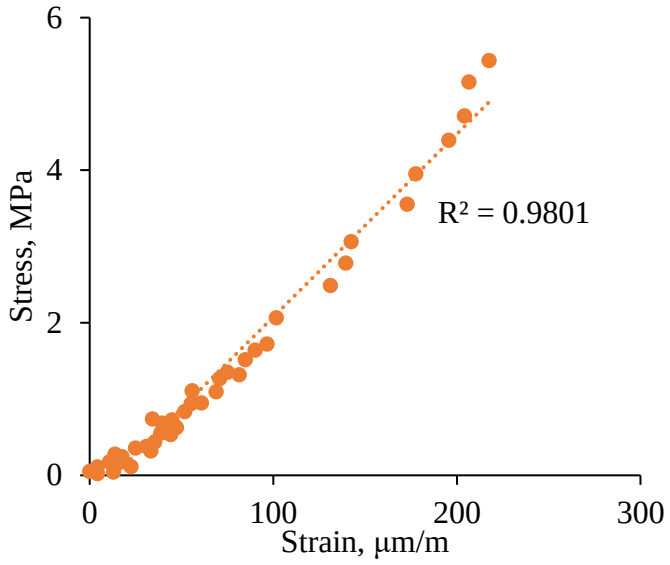

(b)

Fig. 7-9 (a)Axial stress, shrinkage stress, elastic stress and tensile strength development versus age (b) The stress/strain curve at 60 days loading to failure

The fictive elastic stress, shrinkage stress, axial stress are plotted in Fig. 7-9(a) with all extended to 90 days. It can been seen that the shrinkage stress calculated by the method proposed in Chapter 6 is almost the same as the axial stress measured in TSTM test under full restraint. It infers that the shrinkage stress is proportional to the degree of restraint. The fictive elastic stress is shown in orange is calculated by applying Eq. 7-3. It can be seen that by applying the elastic modulus to evaluating the axial stress, it overestimates axial stress a lot. The fictive elastic stress increases with age in a much larger rate than the tensile strength and the two curves intersect with each other at about 90 days. It means that the concrete has potential high risk of cracking if the shrinkages stress follows the development of the fictive elastic stress. The truth is the reverse and thus elastic modulus should not be used for evaluating the shrinkage stress. More importantly, it needs to be noted that since the 7 days loading started, the increase in axial stress TSTM approaches about 1 MPa, which is the same as the increase of the split strength at 60 days. This finding makes it more convincing that shrinkage produces internal 3-D compression, thus potentially increasing the tensile strength.

$$\Delta\sigma_{fe} = \int_{t_0}^{t} E_{e,t}\, d\varepsilon_{sh}(t) \qquad \text{Eq. 7-3}$$

$$\Delta\sigma_{re} = \Delta\sigma_{fe} - \Delta\sigma_{sh} \qquad \text{Eq. 7-4}$$

The relaxation in stress is defined as the difference between fictive elastic and viscoelastic stress as shown in Eq. 7-5. Based on Fig. 7-9, it can be seen that $\Delta\sigma_{re} \approx 2MPa$ at about 90 days. Different from plastics whose relaxation modulus is absolutely a real materials property, relaxation modulus for concrete is fictitious modulus. Intermittent un-loading and re-loading tests also support that the material behavior is remaining elastic in tension.

The stress and autogenous shrinkage are plotted versus time in Fig. 7-10(a) together with the similar plot made by Bjøntegaard (1999) in Fig. 7-10(b). It can be seen that A similar linear development of total stress over time is found by this study and work by Bjøntegaard (1999) which further confirms that relaxation is either instantaneous or not a major factor.

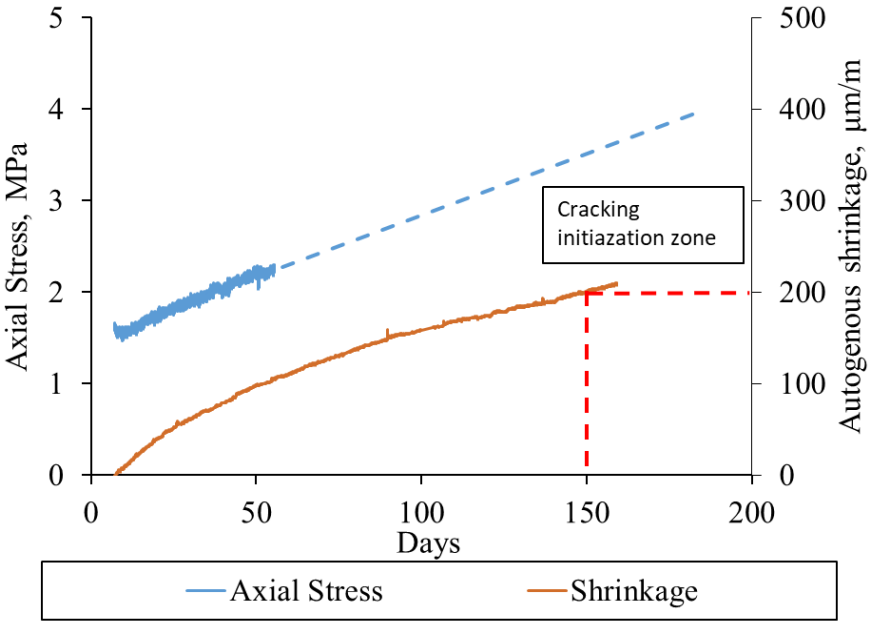

(a)

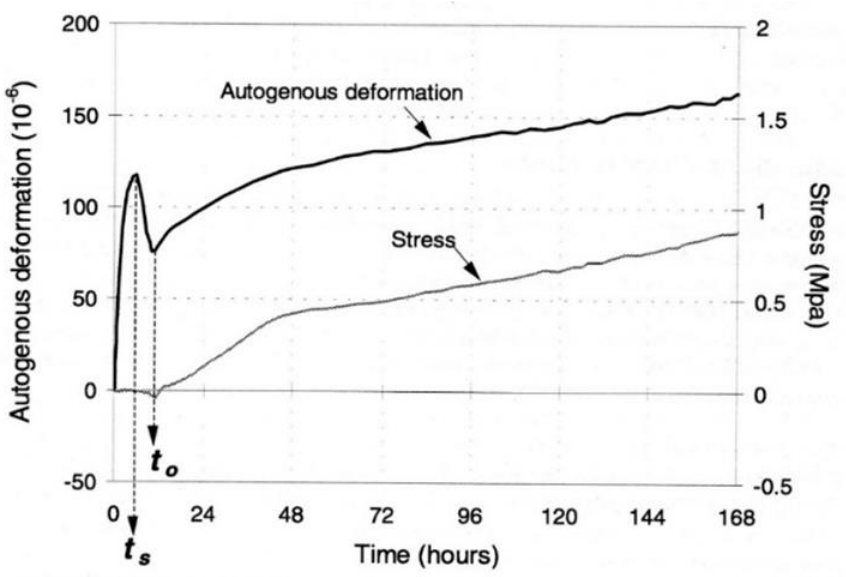

(b)

Fig. 7-10 Stress and shrinkage development versus time (a) tested in this study (b) conducted by Bjøntegaard (1999)

7.6 Estimation of cracking risk and shrinkage modulus

For estimation of cracking risk of concrete under full restraint, the axial stress measured from TSTM test of 0.35-70% is plotted versus autogenous shrinkage in Fig. 7-11(a). An exponential function can be used to perfectly fit the development of axial stress versus autogenous shrinkage. For estimation of the magnitude of axial stress when concrete potentially cracks, the curve is extrapolated to 200 μm, where the cracks may be initiated. It can be seen from Fig. 7-11 that about 3.5 MPa correspond to 200 μm when concrete probably will crack. This correlation can be used to directly evaluate the cracking risk of concrete quantitatively.

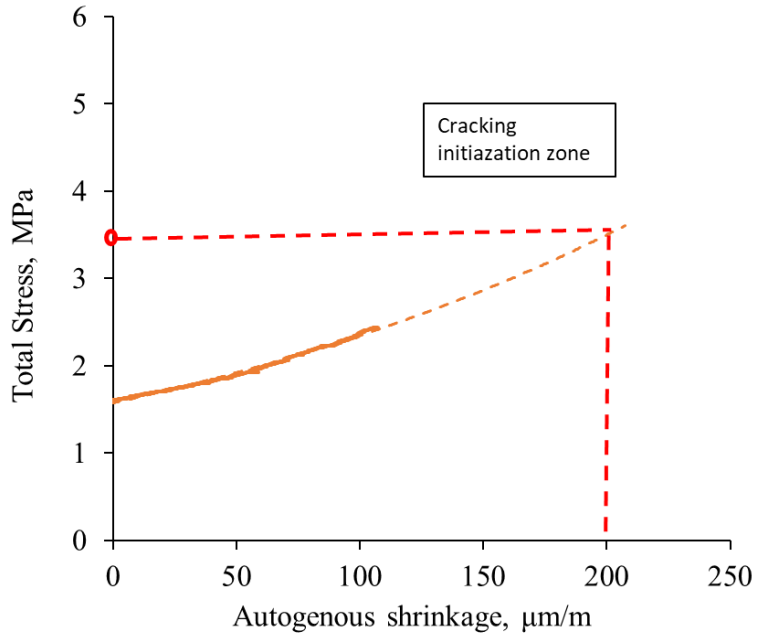

(a)

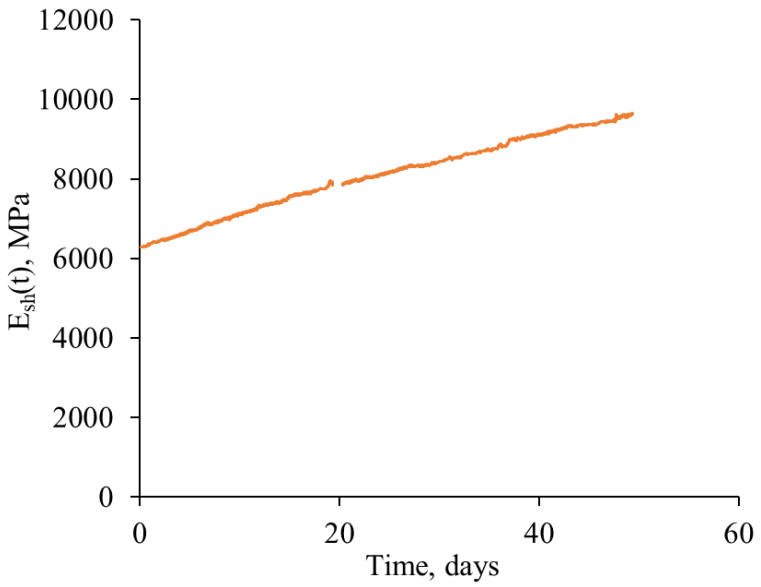

(b)

Fig. 7-11 (a) Total stress plotted versus autogenous shrinkage for 0.35-70% (b) Predicted shrinkage modulus versus time

Since autogenous shrinkage contributes 100% to the development of axial stress within the test period, the derivative of axial stress versus autogenous shrinkage is then defined as the shrinkage modulus, E_{sh} and plotted in Fig. 7-11(b). It can be seen that shrinkage modulus is linearly developing versus time.

$$E_{sh}(t) = \frac{d\sigma(t)}{d\varepsilon_{sh}(t)} \qquad \text{Eq. 7-5}$$

7.7 Summary

In this chapter, the TSTM full restraint test is conducted. By loading and reloading specimens during TSTM test, tensile modulus of HPC is obtained and found lower than the compressive modulus and not increases beyond age of 7 days, while compressive modulus is increasing. With the TSTM results of HPC at later-age (7 days-90 days) under constant strain and shrinkage mitigation due to internal curing of pre-wetted LWA, it suggest that tensile creep is not a factor and relaxation modulus is just a fictitious modulus. The increase in axial stress can be totally attributed to the growth in autogenous shrinkage. Axial stress under full restraint develops exponentially with autogenous shrinkage and it can be used to evaluate the risk of cracking of concrete under external full restraint quantitatively.

Chapter 8 Conclusions and Suggestions for Further work

8.1 Introduction

The major objectives, research approach, summary of major findings and recommendations for further work are discussed in this chapter. It needs to be noted that the major contribution of this research is on the viscoelasticity of HPC starting from later ages (7 days) while most of the previous research is focused on very early age (1-7 days). The conclusions of viscoelasticity effects on HPC from later ages drawn from this research is based on the stage of HPC without effect of substantial change in mechanical properties and volume due to thermal effects.

8.2 Main Objectives and Research Approach

Since it is already known from literature reviews that most of the previous research is focused on the early age (0-7 days) stress relaxation for normal concrete, the focus of this research is on later age (7-90 days) viscoelasticity of HPC and potential for stress relaxation. In the very early age, concrete is undergoing substantial change in mechanical properties and volume due to initial significant thermal effect. The thermal effect from cement hydration is typically insignificant except for mass concrete after 7 days since curing. However, autogenous shrinkage is still a major factor in HPC cured under sealed moisture condition and very few studies have investigated this time period. Therefore the objective of this research is to expand the knowledge by comprehensive study on the viscoelasticity effects on HPC within the period (7-90 days).

This research focuses on the study on the viscoelasticity of HPC with low water/cement ratio (0.35). Aging, material parameters (w/c, aggregate contents) and loading conditions (external or internal) are known to be major factors controlling the viscoelastic development of HPC. Instead

of focusing on modeling and simulation based on data from reference which potentially has lots of uncertainty and variance, numerical modeling and simulation are made based on the experimental tests conducted in this study. Existing models with physical parameters are used in this study for better explanation of viscoelasticity effects on HPC. New findings are made in the research for more accurate assessment of long-term viscoelasticity behavior of HPC starting from later ages. Study on the potential tensile creep is also provided in this research which make it more accurate to estimate cracking risk for HPC.

The findings are split into compressive mode and tensile mode due to the differences in findings discussed in the following chapter.

8.3 Summary of major findings

8.3.1 Compressive mode

Basic creep tests in compression being loaded from three ages (7,28 and 120 days) and two stress levels (5 MPa and 10MPa) in this research extend the knowledge of compressive viscoelasticity effects on HPC. A modified rheological Thomson model is used to simulate the basic creep behavior of HPC due to its ability to capture underlying physical parameters. As one of the parameters of the modified Thomson model, viscoelastic ultimate creep modulus is defined to evaluate the resistance to viscoelastic behavior of HPC under equilibrium condition.

Shrinkage stress development is measured and simulated in free and partial restraint twin shrinkage test. These results demonstrate that shrinkage stress is approximately linear to aggregate content in concrete and proportional to degree of restraint. Pre-wetted lightweight aggregate (LWA) is used in this study to mitigate shrinkage. By the experimental test on the development of internal relative humidity (RH), the effect of internal curing by LWA on shrinkage can be quantified directly by the level of internal RH. It is shown that 50% LWA content by sand replacement can help to maintain the internal RH above 90%. Mitigation of shrinkage is used in TSTM tensile test for studying tensile creep effect at later age.

8.3.2 Tensile mode

Two major factors can potentially cause relaxation, the reduction in total imposed tensile stresses, for constant imposed strain in a TSTM test: (1) initial external tensile loading which is

also the driving force for potential tensile creep, and (2) internal shrinkage stress, which increases linearly with shrinkage. TSTM results of HPC at later-age (7 days-90 days) under constant strain and shrinkage mitigation due to internal curing suggest that tensile creep is not a factor, as no reduction in TSTM tensile stress is obtained for long-term continued relaxation test. Long-term continuous TSTM test at constant total strain with intermittent unloading/re-loading tests lasting less than 30 minutes in duration shows a continued linear elastic stress-strain behavior of HPC of near constant modulus. At end of TSTM testing the stress-strain curve to failure shows linear elastic stress-strain behavior until failure. The total failure strain is in the range of 200-250 micro-strain and failure stress is within expected range based on split tensile test results except for one case. In this case TSTM test duration is extended to 60 days allowing for longer measurement time of the shrinkage stress. During this time-period the increase in stress reaches about 1MPa and total failure stress is increased by same amount over expected tensile strength. These results suggest that shrinkage produces internal 3-D compression, thus potentially increasing the tensile strength. In all cases, no real reduction in tensile stress development is observed during the later-age.

The increase in total time-dependent stress for constant strain is due to shrinkage. Shrinkage stress increase is lower than elastic stress increase. This result in a so-called fictitious stress relaxation modulus. Another major finding is that the tensile modulus of HPC is lower than the compressive modulus and not increasing beyond age of 7 days, while compressive modulus is increasing. This means that tensile stress analysis is different from compressive stress analysis. HPC in tension behaves elastically irrespective of duration of viscoelastic stress development, while HPC in compression behaves viscoelastically and can be simulated by a Thomson model for aging effect.

8.4 Recommendations for further research

Based on the results and limitations of the present work, some recommendations for further work are given:

1. Even though Thomson model can be used to fit the development of basic creep of concrete with not too long loading duration, it has problems with fitting to the basic creep

loading up to 1- 10 years. Optimization of Thomson model could be made to improve the numerical simulation for both mid-span and long –span loading duration.

2. As found by the research that the tensile relaxation behavior at later ages from 7 days is completely different from that at early age, more study and validation need to be made for the mechanisms of the behavior.
3. The study involved in this research can be extended to the viscoelasticity of HPC under drying condition or other environment with changing temperature or humidity. Whether this change may lead to the dramatic difference in the major conclusions is still needed to be validated by experimental test.
4. As HPC is widely used in large structure, the findings by this research need to be extended and calibrated by further field or experimental test on larger structure.

References

ACI 201. 2R-92, Guide to Durable Concrete, Chapter 4, ACI Committee 201.

Aıtcin, P. C. "The durability characteristics of high performance concrete: a review." Cement and concrete composites 25.4-5 (2003): 409-420.

Alfes, C. "Modulus of elasticity and drying shrinkage of high-strength concrete containing silica fume." *Special Publication*132 (1992): 1651-1671.

Al-Manaseer, A. A., et al. "Report on Factors Affecting Shrinkage and Creep of Hardened Concrete. Concrete international, 21." (2005).

Altoubat, S. A., & Lange, D. A. (2001). Creep, shrinkage and cracking of restrained concrete at early age. *Urbana*, *51*, 61801.

Arthanari, S., & Yu, C. W. (1967). Creep of concrete under uniaxial and biaxial stresses at elevated temperatures. *Magazine of Concrete Research*, *19*(60), 149-156.

Atrushi, Dawood Soliman. *Tensile and Compressive Creep of Young Concrete: Testing and Modelling*. Fakultet for ingeniørvitenskap og teknologi, 2003.

Bazant, Z. P., & Chern, J. C. (1985). Concrete creep at variable humidity: constitutive law and mechanism. *Materials and structures*, *18*(1), 1.

Bažant, Z. P., Cusatis, G., & Cedolin, L. (2004). Temperature effect on concrete creep modeled by microprestress-solidification theory. *Journal of engineering mechanics*, *130*(6), 691-699.

Bazant, Z. P., & Li, G. H. (2008). Comprehensive database on concrete creep and shrinkage. *ACI Materials Journal*, *105*(6), 635-637.

Bazant, Z. P., & Kim, S. S. (1979). Approximate relaxation function for concrete. *ASCE J Struct Div*, *105*(12), 2695-2705.

Bažant, Z. P., & Panula, L. (1978). Practical prediction of time-dependent deformations of concrete. *Matériaux et Construction*, *11*(5), 317-328.

Bažant, Z. P., & Prasannan, S. (1988). Solidification theory for aging creep. *Cement and Concrete Research*, *18*(6), 923-932.

Bazant, Z. P., & Wittmann, F. H. (1982). Creep and shrinkage in concrete structures.

Bažant, Z. P., & Wu, S. T. (1974). Rate-type creep law of aging concrete based on Maxwell chain. *Matériaux et Construction*, *7*(1), 45-60.

Bentz, D. P., & Snyder, K. A. (1999). Protected paste volume in concrete: Extension to internal curing using saturated lightweight fine aggregate. *Cement and concrete research*, *29*(11), 1863-1867.

Bentz, D. P., & Weiss, W. J. (2011). *Internal curing: a 2010 state-of-the-art review*. Gaithersburg, Maryland: US Department of Commerce, National Institute of Standards and Technology.

Best, J. F. "Properties and use of fly ash in Portland cement concrete." *Concrete International* 4.07 (1982): 81-92.

Bjøntegaard, Ø., & Sellevold, E. J. (2001). Interaction between thermal dilation and autogenous deformation in high performance concrete. *Materials and structures*, *34*(5), 266-272.

Bjøntegaard, Ø. (1999). Thermal dilation and autogenous deformation as driving forces to self-induced stresses in high performance concrete. Norges Teknisk-Naturvitenskapelige Universitet.

Bissonnette, B., & Pigeon, M. (1995). Tensile creep at early ages of ordinary, silica fume and fiber reinforced concretes. *Cement and concrete research*, *25*(5), 1075-1085.

Bissonnette, B., Pierre, P., & Pigeon, M. (1999). Influence of key parameters on drying shrinkage of cementitious materials. *Cement and Concrete Research*, *29*(10), 1655-1662.

Bosnjak, D., & Kanstad, T. (2001, August). Numerical simulation of temperature and strain development in real concrete structures. In *Creep, Shrinkage and Durability of Concrete and other quasi-brittle Materials, Proceedings of the Sixth International Conference, Cambridge (MA)* (pp. 307-312).

Brooks, J. J., P. J. Wainwright, and M. Boukendakji. "Influence of Slag Type and Replacement Level on Strength Elasticity, Shrinkage and Creep of Concrete." *Special Publication* 132 (1992): 1325-1342.

Byfors, J., (1980): "*plain concrete at early ages"*. Swedish Cement and Concrete Institute. Fo 3:80, Stockholm.

Ceb-Fip, M. C. (1990). Design code. *Comite Euro International du Beton*, 51-59.

Counto, U. J. (1964). The effect of the elastic modulus of the aggregate on the elastic modulus, creep and creep recovery of concrete. *Magazine of Concrete Research*, *16*(48), 129-138.

Copeland, L. E., & Bragg, R. H. (1955). *Self-desiccation in Portland cement pastes* (No. 52).

Cusson, D., & Hoogeveen, T. (2008). Internal curing of high-performance concrete with pre-soaked fine lightweight aggregate for prevention of autogenous shrinkage cracking. *Cement and Concrete Research*, *38*(6), 757-76.

Davis, R. E., & Troxell, G. E. (1954, January). Properties of concrete and their influence on prestress design. In *Journal Proceedings* (Vol. 50, No. 1, pp. 381-391).

Emborg, M. (1998). Development of mechanical behaviour at early ages. Prevention of Thermal Cracking in Concrete at Early Ages; Springenschmid, R., Ed, 76-148.

Grasley, Z. C., & Lange, D. A. (2007). Constitutive modeling of the aging viscoelastic properties of portland cement paste. *Mechanics of Time-Dependent Materials*, *11*(3-4), 175-198.

Hagihara, S., Masuda, Y., & Nakamura, S. (2002, June). Creep behaviour of high-strength concrete in early age. In *6th International Symposium on High Strength/High Performance Concrete*.

Hanehara, S., Hirao, H., and Uchikawa, H., (1999) "Relationship between Autogenous Shrinkage and the Microstructure and Humidity Changes at Inner Part of Hardened Cement Pastes at Early Ages", Proc. Int. Workshop Autoshrink'98, ed. E.-I. Tazawa, Hiroshima, Japan, E & FN SPON, London, pp. 89-10

Hansen, T. C. (1960). *Creep and stress relaxation of concrete: a theoretical and experimental investigation*. Svenska forskningsinstitutet för cement och betong vid Kungl. Tekniska högskolan.

Hansen, P. F., & Pedersen, E. J. (1977). Maturity computer for controlled curing and hardening of concrete (No. Analytic).

Hansen, T. C., & Mattock, A. H. (1966). Influence of Size and Shape of Member on the Shrinkage and Creep of Concrete. In *Journal Proceedings* (Vol. 63, No. 2, pp. 267-290).

Hansen, T. C., & Nielsen, K. E. (1965, July). Influence of aggregate properties on concrete shrinkage. In *Journal Proceedings* (Vol. 62, No. 7, pp. 783-794).

Hansen, W., Liu, Z., & Koenders, E. A. (2014). Internal Viscoelastic Modulus Associated with Autogenous Shrinkage in Cementitious Materials. *Journal of Advanced Concrete Technology*, *12*(11), 496-502.

Haranki, B. (2009). Strength, modulus of elasticity, creep and shrinkage of concrete used in Florida (Doctoral dissertation, University of Florida).

Lee, K. M., Lee, H. K., Lee, S. H., & Kim, G. Y. (2006). Autogenous shrinkage of concrete containing granulated blast-furnace slag. *Cement and Concrete Research*, *36*(7), 1279-1285.

Liu, N., Plucinsky, P., & Jeffers, A. E. (2017). Combining load-controlled and displacement-controlled algorithms to model thermal-mechanical snap-through instabilities in structures. *Journal of Engineering Mechanics*, *143*(8), 04017051.

Jonasson, J. E., (1985): "*Early Strength Growth in Concrete – Preliminary Test Results Concerning Hardening at Elevated Temperatures"*, International Symposium on Winter Concreting (RILEM)), Espoo, Technical Research Center of Finland (VTT), pp. 249-254.

Lura, P., (2003) “Autogenous Deformation and Internal Curing of Concrete”, Delft, The Netherlands, Delft University.

Lura, P., Van Breugel, K., Maruyama, I., (2000): *“Effect of Curing Temperature and Type of Cement on Early-Age Shrinkage of High Performance Concrete”*, Submitted to Cement Concrete Research Special issue, Proc. of Symposium ‘Materials Science of High Performance Concrete’, Boston.

Lura, P., van Breugel, K., & Maruyama, I. (2001). Effect of curing temperature and type of cement on early-age shrinkage of high-performance concrete. *Cement and Concrete Research*, *31*(12), 1867-1872.

Kanstad, T., Hammer, T. A., Bjřntegaard, Ř., & Sellevold, E. J. (1999). Mechanical Properties of Young Concrete-Evaluation of Test Methods for Tensile Strength and Modulus of Elasticity-Determination of Models Parameters. NOR-IPACS Report STF22 A99762. ISBN 82-14-01062-4, Trondheim.

Kaplan, M. F. (1959). Ultrasonic Pulse Velocity, Dynamic Modulus of Elasticity, Poisson's Ratio and the Strength of Concrete Made with Thirteen Different Cements' Aggregate. *Rilem Synpo. Paris*.

Kasai, Y. *"Durability of Concrete Using Recycled Coarse Aggregate, RILEM; Reuse of Demolition Waste."* V 2 (1974): 623-632.

Khan, Arshad A., William D. Cook, and Denis Mitchell. "*Tensile strength of low, medium, and high-strength concretes at early ages.*" Materials Journal 93.5 (1996): 487-493.

Klug, P., & Wittmann, F. (1970). The correlation between creep deformation and stress relaxation in concrete. *Matériaux et Construction*, *3*(2), 75-80.

Koenders, E. A. B. (1997). Simulation of volume changes in hardening cement-based materials (Doctoral dissertation, TU Delft, Delft University of Technology).

Koenders, E. A. B., & Van Breugel, K. (1997). Numerical modelling of autogenous shrinkage of hardening cement paste. *Cement and Concrete Research*, *27*(10), 1489-1499.

Kovler, K. (1994). Testing system for determining the mechanical behaviour of early age concrete under restrained and free uniaxial shrinkage. *Materials and structures*, *27*(6), 324.

Mazloom, M., Ramezanianpour, A. A., & Brooks, J. J. (2004). Effect of silica fume on mechanical properties of high-strength concrete. *Cement and Concrete Composites*, *26*(4), 347-357.

Maslov, G. N. (1940). “Thermal stress states in concrete masses, with account of concrete creep.” Izvestia Nauchno-Issledovatel’skogo Instituta Gidrotechniki, Vol. 28, Gosenergoizdat, Moscow, 28, 175–188.

Morimoto, H., & Koyanagi, W. (2014, April). 12 ESTIMATION OF STRESS RELAXATION IN CONCRETE AT EARLY AGES. In *Thermal Cracking in Concrete at Early Ages: Proceedings of the International RILEM Symposium* (p. 95). CRC Press.

McDonald, D., & Roper, H. (1993). Prediction of drying shrinkage of concrete from internal humidities and finite element techniques. In *RILEM PROCEEDINGS* (pp. 259-259). CHAPMAN & HALL.

Nasser, K. W., & Neville, A. M. (1965, December). Creep of concrete at elevated temperatures. In *Journal Proceedings*(Vol. 62, No. 12, pp. 1567-1580).

Neville, A.M, and Aitcin,P.C. "High performance concrete—an overview." *Materials and structures* 31.2 (1998): 111-117.

Neville, A. M. (1971). Creep of concrete: plain, reinforced, and prestressed.

Neville, A., & Aitcin, P. C. (1998). High performance concrete—an overview. *Materials and structures*, *31*(2), 111-117.

Neville, A. M., Dilger, W. H., and Brooks, J. J. (1983). *Creep of plain and structural concrete*, Construction Press, New York.

Onken, P., & Rostasy, F. S. (1995). A practical planning tool for the simulation of thermal stresses and for the prediction of early thermal cracks in massive concrete structures. In *RILEM PROCEEDINGS* (pp. 289-289). CHAPMAN & HALL.

Paillere, A., Buil, M., & Serrano, J. J. (1989). Effect of fiber addition on the autogenous shrinkage of silica fume. *Materials Journal*, *86*(2), 139-144.

Pickett, G. (1956). Effect of aggregate on shrinkage of concrete and a hypothesis concerning shrinkage. In *Journal Proceedings* (Vol. 52, No. 1, pp. 581-590).

Polivka, M., Pirtz, D. and Adams, R. F. (1964): *"Studies f Creep in Mass Concrete",* Symposium on 'Mass Concrete', ACI, Special Publication, NO. 6, pp 257-83.

Ranaivomanana, N., Multon, S., & Turatsinze, A. (2013). Tensile, compressive and flexural basic creep of concrete at different stress levels. *Cement and Concrete Research*, *52*, 1-10.

Report of ACI Committee 233, Slag Cement in Concrete and Mortar, ACI 233R-03, American Concrete Institute, Farmington Hills, Mich, 2003.

RILEM TC-196, Internal curing of concrete, state-of-the-art report of RILEM technical committee 196-ICC, in: K. Kovler, O.M. Jensen (Eds.), RILEM Publications S.A.R.L. France, Bagneux, 2007, 139 pp.

Rossi, P., Tailhan, J. L., & Le Maou, F. (2013). Creep strain versus residual strain of a concrete loaded under various levels of compressive stress. *Cement and concrete research*, *51*, 32-37.

Ruiz, M. F., Muttoni, A., & Gambarova, P. G. (2007). Relationship between nonlinear creep and cracking of concrete under uniaxial compression. *Journal of Advanced Concrete Technology, 5*(3), 383-393.

Springenschmid R., Breitenbücher R., Mangold M., "Development of the cracking frame and the temperature-stress testing machine", Thermal Cracking in Concrete at Early Ages, Proceedings of the International RILEM Symposium, Munich, Germany, 10-12 October, 1994, p. 137-144.

Smadi, M. M., Slate, F. O., & Nilson, A. H. (1987). Shrinkage and creep of high-, medium-, and low-strength concretes, including overloads. *Materials Journal*, *84*(3), 224-234.

Standard, A. S. T. M. C192. 2007. Standard Practice for Making and Curing Concrete Test Specimens in the Laboratory (ASTM C192-07). West Conshohocken, PA: ASTM International.

Standard, A. S. T. M. (2010). Standard Test Methods for Compressive Strength of Cylindrical Concrete Specimens. *ASTM C39*.

Suter, M., & Benipal, G. S. (2006). Time-dependent behaviour of reacting concrete I: Mechanism and theory. *Mechanics of Time-Dependent Materials*, *10*(1), 51-62.

Tazawa, E. I., & Miyazawa, S. (1995). Influence of cement and admixture on autogenous shrinkage of cement paste. *Cement and concrete research*, *25*(2), 281-287.

Tazawa, E., Miyazawa, S., and Kasai T., (1995) "Chemical Shrinkage and Autogenous Shrinkage of Hydrating Cement Paste", *Cement and Concrete Research*, Vol. 25 (2), pp. 288-292.

Yıldırım, H., & Sengul, O. (2011). Modulus of elasticity of substandard and normal concretes. *Construction and Building Materials*, *25*(4), 1645-1652.

Yue, L. L., & Taerwe, L. (1992). Creep recovery of plain concrete and its mathematical modelling. *Magazine of concrete research*, *44*(161), 281-290.

Zhang, M. H., Tam, C. T., & Leow, M. P. (2003). Effect of water-to-cementitious materials ratio and silica fume on the autogenous shrinkage of concrete. Cement and Concrete Research, 33(10), 1687-1694.

Zhang, J., Dongwei, H., & Wei, S. (2010). Experimental study on the relationship between shrinkage and interior humidity of concrete at early age. *Magazine of Concrete Research*, *62*(3), 191-199.

APPENDICES

APPENDIX A: Total Creep Strain and Creep Compliance

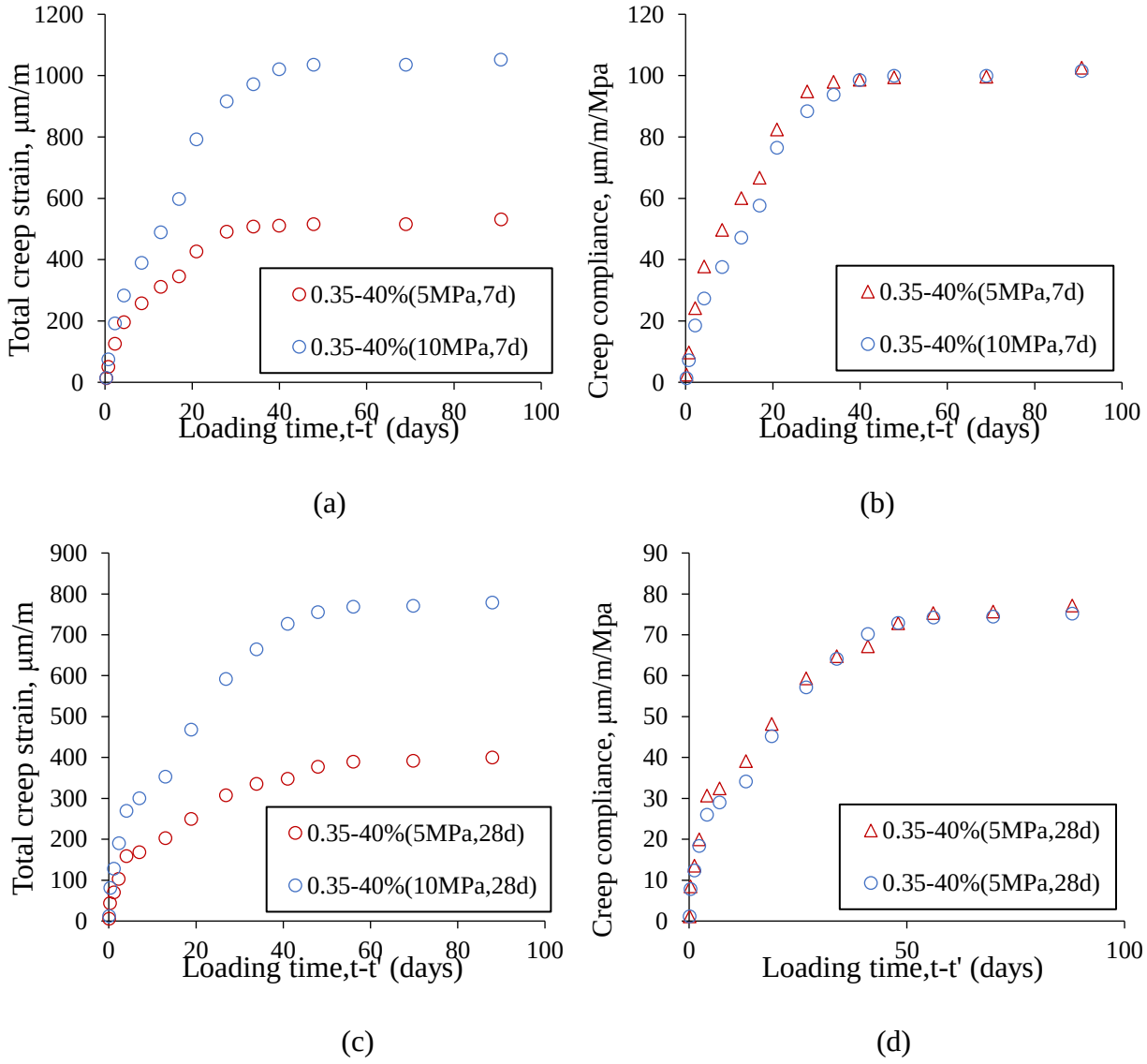

Fig. A-1 The tensile creep strain and creep compliance for 0.35-40% with loading age (7 and 28 days) with two stress load (5MPa and 10MPa)

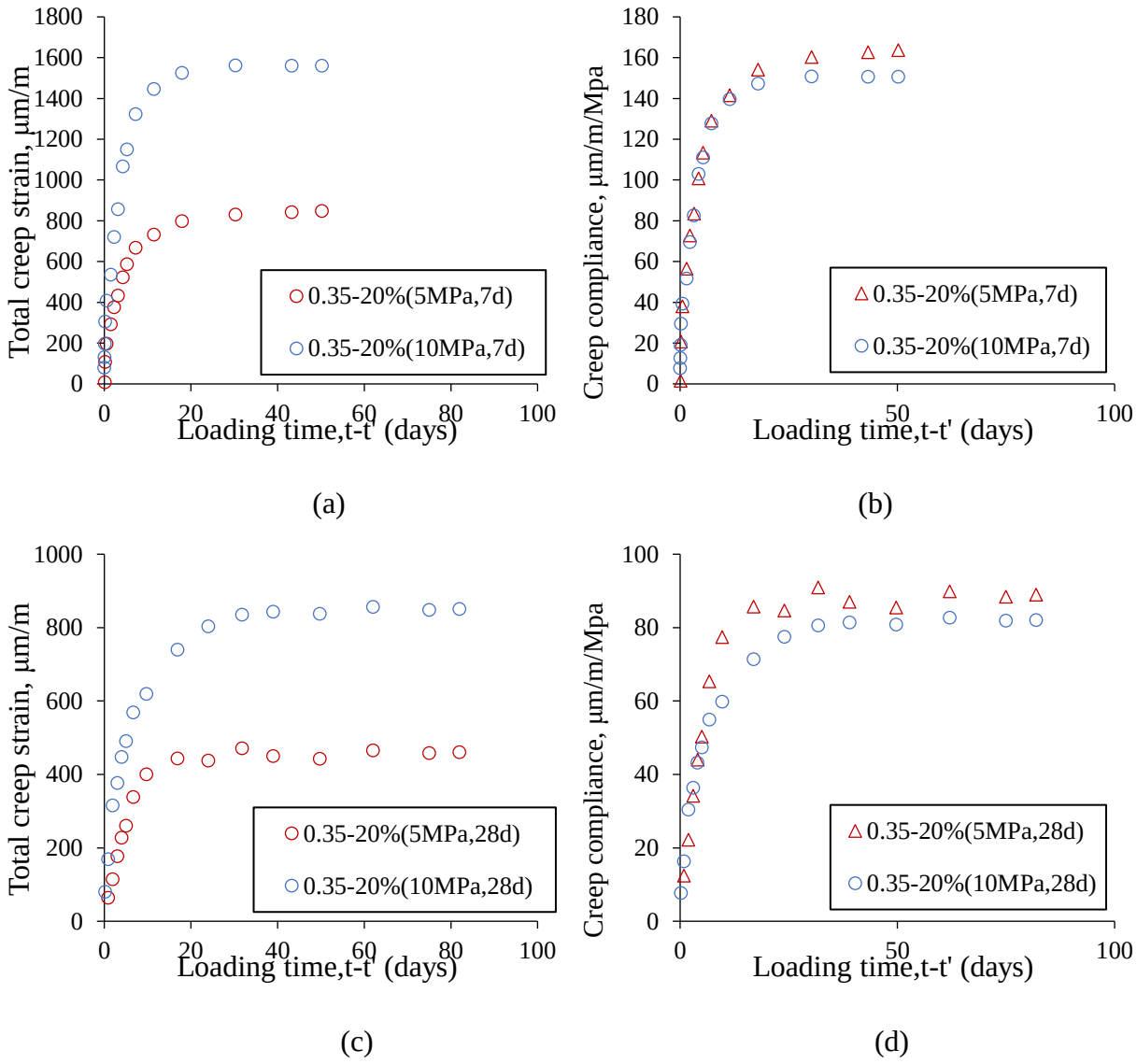

Fig. A-2 The tensile creep strain and creep compliance for 0.35-20% with loading age (7 and 28 days) with two stress load (5MPa and 10MPa)

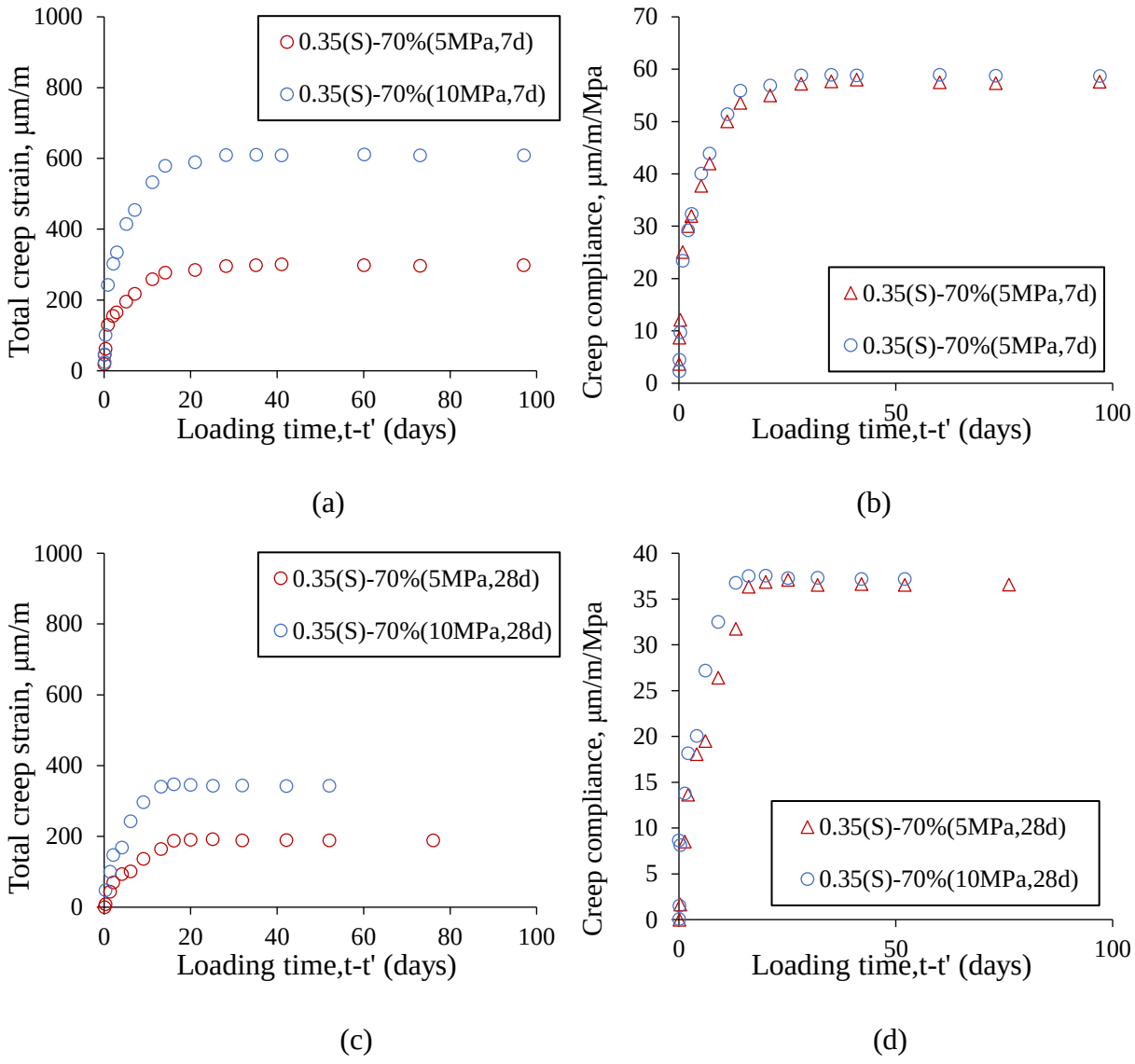

Fig. A-3 The tensile creep strain and creep compliance for 0.35(S)-70% with loading age (7 and 28 days) with two stress load (5MPa and 10MPa)

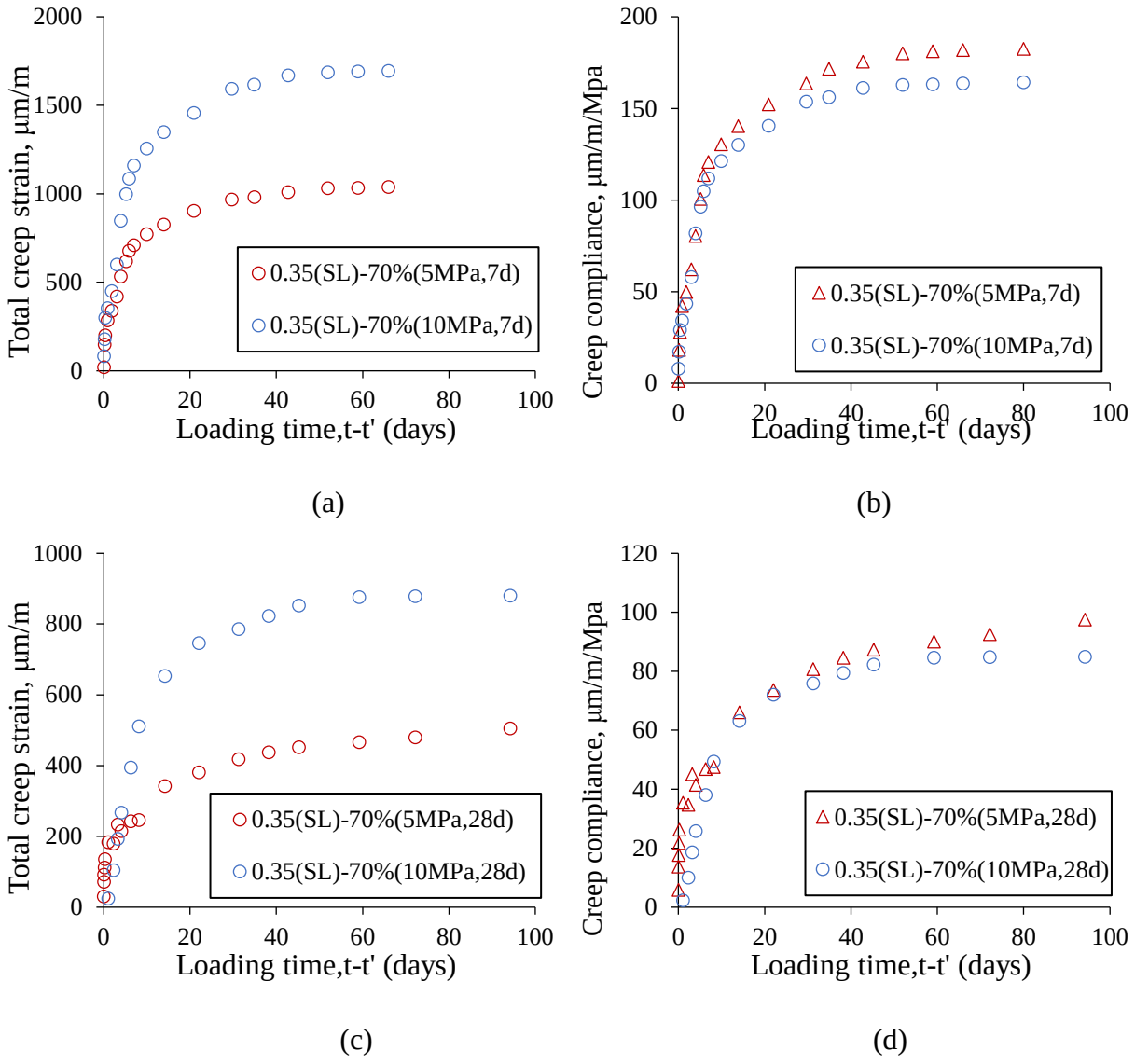

Fig. A-4 The tensile creep strain and creep compliance for 0.35(SL)-70% with loading age (7 and 28 days) with two stress load (5MPa and 10MPa)

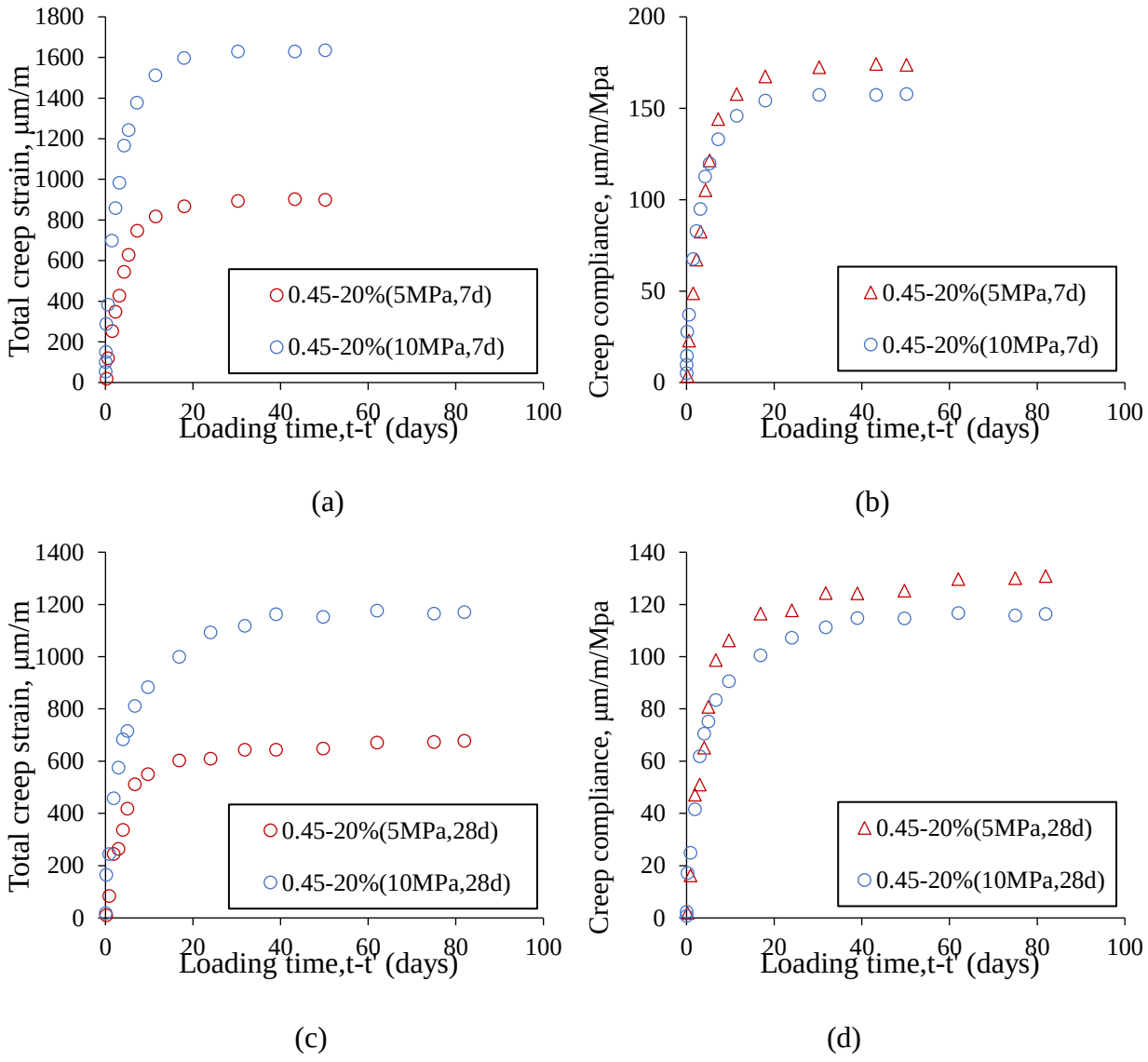

Fig. A-5 The tensile creep strain and creep compliance for 0.45-20% with loading age (7, 28 and 120 days) with two stress load(5MPa and 10MPa)

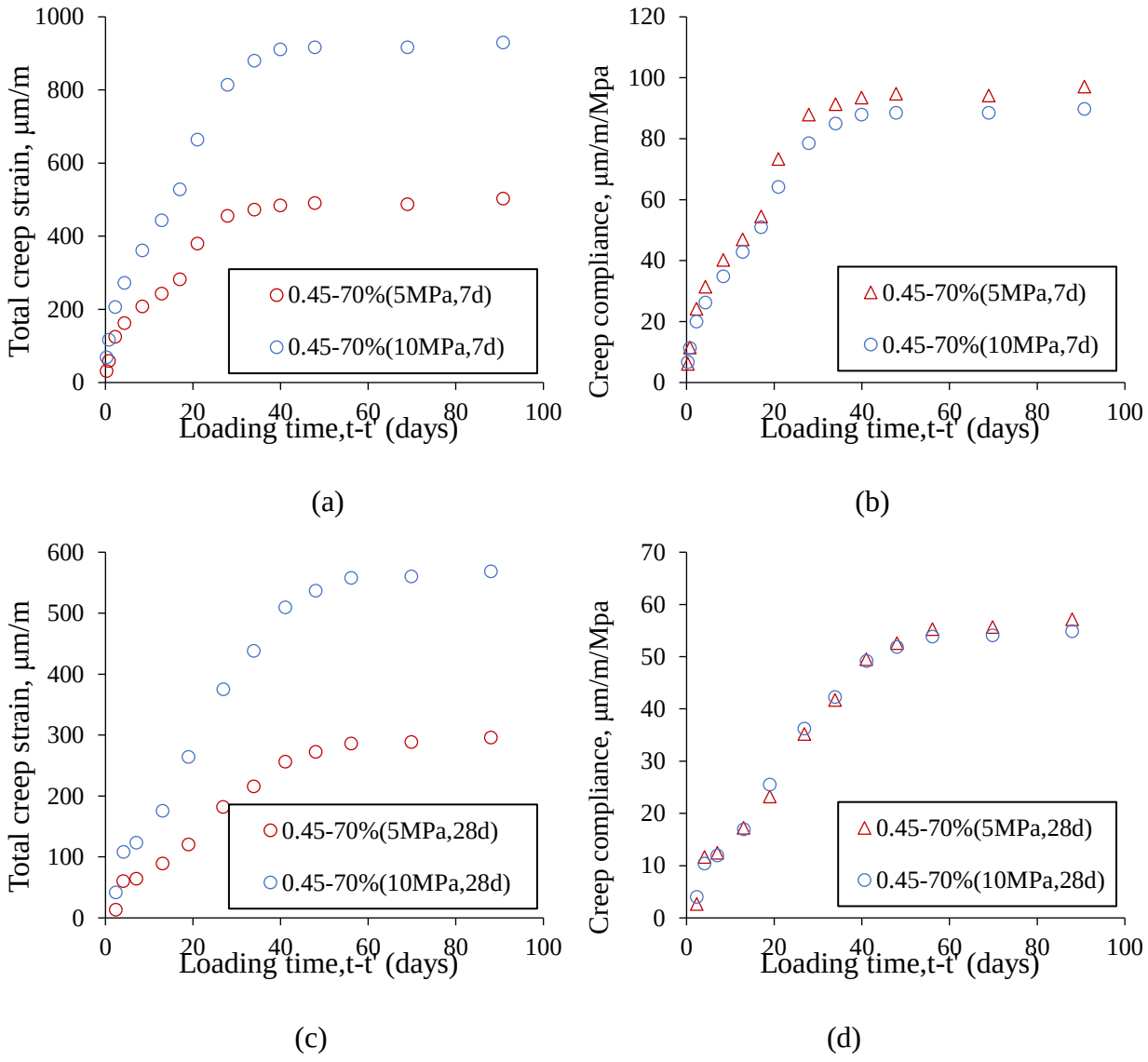

Fig. A-6 The tensile creep strain and creep compliance for 0.45-70% with loading age (7, 28 and 120 days) with two stress load(5MPa and 10MPa)

APPENDIX B: Compliance Development with Simulation versus Time

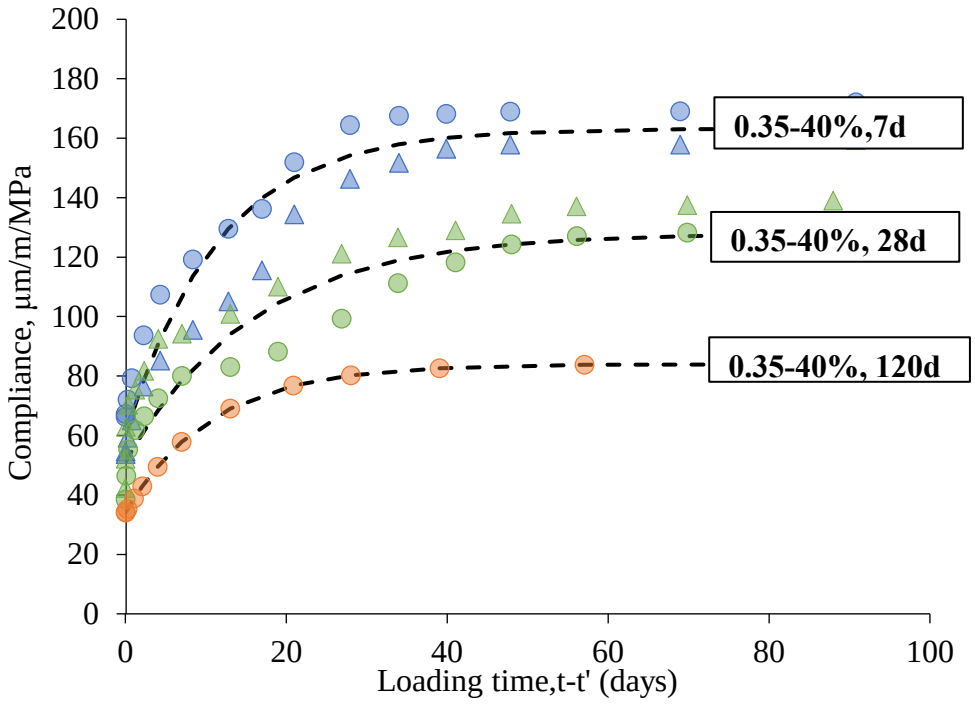

Fig. B-1 The compliance of 0.35-40% starting from 7, 28 and 120 days

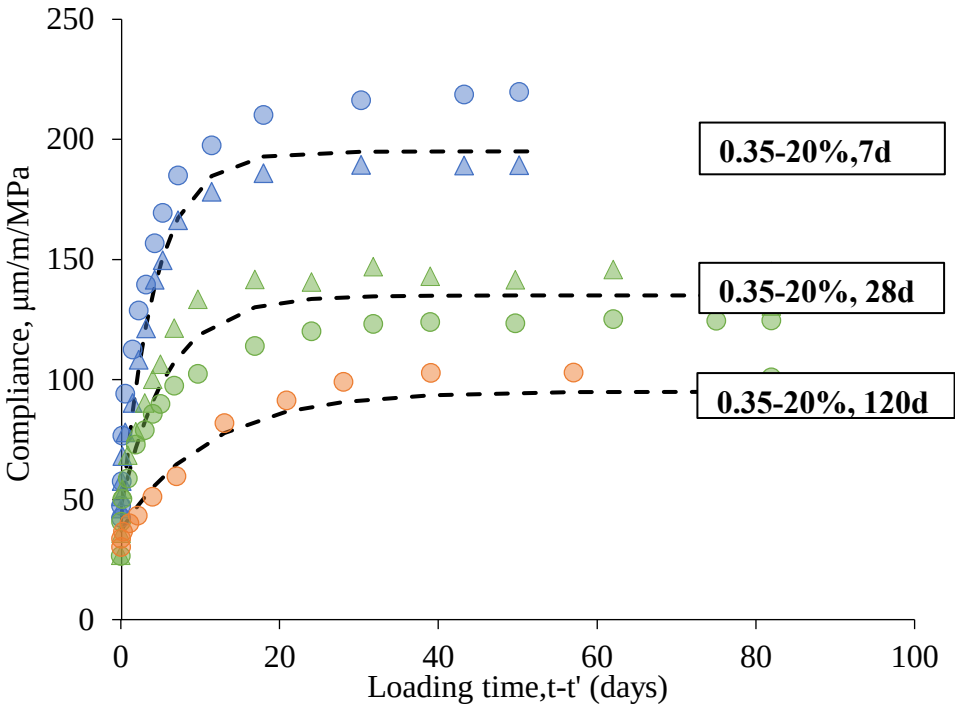

Fig. B-2 The compliance of 0.35-40% starting from 7, 28 and 120 days

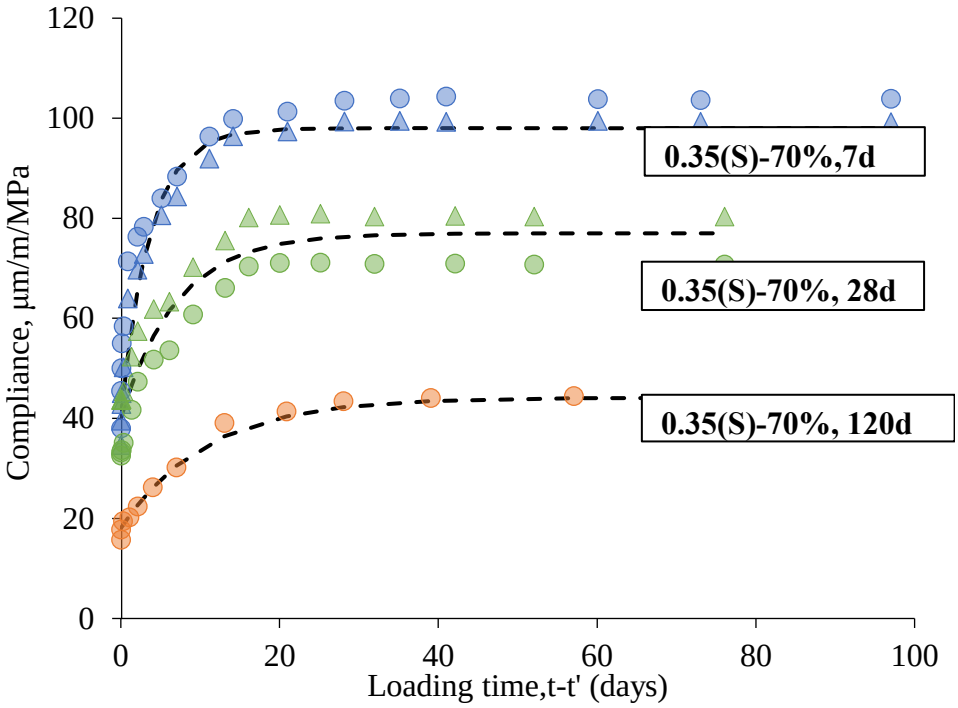

Fig. B-3 The compliance of 0.35(S)-70% starting from 7, 28 and 120 days

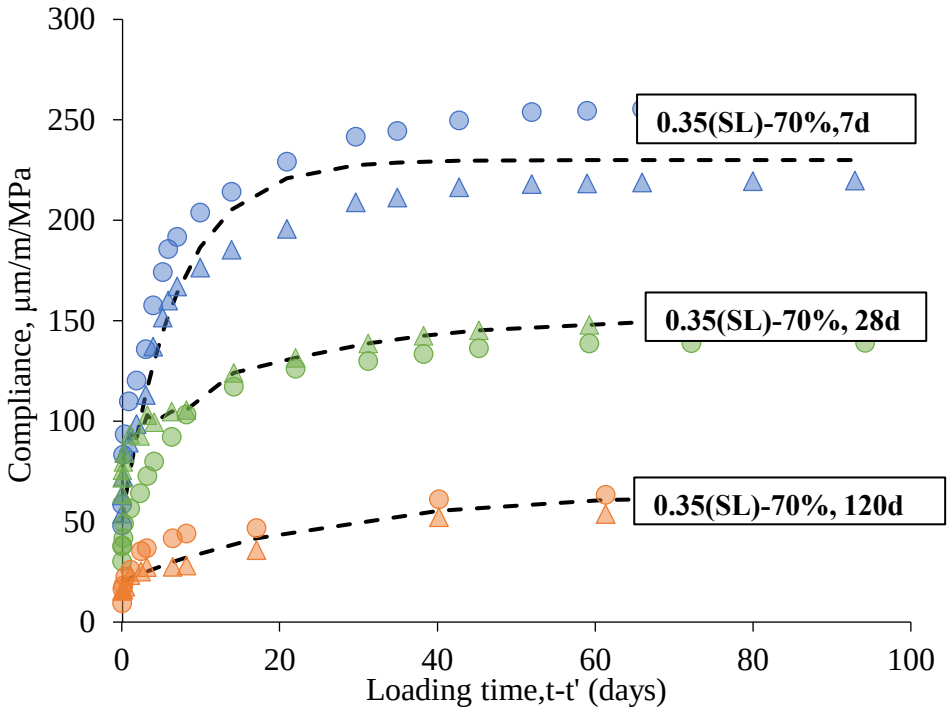

Fig. B-4 The compliance of 0.35(SL)-70% starting from 7, 28 and 120 days

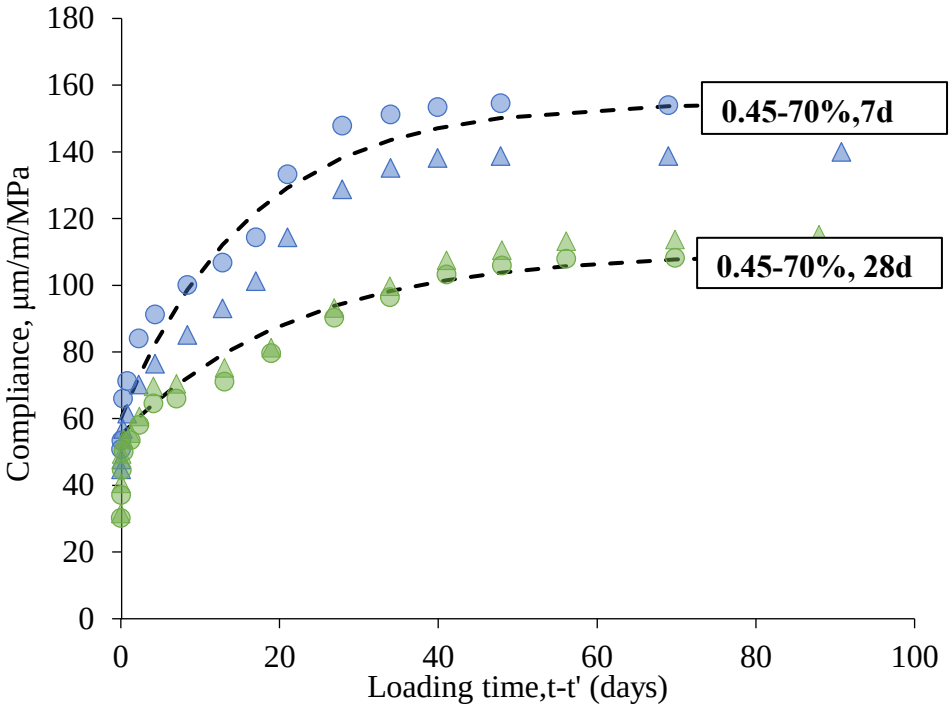

Fig. B-5 The compliance of 0.45-70% starting from 7 and 28 days

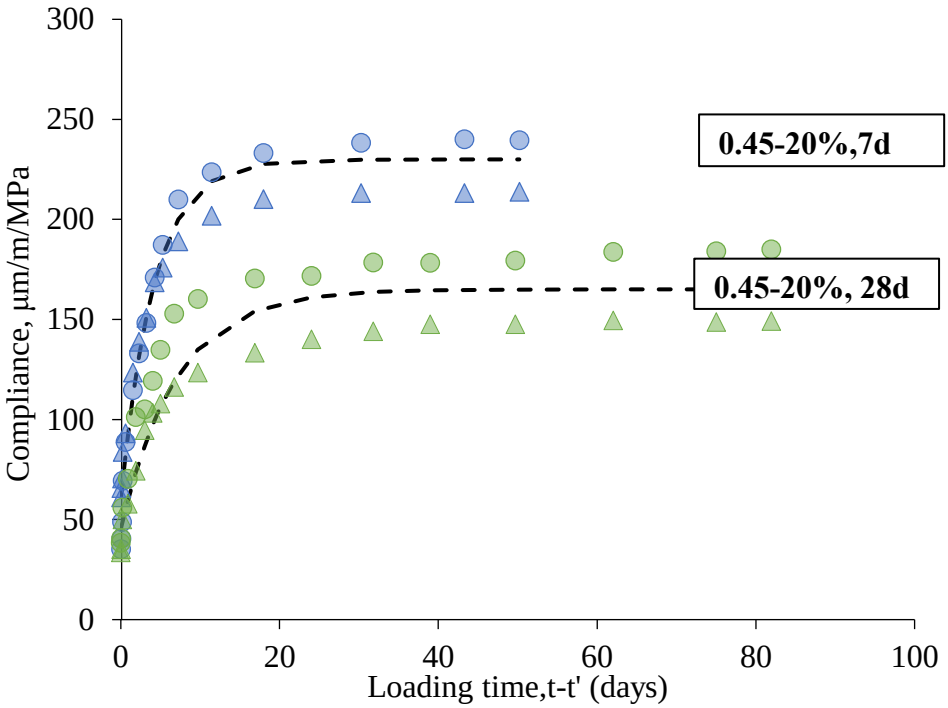

Fig. B-6 The compliance of 0.45-20% starting from 7 and 28 days

APPENDIX C: Numerical Simulation of Relaxation

If we assume that $\varepsilon_{cr}(t)$ is constant ε_0 all the time, Eq. 5-9 can be converted to Eq. (1) by dividing ε_0 :

$$\frac{\sigma_c(t_0)J(t,t_0)}{\varepsilon_0} + \int_{t_0}^{t} J(t,t')d\frac{\sigma(t')}{\varepsilon_0} = J(t,t_0)R(t_0,t_0) + \int_{t_0}^{t} J(t,t')d\frac{\sigma(t')}{\varepsilon_0}$$

$$= J(t,t_0)E_e(t_0) + \int_{t_0}^{t} J(t,t')d\frac{\sigma(t')}{\varepsilon_0} = 1 \qquad \text{Eq. C-1}$$

$E_e(t_0)$ means the elastic modulus, the first part in the equation above $J(t,t_0)E_e(t_0)$ means the strain part related to elastic modulus. And the second part is the strain related to creep. The sum of the two parts keeps constant.

Then assume that uniaxial load is applied at $t_0 = 0$,

$$\frac{\sigma(t_0)}{\varepsilon_0} = d\left(\frac{\sigma(t_0)}{\varepsilon_0}\right) \qquad \text{Eq. C-2}$$

Then Eq. (2) can be written as:

$$1 = \frac{\sigma_c(t_0)J(t,t_0)}{\varepsilon_0} + \int_{t_0}^{t} J(t,t')d\frac{\sigma(t')}{\varepsilon_0} =$$

$$\int_{0}^{t_0} J(t,t_0)d\frac{\sigma(t_0)}{\varepsilon_0} + \int_{t_0}^{t} J(t,t')d\frac{\sigma(t')}{\varepsilon_0} = \int_{0}^{t} J(t,t')dR(t') = 1 \qquad \text{Eq. C-3}$$

Then, the approximation equation can be obtained:

$$\sum_{i=1}^{k} J(t_k, t_i)\,\Delta R(t_i) = constant \qquad \text{Eq. C-4}$$

Then the equation above can be written as

$$\sum_{i=1}^{k} \frac{1}{2}[J(t_k, t_i) + J(t_k, t_{i-1})]\,\Delta R(t_i) = 1 \qquad \text{Eq. C-5}$$

Then when t=k-1:

$$\sum_{i=1}^{k-1} \frac{1}{2}[J(t_{k-1}, t_i) + J(t_{k-1}, t_{i-1})]\,\Delta R(t_i) = 1 \qquad \text{Eq. C-6}$$

Eq. (6) can be written as:

$$\sum_{i=1}^{k} \frac{1}{2}[J(t_{k-1}, t_i) + J(t_{k-1}, t_{i-1})]\,\Delta R(t_i) - \frac{1}{2}[J(t_k, t_k) + J(t_k, t_{k-1})]\Delta R(t_k) = 1 \qquad \text{Eq. C-7}$$

Then based on Eq. C-5 to Eq. C-7**,**

$$\sum_{i=1}^{k} \frac{1}{2}[J(t_{k-1}, t_i) + J(t_{k-1}, t_{i-1})]\,\Delta R(t_i) -$$

$$\sum_{i=1}^{k} \frac{1}{2}[J(t_k, t_i) + J(t_k, t_{i-1})]\,\Delta R(t_i) - \frac{1}{2}[J(t_k, t_k) + J(t_k, t_{k-1})]\Delta R(t_k) = 0 \qquad \text{Eq.C-8}$$

$\Delta R(t_k)$ can be obtained by:

$$\Delta R(t_k) = \frac{\sum_{i=1}^{k} \frac{1}{2}\{[J(t_{k-1},t_i)+J(t_{k-1},t_{i-1})]-[J(t_k,t_i)+J(t_k,t_{i-1})]\}}{\frac{1}{2}[J(t_k,t_k)+J(t_k,t_{k-1})]}\Delta R(t_i) \qquad \text{Eq. C-9}$$

$$= \frac{\sum_{i=1}^{k} \{[J(t_{k-1},t_i)+J(t_{k-1},t_{i-1})]-[J(t_k,t_i)+J(t_k,t_{i-1})]\}}{[J(t_k,t_k)+J(t_k,t_{k-1})]}\Delta R(t_i) \qquad \text{Eq. C-10}$$

APPENDIX D: Code for Simulating Relaxation

```
clear all;
clc;
ultcreep=zeros(100,1);    % ultimate creep matrix
time=zeros(100,1);
t=[7,28,120];
Relaxation=zeros(100,3);
Eelastict = zeros(3,1);

num=1;
while num<101
    time(num)=(num)*10;   %in hrs
    num=num+1;
end
for j=1:3

%0.35-20
% Ae = 9878;
% Be = -27033;
% Ac = 3799;
% Bc = -13135;
% At = 49.43;
% Bt = - 162.94;



%0.35-40
% Ae=6394;
% Be=- 17793;
% Ac=3717.2;
% Bc = -10135;
% At = 23.87;
% Bt =138.75;
%
% %0.35-70
Ae=2254;
Be=20671;
Ac=6431.3;
Bc = -18724;
At = 14.777;
Bt = 9.28;


creep=zeros(100,100);
%J function for J curve including elastic and creep strain.
for num=1:100
    for num2=num:100
```

```
Ecreep=Ac*log(time(num)+24*t(j)) + Bc;
        Eelastict2=Ae*log(time(num)+24*t(j)) + Be;
        taut=At*log(time(num)+24*t(j)) + Bt;
        creep(num2,num)=1/Eelastict2+(1-1/exp((time(num2)-
time(num))/taut))/Ecreep;
    end
end
%Generating relaxation modulus matrix
R=zeros(100,1);
%Generating the intial value for R curve modulus
R(1)=Ae*log(24*t(j))+Be;
%Generating the intial value for R curve modulus
R(2)=R(1);
%Generating the intial value for R curve modulus
dR=zeros(100,1);
%Generating the intial value for R curve modulus
dR(2)=R(1);
% Calculating relaxation modulus
for k=3:100
    sum=0;
    for i=2:k-1
        sum=sum-(creep(k,i)+creep(k,i-1)-creep(k-1,i)-creep(k-1,i-1))*dR(i);
    end
    dR(k)=sum/(creep(k,k)+creep(k,k-1));
    R(k)=R(k-1)+dR(k);
end
Relaxation(:,j)=R;
end

figure();
semilogx([time(2:end)/24 time(2:end)/24
time(2:end)/24],Relaxation(2:end,1:3));
xlabel('Loading age,(t-t0)');
ylabel('Relaxtion modulus, in MPa');
legend('t0=7days','t0=28days','t0=120days','Location','northeast
```

APPENDIX E: Total Strain and Compliance versus Loading Age

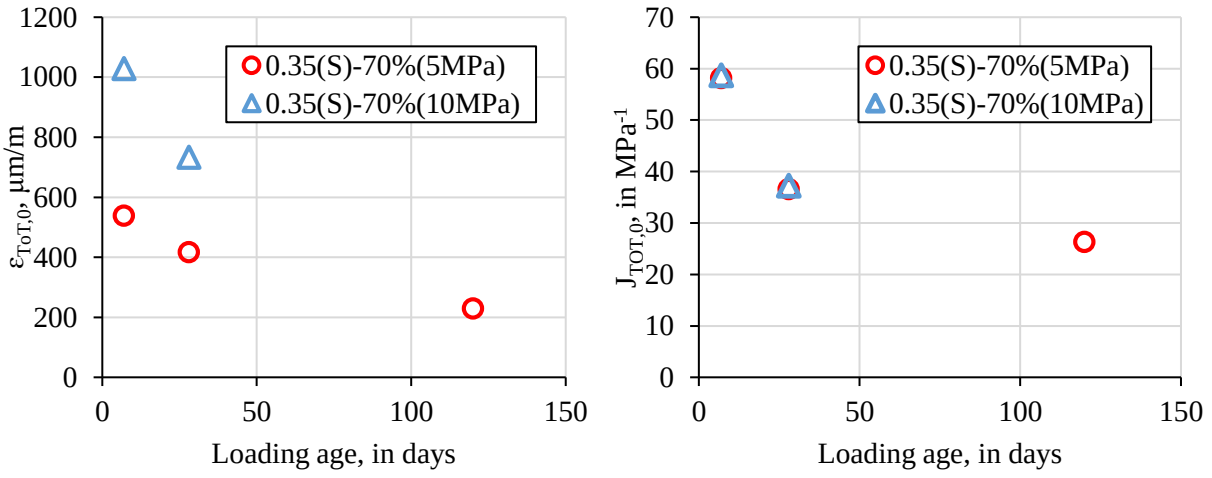

(a) (b)

Fig. E-1 The ultimate total strain and compliance for 0.35(S)-70% at 7, 28 and 120 days.

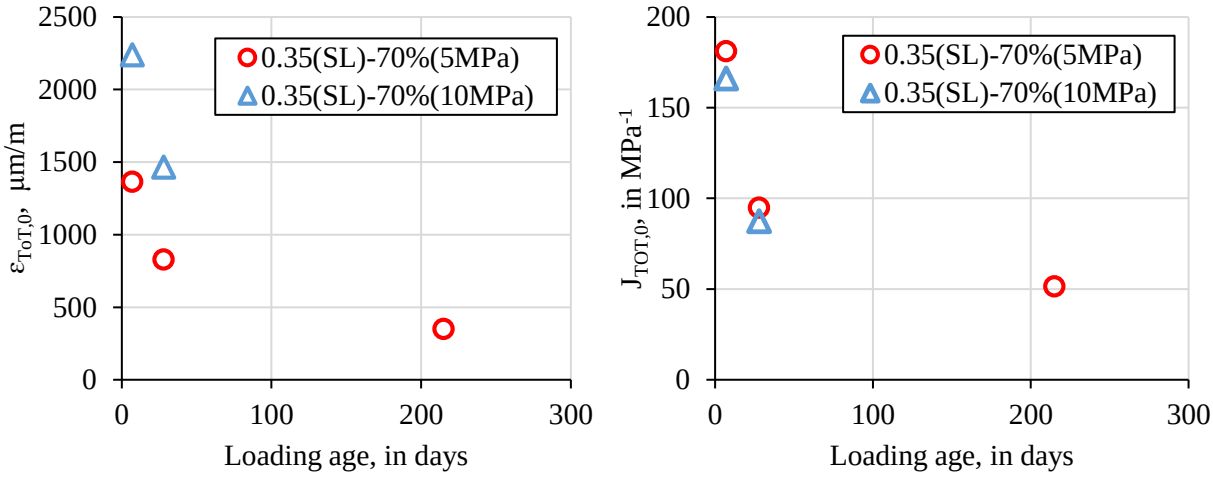

(a) (b)

Fig. E-2 The ultimate total strain and compliance for 0.35(SL)-70% at 7, 28 and 120 days.

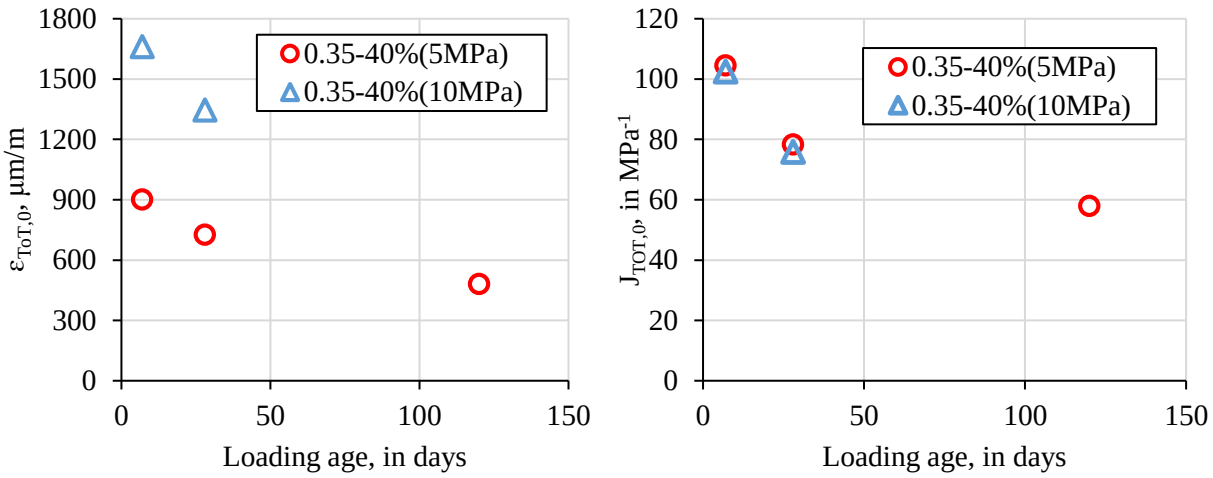

(a) (b)

Fig. E-3 The ultimate total strain and compliance for 0.35-40% at 7, 28 and 120 days.

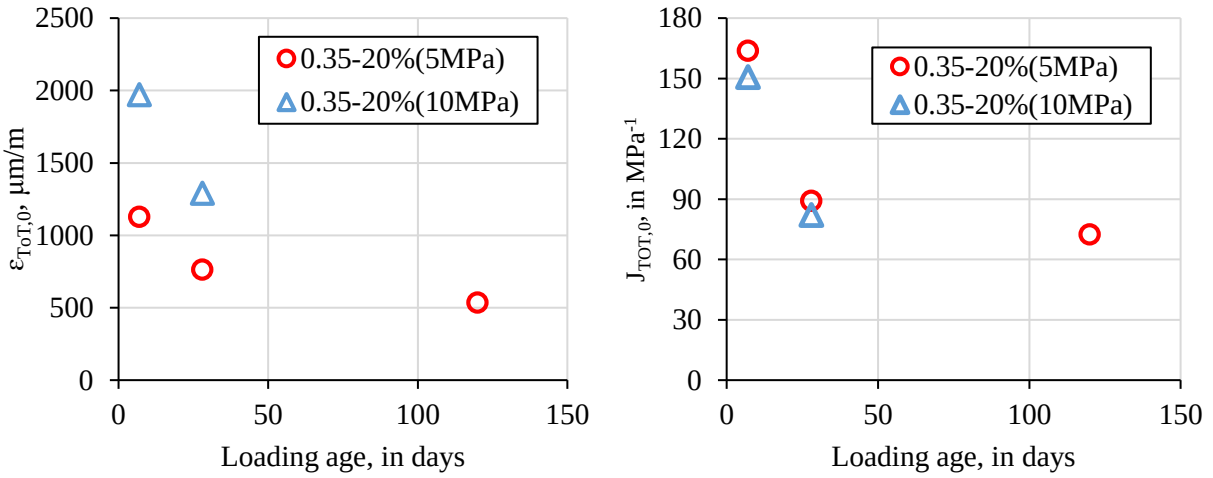

(a) (b)

Fig. E-4 The ultimate total strain and compliance for 0.35-20% at 7, 28 and 120 days.

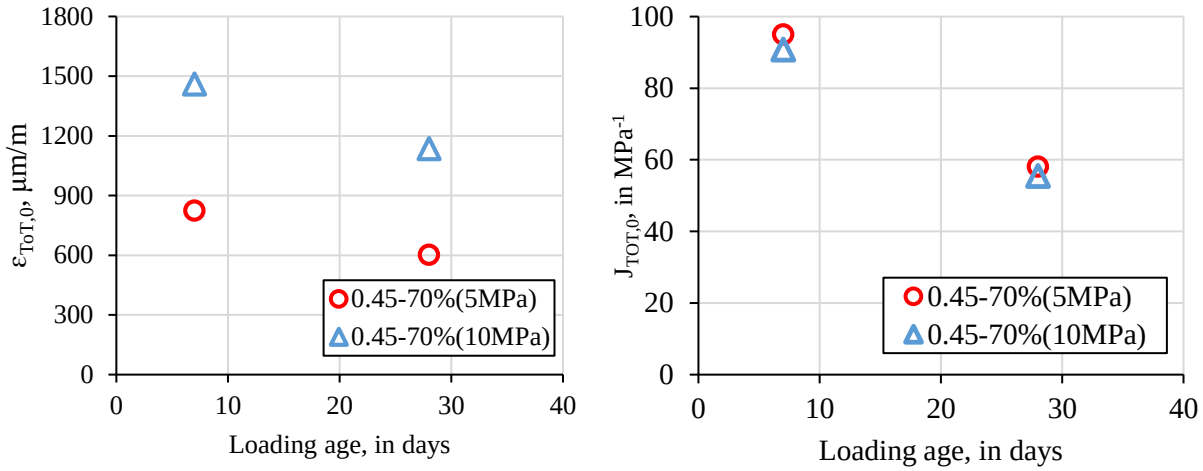

(a) (b)

Fig. E-5 The ultimate total strain and compliance for 0.45-70% at 7, 28 and 120 days.

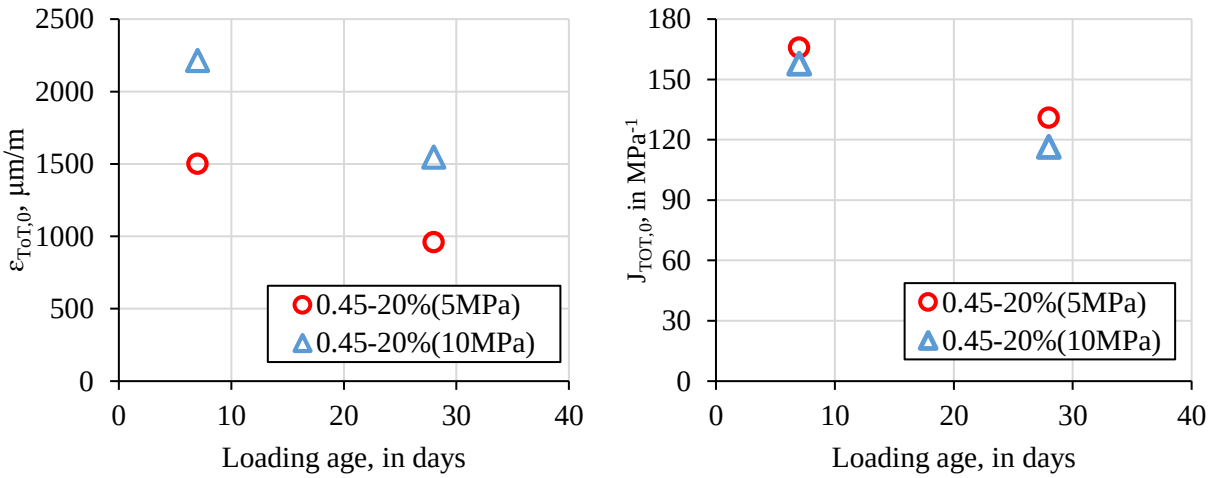

(a) (b)

Fig. E-6 The ultimate total strain and compliance for 0.45-20% at 7, 28 and 120 days